



Norwegian University of
Science and Technology

Effective Polyakov Loop Modeling of QCD

A Field Theoretical Study of the Phase

Diagram of Quark Matter

Åsmund Schiager Folkestad

Master of Science in Physics and Mathematics

Submission date: June 2018

Supervisor: Jens Oluf Andersen, IFY

Norwegian University of Science and Technology
Department of Physics

Preface

This master's thesis represents 20 weeks of work over the course of the 2018 spring semester. It is the continuation of a project on the quark-meson model carried out during the fall of 2017 [1]. I assume that the reader is familiar with elementary classical and quantum field theory, statistical mechanics, and phase transitions. Only a minimum of thermal field theory is assumed, with clear statements included when results from the field are used. The specifics of the models studied are covered in full detail, and no preexisting knowledge is required.

Chapters 2 and 3 consist of a relatively lengthy introduction to the Polyakov loop since I could not find a self-contained introduction at the level appropriate for an early graduate student without a background in the literature. Especially the literature derivations of the formula relating the Polyakov loop and the quark free energy appeared obscure to me, and I thus provided a step-by-step field theoretic derivation of the formula.

Finally, I owe gratitude to the people supporting me during this work. I would like to thank Professor Jens O. Andersen for excellent supervision, interesting discussions and thorough feedback on my work. I would also like to thank my housemates and friends for providing a fantastic atmosphere in which to decouple from physics, with a special mention to my gym partner Simen Kjernlie. Lastly, I am indebted to my partner Ana Trišović, who always supports me and forgives me when I am fully absorbed by my work.

Abstract

In this thesis we study the phase diagram of two-flavor quantum chromodynamics with effective models. We investigate the phase diagram in the baryon chemical potential–temperature and magnetic field–temperature planes. As approximations to QCD we use the Polyakov-loop extended quark-meson model (PQM) and the Pisarski-Skokov chiral matrix model (χM). We take quantum and thermal fluctuations of quarks into account to one loop, while we neglect bosonic fluctuations. Bosonic self-energy corrections are calculated in order to consistently fix coupling constants at the one-loop level in the large- N_c limit.

We find that both models have coinciding chiral and deconfinement phase crossovers at zero chemical potential, and the pseudocritical temperatures agree with two-flavor lattice QCD simulations. For temperatures up to $T \approx 2T_c$ the models agree reasonably with the pressure, energy density, and interaction measure as calculated on the lattice. However, the Polyakov loop temperature dependence disagrees with the lattice results.

For quark chemical potentials satisfying $\mu \leq T$, the PQM model agrees well with the pressure and quark number density from lattice simulations. The χM model overshoots these quantities. In the regime $\mu \gg T$ the PQM model predicts a quarkyonic phase while the χM model predicts a deconfined and chirally restored phase.

At constant magnetic fields the two models display magnetic catalysis at all temperatures, which is in disagreement with lattice data. We show that the chiral sector is responsible for magnetic catalysis. Furthermore, we find that a Polyakov loop model without a chiral sector displays inverse magnetic catalysis. Finally, we show that inverse magnetic catalysis does not occur in the χM model even when the deconfinement temperature in the gluonic sector is made to decrease with the magnetic field.

Sammendrag

I denne avhandlingen studerer vi fase-diagrammet til kvantekromodynamikk (QCD) med to kvarktyper ved hjelp av effektiv modellering. Vi undersøker fase-diagrammet i kjemisk potensial–temperatur planet og magnetisk felt–temperatur planet. Som tilnærming til QCD benytter vi en kiral matrisemodell og kvark-meson-modellen (PQM) utvidet med Polyakovløkka. Vi tar høyde for kvantefluktuasjoner og termiske fluktuasjoner til en løkke, mens bosonfluktuasjoner blir neglisjert. Bosoniske selvenergi-korreksjoner regnes ut slik at vi kan bestemme koblingskonstantene konsistent på en-løkke nivået i grensen der N_c er stor.

Ved null kjemisk potensial finner vi at begge modellene har samtidige faseoverganger for kvarkfrigjøring og gjenopprettelse av kiral symmetri. De pseudokritiske temperaturene overenstemmer med QCD-simuleringer på gitteret med to kvarktyper. For temperaturer opp til $T \approx 2T_c$ reproduserer begge modeller gitterverdier for trykk, energitetthet og interaksjonsmål til relativt høy grad. Polyakovløkkas temperaturavhengighet overenstemmer ikke med gittersimuleringer i noen av modellene.

For kjemiske potensial $\mu \leq T$ finner vi at PQM-modellen reproduserer trykket og kvark-tettheten på gitteret, mens χM -modellen overestimerer disse størrelsene. I regimet $\mu \gg T$ forutsier PQM-modellen en kvarkyonisk fase, mens χM -modellen forutsier en fase der kiral symmetri er gjenopprettet og hvor kvarkene er frigjort.

Ved konstante magnetfelt finner vi at begge modeller har magnetisk katalyse ved alle temperaturer, og de reproduserer dermed ikke gittersimuleringer. Vi viser at det er den kirale sektoren som er ansvarlig for magnetisk katalyse og at en Polyakovløkke-modell uten en kiral sektor har invers magnetisk katalyse. Til slutt viser vi at invers magnetisk katalyse ikke oppstår i χM modellen selv når man lar den kritiske temperaturen i gluonsektoren avta med magnetfeltet.

Contents

Preface	i
Abstract	iii
Sammendrag	v
Conventions	x
1 Introduction	1
1.1 The Discovery of the Strong Force	1
1.2 Quantum Chromodynamics and the Standard Model	2
1.3 The QCD Phase Diagram	3
1.4 Thesis Outline	4
2 The Polyakov Loop	7
2.1 Yang-Mills Theory	7
2.2 Quantum Chromodynamics	9
2.3 Heavy Quark Dynamics	10
2.4 The Polyakov Loop and Deconfinement	12
2.5 Dual Systems	18
2.6 Center Symmetry and its Spontaneous Breaking	19
2.7 The Polyakov Gauge	22
3 Modeling Quark Confinement	25
3.1 The Partition Function of Fermions in a Gluonic Background	26
3.2 Quarks in a $N_c = 3$ Gluonic Background	29
3.3 The Effective Potential	31
3.4 Phenomenological Polyakov Loop Potentials	34
3.5 The Relation Between Φ and $\bar{\Phi}$ at $\mu \neq 0$	37
4 The Polyakov Loop Quark-Meson Model	41
4.1 An $O(4)$ Model with Spontaneous Symmetry Breaking	41
4.2 The Quark-Meson Model	44
4.3 Chiral Symmetry Breaking in the QM Model	47

4.4	Parameters of the QM Model at One Loop	48
4.5	The Pion Decay Constant	51
4.6	The PQM Partition Function in the One-Loop Large- N_c Limit	52
4.7	The PQM Model as an Effective Model of QCD	54
5	Thermodynamics of the PQM and χM Models	59
5.1	The Gluonic Sector of the χM Model	60
5.2	A Phenomenological Quark Term	62
5.3	The Complete PQM and χM Models	64
5.4	QCD Lattice Results	66
5.5	Numerical Results: PQM and χM Model Thermodynamics at $\mu = 0$	68
5.6	Minimizing Ω at $\mu \neq 0$	79
5.7	Numerical Results: PQM and χM Model Thermodynamics at $\mu > 0$	81
6	The PQM Model in a Magnetic Field	87
6.1	The PQM Lagrangian Coupled to the EM field	88
6.2	Quarks in a Constant Magnetic Field	89
6.3	Landau Levels	90
6.4	The Quark Partition Function at One Loop: Part I	92
6.5	Interlude: Regularization of the Vacuum Energy	94
6.6	The Quark Partition Function to One Loop: Part II	95
6.7	The PQM Partition Function	97
6.8	A Fugacity Expansion of Ω_T	101
6.9	Numerical Methods	102
6.10	Numerical Results: The Effective Potential	103
6.11	Numerical Results: Magnetic Catalysis	105
6.12	Numerical Results: The Effect of the Chiral Sector on Magnetic Catalysis	105
6.13	Inverse Magnetic Catalysis	107
6.14	Numerical Results: A B -Dependent Gluonic Sector	111
7	Conclusion and Outlook	113
7.1	Summary	113
7.2	Conclusion	115
7.3	Outlook	115
	Bibliography	117
A	Additional Derivations	129
A.1	Calculation of the Fermion Partition Function	129
A.2	Matsubara Frequency Sums	130
A.3	Symmetries of the QM Model	133
A.4	One-Loop Renormalization of the QM Model	136
B	Code	151
B.1	Implementation of the Effective Potential in Python	151

CONTENTS

B.2 Implementation of the Thermal Quark Integrand in C	159
B.3 Implementation of the Global Minimization in Python	160

Conventions

Units

We use natural units where $\hbar = c = k_B = 1$. For electromagnetic units we use Lorentz-Heaviside units, which implies $\epsilon_0 = \mu_0 = 1$. This gives a fine structure constant of $\alpha = \frac{e^2}{4\pi}$ and an electromagnetic Lagrangian $\mathcal{L} = -\frac{1}{4}F_{\mu\nu}F^{\mu\nu}$.

Metric, Indices and Gamma Matrices

Vectors in space-time are written as $v^\mu = v = (v^0, \mathbf{v})$, where bold font indicates a spatial vector with three components. We use Einstein summation convention when summing over vectors. Unless otherwise specified, greek indices sum over space-time while Latin indices sum over space. We choose the Minkowski metric signature $g_{\mu\nu} = \text{diag}(1, -1, -1, -1)$, and repeated latin indices do not have an implicit minus sign, meaning

$$u^\mu v_\mu = g_{\mu\nu} u^\mu v^\nu = v^0 v^0 - v^i v^i. \quad (0.0.1)$$

We use the Dirac representation of the gamma matrices

$$\gamma^0 = \begin{pmatrix} 1 & 0 \\ 0 & 1 \end{pmatrix}, \quad \gamma^i = \begin{pmatrix} 0 & \sigma^i \\ -\sigma^i & 0 \end{pmatrix}, \quad (0.0.2)$$

where σ^i are the standard Pauli matrices.

$SU(3)$ and Gell-Mann Matrices

We refer to the Lie algebra of $SU(3)$ as $\mathfrak{su}(3)$. As a basis for $\mathfrak{su}(3)$ and as generators for $SU(3)$ in fundamental representation, we use $T^a = \frac{1}{2}\lambda^a$, where λ^a are the Gell-Mann matrices. The index a runs from 1 to 8. The diagonal matrices are λ^3 and λ^8 , which reads

$$\lambda^3 = \begin{pmatrix} 1 & 0 & 0 \\ 0 & -1 & 0 \\ 0 & 0 & 0 \end{pmatrix}, \quad \lambda^8 = \frac{1}{\sqrt{3}} \begin{pmatrix} 1 & 0 & 0 \\ 0 & 1 & 0 \\ 0 & 0 & -2 \end{pmatrix}. \quad (0.0.3)$$

We write the matrix gluon field in a bold font, $\mathbf{A}_\mu = A_\mu^a T^a$.

Introduction

In this introductory chapter we start with a brief history of the strong force. We then give a non-technical description of quantum chromodynamics and its relevance to physical phenomena.¹ Finally, we describe how this thesis is structured.

1.1 The Discovery of the Strong Force

After the discovery of the atomic nucleus by Rutherford [2] an obvious question arose: what holds it together? Some force must overcome the electrical repulsion between the positively charged protons, yet no such force had been observed at the time. This force came to be known as the strong nuclear force, and several scientists attempted to explain its origins in the following years. Most important was Yukawa's proposition that the protons and neutrons interact attractively as the result of exchanging a massive particle known as a meson. There is truth to this idea, and Yukawa was in 1949 awarded the Nobel Prize in physics for his prediction of the particles that we now call pions [3].

Gell-Mann [4] and Zweig [5] made a breakthrough in 1964 when they realized that the nucleons, pions, and myriad of new particles discovered in the fifties could be understood as bound states of more fundamental particles. These came to be known as quarks. However, it was not until the 1970's that a proper understanding of the strong forces was achieved. It turned out that the strong nuclear force acting to bind nucleons was a remnant effect of the more fundamental strong interaction between quarks. In 1973 the theory of quantum chromodynamics (QCD) was finally published [6], and it is this theory that today is held to be the correct theory of the strong interactions.

¹We remark that the first two sections in this chapter are nearly identical to the introduction in the specialization project leading up to this thesis [1].

1.2 Quantum Chromodynamics and the Standard Model

QCD is a part of a collective of quantum field theories together known as the Standard Model. The Standard Model describes three out of the four known forces of nature: the strong, the weak and the electromagnetic forces. QCD describes the strong force, while quantum electrodynamics (QED) and Glashow-Weinberg-Salam (GWS) theory describe the electromagnetic and the weak forces, respectively.² The Standard Model has time and again been tested successfully in particle accelerators, and the model describes nearly all of the observed interactions between elementary particles.³ A comprehensive summary of the most up to date experimental measurements pertaining to the Standard Model are found in *The Review of Particle Physics* [8].

		Fermion generations			Gauge bosons	Scalar bosons
		I	II	III		
Quarks	u up	c charm	t top	g gluons	H Higgs	
	d down	s strange	b bottom	γ photon		
Leptons	e electron	μ muon	τ tau	Z^0 Z boson	W^\pm W bosons	
	ν_e electron neutrino	ν_μ muon neutrino	ν_τ tau neutrino			

Table 1.1: Elementary particles in the Standard Model of particle physics.

The Standard Model contains three classes of fundamental particles: the matter particles, which are spin- $\frac{1}{2}$ fermions, the force carriers, which are spin-1 bosons, and the spin-0 Higgs boson, which is responsible for generating the elementary fermion masses. The fermions are additionally separated into leptons and quarks, and only the latter interact via the strong force. It turns out that there are three generations of fermions, with two quarks and two leptons in each generation. Thus, there are six quarks known to exist, and we refer to them as having different flavors. Table 1.1 shows the particle content of the Standard Model. In this work we will deal with the two lightest quark

²Technically, GWS theory also describes electromagnetic forces.

³Combined recent observations by the LHCb, Belle, and BaBar experiments, summarized in the preprint [7], appears to be showing violations of a property known as lepton universality at the 5σ confidence level.

flavors, the up and down quarks, which have bare masses at the order of $\sim \text{MeV}$ [8]. The different quark flavors get progressively heavier with each generation, and at sufficiently low energies only the lightest flavors influence observed physics.

QCD shares many structural features with QED. In the former the interactions between quarks are mediated via massless particles known as gluons, which are the analogs to the photon in the electromagnetic force. Similarly to the photons which only interact with electrically charged particles, the gluons only interact with particles having a property known as color. However, while there is only one type of electric charge, there are three types of color charges, and eight different gluons exist. Furthermore, the gluons carry color, causing them to interact among themselves.

The fact that gluons carry color causes QCD to become increasingly weakly interacting at high energies. This effect is known as asymptotic freedom, and Gross, Wilczek [9] and Politzer [10] were awarded the Nobel Prize in 1973 for its discovery. Asymptotic freedom also implies that the theory becomes increasingly strongly interacting at low energies, and a result of this is that perturbation theory breaks down at energies lower than $\sim 1 \text{ GeV}$ [11]. This is the regime relevant to hadrons and arguably the most interesting regime of the theory. Studying QCD below this scale is extremely hard and requires non-perturbative techniques. As a result, there is still active research on QCD, and several important unsolved problems exist, with perhaps the most prominent one being the problem of confinement, which we describe in the following.

1.3 The QCD Phase Diagram

The property of confinement is an essential aspect of QCD. It implies that objects with net color can never exist freely at low energies, which explains why free quarks have never been observed.⁴ Confinement has not been proven rigorously, but its existence is well establishing by simulations that use a numerical technique known as lattice QCD, where QCD is defined on a discretized space-time.

It is however well known that at high temperatures, nuclear matter undergoes a phase transition to a state where quarks and gluons are no longer confined. The first direct observation of this phase was announced by experiments at the Relativistic Heavy Ion Collider in 2005 [12–15] and later also at the Large Hadron Collider [16]. The transition is known as the deconfinement phase transition, and the state of matter obtained at high temperatures is called a quark-gluon plasma (QGP). The deconfinement phase transition in lattice QCD simulations is found to happen at a temperature $T \approx 160 \text{ MeV}$ [17], which is outside the perturbative regime of QCD.

It turns out that QCD has a rich phase structure, and there is a large body of work on the subject [18]. Figure 1.1 shows a sketch of the conjectured phase diagram of QCD. In addition to the deconfinement phase transition, there is a transition known as the chiral phase transition. For zero baryon chemical potential lattice QCD indicates that

⁴Technically, only $SU(3)$ color singlets can exist freely.

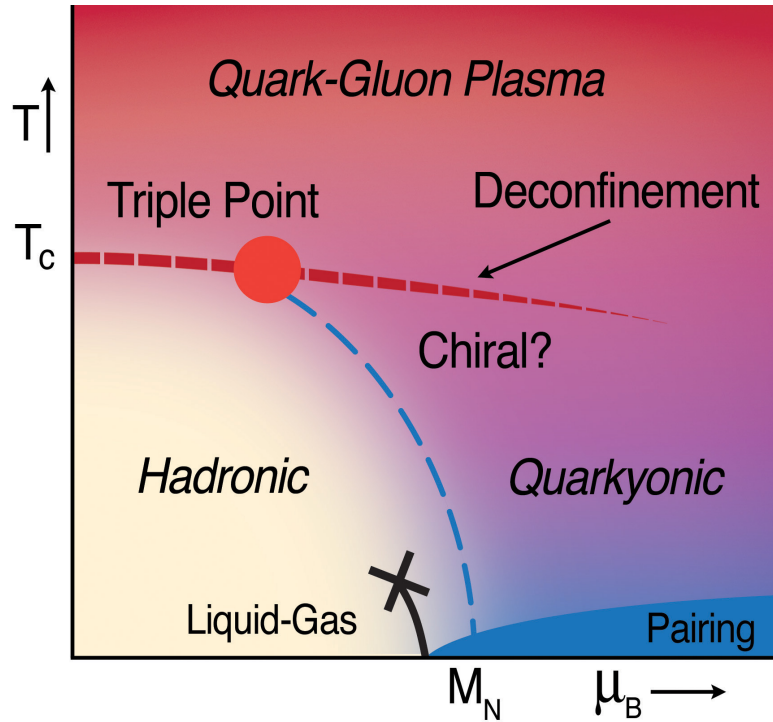


Figure 1.1: Sketch of the conjectured phase diagram of QCD in the plane of temperature and baryon chemical potential. Figure from Ref. [19].

the chiral transition happens at the same temperature as deconfinement [17].⁵ The chiral phase transition is related to that fact that for the lightest quark flavors, QCD has an approximate symmetry under mixing of the light quark flavors. For massless quarks this symmetry is exact and is known as chiral symmetry. In the vacuum, chiral symmetry is broken spontaneously, and as a consequence the pions arise as (approximate) Nambu-Goldstone bosons, which is a type of particle that appears when a continuous symmetry is spontaneously broken. At high temperatures, the approximate chiral symmetry is restored in the chiral phase transition.

1.4 Thesis Outline

Since the most interesting features of the phase diagram lie outside the regime where we can use QCD perturbation theory, other methods must be employed. Lattice QCD is a method to study QCD non-perturbatively from first principles, but a technicality known as the sign problem makes its use at non-zero baryon chemical potential infeasible at present day [20]. In this work we will instead use phenomenological models to study the QCD phase diagram and thermodynamics. In particular, we employ the quark-meson

⁵Zero baryon chemical potential means vanishing baryon density. Increasing baryon chemical potential means increasing baryon density.

(QM) model extended with the Polyakov loop and a recently published [21] model that we refer to as the chiral matrix (χM) model.

To better understand the deconfinement phase transition, we start out in Chapter 2 by reviewing the basics of Yang-Mills theory and QCD, and we investigate the dynamics of heavy quarks in a gluonic background. Following this we show how the free energy F_q of a heavy quark in a gluonic background at temperature T is related to the expectation value of an operator Φ known as the Polyakov loop:⁶

$$e^{-F_q/T} = \langle \Phi \rangle. \quad (1.4.1)$$

This formula was originally derived by McLerran and Svetitsky in Ref. [22]. However, since the original paper lacks a step-by-step derivation and the author could not find one in the literature, an independent field theoretic derivation of the formula is provided. The derivation is based on a similar relation for the Wilson loop at zero temperature obtained in Ref. [23]. Once (1.4.1) is established we discuss gauge transformations at finite temperature and the closely related concept of center symmetry. We show that the deconfinement phase transition for heavy quarks is associated with the breaking of center symmetry.

In Chapter 3 we construct a toy model for quark confinement by coupling free fermions to a constant temporal gluonic background, following the procedure pioneered by Fukushima in Ref. [24]. We furthermore discuss the effective potential in QFT at finite temperature, its relation to the thermodynamic grand potential, and phenomenological Polyakov loop potentials. We round off the chapter with a discussion of the relation between the Polyakov loop $\langle \Phi \rangle$ and the conjugate Polyakov loop $\langle \bar{\Phi} \rangle$ at non-zero baryon chemical potential, which appears to be a subject of confusion in the literature.

The topic of Chapter 4 is the quark-meson model and its Polyakov-loop extended version. We summarize work from the project leading up to this thesis [1], which consists of a one-loop renormalization of the QM model at zero temperature in the large- N_c limit. We also justify why the PQM model provides an approximation to QCD and discuss the relationship between the symmetries of the two.

We proceed to study the phase diagram and thermodynamics of the PQM model numerically in Chapter 5. We do this in the large- N_c limit where we can neglect mesonic fluctuations, and we fix the coupling constants consistently at the one-loop level, which is typically not done in the literature. Furthermore, we carry out the same study on a modified version of the χM model. We also study the models at finite baryon chemical potential, which at the time of writing has not been done for the χM model in the literature. We carry out a comprehensive comparison of model results with lattice data.

In Chapter 6 we augment the PQM and χM models with a constant magnetic field. We study the concept of magnetic catalysis and investigate the interplay between the critical temperature for the deconfinement and chiral transitions. Finally, we study the effect of making the gluonic sector of the χM model dependent on the magnetic field, and we compare the resulting $T_c(B)$ -phase diagram with lattice data.

⁶It is not clear that F_q is a free energy in the technical sense. We discuss this in Chapter 2.

The Polyakov Loop

In this chapter we first summarize the basics of Yang-Mills theory and briefly discuss how it describes the strong force. We proceed to show how the expectation value of the Polyakov loop operator can be used as an order parameter for confinement in a pure gluonic theory with static (infinitely heavy) quarks. We then discuss gauge transformations at finite temperature and how the spontaneous breaking of a symmetry known as center symmetry is related to confinement. Using center symmetry, we show that only static quark configurations with integer baryon numbers can exist in the confined phase.

2.1 Yang-Mills Theory

The quantum theory of electromagnetism, QED, is described by a Lagrangian

$$\mathcal{L} = -\frac{1}{4}F^{\mu\nu}F_{\mu\nu} + \bar{\psi}[i\gamma^\mu(\partial_\mu - ieA_\mu) - m]\psi, \quad (2.1.1)$$

where ψ is a Dirac spinor field, A_μ the photon field, e the electric charge of the ψ field and $F_{\mu\nu}$ the field strength tensor

$$F_{\mu\nu} = \partial_\mu A_\nu - \partial_\nu A_\mu. \quad (2.1.2)$$

Equation (2.1.1) is invariant under a local phase change of the fields given by

$$\psi(x) \rightarrow e^{-i\alpha(x)}\psi(x), \quad (2.1.3)$$

$$A_\mu(x) \rightarrow A_\mu(x) + \frac{1}{e}\partial_\mu\alpha(x), \quad (2.1.4)$$

where $\alpha(x)$ is some arbitrary smooth function on space-time. This symmetry is known as a gauge symmetry. It is a mathematical redundancy in the description of QED that is needed to describe a massless spin-1 particle, which only can have two possible spin

polarizations, with a four-component vector object. That a massless spin-1 particle can only have two spin polarizations is a classic result shown by Wigner in 1939 [25], and it only assumes that particles transform under irreducible unitary representations of the Poincaré group.¹ Fixing the gauge, meaning that we fix a particular property of A_μ that is not gauge invariant but which has no physical consequences, removes two degrees of freedom and leaves only two [26].

In 1954 Yang and Mills [27] showed that the gauge symmetry in (2.1.3)–(2.1.4) could be generalized to symmetry transformations that mix components of different spinors and vectors fields. In the case of electromagnetism, the gauge transformation at each space-time point constitutes a transformation in the Lie group $U(1)$, which can be defined as the group of complex numbers with unit modulus. We obtain the Yang-Mills generalization by constructing a Lagrangian with $N > 1$ Dirac spinor fields that are invariant under local $SU(N)$ transformations, where $SU(N)$ is the group of N -dimensional unitary matrices with unit determinant.² As is shown in standard texts on QFT [11, 26, 28], the resulting Lagrangian is

The Yang-Mills Lagrangian

$$\mathcal{L} = -\frac{1}{4}F^{a\mu\nu}F_{\mu\nu}^a + \bar{\psi}(i\gamma^\mu D_\mu - m)\psi. \quad (2.1.5)$$

Here ψ is an N -plet of Dirac spinors, γ^μ the gamma matrices, $\bar{\psi} = \psi^\dagger\gamma^0$ the N -plet of Dirac conjugate spinors, A_μ^a the a -th gauge field, m the fermion mass and D_μ the gauge covariant derivative,

$$D_\mu = \partial_\mu - igA_\mu^a T^a. \quad (2.1.6)$$

The matrices T^a are the generators of $SU(N)$ in the fundamental representation and act on the N -plet of spinors, where a runs from 1 to $N^2 - 1$.³ The quantity g is a real coupling constant and $F_{\mu\nu}^a$ are the field strength tensors,

$$F_{\mu\nu}^a = (\partial_\mu A_\nu^a - \partial_\nu A_\mu^a) + gf^{bca}A_\mu^b A_\nu^c. \quad (2.1.7)$$

The numbers f^{abc} are the structure constants of the Lie algebra of $SU(N)$, which we refer to as $\mathfrak{su}(N)$, and are defined by the relation⁴

$$[T^a, T^b] = if^{abc}T^c. \quad (2.1.8)$$

From (2.1.5) and (2.1.7) we see that $SU(N)$ Yang-Mills theory consists of $N^2 - 1$ massless spin-1 fields. Furthermore, from (2.1.7) it is clear that they interact among themselves if $f^{abc} \neq 0$, which is the case for all $N > 1$.⁵

¹The Poincaré group is the group of space-time translations, spatial rotations, and Lorentz boosts.

²Other gauge groups than $SU(N)$ are also possible.

³The fundamental representation in the case of $SU(N)$ means a representation with N -dimensional matrices.

⁴The Lie algebra is the vector space spanned by $\{T^a\}$ that is equipped with the bilinear commutator map.

⁵ $N = 1$ just gives the trivial group and is not considered.

It is convenient to define the $N \times N$ matrix field

$$\mathbf{A}_\mu = A_\mu^a T^a. \quad (2.1.9)$$

Note that \mathbf{A}_μ is in the Lie algebra of $SU(N)$ since A_μ^a is a real field. In this notation we can write a general gauge transformation $\Omega(x) \in SU(N)$ as

$$\psi(x) \rightarrow \Omega(x)\psi(x), \quad (2.1.10)$$

$$\mathbf{A}_\mu(x) \rightarrow \Omega(x)\mathbf{A}_\mu(x)\Omega^\dagger(x) - \frac{i}{g} [\partial_\mu\Omega(x)]\Omega^\dagger(x). \quad (2.1.11)$$

The Yang-Mills Lagrangian is constructed by looking for the simplest fermionic Lagrangian that is invariant under (2.1.10).⁶ This forces us to introduce the gauge fields, their interactions with the fermions and their gauge transformation properties. Another way to look at it is that for a given gauge group, the Yang-Mills Lagrangian is the simplest Lorentz-invariant Lagrangian that contains massless spin-1 particles that interact with fermions.

We note that since two general transformations in $SU(N)$ do not commute, Yang-Mills theory is also known as non-Abelian gauge theory. For a discussion of non-Abelian gauge theory and derivations of the results in this section, the reader is referred to Refs. [11, 26, 28].

2.2 Quantum Chromodynamics

If we include N_f different N_c -plets of Dirac spinors in the Yang-Mills Lagrangian, each representing a different quark flavor with a separate mass m_j , we get:

$$\mathcal{L} = -\frac{1}{4}F^{\alpha\mu\nu}F_{\mu\nu}^a + \sum_{j=1}^{N_f} \bar{\psi}_j(i\gamma^\mu D_\mu - m_j)\psi_j. \quad (2.2.1)$$

If we choose $N_c = 3$ and $N_f = 6$, we get the QCD Lagrangian.⁷ We use the symbol N_c since this value determines the number of different quark colors. With the appropriate values for the six quark masses and the coupling g , (2.2.1) describes the strong force.

Upon renormalizing the QCD Lagrangian and calculating the running coupling, we find that the strong force analogue to the fine structure constant at the one-loop level is [11, 26]

$$\alpha(\Lambda) \equiv \frac{g(\Lambda)^2}{4\pi} = \frac{2\pi}{b_0} \frac{1}{\ln\left(\frac{\Lambda}{\Lambda_{\text{QCD}}}\right)}, \quad (2.2.2)$$

where Λ is the momentum scale at which the coupling is evaluated, Λ_{QCD} a dimensionful energy scale characteristic of QCD and

$$b_0 = 11 - \frac{2}{3}N_f. \quad (2.2.3)$$

⁶Technically the Lagrangian without the gauge field kinetic terms is also gauge-invariant, but this is not interesting since the gauge fields then have no dynamics.

⁷ $N_f = 6$ is because six quark flavors are observed in nature.

For $N_f = 6$, where $b_0 > 0$, the coupling becomes weaker at higher energies. This is the phenomenon of asymptotic freedom. As $\Lambda \rightarrow \Lambda_{\text{QCD}}$ from above we have that $g \rightarrow \infty$. Thus, QCD becomes strongly coupled and perturbation theory breaks down at low energies. The value of Λ_{QCD} quoted in the literature varies due to different approximation schemes used for calculating $\alpha(\Lambda)$, but it is typically of the order $\Lambda_{\text{QCD}} \sim 100 \text{ MeV}$ to 200 MeV [11, 26]. As a consequence, QCD perturbation theory becomes valid only at energies higher than $\sim 1 \text{ GeV}$.

As described in Chapter 1, confinement is a characteristic property of QCD. It refers to the fact that quarks are only observed in composite states that are $SU(3)$ color singlets.⁸ It has never been proven rigorously that confinement takes place in QCD, and it is not seen in perturbation theory. However, its existence is strongly supported by lattice QCD simulations [29, 30]. The strong coupling of QCD at low energies likely gives rise to the confinement of color charge as a non-perturbative effect.

2.3 Heavy Quark Dynamics

To discuss confinement, we will as an intermediate step look at the simplified case of QCD with a single heavy quark flavor. In the following, we use the same approach as Lowell and Weisberger [23] to construct the non-relativistic limit of the fermion sector of the QCD Lagrangian.

Take the quark mass m to be much larger than any other energy scale in the problem, informally written as $m \rightarrow \infty$. This is an assumption on the dynamics of the problem and means that we are working in the extreme non-relativistic limit. We remind that the quark sector of the QCD Lagrangian reads

$$\mathcal{L}_q = \bar{\psi}(i\gamma^\mu D_\mu - m)\psi. \quad (2.3.1)$$

Define the operator

$$U = \exp\left(-\frac{i}{2m}\gamma^j D_j\right), \quad (2.3.2)$$

where the latin indices only sum over spatial components. Define also the spinor Ψ via⁹

$$\psi = U\Psi. \quad (2.3.3)$$

The argument of the exponential is skew-Hermitian,

$$\begin{aligned} (i\gamma^j D_j)^\dagger &= (\partial_j - igA_j^a T^a)^\dagger (\gamma^j)^\dagger (-i) \\ &= (-i)(-\partial_j + igA_j^a T^a)(-\gamma^j) \\ &= -i\gamma^j D_j, \end{aligned} \quad (2.3.4)$$

⁸Meaning they are invariant under $SU(3)$.

⁹For this to uniquely define Ψ we must have that U is invertible, which is the case for a matrix exponential.

and we get

$$U^\dagger = \exp\left(\left[-\frac{i}{2m}\gamma^j D_j\right]^\dagger\right) = \exp\left(\frac{i}{2m}\gamma^j D_j\right) = U^{-1}, \quad (2.3.5)$$

meaning that U is unitary. We used the fact that T^a and γ^j commute since they act on different objects, that $(\partial_i)^\dagger = -\partial_i$, that A_j^a is a real quantum field, that $(\gamma^j)^\dagger = -\gamma^j$, and that T^a is Hermitian. The generators of $SU(N)$ are always Hermitian, since for a general infinitesimal $SU(N)$ -transformation Ω we can write

$$1 = \Omega^\dagger \Omega = e^{i\alpha^a T^{a\dagger}} e^{-i\alpha^b T^b} = 1 + i\alpha^a (T^a - T^{a\dagger}) + \mathcal{O}(\alpha^2), \quad (2.3.6)$$

for arbitrary infinitesimal parameters $\{\alpha^a\}$.

Since U is unitary, we can treat Ψ as the new fundamental field. Substituting (2.3.3) into (2.3.1) and expanding in m^{-1} , we find

$$\begin{aligned} \mathcal{L}_q &= \Psi^\dagger U^\dagger \gamma^0 (i\gamma^0 D_0 - i\gamma^i D_i - m) U \Psi \\ &= \Psi^\dagger \left(1 + \frac{i}{2m}\gamma^j D_j + \dots\right) \gamma^0 (i\gamma^0 D_0 - i\gamma^i D_i - m) \left(1 - \frac{i}{2m}\gamma^j D_j + \dots\right) \Psi \\ &= \Psi^\dagger (-\gamma^0 m + iD_0) \Psi + \mathcal{O}(m^{-1}) \\ &= \Psi^\dagger (-\gamma^0 m + i\partial_t + gA_0^a T^a) \Psi + \mathcal{O}(m^{-1}), \end{aligned} \quad (2.3.7)$$

where we used $\{\gamma^j, \gamma^0\} = 0$, where $\{\cdot, \cdot\}$ is the anti-commutator. This transformation is a special case of what is known as a Foldy-Wouthuysen transformation [31]. It shows that in the $m \rightarrow \infty$ limit, only the temporal component of the gauge fields govern the quark dynamics.¹⁰ If we kept terms to order m^{-1} and derived the equations of motion, we would get the QCD analogue of the Pauli equation.

Let us consider the Dirac representation of the gamma matrices, where

$$\gamma^0 = \text{diag}(1, 1, -1, -1). \quad (2.3.8)$$

Define

$$\Psi = \begin{pmatrix} q \\ \tilde{q}^\dagger \end{pmatrix}, \quad (2.3.9)$$

where q and \tilde{q}^\dagger are column N_c -plets with the upper and lower two spinor components of the spinors in Ψ , respectively. Inserting (2.3.8) and (2.3.9) into (2.3.7), we find

$$\mathcal{L}_q = q^\dagger (-m + i\partial_t + gA_0^a T^a) q + \tilde{q} (m + i\partial_t + gA_0^a T^a) \tilde{q}^\dagger + \mathcal{O}(m^{-1}). \quad (2.3.10)$$

In the Dirac representation the upper and lower two components of the Dirac spinors can be interpreted as particle and antiparticle [32], and we thus see that the quark and antiquark degrees of freedom decouple in the $m \rightarrow \infty$ limit, which is what we expect for a non-relativistic theory. To get the Lagrangian on the final form, we use that

$$\tilde{q} T^a \tilde{q}^\dagger = \tilde{q}_i T_{ij}^a \tilde{q}_j^\dagger = -\tilde{q}_j^\dagger T_{ij}^a \tilde{q}_i = -\tilde{q}^\dagger (T^a)^T \tilde{q} = (\tilde{q}^\dagger)^T \tilde{T}^a \tilde{q}^T, \quad (2.3.11)$$

¹⁰We avoid the gauge where $A_0^a = 0$, which would require us to include higher order contributions in m^{-1} in (2.3.7).

where we defined

$$\tilde{T}^a = -(T^a)^T \quad (2.3.12)$$

and used that the spinor components are Grassmann numbers and thus anticommute.¹¹ Furthermore, we use that a partial integration gives an equivalent Lagrangian:

$$\tilde{q}\partial_t\tilde{q}^\dagger \simeq -(\partial_t\tilde{q})\tilde{q}^\dagger = (\tilde{q}^\dagger)^T\partial_t\tilde{q}^T. \quad (2.3.13)$$

Redefining \tilde{q}^\dagger to be a row object, i.e. $(\tilde{q}^\dagger)^T \rightarrow \tilde{q}^\dagger$ and $\tilde{q}^T \rightarrow \tilde{q}$, and inserting (2.3.11) and (2.3.13) into (2.3.10), the Lagrangian becomes

$$\begin{aligned} \mathcal{L}_q &= q^\dagger(-m + i\partial_t + gA_0^a T^a)q + \tilde{q}^\dagger(-m + i\partial_t + gA_0^a \tilde{T}^a)\tilde{q} + \mathcal{O}(m^{-1}) \\ &= q^\dagger Dq + \tilde{q}^\dagger \tilde{D}\tilde{q} + \mathcal{O}(m^{-1}), \end{aligned} \quad (2.3.14)$$

where we have defined the operators

$$D = -m + i\partial_t + gA_0^a T^a, \quad (2.3.15)$$

$$\tilde{D} = -m + i\partial_t + gA_0^a \tilde{T}^a, \quad (2.3.16)$$

for later convenience.

Finally, we have that the Hamiltonian density is given by

$$\mathcal{H}_q = iq^\dagger\partial_t q + i\tilde{q}^\dagger\partial_t\tilde{q} - \mathcal{L}_q = q^\dagger(m - gA_0^a T^a)q + \tilde{q}^\dagger(m - gA_0^a \tilde{T}^a)\tilde{q}, \quad (2.3.17)$$

where we used that the conjugate momenta are $\pi_q = iq^\dagger$, $\pi_{\tilde{q}} = i\tilde{q}^\dagger$, $\pi_{q^\dagger} = \pi_{\tilde{q}^\dagger} = 0$. The static quark Hamiltonian thus is

$$H_q = \int d^3x \mathcal{H}_q. \quad (2.3.18)$$

2.4 The Polyakov Loop and Deconfinement

We will now consider a thermal system of gluons and study the effect of adding a single heavy quark. By adding a heavy quark, we probe the gluon dynamics in the presence of a static color test charge. Combining aspects of the derivations of Lowell and Weisberger [23], and McLerran and Svetitsky [22], we show that the “free energy” cost of adding this test charge is related to the expectation value of the Polyakov loop operator and that the expectation value of the Polyakov loop acts as an order parameter for confinement.¹² The free energy appears in quotation marks since it is not entirely clear that what in the literature is referred to as a free energy actually is a free energy, as we will discuss in the following.

A theory with only gluons, which we refer to as pure gauge theory, is described by

$$\mathcal{L}_A = -\frac{1}{4}F^{a\mu\nu}F_{\mu\nu}^a. \quad (2.4.1)$$

¹¹We suppressed the Dirac spinor indices which are not relevant to the calculation.

¹²The Polyakov loop was first studied by Polyakov [33] and Susskind [34] using lattice methods.

Let $H_A(A)$ be the Hamiltonian corresponding to this Lagrangian density. The partition function Z and free energy F of a thermal system of gluons in the canonical ensemble at inverse temperature β is given by

$$Z = e^{-\beta F} = \widetilde{\sum}_A \langle A | e^{-\beta H_A(A)} | A \rangle = \text{Tr} \left(e^{-\beta H_A(A)} P \right). \quad (2.4.2)$$

Here $\widetilde{\sum}_A$ is a Hilbert-space sum over gauge-inequivalent physical states $|A\rangle$ which can alternatively be written as a trace if one includes an operator P that projects out only physical states.¹³ Carrying out this sum is complicated by the gauge redundancy, but we will not deal with it explicitly and refer the reader to Ref. [35] for details. When the sum is explicitly written out as a path integral, the integral only runs over field configurations that are β -periodic in imaginary time τ ,

$$A_\mu(\mathbf{x}, -i\tau) = A_\mu(\mathbf{x}, -i\tau - i\beta). \quad (2.4.3)$$

That the partition function for bosons is obtained by summing over periodic field configurations in imaginary time is an elementary result from thermal quantum field theory [36, 37]. It follows from the commutation relations of the fields and the fact that the initial and final states of the matrix elements in (2.4.2) are the same.

We proceed to consider states containing both gluons and heavy quarks, i.e. product states

$$|\psi\rangle \otimes |A\rangle, \quad (2.4.4)$$

where the first ket represents the fermion state. It is intuitive to assume that the free energy of a system of gluons with a single heavy quark of color a added at \mathbf{x} is given by

$$\begin{aligned} e^{-\beta F_{q,a}(\mathbf{x})} &= V \widetilde{\sum}_A \langle A | \otimes \langle q_a(\mathbf{x}) | e^{-\beta H} | q_a(\mathbf{x}) \rangle \otimes | A \rangle \\ &= V \widetilde{\sum}_A \langle A | \otimes \langle 0 | q_a(\mathbf{x}, 0) e^{-\beta H} q_a^\dagger(\mathbf{x}, 0) | 0 \rangle \otimes | A \rangle, \end{aligned} \quad (2.4.5)$$

where there is no sum over a and $H = H_A(A) + H_q(A, q, \tilde{q})$. That is, we sum over all gluonic states that contain a single quark of color a at \mathbf{x} . The volume factor is needed for dimensional reasons, since we have the normalization $[qq^\dagger] = [x]^{-3}$. Averaging over colors, we have the average quark free energy

$$e^{-\beta F_q(\mathbf{x})} = V \sum_a \frac{1}{N_c} \widetilde{\sum}_A \langle A | \otimes \langle 0 | q_a(\mathbf{x}, 0) e^{-\beta H} q_a^\dagger(\mathbf{x}, 0) | 0 \rangle \otimes | A \rangle. \quad (2.4.6)$$

This is the starting assumption of McLerran and Svetitsky's original paper [22]. Most authors in the literature claim that F_q is a free energy, but it is not entirely obvious that this is the case. The definition of the partition function of a system, and thus its free energy, crucially depends on the fact that we sum over all physical states. By inserting the creation operators by hand we assume that the trace over quark space reduces to

¹³The sum $\widetilde{\sum}_A \langle A | \cdot | A \rangle$ is not a trace, since it is not a sum over a complete set, but rather a sum over the subspace of states that are physical. See Ref. [35] for how to construct P .

a single term and that the projection operator P is unchanged.¹⁴ Furthermore, the fact that we sum over different colors means that we take the average of the partition functions of different physical systems. It is indeed argued by Dumitru, Pisarski and Zschieche in Ref. [38] that $F_q(\mathbf{x})$ is not a free energy, since it does not have the correct monotonicity properties required of a true free energy. Instead, it is just the thermal expectation value of the propagator of a heavy test quark, and this does not necessarily satisfy all the properties that a free energy does.

Whether or not F_q is a free energy, let us show how it is related to the quark propagator. We manipulate (2.4.6) to find

$$\begin{aligned}
e^{-\beta F_q(\mathbf{x})} &= V \sum_a \frac{1}{N_c} \widetilde{\sum}_A \langle A | \otimes \langle 0 | q_a(\mathbf{x}, 0) e^{-\beta H} q_a^\dagger(\mathbf{x}, 0) e^{\beta H} e^{-\beta H} | 0 \rangle \otimes | A \rangle \\
&= V \sum_a \frac{1}{N_c} \widetilde{\sum}_A \langle A | \otimes \langle 0 | q_a(\mathbf{x}, 0) \left(e^{\beta H_q} q_a(\mathbf{x}, 0) e^{-\beta H_q} \right)^\dagger | 0 \rangle \otimes e^{-\beta H_A(A)} | A \rangle \\
&= V \sum_a \frac{1}{N_c} \widetilde{\sum}_A \langle A | \left[\langle 0 | q_a(\mathbf{x}, 0) q_a^\dagger(\mathbf{x}, -i\beta) | 0 \rangle \right] e^{-\beta H_A(A)} | A \rangle \\
&= V \sum_a \frac{1}{N_c} \widetilde{\sum}_A \langle A | \langle q_a(\mathbf{x}, 0) | q_a(\mathbf{x}, -i\beta) \rangle e^{-\beta H_A(A)} | A \rangle.
\end{aligned} \tag{2.4.7}$$

In the first line we used $1 = e^{\beta H} e^{-\beta H}$. In the second line we used that

$$H_q(q, \tilde{q}, A) | 0 \rangle \otimes | A \rangle = 0, \tag{2.4.8}$$

in addition to

$$H_A(A) [| 0 \rangle \otimes | A \rangle] = | 0 \rangle \otimes H_A(A) | A \rangle, \tag{2.4.9}$$

and

$$e^{\beta H} q_a e^{-\beta H} = e^{\beta H_q} q_a e^{-\beta H_q}. \tag{2.4.10}$$

The latter holds true since $[H_A, q_a] = [H_A, H_q] = 0$, where the second commutator is correct because H_q contains only A_μ^a for $\mu = 0$, and $[A_0^a T^a, H_A(A)] = 0$ since the canonical momentum of A_0^a vanishes.¹⁵ In the third line we analytically continued the formula

$$e^{iHt'} O(t) e^{-iHt'} = O(t + t') \tag{2.4.11}$$

to imaginary times.

To proceed we must evaluate $\langle q_a(\mathbf{x}, 0) | q_a(\mathbf{x}, -i\beta) \rangle$. We see that it is the zero temperature Green's function for a quark state evolving under H_q ,

$$[G(\mathbf{x}, t; \mathbf{x}, 0)]_{aa} = \langle q_a(\mathbf{x}, 0) | e^{-iH_q t} | q_a(\mathbf{x}, 0) \rangle, \tag{2.4.12}$$

analytically continued to imaginary time $t = -i\tau$ with $\tau = \beta$. Furthermore, we note that the gauge field contained in H_q is a classical field and not a quantum field, since A_0^a

¹⁴Saying that the quark trace reduces to one term corresponds to saying there are no quark fluctuations, which seems reasonable in the $m \rightarrow \infty$ limit.

¹⁵ H_A contains no T^a matrices, only products of the gauge fields and their derivatives. But $\pi_{A_0}^a = \frac{\partial \mathcal{L}}{\partial(\partial_0 A_0^a)} = 0$, which is the only potential term in H_A which would not commute with the A_0^a in H_q .

commutes with q , \tilde{q} and $H_A(A)$, and thus the A_0^a in H_q can always act either to the left or the right on an A -eigenstate. Since \mathcal{L}_q is quadratic in the quark fields, the propagator is in practice given by a free quantum field theory. It is known that the propagator for a quadratic Lagrangian $\mathcal{L} = q^\dagger Dq$ is the solution to the equation [26, 28]

$$DG(\mathbf{x}, t; \mathbf{x}', 0) = i\delta(\mathbf{x} - \mathbf{x}')\delta(t). \quad (2.4.13)$$

With D as defined in (2.3.15), we find

$$[i\partial_t + gA_0^a(\mathbf{x}, t)T^a - m]G(\mathbf{x}, t; \mathbf{x}', 0) = i\delta(\mathbf{x} - \mathbf{x}')\delta(t). \quad (2.4.14)$$

When the delta functions are zero this is just the Schrödinger equation, which for a time-dependent Hamiltonian $H(t)$ has the well-known solution

$$\mathbb{T} e^{-i\int_0^t dt' H(t')} = e^{-imt} \mathbb{T} e^{ig\int_0^t dt' A_0^a(\mathbf{x}, t')T^a}, \quad (2.4.15)$$

where \mathbb{T} is the time ordering operator. With the delta functions included we see by direct insertion that a solution is given by

$$G(\mathbf{x}, t; \mathbf{x}', 0) = \theta(t)\delta(\mathbf{x} - \mathbf{x}')e^{-imt} \mathbb{T} e^{ig\int_0^t dt' A_0^a(t')T^a}, \quad (2.4.16)$$

where $\theta(t)$ is the Heaviside step function. This is the retarded propagator, which we choose since we work in the non-relativistic limit. In analytically continuing this formula to imaginary times, we will have that that $G(-i\tau, \mathbf{x}; \mathbf{x}', 0) = 0$ for imaginary times $\tau < 0$. This is because we should analytically continue to imaginary time before carrying out the path integral to get an analogue of (2.4.14) in imaginary time. Since time and space are treated equally in this case, and space appears as $\delta(\mathbf{x} - \mathbf{x}')$, time will appear as $\delta(\tau)$. Thus, we find

$$\begin{aligned} G(\mathbf{x}, -i\beta; \mathbf{x}', 0) &= \theta(\beta)\delta(\mathbf{x} - \mathbf{x}')e^{-\beta m} \mathbb{T}_\tau e^{ig\int_0^{-i\beta} dt' A_0^a(\mathbf{x}, t')T^a}, \\ &= \delta(\mathbf{x} - \mathbf{x}')e^{-\beta m} \mathbb{T}_\tau e^{g\int_0^\beta d\tau A_0^a(\mathbf{x}, -i\tau)T^a}, \end{aligned} \quad (2.4.17)$$

where we used that $\beta > 0$ and defined the imaginary time ordering operator \mathbb{T}_τ . We now define the Polyakov loop to be

The Polyakov Loop

$$L(\mathbf{x}) = \mathbb{T}_\tau \exp \left[ig \int_0^\beta d\tau A_4^a(\mathbf{x}, \tau)T^a \right], \quad (2.4.18)$$

where we have introduced the Euclidean gauge field A_4^a

$$A_4^a(\mathbf{x}, \tau) = -iA_0^a(\mathbf{x}, -i\tau). \quad (2.4.19)$$

Hence, we find

$$\langle q_a(\mathbf{x}, 0) | q_a(\mathbf{x}, -i\beta) \rangle = [G(\mathbf{x}, -i\beta; \mathbf{x}, 0)]_{aa} = V^{-1} e^{-\beta m} [L(\mathbf{x})]_{aa}, \quad (2.4.20)$$

where we used that $\delta(\mathbf{x} = 0) = V^{-1}$ in a finite volume. Inserting (2.4.20) into (2.4.7), we find

$$\begin{aligned} e^{-\beta[F_q(\mathbf{x})-m]} &= \sum_a \frac{1}{N_c} \widetilde{\sum}_A \langle A | [L(\mathbf{x})]_{aa} e^{-\beta H_A(A)} | A \rangle \\ &= \frac{1}{N_c} \widetilde{\sum}_A \langle A | e^{-\beta H_A(A)} \text{tr}_c L(\mathbf{x}) | A \rangle, \end{aligned} \quad (2.4.21)$$

where tr_c is the matrix trace in color space. We did not assume any cyclic property of the sum over $|A\rangle$, since this does not hold as the sum is not over a complete set, i.e. it is not a trace. Rather, L contains a classical field and can be moved past $e^{-\beta H_A(A)}$. Dividing (2.4.21) by the partition function of the pure gluon system, $Z = e^{-\beta F}$, we find

$$e^{-\beta \Delta F_q(\mathbf{x})} = \frac{1}{N_c} \langle \text{tr}_c L(\mathbf{x}) \rangle, \quad (2.4.22)$$

where $\langle \cdot \rangle$ is the thermal expectation value, defined for an operator O as

$$\langle O \rangle = \frac{1}{Z} \text{Tr} \left(e^{-\beta H} O \right), \quad (2.4.23)$$

and $\Delta F_q(\mathbf{x}) = F_q(\mathbf{x}) - F - m$. If it is correct that F_q is a free energy, then ΔF would be interpreted as is the average change in free energy not coming from the rest mass upon adding a quark to the system.

Defining the traced Polyakov loop operator

$$\Phi(\mathbf{x}) = \frac{1}{N_c} \text{tr}_c L(\mathbf{x}), \quad (2.4.24)$$

which we will also refer to as just the Polyakov loop, we find

$$e^{-\beta \Delta F_q(\mathbf{x})} = \langle \Phi(\mathbf{x}) \rangle. \quad (2.4.25)$$

If we accept that F_q represents the average energy cost of adding a single quark to the gluonic system, we draw the conclusion that

The Polyakov Loop as an Order Parameter

$$\begin{aligned} \langle \Phi \rangle = 0 &\Rightarrow \Delta F_q = \infty \Rightarrow \text{Free quarks cannot exist.} \\ \langle \Phi \rangle > 0 &\Rightarrow \Delta F_q < \infty \Rightarrow \text{Free quarks can exist.} \end{aligned} \quad (2.4.26)$$

Alternatively, we can instead use (2.4.20) to say that

The Polyakov Loop as an Order Parameter

$$\begin{aligned} \langle \Phi \rangle = 0 &\Rightarrow \text{The expected color-averaged quark propagator vanishes.} \\ &\Rightarrow \text{Single propagating quarks does not exist (on average).} \end{aligned}$$

Hence, it is natural to interpret $\langle \Phi \rangle = 0$ as a criterion for confinement, and in a pure gauge theory we should have $\langle \Phi \rangle = 0$ for a confined phase and $\langle \Phi \rangle > 0$ for a deconfined phase.¹⁶

The derivation above is readily generalized to n_q quarks and $n_{\bar{q}}$ antiquarks by inserting the relevant creation and annihilation operators for each quark and antiquark in (2.4.7). The result is

$$\exp[-\beta\Delta F(\mathbf{x}_1, \dots, \mathbf{x}_{n_q}, \mathbf{y}_1, \dots, \mathbf{y}_{n_{\bar{q}}})] = \langle \Phi(\mathbf{x}_1) \dots \Phi(\mathbf{x}_{n_q}) \bar{\Phi}(\mathbf{y}_1) \dots \bar{\Phi}(\mathbf{y}_{n_{\bar{q}}}) \rangle, \quad (2.4.27)$$

where ΔF is the change in “free energy” upon addition of quarks at $\mathbf{x}_1, \dots, \mathbf{x}_{n_q}$ and antiquarks at $\mathbf{y}_1, \dots, \mathbf{y}_{n_{\bar{q}}}$ in a pure gluon system. The quantities $\bar{\Phi}$ for antiquarks appear since we must replace $T^a \rightarrow \tilde{T}^a$ in the Polyakov loop. This gives

$$\begin{aligned} \bar{\Phi}(\mathbf{x}) &\equiv \frac{1}{N_c} \text{tr}_c \mathbf{T}_\tau e^{ig \int_0^\beta d\tau A_4^a(\mathbf{x}, \tau) \tilde{T}^a} \\ &= \frac{1}{N_c} \text{tr}_c \mathbf{T}_\tau e^{-ig \int_0^\beta d\tau A_4^a(\mathbf{x}, \tau) (T^a)^T} \\ &= \frac{1}{N_c} \text{tr}_c \left(\mathbf{T}_\tau e^{ig \int_0^\beta d\tau A_4^a(\mathbf{x}, \tau) (T^a)^\dagger} \right)^* \\ &= \frac{1}{N_c} \text{tr}_c \left(\mathbf{T}_\tau e^{ig \int_0^\beta d\tau A_4^a(\mathbf{x}, \tau) T^a} \right)^* \\ &= \frac{1}{N_c} \text{tr}_c \left(\mathbf{T}_\tau e^{ig \int_0^\beta d\tau A_4^a(\mathbf{x}, \tau) T^a} \right)^\dagger \\ &= \frac{1}{N_c} \text{tr}_c L^\dagger(\mathbf{x}), \end{aligned} \quad (2.4.28)$$

where we assumed that A_4^a is real and that T^a is Hermitian. Furthermore, we used that the matrix trace is invariant under transposition.

Assuming that A_4^a is real requires a comment. From the definition $iA_4^a(\tau) = A_0^a(-i\tau)$ and the knowledge that $A_0(t)$ is a real field, it would be natural to assume that A_4^a is imaginary. However, it is not clear that A_0 should stay real when analytically continued to imaginary times. It turns out that when converting (2.4.2) to a path integral in a way such that only gauge-inequivalent and gauge-invariant states are counted, one can initially set $A_0^a = 0$ as a gauge choice. However, in the process of implementing the sum over only gauge invariant states in the path integral, auxiliary real fields A_4^a are introduced. It turns out that these fields occur in the Lagrangian exactly where $-iA_0^a$ occurred in the original Lagrangian. Thus, we can directly replace $A_0^a \rightarrow iA_4^a$, as long as we remember that A_4^a is real. For a discussion of the Euclidean gauge field and its properties, the reader is referred to Ref. [39].

¹⁶Note that we have only shown that Φ is an order parameter for heavy quark confinement. We have not shown any relation between gluon confinement and Φ , even though it might exist.

If we want to evaluate the Polyakov loop for an A_4^a that is complex, $\bar{\Phi}$ is given by

$$\begin{aligned}
\bar{\Phi}(\mathbf{x}) &= \frac{1}{N_c} \text{tr}_c \mathbb{T}_\tau e^{-ig \int_0^\beta d\tau A_4^a(\mathbf{x}, \tau)(T^a)^T} \\
&= \frac{1}{N_c} \text{tr}_c \left(\bar{\mathbb{T}}_\tau e^{-ig \int_0^\beta d\tau A_4^a(\mathbf{x}, \tau)(T^a)} \right)^T \\
&= \frac{1}{N_c} \text{tr}_c \bar{\mathbb{T}}_\tau e^{-ig \int_0^\beta d\tau A_4^a(\mathbf{x}, \tau)(T^a)} \\
&= \frac{1}{N_c} \text{tr}_c \bar{L}(\mathbf{x}), \tag{2.4.29}
\end{aligned}$$

where $\bar{\mathbb{T}}_\tau$ is anti-time ordering, which orders terms in the opposite order from the time ordering operation. We must change to anti-time ordering upon pulling the time ordering inside the transposition operation since transposition reverses the order of a product of matrices. In the last line we defined the conjugate Polyakov loop \bar{L} , which is a term we will also use to refer to $\bar{\Phi}$. Why we would want to consider a complex gauge field is at first sight puzzling. It is related to the case of $\mu \neq 0$, where the Euclidean action becomes complex. We will postpone the discussion of this until Sec. 3.5.

2.5 Dual Systems

Since confinement happens at low temperatures, we should have that $\langle \Phi \rangle = 0$ at low T and $\langle \Phi \rangle \neq 0$ at high T . In other words, the system is disordered at low temperatures and ordered at high temperatures. This behavior is opposite to typical order parameters such as magnetization in an Ising system and is at first sight puzzling. However, one can gain insight into this behavior by studying so-called dual systems. It turns out, as first discovered by Kramers and Wannier [40, 41], that if we write high-temperature and low-temperature series expansions of the partition function of a 2D Ising model on a square lattice, there is a special one-to-one correspondence between the terms in the two series. With a modification of the coupling, one can transform the low-temperature expansion of the 2D Ising model into the high-temperature expansion, and vice versa. More precisely, this means that the series expansions of the free energy at low and high temperatures, F_L and F_H respectively, can be written as

$$F_L(\beta, J) = l(K) + s(K), \tag{2.5.1}$$

$$F_H(\beta, J) = h(\tilde{K}) + s(\tilde{K}), \tag{2.5.2}$$

where $s(x)$ is an infinite series in x , $h(x)$ and $l(x)$ some finite series in x , and K and \tilde{K} two functions of βJ , where J is the coupling between two neighbouring spins. The significance of these equations lies in the fact that the same series expansion $s(x)$ occurs in both expressions, only evaluated at different arguments. Since both series give the exact free energy when they are not truncated, we can write

$$F_L(\beta, J) = F_H(\beta, J) = h(\tilde{K}(K)) + s(\tilde{K}(K)). \tag{2.5.3}$$

Thus, with the appropriate modification of the temperature, realized as $K \rightarrow \tilde{K}$, the low-temperature Ising model can be described by an Ising model at high temperature. Since the mapping $K \leftrightarrow \tilde{K}$ interchanges low and high temperatures, we have that the dual description of the Ising model has net magnetization at high temperatures. This is exactly how the Polyakov loop expectation value is shown to behave at the qualitative level.

While most systems are not self-dual, we can sometimes find two different systems such that the low-temperature description of one system is dual to the high-temperature description of the other. Interestingly, the 3D Ising model on a square lattice is dual to a lattice \mathbb{Z}_2 gauge theory on the same lattice [42], indicating the possibility of $SU(N)$ gauge theory being dual to some Ising-like system which is ordered at low temperatures. Feeding this idea is Svetitsky and Yaffe's conjecture [43], which is obtained using universality arguments, that a $(d+1)$ dimensional gauge theory has the same critical behavior as a d -dimensional spin model with the same global symmetry.

Finally, we mention, as pointed out in Ref. [44], that in the strong coupling limit an $SU(N)$ gauge theory at temperature T can be approximately described as an XY -model at temperature $\sim T^{-1}$, where $\langle \Phi \rangle$ corresponds to the order parameter for magnetization in the latter model.¹⁷ With the knowledge of dual systems in mind, the behavior of the Polyakov loop is less perplexing.

2.6 Center Symmetry and its Spontaneous Breaking

In the study of phase transitions one finds that when an order parameter becomes non-zero, it is associated with the spontaneous breaking of some symmetry. As was first shown by t'Hooft [45], and as will be described in the following, this is also the case in the deconfined phase.

We pointed out in Sec. 2.1 that the gauge transformation of the gluon field takes the form

$$\mathbf{A}_\mu(x) \rightarrow \Omega(x)\mathbf{A}_\mu(x)\Omega^\dagger(x) - \frac{i}{g} [\partial_\mu\Omega(x)]\Omega^\dagger(x) \quad (2.6.1)$$

for any $\Omega(x) \in SU(N_c)$. This transformation leaves the gluonic Lagrangian (2.4.1) invariant and is thus a symmetry of the action of pure gauge theory. However, for a generic $\Omega(x)$ this transformation ruins the periodicity in imaginary time, as required for the field configurations summed over in the partition function. Let us rename the gauge fields $A_\mu^a(\mathbf{x}, -i\tau) \rightarrow A_\mu^a(\mathbf{x}, \tau)$, and similarly for the gauge transformations and other time-dependent fields to be introduced. Restricting to transformations that satisfy

$$\Omega(\mathbf{x}, \tau) = \Omega(\mathbf{x}, \tau + \beta) \quad (2.6.2)$$

solves the problem, but it turns out that there is a larger group of symmetries that leaves the action invariant. Assume instead a generic gauge transformation that satisfies

$$\Omega(\mathbf{x}, \tau + \beta) = G(\mathbf{x}, \tau)\Omega(\mathbf{x}, \tau), \quad (2.6.3)$$

¹⁷The XY -model is a generalization of the Ising model, where the direction of the spins can take continuous values in a $2D$ plane.

for some $G(\mathbf{x}, \tau) \in SU(N_c)$. Let \mathbf{A}'_μ be the transformed field:

$$\mathbf{A}'_\mu(\mathbf{x}, \tau) = \Omega(\mathbf{x}, \tau) \mathbf{A}_\mu(\mathbf{x}, \tau) \Omega^\dagger(\mathbf{x}, \tau) - \frac{i}{g} [\partial_\mu \Omega(\mathbf{x}, \tau)] \Omega^\dagger(\mathbf{x}, \tau). \quad (2.6.4)$$

We then get

$$\mathbf{A}'_\mu(\mathbf{x}, \tau + \beta) = G(\mathbf{x}, \tau) \mathbf{A}'_\mu(\mathbf{x}, \tau) G^\dagger(\mathbf{x}, \tau) - \frac{i}{g} [\partial_\mu G(\mathbf{x}, \tau)] G(\mathbf{x}, \tau)^\dagger. \quad (2.6.5)$$

If $G(\mathbf{x}, \tau)$ is constant in space and time and commutes with \mathbf{A}'_μ for all (\mathbf{x}, τ) , then

$$\mathbf{A}'_\mu(\mathbf{x}, \tau + \beta) = \mathbf{A}'_\mu(\mathbf{x}, \tau). \quad (2.6.6)$$

Since \mathbf{A}_μ is a matrix in the fundamental representation of $SU(N_c)$, which is irreducible, G is proportional to the identity matrix by Schur's lemma. Let $G = \lambda I_{N_c}$, where I_{N_c} is the $N_c \times N_c$ identity matrix and $\lambda \in \mathbb{C}$. Since we know that $G \in SU(N_c)$, we must have

$$\det G = \lambda^{N_c} = 1. \quad (2.6.7)$$

Thus, $\lambda = \lambda_n$ is one of the N_c -th roots of unity, and all possible matrices G are given by

$$G_n = \lambda_n I_{N_c} = e^{-2\pi i n / N_c} I_{N_c}, \quad n = 0, \dots, N_c - 1. \quad (2.6.8)$$

Clearly $\{G_n\}$ forms a finite group under matrix multiplication that is isomorphic to \mathbb{Z}_{N_c} . Since $\{G_n\}$ contains all elements that commute with all other elements of $SU(N_c)$, it is the center subgroup of $SU(N_c)$.¹⁸

Before proceeding, a comment about terminology is warranted. Non-periodic transformations of the kind shown in (2.6.3) are perfectly valid gauge transformations as normally defined in Minkowski space. However, if we restrict the term ‘‘gauge transformation’’ to mean transformations that satisfy imaginary time periodicity, as is often done in the literature on thermal field theory, then we might refer to the transformation in (2.6.3) with $G = G_n \neq 1_{N_c}$ as a twisted gauge transformation or a center transformation. In this language, twisted gauge transformations are not a subset of gauge transformations. If we take the view that our fields are defined on a Euclidean space-time, which then corresponds to the space $S^1 \times \mathbb{R}^3$, it appears natural to ask that our gauge transformations are single-valued on that space-time. We will refer to invariance under twisted gauge transformations as center symmetry.

Restricting the definition of gauge transformations is also useful upon the introduction of dynamical fermions. A basic result from thermal QFT in the imaginary time formalism states that for a partition that includes fermions, only fermionic fields satisfying

$$\psi(\mathbf{x}, \tau + \beta) = -\psi(\mathbf{x}, \tau) \quad (2.6.9)$$

¹⁸For any group G , the center group is the subgroup of elements that commute with all elements in G .

are included in the sum over field configurations [36, 37]. However, a fermionic field that changes as $\psi \rightarrow \psi'$ under a twisted gauge transformation satisfies

$$\psi'(\mathbf{x}, \tau + \beta) = \Omega(\mathbf{x}, \tau + \beta)\psi(\mathbf{x}, \tau + \beta) = -\lambda_n \Omega(\mathbf{x}, \tau)\psi(\mathbf{x}, \tau) = -\lambda_n \psi'(\mathbf{x}, \tau), \quad (2.6.10)$$

which does not have the required anti-periodicity for $n \neq 0$.

Under a gauge transformation, the Polyakov loop transforms as

$$L(\mathbf{x}) \rightarrow L'(\mathbf{x}) = \Omega(\mathbf{x}, \beta)L(\mathbf{x})\Omega^\dagger(\mathbf{x}, 0). \quad (2.6.11)$$

This follows from the gauge-transformation properties of the so-called Wilson line, which is a Minkowski space generalization of L . We do not prove this equation and instead refer the reader to the proof in Ref. [11]. We note from (2.6.11) that L is not a gauge invariant quantity, although its trace might be. Since equation (2.6.11) also holds true for a twisted gauge transformation, it gives that the traced Polyakov loop transforms into

$$\Phi'(\mathbf{x}) = \frac{1}{N_c} \text{Tr} \left[\lambda_n \Omega(0, \mathbf{x})L(\mathbf{x})\Omega^\dagger(0, \mathbf{x}) \right] = \lambda_n \frac{1}{N_c} \text{Tr} [L(\mathbf{x})] = \lambda_n \Phi(\mathbf{x}). \quad (2.6.12)$$

Thus, we see that the traced Polyakov loop is gauge invariant ($n = 0$), but not center invariant. This means that

$$\langle \Phi \rangle \rightarrow \lambda_n \langle \Phi \rangle, \quad (2.6.13)$$

under a twisted gauged transformation. However, if center symmetry is a symmetry of the partition function, we conclude that

Center Symmetry and the Polyakov Loop

$\langle \Phi \rangle \neq 0 \Rightarrow$ Center symmetry is spontaneously broken.

Thus, deconfinement in pure gauge theory with static quarks is associated with spontaneous center symmetry breaking.

From (2.4.28) we see that $\bar{\Phi}$ transforms as

$$\bar{\Phi} \rightarrow \lambda_n^* \bar{\Phi} = \lambda_n^{-1} \bar{\Phi} \quad (2.6.14)$$

under a twisted gauge transformation associated with the center element λ_n . Consider the correlator C between n_q quarks located at $\mathbf{x}_1, \dots, \mathbf{x}_{n_q}$ and $n_{\bar{q}}$ antiquarks located at $\mathbf{y}_1, \dots, \mathbf{y}_{n_{\bar{q}}}$:

$$C \equiv \left\langle \Phi(\mathbf{x}_1) \dots \Phi(\mathbf{x}_{n_q}) \bar{\Phi}(\mathbf{y}_1) \dots \bar{\Phi}(\mathbf{y}_{n_{\bar{q}}}) \right\rangle. \quad (2.6.15)$$

Under a center transformation the correlator transforms as

$$C \rightarrow (\lambda_n)^{n_q - n_{\bar{q}}} C. \quad (2.6.16)$$

Assume now that we are in a phase where center symmetry is not broken. Then C should transform into itself under (2.6.16). But this is only possible if either $C = 0$ or if

$$(n_q - n_{\bar{q}}) = 0 \pmod{N_c}, \quad (2.6.17)$$

since λ_n is an N_c -th root of unity. Consequently, in the confined phase $C = 0$ unless the correlator probes a configuration of quarks with integer baryon number, where the baryon number is defined as

$$B = (n_q - n_{\bar{q}})/N_c. \quad (2.6.18)$$

Thus, a configuration with non-integer baryon number will (on thermal average) not propagate. If we accept that ΔF is an energy cost, we have that $e^{-\beta\Delta F} = C = 0$ implies infinite energy cost associated with a quark configuration with non-integer baryon number.

2.7 The Polyakov Gauge

In choosing a gauge for the \mathbf{A}_μ fields, it is convenient to use a gauge which simplifies the Polyakov loop as much as possible. An obvious candidate would be the Weyl gauge where $\mathbf{A}_4 = 0$, in which the Polyakov loop would be trivial. However, quite reassuringly, it turns out that the Weyl gauge is not compatible with the time-periodicity required of the thermal gauge fields [46, 47]. Instead, we can choose a so-called static gauge, where

$$\partial_\tau \mathbf{A}_4 = 0. \quad (2.7.1)$$

That we can choose such a gauge is shown in Ref. [48]. One can furthermore rotate the gauge fields so that \mathbf{A}_4 is in the Cartan subalgebra of $\mathfrak{su}(N_c)$ [44], which is the algebra spanned by the generators of $SU(N_c)$ that commute with each other. Combining these gauge choices gives us the Polyakov gauge, in which \mathbf{A}_4 is diagonal and time independent. We then see that the Polyakov loop takes the simple form

$$L(\mathbf{x}) = e^{ig\beta\mathbf{A}_4(\mathbf{x})} = \text{diag}(e^{ig\beta[\mathbf{A}_4(\mathbf{x})]_{11}}, \dots, e^{ig\beta[\mathbf{A}_4(\mathbf{x})]_{N_c N_c}}), \quad (2.7.2)$$

where square brackets $[\cdot]_{ij}$ mean that we are referring to the (i, j) matrix element. This is a significant simplification, especially since we could drop the time ordering operator which makes the Polyakov loop hard to manipulate in practical calculations.

In the case of $SU(3)$ there are two Cartan generators. We use the most common set of generators for $SU(3)$ in the fundamental representation, which is given by $T^a = \frac{1}{2}\lambda_a$, where λ_a are the Gell-Mann matrices [11, 26]. We can then write

$$\mathbf{A}_4 = \frac{1}{2}(\lambda_3 A_4^3 + \lambda_8 A_4^8), \quad (2.7.3)$$

where λ_3 and λ_8 are the two diagonal Gell-Mann matrices, given by

$$\lambda_3 = \begin{pmatrix} 1 & 0 & 0 \\ 0 & -1 & 0 \\ 0 & 0 & 0 \end{pmatrix}, \quad \lambda_8 = \frac{1}{\sqrt{3}} \begin{pmatrix} 1 & 0 & 0 \\ 0 & 1 & 0 \\ 0 & 0 & -2 \end{pmatrix}. \quad (2.7.4)$$

Defining

$$q = \frac{3}{4\pi}g\beta A_4^3, \quad r = \frac{\sqrt{3}}{4\pi}g\beta A_4^8, \quad (2.7.5)$$

we get

$$g\beta\mathbf{A}_4 = \frac{2\pi}{3} \text{diag}(q+r, -q+r, -2r), \quad (2.7.6)$$

which gives that the Polyakov loop is

$$L(\mathbf{x}) = \begin{pmatrix} e^{i\frac{2\pi}{3}[q(\mathbf{x})+r(\mathbf{x})]} & 0 & 0 \\ 0 & e^{i\frac{2\pi}{3}[-q(\mathbf{x})+r(\mathbf{x})]} & 0 \\ 0 & 0 & e^{i\frac{2\pi}{3}[-2r(\mathbf{x})]} \end{pmatrix}. \quad (2.7.7)$$

From (2.4.29) we see that the conjugate Polyakov loop is given by

$$\bar{L}(\mathbf{x}) = \begin{pmatrix} e^{-i\frac{2\pi}{3}[q(\mathbf{x})+r(\mathbf{x})]} & 0 & 0 \\ 0 & e^{-i\frac{2\pi}{3}[-q(\mathbf{x})+r(\mathbf{x})]} & 0 \\ 0 & 0 & e^{i\frac{2\pi}{3}[2r(\mathbf{x})]} \end{pmatrix}. \quad (2.7.8)$$

If A_4^q is real, then $\bar{L}(\mathbf{x}) = L^\dagger(\mathbf{x})$. Irrespective of whether this is the case, the traced Polyakov loops are

$$\Phi = \frac{e^{2\pi ir/3}}{3} \left[e^{-2\pi ir} + 2 \cos\left(\frac{2\pi q}{3}\right) \right], \quad (2.7.9)$$

$$\bar{\Phi} = \frac{e^{-2\pi ir/3}}{3} \left[e^{2\pi ir} + 2 \cos\left(\frac{2\pi q}{3}\right) \right], \quad (2.7.10)$$

When \mathbf{A}_4 is constant in space, and thus also r and q , we have

$$\Phi = \begin{cases} 0, & q = 1, r = 0 \\ 1, & q = 0, r = 0 \end{cases}, \quad (2.7.11)$$

at the classical level. Recalling (2.4.26) we conclude that a state with $q = 1$, $r = 0$ is a confined state, while a state with $q = 0$, $r = 0$ is a deconfined state. For a quantum state we reach the same conclusion if the given state is a simultaneous eigenstate of r and q with the eigenvalues being the above combinations.

Note that if we in (2.7.9) and (2.7.10) set r to some integer, we get states which only differ by a center transformation, and $|\Phi|$ is identical for any $r \in \mathbb{Z}$. Furthermore, Φ is periodic in q and r , with both having periods of 3. Thus, we can with full generality restrict $q \in [0, 3]$ and $r \in [0, 3]$.

Finally, assuming that \mathbf{A}_4 is spatially constant means that we ignore the possible formation of domains with different ‘‘center phases’’. This is analogous to how we can have domains with opposite magnetizations in an Ising model.

Modeling Quark Confinement

In Chapter 2 it was shown how the Polyakov loop is an exact order parameter for a gauge theory with infinitely heavy quarks. However, in theories with quarks of finite mass, such as QCD, our analysis breaks down, and center symmetry is explicitly broken by fermionic terms. Despite this, lattice studies have shown that the Polyakov loop still is an approximate order parameter for deconfinement [44]. This is analogous to the fact that magnetization in an Ising model is an approximate order parameter upon the introduction of an external magnetic field.

Due to the challenging nature of studying non-Abelian gauge theories, the QCD phase diagram is often instead studied with effective models without gauge fields. Examples of such models include the Nambu-Jona-Lasinio (NJL) model [49, 50] and the linear sigma model [51]. The latter initially described nucleons and mesons but was later reinterpreted to describe mesons and quarks, and it is usually referred to as the quark-meson model. These models do not take confinement into account in their standard form, but in 2004 Fukushima [24] showed how the NJL model could be extended to also have a confining mechanism. This involves including a static temporal background gauge field and a phenomenological potential associated with it. In this chapter we show how the Polyakov loop can be incorporated into a fermionic Lagrangian to model quark confinement.

For a review on effective Polyakov loop modeling, on which this section is partly based, see Ref. [44].

3.1 The Partition Function of Fermions in a Gluonic Background

One of the elementary results of thermal QFT in imaginary time is that the grand canonical partition function of a field ϕ with canonical momentum π is given by the path integral [36, 37]

$$Z = \int_{(\text{A})\text{PBC}} \mathcal{D}\phi \int \mathcal{D}\pi \exp \left\{ \int_0^\beta d\tau \int d^3x [i\pi\partial_\tau\phi - \mathcal{H}(\pi, \phi) + \mu\mathcal{N}(\pi, \phi)] \right\}, \quad (3.1.1)$$

where μ is the chemical potential corresponding to the conserved charge density \mathcal{N} . (A)PBC refers to the fact that in imaginary time, we should only integrate over fields satisfying either periodic and anti-periodic boundary conditions, where the latter must be chosen for fermions. More precisely

$$\phi(\mathbf{x}, \tau + \beta) = \phi(\mathbf{x}, \tau) \quad \text{if } \phi \text{ is bosonic,} \quad (3.1.2)$$

$$\phi(\mathbf{x}, \tau + \beta) = -\phi(\mathbf{x}, \tau) \quad \text{if } \phi \text{ is fermionic.} \quad (3.1.3)$$

Note that Z must be dimensionless, and thus so must $\mathcal{D}\phi\mathcal{D}\pi$. This is achieved by interpreting the path integrals as integrals over the dimensionless Fourier coefficients of the fields.

Consider an N_c -plet of Dirac spinor fields in a background temporal gauge field that is treated classically. The Lagrangian reads

$$\mathcal{L} = \bar{\psi} [i\gamma^\mu(\partial_\mu - ig\delta_{\mu 0}\mathbf{A}_0) - m] \psi, \quad (3.1.4)$$

where we remind that $\mathbf{A}_0 = A_0^a T^a$. We can think of the background gauge field as the mean value of the quantum gauge field $\mathbf{A}_0 = \langle \mathbf{A}_0^{qu} \rangle$. The Lagrangian is clearly symmetric under $\psi \rightarrow e^{-i\alpha} \psi$, which via Noether's theorem leads to the conserved current

$$j^\mu = \bar{\psi} \gamma^\mu \psi. \quad (3.1.5)$$

This gives the conserved charge

$$Q = \int d^3x j^0 = \int d^3x \psi^\dagger \psi, \quad (3.1.6)$$

which is the conservation of quark number (and thus also baryon number). We refer to the chemical potential corresponding to this conserved charge, μ , as the quark chemical potential, and define $\mu_B = 3\mu$ to be the baryon chemical potential.

The conjugate momenta for ψ and ψ^\dagger are $\pi_\psi = i\psi^\dagger$ and $\pi_{\psi^\dagger} = 0$. Deriving the Hamiltonian corresponding to (3.1.4) in the usual way, setting $\mathcal{N} = j^0$ and introducing the Euclidean gauge field, we find that

$$\begin{aligned} \mathcal{H} - \mu\mathcal{N} &= \bar{\psi} \left[i\gamma^i \partial_i - ig\gamma^0 \mathbf{A}_4 + m \right] \psi - \mu \bar{\psi} \gamma^0 \psi \\ &= \bar{\psi} \left[i\gamma^i \partial_i - \gamma^0 (ig\mathbf{A}_4 + \mu) + m \right] \psi. \end{aligned} \quad (3.1.7)$$

Thus, we see that \mathbf{A}_4 plays the role of an imaginary chemical potential. Alternatively, the chemical potential acts as an imaginary gauge field. Combining (3.1.1) and (3.1.7), we have that the partition function is

$$\begin{aligned} Z &= \int_{\text{ABPC}} i\mathcal{D}\psi^\dagger \mathcal{D}\psi \exp \left\{ \int_0^\beta d\tau \int d^3x \psi^\dagger \left[-\partial_\tau - i\gamma^0 \gamma^i \partial_i + ig\mathbf{A}_4 + \mu - \gamma^0 m \right] \psi \right\} \\ &= \int_{\text{ABPC}} i\mathcal{D}\psi^\dagger \mathcal{D}\psi \exp(-S_E), \end{aligned} \quad (3.1.8)$$

where we in the second line defined the Euclidean action S_E .

Assume that we are in the Polyakov gauge, as described in Sec. 2.7, and that \mathbf{A}_4 does not depend on the spatial position. Since \mathbf{A}_4 by assumption is spatially constant and, by gauge choice, time-independent, we can write the action as a sum over Fourier modes. We insert the Fourier expanded fields

$$\psi(\mathbf{x}, \tau) = \frac{1}{\sqrt{V}} \sum_{\mathbf{p}, n} \psi(\mathbf{p}, n) e^{i(\mathbf{p}\cdot\mathbf{x} + \omega_n \tau)}, \quad (3.1.9)$$

$$\psi^\dagger(\mathbf{x}, \tau) = \frac{1}{\sqrt{V}} \sum_{\mathbf{p}, n} \psi^\dagger(\mathbf{p}, n) e^{-i(\mathbf{p}\cdot\mathbf{x} + \omega_n \tau)}, \quad (3.1.10)$$

where the factors $V^{-\frac{1}{2}}$ are separated out to make the Fourier coefficients dimensionless. The antiperiodicity of the fermion fields give

$$e^{i\omega_n \beta} = -1 \quad \Rightarrow \quad \omega_n = (2n + 1)\pi T. \quad (3.1.11)$$

The energies ω_n are known as the fermionic Matsubara frequencies. After inserting the Fourier expansions, the Euclidean action is given by

$$-S_E = \beta \sum_{\mathbf{p}, n} \psi^\dagger(\mathbf{p}, n) \left[-i\omega_n + ig\mathbf{A}_4 + \mu + \gamma^0 \gamma^i p_i - \gamma^0 m \right] \psi(\mathbf{p}, n) \quad (3.1.12)$$

Inserting (3.1.12) into the partition function and writing the path integral as integrals over the Fourier coefficients, we find

$$Z = \prod_{n, \mathbf{p}} \int i d[\psi^\dagger(\mathbf{p}, n)] d[\psi(\mathbf{p}, n)] e^{-i\psi^\dagger(\mathbf{p}, n) D(\mathbf{p}, n) \psi(\mathbf{p}, n)}, \quad (3.1.13)$$

where

$$\begin{aligned} D(\mathbf{p}, n) &= i\beta \left[-i\omega_n + ig\mathbf{A}_4 + \mu + \gamma^0 \gamma^i p_i - \gamma^0 m \right], \\ &= i\beta \left[(-i\omega_n + \mu + \gamma^0 \gamma^i p_i - \gamma^0 m) \otimes I_{N_c} + igI_4 \otimes \mathbf{A}_4 \right], \end{aligned} \quad (3.1.14)$$

In the second line we wrote out explicitly the identity matrices to emphasize that $D(\mathbf{p}, n)$ are $4N_c \times 4N_c$ matrices. Changing integration variable $i\psi^\dagger \rightarrow \psi^\dagger$ and using the well known formula for a Gaussian Grassmann integral [11, 26]

$$\int d\psi^\dagger d\psi e^{-\psi^\dagger A \psi} = \det A, \quad (3.1.15)$$

we find that

$$\ln Z = \ln \prod_{n, \mathbf{p}} \det D(\mathbf{p}, n) = \sum_{n, \mathbf{p}} \ln \det D(\mathbf{p}, n). \quad (3.1.16)$$

Defining the 4×4 matrix

$$K = -i\omega_n + \mu + \gamma^0 \gamma^i p_i - \gamma^0 m, \quad (3.1.17)$$

$D(\mathbf{p}, n)$ takes the block matrix form

$$D(\mathbf{p}, n) = i\beta \begin{pmatrix} K + (ig[\mathbf{A}_4]_{11})I_4 & 0 & \dots & 0 \\ 0 & K + (ig[\mathbf{A}_4]_{22})I_4 & & \vdots \\ \vdots & & \ddots & \\ 0 & \dots & & K + (ig[\mathbf{A}_4]_{N_c N_c})I_4 \end{pmatrix}. \quad (3.1.18)$$

Using that the determinant of a block diagonal matrix is the product of the determinant of the blocks, we find

$$\begin{aligned} \ln Z &= \sum_{n, \mathbf{p}} \ln \left[(i\beta)^{N_c} \prod_{j=1}^{N_c} \det \left(K + ig[\mathbf{A}_4]_{jj} \right) \right] \\ &= \sum_{n, \mathbf{p}} \sum_{j=1}^{N_c} \ln \det \left[i\beta \left(K + ig[\mathbf{A}_4]_{jj} \right) \right]. \end{aligned}$$

Note that $K(\mu) + ig[\mathbf{A}_4]_{jj} = K(\mu + ig[\mathbf{A}_4]_{jj})$, where μ is to be interpreted an argument of K . Thus, from here our derivation coincides with the derivation of the partition function for a free Fermi gas, except we have N_c independent fermion types labeled by c which each have a different effective chemical potential that is given by

$$\tilde{\mu}_j = \mu + ig[\mathbf{A}_4]_{jj}. \quad (3.1.19)$$

The next step is to calculate the determinant of the matrices $K(\tilde{\mu}_c)$ and carry out the sum over the Matsubara frequencies. This procedure can be found in any treatment on elementary thermal field theory [36, 37] and is also carried out explicitly in Appendix A.1. The result, after taking the thermodynamic limit where can replace

$$\sum_{\mathbf{p}} \rightarrow V \int \frac{d^3 p}{(2\pi)^3}, \quad (3.1.20)$$

is

$$\ln Z = 2V \sum_{j=1}^{N_c} \int \frac{d^3 p}{(2\pi)^3} \left\{ \beta \omega_{\mathbf{p}} + \ln \left[1 + e^{-\beta(\omega_{\mathbf{p}} - \tilde{\mu}_j)} \right] + \ln \left[1 + e^{-\beta(\omega_{\mathbf{p}} + \tilde{\mu}_j)} \right] \right\}, \quad (3.1.21)$$

which is the well known result for the partition function of a free Fermi gas, except that we have N_c fermion species with different chemical potentials $\tilde{\mu}_c$. The different signs

of the chemical potential correspond to particles and antiparticles. The factor of two arises because each spin- $\frac{1}{2}$ fermion has two spin polarizations. We finally note that the first term is divergent. It is the famous vacuum energy, which we for the time being will ignore, but whose divergence we cure with renormalization in Chapter 4.

We can rewrite (3.1.21) in terms of the Polyakov loop, by using that

$$\begin{aligned} \sum_{j=1}^{N_c} \ln \left[1 + e^{-\beta(\omega_{\mathbf{p}} - \tilde{\mu}_j)} \right] &= \sum_{j=1}^{N_c} \ln \left[1 + e^{i\beta g [\mathbf{A}_4]_{jj}} e^{-\beta(\omega_{\mathbf{p}} - \mu)} \right] \\ &= \sum_{j=1}^{N_c} \ln \left[1 + [L]_{jj} e^{-\beta(\omega_{\mathbf{p}} - \mu)} \right] \\ &= \text{tr}_c \ln \left[1 + L e^{-\beta(\omega_{\mathbf{p}} - \mu)} \right], \end{aligned} \quad (3.1.22)$$

where we in the last line use that the logarithm of a diagonal matrix is taken by applying the logarithm to each diagonal element. Analogously we get the conjugate Polyakov loop for the antiquark contribution with the opposite sign of $\tilde{\mu}_j$. Thus, we achieve the result commonly cited in the literature:

Partition Function of Free Fermi Gas in Background Temporal Gauge Field

$$\begin{aligned} \ln Z = & 2V \int \frac{d^3 p}{(2\pi)^3} \left\{ \text{tr}_c \ln \left[1 + L e^{-\beta(\omega_{\mathbf{p}} - \mu)} \right] + \text{tr}_c \ln \left[1 + \bar{L} e^{-\beta(\omega_{\mathbf{p}} + \mu)} \right] \right\} \\ & + 2V N_c \beta \int \frac{d^3 p}{(2\pi)^3} \omega_{\mathbf{p}}. \end{aligned} \quad (3.1.23)$$

We emphasize that the derivation of this formula required the Polyakov gauge and that \mathbf{A}_4 is spatially constant. By writing \bar{L} instead of L^\dagger we also allow for A_4^a being complex, which is a topic we return to at the end of the chapter.

3.2 Quarks in a $N_c = 3$ Gluonic Background

Let us consider the case of $SU(3)$. Equation (3.1.23) is not the most useful way to write the partition function. Instead, we write

$$\sum_{j=1}^{N_c} \ln \left[1 + [L]_{jj} e^{-\beta(\omega_{\mathbf{p}} - \mu)} \right] = \ln \left[\prod_{j=1}^3 \left(1 + [L]_{jj} e^{-\beta(\omega_{\mathbf{p}} - \mu)} \right) \right]. \quad (3.2.1)$$

The argument of the logarithm on the left hand side reads

$$1 + (L_{11} + L_{22} + L_{33})e^{-y} + (L_{11}L_{22} + L_{22}L_{33} + L_{33}L_{11})e^{-2y} + L_{11}L_{22}L_{33}e^{-3y}, \quad (3.2.2)$$

where $y = \beta(\omega_{\mathbf{p}} - \mu)$. From (2.7.7), which gives the matrix form of L in the $N_c = 3$ Polyakov gauge, we see that

$$L_{11} + L_{22} + L_{33} = 3\bar{\Phi}, \quad (3.2.3)$$

$$L_{11}L_{22} + L_{22}L_{33} + L_{33}L_{11} = 3\bar{\Phi}, \quad (3.2.4)$$

$$L_{11}L_{22}L_{33} = 1. \quad (3.2.5)$$

The result for antiparticles is obtained by interchanging $\Phi \leftrightarrow \bar{\Phi}$ and $\mu \rightarrow -\mu$. Hence, for $N_c = 3$ the partition function reads

$$\begin{aligned} \ln Z &= 2V \int \frac{d^3p}{(2\pi)^3} \ln \left[1 + 3\bar{\Phi}e^{-\beta(\omega_{\mathbf{p}}-\mu)} + 3\Phi e^{-2\beta(\omega_{\mathbf{p}}-\mu)} + e^{-3\beta(\omega_{\mathbf{p}}-\mu)} \right] \\ &+ 2V \int \frac{d^3p}{(2\pi)^3} \ln \left[1 + 3\Phi e^{-\beta(\omega_{\mathbf{p}}+\mu)} + 3\bar{\Phi}e^{-2\beta(\omega_{\mathbf{p}}+\mu)} + e^{-3\beta(\omega_{\mathbf{p}}+\mu)} \right] \\ &+ 2VN_c\beta \int \frac{d^3p}{(2\pi)^3} \omega_{\mathbf{p}}. \end{aligned} \quad (3.2.6)$$

The expectation value of the quark number, where quarks and antiquarks count oppositely, is

$$\langle N \rangle = \left\langle \int d^3x \mathcal{N} \right\rangle = \frac{1}{\beta} \frac{\partial}{\partial \mu} \ln Z, \quad (3.2.7)$$

since for a general system in the grand canonical ensemble with a conserved quantity N ,

$$\frac{1}{\beta} \frac{\partial}{\partial \mu} \ln Z = \frac{1}{\beta} \frac{1}{Z} \frac{\partial}{\partial \mu} \sum_n \langle n | e^{-\beta(E_n - \mu N)} | n \rangle = \frac{1}{Z} \text{Tr} \left\{ e^{-\beta(H - \mu N)} N \right\}. \quad (3.2.8)$$

Differentiating (3.2.6) with respect to μ , we get

$$n_q \equiv \langle N \rangle / V = 6 \int \frac{d^3p}{(2\pi)^3} \left\{ n_F(\beta[\omega_{\mathbf{p}} - \mu], \Phi, \bar{\Phi}) - \tilde{n}_F(\beta[\omega_{\mathbf{p}} + \mu], \Phi, \bar{\Phi}) \right\} \quad (3.2.9)$$

where

$$n_F(y, \Phi, \bar{\Phi}) = \frac{1 + 2\bar{\Phi}e^y + \Phi e^{2y}}{1 + 3\bar{\Phi}e^y + 3\Phi e^{2y} + e^{3y}}, \quad (3.2.10)$$

$$\tilde{n}_F(y, \Phi, \bar{\Phi}) = \frac{1 + 2\Phi e^y + \bar{\Phi}e^{2y}}{1 + 3\Phi e^y + 3\bar{\Phi}e^{2y} + e^{3y}}, \quad (3.2.11)$$

are the effective Fermi distribution functions for the quarks and antiquarks, respectively.

In the confined limit where $\Phi = \bar{\Phi} = 0$, we have that the distribution functions are

Fermi Distribution Functions in the Confined State

$$n_F(\beta[\omega_{\mathbf{p}} - \mu], 0, 0) = \frac{1}{1 + e^{\beta(3\omega_{\mathbf{p}} - 3\mu)}} \quad (3.2.12)$$

$$\tilde{n}_F(\beta[\omega_{\mathbf{p}} + \mu], 0, 0) = \frac{1}{1 + e^{\beta(3\omega_{\mathbf{p}} + 3\mu)}} \quad (3.2.13)$$

These functions are exactly the Fermi distribution functions for free fermions with energy $3\omega_{\mathbf{p}}$ and chemical potential $\pm 3\mu = \pm\mu_B$. We interpret this result to mean that in the state where $\Phi = \bar{\Phi} = 0$, the relevant degrees of freedom are baryons and antibaryons, at least in a statistical sense. We have not yet implemented any mechanism for determining Φ as a function of T , but knowing that $\Phi = 0$ should occur at low temperatures, we might reasonably call the above the low-temperature limit.

Let us also consider the case where $\Phi = \bar{\Phi} = 1$. The Fermi distribution functions then take the form

$$n_F(y, 1, 1) = \tilde{n}_F(y, 1, 1) = \frac{1 + 2e^y + e^{2y}}{1 + 3e^y + 3e^{2y} + e^{3y}} = \frac{(1 + e^y)^2}{(1 + e^y)^3} = \frac{1}{1 + e^y}. \quad (3.2.14)$$

Hence, we have Fermi distribution functions

$$n_F(\beta[\omega_{\mathbf{p}} - \mu], 1, 1) = \frac{1}{1 + e^{\beta(\omega_{\mathbf{p}} - \mu)}}, \quad (3.2.15)$$

$$\tilde{n}_F(\beta[\omega_{\mathbf{p}} + \mu], 1, 1) = \frac{1}{1 + e^{\beta(\omega_{\mathbf{p}} + \mu)}}, \quad (3.2.16)$$

that describes free quarks and antiquarks, as expected in the deconfined phase. Since we should have $\Phi = \bar{\Phi} = 1$ at high temperatures, we refer to the above as the high-temperature limit.

If $\mu = 0$ the quark number satisfies $\langle N_q \rangle = 0$. This is as expected since with $\mu = 0$ we have not introduced any imbalance in the numbers of quarks and antiquarks.

We should also ask if two-quark bound states form in the confined state, thus describing mesons in a statistical sense. In the expression for $\langle N \rangle$ in the confined limit, we did not find any terms $(1 + e^{-2\beta\omega})^{-1}$, indicating that mesons do not form. However, such a state would not contribute to the quark number $\langle N \rangle$, since each meson state has net quark number zero. On the other hand, mesonic states should contribute to the energy density. The energy density $\epsilon = \langle H \rangle / V$ is given by

$$\epsilon = \frac{1}{V} \left[\mu \frac{\partial}{\partial \mu} (T \ln Z) - \frac{\partial}{\partial \beta} (\ln Z) \right], \quad (3.2.17)$$

which one can promptly work out from the definition of Z . Carrying out these derivatives and setting $\Phi = \bar{\Phi} = 0$, i.e. considering the confined limit, gives

$$\epsilon = 2V \int \frac{d^3p}{(2\pi)^3} \left[\frac{3\omega_{\mathbf{p}}}{1 + e^{\beta(3\omega_{\mathbf{p}} - 3\mu)}} + \frac{3\omega_{\mathbf{p}}}{1 + e^{\beta(3\omega_{\mathbf{p}} + 3\mu)}} \right]. \quad (3.2.18)$$

Thus, it appears that the quarks confine into only baryonic states in our toy model. In Chapter 4 we will see that this makes it natural to combine the model presented here with separate mesonic fields.

3.3 The Effective Potential

In the previous section we showed how a constant classical background gauge field \mathbf{A}_4 could induce quark confinement, given that its value is chosen appropriately. However,

\mathbf{A}_4 , and thus also $\Phi(\mathbf{A}_4)$ and $\bar{\Phi}(\mathbf{A}_4)$, is a free parameter since we have not included any dynamical mechanism for determining \mathbf{A}_4 as a function of temperature and chemical potential. We do not want \mathbf{A}_4 to remain free since the external gluon field is not a quantity we can manipulate in the laboratory. Thus, we need to find a way to determine \mathbf{A}_4 . To do this, we will use the concept of an effective potential.

We first consider some thermodynamics. The grand canonical potential \mathcal{G} for a system in the grand canonical ensemble is defined as [52]

$$\mathcal{G}(T, \mu, V) = \Omega(T, \mu)V = -T \log Z, \quad (3.3.1)$$

where we also defined the grand canonical potential density Ω .¹ As indicated by the name, \mathcal{G} is a thermodynamical potential, meaning that it is a Legendre transform of the internal energy $E(S, \langle N \rangle, V) \equiv \langle H \rangle$, and it can be written as

$$\mathcal{G}(T, \mu, V) = E - TS - \mu \langle N \rangle, \quad (3.3.2)$$

where S is the entropy. Since \mathcal{G} is a thermodynamical potential, it is subject to a general minimum principle which states that in a system in equilibrium, any unconstrained dynamical parameter in the potential will attain a value which minimizes the potential for the given state variables [53]. Thus, the equations we need to determine $\mathbf{A}_4(\mu, T)$, and by extension $\Phi(\mu, T)$ and $\bar{\Phi}(\mu, T)$, are

$$\frac{\partial}{\partial q} \mathcal{G}(\mu, T) = 0, \quad \frac{\partial}{\partial r} \mathcal{G}(\mu, T) = 0, \quad (3.3.3)$$

where q, r are the parameters used to parametrize \mathbf{A}_4 in Sec. 2.7. However, using the partition function in (3.2.6) to calculate \mathcal{G} does not provide a good model since we have excluded all gluon dynamics. We are not modeling the energy cost of having a gluonic background field \mathbf{A}_4 . To address this problem, it is useful to consider the effective potential. We cover the subject following the approach of Ref. [39], which is based on the original work in Ref. [54].

For simplicity, let us consider the partition function for a real scalar field ϕ with Euclidean action S_E , which is given by

$$Z = \int \mathcal{D}\phi e^{-S_E} \quad (3.3.4)$$

after the conjugate momentum is integrated out.² Consider writing S_E and $\mathcal{D}\phi$ in terms of the dimensionless Fourier modes $\phi_{\mathbf{p},n}$ of $\phi(x)$, so we get

$$\exp[-\beta V \Omega] = Z = \int_{-\infty}^{\infty} d\phi_{0,0} \int \left[\prod_{(\mathbf{p},n) \neq (0,0)} d\phi_{\mathbf{p},n} \right] e^{-S_E(\{\phi_{\mathbf{p},n}\})}, \quad (3.3.5)$$

where we in the first equality just inserted the definition of Ω in terms of Z and in the second factored out the $(0,0)$ -mode. Let us rename $\phi_{0,0} = \bar{\phi}$ and refer to it as the

¹Writing $\mathcal{G}(T, \mu, V) = \Omega(T, \mu)V$ assumes that the system under study is homogeneous.

²We implicitly assume the imaginary time periodicity requirement.

condensate. Imagine now carrying out the integral over all Fourier modes except $\bar{\phi}$. Define the result to be

$$\exp[-\beta V \Omega] = \int_{-\infty}^{\infty} d\bar{\phi} \exp[-\beta V \mathcal{U}_{\text{eff}}(\bar{\phi})], \quad (3.3.6)$$

where \mathcal{U}_{eff} is the effective potential density, which we usually just refer to as the effective potential. Expanding \mathcal{U}_{eff} about a minimum $\bar{\phi}_m$,³

$$\mathcal{U}_{\text{eff}}(\bar{\phi}) = \mathcal{U}_{\text{eff}}(\bar{\phi}_m) + \frac{1}{2} \mathcal{U}_{\text{eff}}''(\bar{\phi}_m) (\bar{\phi} - \bar{\phi}_m)^2 + \dots, \quad (3.3.7)$$

we can approximate the partition function to be

$$\begin{aligned} \exp[-\beta V \Omega] &\approx \exp[-\beta V \mathcal{U}_{\text{eff}}(\bar{\phi}_m)] \int_{-\infty}^{\infty} d\bar{\phi} \exp\left[-\frac{\beta V}{2} \mathcal{U}_{\text{eff}}''(\bar{\phi}_m) (\bar{\phi} - \bar{\phi}_m)^2\right] \\ &= \exp[-\beta V \mathcal{U}_{\text{eff}}(\bar{\phi}_m)] \sqrt{\frac{2\pi}{\beta V \mathcal{U}_{\text{eff}}''(\bar{\phi}_m)}}, \end{aligned} \quad (3.3.8)$$

which gives that

$$\Omega = \mathcal{U}_{\text{eff}}(\phi_{\text{min}}) + \mathcal{O}\left(\frac{\ln V}{V}\right). \quad (3.3.9)$$

From this equation we draw the conclusion that in the thermodynamic limit, when $V \rightarrow \infty$, the effective potential evaluated at the minimum coincides with the grand potential density. Thus, in the thermodynamic limit we need not consider fluctuations in the condensate mode, and it will take on the value that minimizes $\mathcal{U}_{\text{eff}}(\bar{\phi})$.

It should be noted that the way we have defined the effective potential here differs slightly from the typical definition used in texts on QFT, such as Refs. [11, 26, 28], which is based on the Legendre transform of the generating functional in the presence of an external source. However, the two definitions are entirely equivalent, as pointed out in Ref. [54].

We now have a hypothetical process that can be used to generate an effective potential for the static background field \mathbf{A}_4 . Namely, using the pure gluonic Lagrangian (2.4.1), we can integrate out all the spatial gauge fields and all the Fourier modes of \mathbf{A}_4 except the condensate mode,⁴ in the same way as in (3.3.6), to obtain a potential for the background gauge field. Physically it means that we integrate out all quantum and thermal fluctuations on top of the constant background field \mathbf{A}_4 . As a result we get a potential $\mathcal{U}_{\text{glue}}(q, r, T)$ that represents the free energy cost of having a constant temporal background gauge field in a pure gauge theory. We can then add $\mathcal{U}_{\text{glue}}$ to the grand potential obtained from (3.2.6) to get a model that incorporates a sensible dynamical way of determining $\Phi(\mu, T)$ and $\bar{\Phi}(\mu, T)$. Note that this process still is an approximation, since we do not include the fermion-gluon interaction term $\bar{\Psi} i \gamma^\mu A_\mu^a T^a \Psi$ when we are integrating out gauge fields to obtain $\mathcal{U}_{\text{glue}}$, and we are still coupling only the temporal gauge field to the quarks.

³If there is no unique minimum, as is the case when there is spontaneous symmetry breaking, we must choose a particular minimum by adding a source to the action [39].

⁴The temporal Fourier modes of \mathbf{A}_4 are zero by gauge choice and need not be integrated out.

3.4 Phenomenological Polyakov Loop Potentials

Calculating $\mathcal{U}_{\text{glue}}$ from first principles is highly non-trivial, and one usually instead utilizes phenomenological potentials $\mathcal{U}_{\text{glue}}(\Phi, \bar{\Phi}, T)$ whose form are based on symmetry considerations and whose parameters are fitted with data from pure glue lattice simulations. To understand common choices of potentials we should summarize some of the results from $SU(3)$ lattice gauge theory.

It is known from lattice simulations that a pure $SU(3)$ gauge theory undergoes a first-order phase transition, corresponding to gluonic deconfinement, at $T_0 = 270 \text{ MeV}$ [55]. A first-order transition is expected on the basis of universality, as argued by Svetitsky and Yaffe in Refs. [43, 56]. In addition to the location of the phase transition, various thermodynamical properties such as the pressure and internal energy as functions of temperature have been established [57–59]. Finally, one also has simulations of the Polyakov loop as a function of temperature [60].

With knowledge about pure $SU(3)$ gauge theory from the lattice one can fit a phenomenological potential. We can for example fit the potential so that three quantities from lattice simulations are reproduced: the critical temperature where $\mathcal{U}_{\text{glue}}$ admits a phase transition, the pressure of the gluonic system at the phase transition, and the value of the Polyakov loop at the phase transition, i.e. T_0 , $P(T_0)$ and $\Phi(T_0)$. The first requirement necessitates that the form of the effective potential admits a first-order transition in the first place. For the second criterion, we can find the pressure from the effective potential as

$$P = -\mathcal{U}_{\text{glue}}(\Phi, \bar{\Phi}, T) \quad (3.4.1)$$

by using the general relation $P = -\frac{\partial \mathcal{G}}{\partial V}$. It should be noted that the above argument only justifies why three fit parameters are likely to be needed, and it is not meant to be a claim on how to best perform the fit. In reality one would likely obtain better results with first fixing the phase transition point and then doing a simultaneous least squares fits of $P(T)$ and $\Phi(T)$ versus lattice data.

Multiple things can be said about the form of $\mathcal{U}_{\text{glue}}$ on the basis of general considerations. $\mathcal{U}_{\text{glue}}$ must be symmetric under center transformations since the gluonic action is center symmetric. Remembering the transformation rule for Φ and $\bar{\Phi}$ under center transformations, (2.6.12) and (2.6.14), we see that the potential can be a function the terms $\Phi\bar{\Phi}$, Φ^3 and $\bar{\Phi}^3$ only. Additionally, there is no reason for any asymmetry between Φ and $\bar{\Phi}$ in a pure gluonic system, and we thus require that the potential be symmetric under $\Phi \leftrightarrow \bar{\Phi}$. Finally, we must demand that the minimum of $\mathcal{U}_{\text{glue}}$ at low temperatures is at $\Phi = \bar{\Phi} = 0$. At high temperatures it should preferably equal to or asymptotically approach $\Phi = \bar{\Phi} = 1$.

Several potentials have been suggested in the literature [61–64], and some of the most frequently used are compared in Ref. [65]. The number of fit parameters vary from two [63] to seven [61]. One of the models by Ratti, Rößner, Thaler and Weise [62] takes the form

$$\frac{\mathcal{U}_{\text{RRTW}}}{T^4} = -\frac{1}{2}a(T)\Phi\bar{\Phi} + b(T) \ln \left[1 - 6\Phi\bar{\Phi} + 4(\Phi^3 + \bar{\Phi}^3) - 3(\Phi\bar{\Phi})^2 \right], \quad (3.4.2)$$

with the temperature dependent parameters

$$a(T) = a_1 + a_2 \left(\frac{T_0}{T}\right) + a_3 \left(\frac{T_0}{T}\right)^2, \quad (3.4.3)$$

$$b(T) = b_1 \left(\frac{T_0}{T}\right)^3, \quad (3.4.4)$$

with $T_0 = 270$ MeV and fit parameters $a_1 = 3.51$, $a_2 = -2.47$, $a_3 = 15.22$, $b_1 = -1.75$. Fukushima proposes a similar potential of the form [63]

$$\frac{\mathcal{U}_{\text{Fuku}}}{T^4} = -\frac{b}{T} \left\{ ce^{-aT_0/T} \Phi \bar{\Phi} + \ln \left[1 - 6\Phi \bar{\Phi} + 4(\Phi^3 + \bar{\Phi}^3) - 3(\Phi \bar{\Phi})^2 \right] \right\}, \quad (3.4.5)$$

with free parameters a, b, c, T_0 . The parameters a and T_0 occur as a product, and they can thus be considered together as one independent parameter $\alpha = aT_0$. In his original work Fukushima does not fit α and b to lattice data, but instead chooses α so the deconfinement temperature is reproduced and b so that the chiral and deconfinement phase transitions happen at the same temperature when the potential is combined with the NJL model. c is chosen to be $c = 54$.

Figure 3.1 shows the potential $\mathcal{U}_{\text{Fuku}}$ as function of $\Phi = \bar{\Phi}$ at three different temperatures with $a = 2.46$. The latter chosen so a phase transition occurs roughly at T_0 . Figure 3.2 compares the minimum location of the Fukushima and RRTW potentials as function of temperature.

The appearance of the same logarithmic factor in both potentials deserves a comment. The term is motivated by the integration measure, also known as the Haar measure, of group integration over $SU(3)$. It turns out that for the Polyakov gauge, the argument of the logarithm in the potentials (3.4.2) and (3.4.5) corresponds to the Haar measure [63].

The potentials presented above do not take into account the backreaction of quarks onto the gluonic sector. This is due to the approximations noted at the end of Sec. 3.3. However, from the fact that the running coupling in QCD depends on the number of quark flavors, as evident from the one-loop expression

$$\frac{g(\Lambda, N_f)^2}{4\pi} = \frac{2\pi}{(11 - \frac{2}{3}N_f) \ln\left(\frac{\Lambda}{\Lambda_{\text{QCD}}}\right)}, \quad (3.4.6)$$

we conclude that the behavior in the gluonic sector should also depend on N_f , since g determines the strength of the interactions between the gauge fields. The authors in Refs. [66, 67] parametrize this dependence as

$$T_0(N_f) = \hat{T} e^{-\frac{2\pi}{\alpha_0} (11 - \frac{2}{3}N_f)^{-1}}, \quad (3.4.7)$$

where $\hat{T} = 1.77$ GeV and $\alpha_0 = 0.304$, which yields $T_0(N_f = 0) = 270$ MeV. This expression is heuristically obtained by assuming that the temperature dependence of g is governed by (3.4.6) with $\Lambda = T$ and that the phase transition occurs at a specific coupling, so that we can solve

$$g(T_0(N_f), N_f) = g(T_0(0), 0) \quad (3.4.8)$$

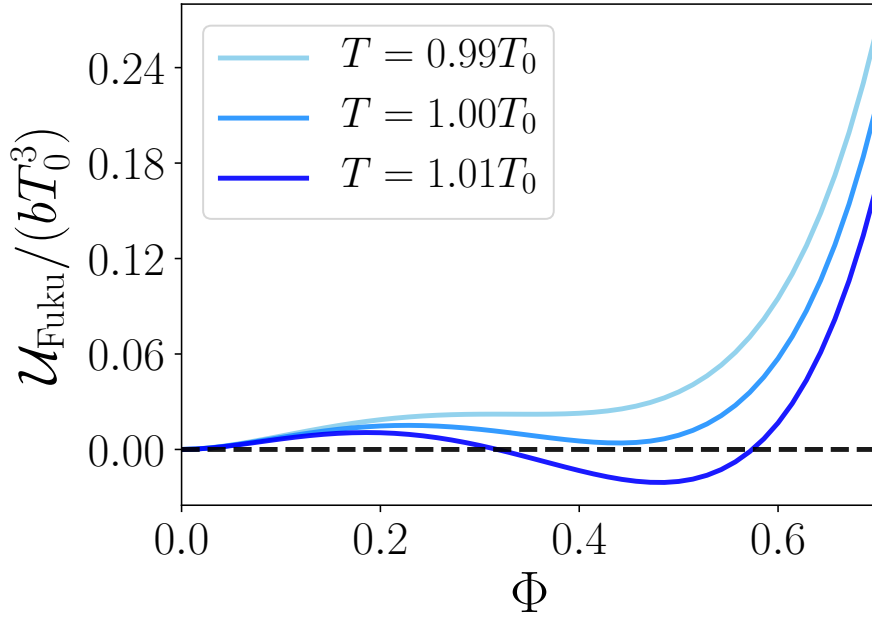


Figure 3.1: $\mathcal{U}_{\text{Fuku}}/(bT_0^3)$ as function of $\Phi = \bar{\Phi}$ for $a = 2.46$ for three different temperatures. A first-order phase transition happens at roughly T_0 .

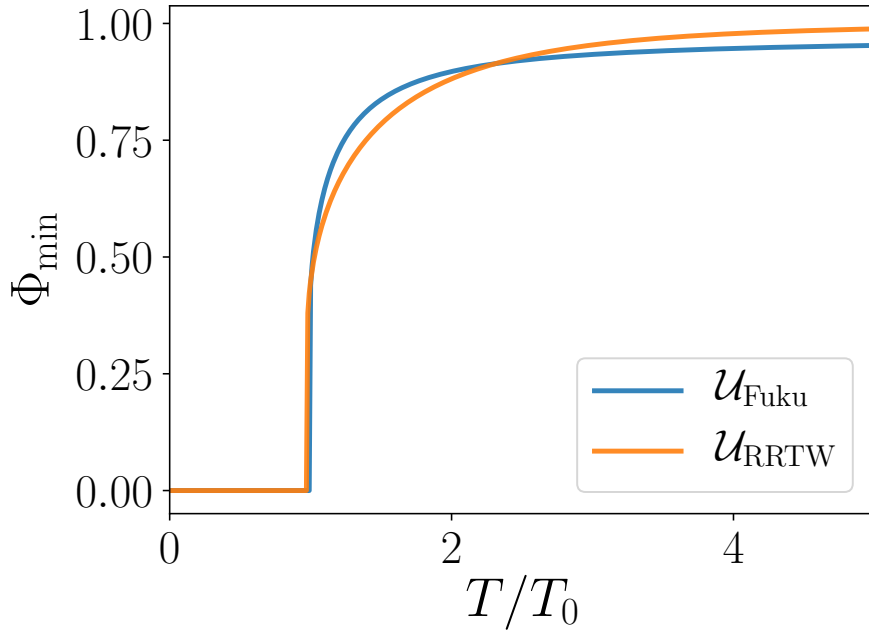


Figure 3.2: Comparison of the minimum location of $\mathcal{U}_{\text{Fuku}}$ and $\mathcal{U}_{\text{RRTW}}$ as function of temperature. Note that $\Phi_{\text{min}} = \bar{\Phi}_{\text{min}}$, and that a first-order phase transition occurs at $T \approx T_0$.

for $T_0(N_f)$. With $N_f = 2$ the relation (3.4.7) yields

$$T_0 \approx 208 \text{ MeV}. \quad (3.4.9)$$

Finally, we point out that some works introduce a μ -dependence in T_0 [66]. However, it was shown in Ref. [68] that the phase diagram is highly sensitive to the exact parametrization of $T_0(\mu)$. For this reason, to avoid overfitting, we do not use such a dependence in this thesis.

3.5 The Relation Between Φ and $\bar{\Phi}$ at $\mu \neq 0$

In Sec. 2.4 we defined the Polyakov loop and the conjugate Polyakov loop:

$$L[\mathbf{A}_4] = \text{T}_\tau e^{ig \int_0^\beta d\tau \mathbf{A}_4(\mathbf{x}, \tau)} = e^{ig\beta \mathbf{A}_4(\mathbf{x})}, \quad (3.5.1)$$

$$\bar{L}[\mathbf{A}_4] = \bar{\text{T}}_\tau e^{-ig \int_0^\beta d\tau \mathbf{A}_4(\mathbf{x}, \tau)} = e^{-ig\beta \mathbf{A}_4(\mathbf{x})}, \quad (3.5.2)$$

where the rightmost equations apply in the Polyakov gauge only. We also defined (in the Polyakov gauge)

$$\Phi = \frac{1}{N_c} \text{tr}_c e^{ig\beta \mathbf{A}_4(\mathbf{x})}, \quad \bar{\Phi} = \frac{1}{N_c} \text{tr}_c e^{-ig\beta \mathbf{A}_4(\mathbf{x})}. \quad (3.5.3)$$

These are operators in a quantum theory, and the quantities which are related to the quark (possibly pseudo) free energies are $\langle \Phi \rangle$ and $\langle \bar{\Phi} \rangle$.

It turns out that $\langle \Phi \rangle^* = \langle \bar{\Phi} \rangle$ for $\mu = 0$, while for $\mu \neq 0$ we have $\langle \Phi \rangle^* \neq \langle \bar{\Phi} \rangle$ [38, 44, 69, 70]. Furthermore, it is found that $\langle \Phi \rangle$ and $\langle \bar{\Phi} \rangle$ are both real, and with $\langle \bar{\Phi} \rangle \neq \langle \Phi \rangle$ for $\mu \neq 0$ [44, 70, 71]. In Ref. [44] this is shown nonperturbatively.

Exactly how to treat the $\mu \neq 0$ case appears to be the subject of some disagreement, and various solutions and explanations are proposed in the literature [38, 69, 72–74]. To discuss it, let us start by examining how we constructed our toy model for confinement in Sec. 3.2.

In Sec. 3.2 we considered quantum fermionic fields which were in a constant temporal background field \mathbf{A}_4^{bk} . As we did not consider fluctuations in \mathbf{A}_4^{bk} it was considered to represent the mean value of the quantum field: $\langle \mathbf{A}_4^{qu} \rangle = \mathbf{A}_4^{bk}$. Thus, the quantity which appeared in our theory really was $L[\langle \mathbf{A}_4^{qu} \rangle]$ and not $\langle L[\mathbf{A}_4^{qu}] \rangle$ (and similar for \bar{L}). Let us now include a 0-subscript to refer to these approximations to $\langle \Phi \rangle$ and $\langle \bar{\Phi} \rangle$:

$$\Phi_0 = \frac{1}{N_c} \text{tr}_c e^{ig\beta \langle \mathbf{A}_4^{qu} \rangle}, \quad \bar{\Phi}_0 = \frac{1}{N_c} \text{tr}_c e^{-ig\beta \langle \mathbf{A}_4^{qu} \rangle}. \quad (3.5.4)$$

Perturbative QCD shows that [75–77]

$$\langle \Phi \rangle = \Phi_0 + \mathcal{O}(g^2), \quad \langle \bar{\Phi} \rangle = \bar{\Phi}_0 + \mathcal{O}(g^2), \quad (3.5.5)$$

so that in the regime above the deconfinement phase transition, where g is small, we are at least approximately dealing with $\langle\Phi\rangle$ and $\langle\bar{\Phi}\rangle$. If we assume that \mathbf{A}_4^{bk} is Hermitian,⁵ we necessarily find that

$$\Phi_0^* = \bar{\Phi}_0 \Rightarrow |\Phi_0| = |\bar{\Phi}_0|, \quad (3.5.6)$$

However, as mentioned, it is seen analytically [44] that for $\mu > 0$ one has $\langle\Phi\rangle \neq \langle\bar{\Phi}\rangle$ with both being real.⁶ Thus, we want our model to capture $|\Phi_0| \neq |\bar{\Phi}_0|$, but this cannot be obtained when choosing a mean field $\mathbf{A}_4^{bk} \in \mathfrak{su}(3)$, since it implies that \mathbf{A}_4^{bk} is Hermitian.

In Ref. [73] it is argued that it is fluctuations that cause $\langle\Phi\rangle^* \neq \langle\bar{\Phi}\rangle$, and by using $\mathbf{A}_4^{bk} = \langle\mathbf{A}_4^{qu}\rangle \in \mathfrak{su}(3)$ from the beginning we necessarily cannot obtain this difference for Φ_0 and $\bar{\Phi}_0$. Thus, it seems reasonable that fluctuations cause $|\langle\Phi\rangle| \neq |\langle\bar{\Phi}\rangle|$, since evaluating (3.5.3) for a single configuration $\mathbf{A}_4 \in \mathfrak{su}(3)$ can never yield $\Phi^* \neq \bar{\Phi}$. The authors of Ref. [73] conclude that the mean field treatment of \mathbf{A}_4 involves $|\Phi_0| = |\bar{\Phi}_0|$, and they use a more elaborate scheme to account for fluctuations.

However, if we realize that when $\mu \neq 0$ we can have $\langle\mathbf{A}_4\rangle \notin \mathfrak{su}(3)$ even though each configuration \mathbf{A}_4 separately is in $\mathfrak{su}(3)$, then we might also obtain $|\Phi_0| \neq |\bar{\Phi}_0|$. This is possible since the introduction of a chemical potential makes the exponential weighting factor e^{-S_E} complex [20]. Thus, in calculating $\langle\mathbf{A}_4\rangle$ for $\mu \neq 0$, one might obtain that $\langle\mathbf{A}_4\rangle$ is non-Hermitian even though each single gauge field configuration \mathbf{A}_4 is, since one in practice is adding up $\mathfrak{su}(3)$ matrices weighted with the complex “probability measure” e^{-S_E} . The case that $\langle\mathbf{A}_4\rangle$ is not in $\mathfrak{su}(3)$, and thus non-Hermitian, is proposed and discussed in Refs. [77, 78]. Pisarski and Skokov in their paper on the χM model [21], which we will study in Chapter 5, propose an imaginary value for the gauge field parameter r , which leads to to a non-Hermitian $\langle\mathbf{A}_4\rangle$.

A third approach taken in several papers, including for example Refs. [79, 80], is to forget about the parametrization $\Phi_0(q, r)$ and $\bar{\Phi}_0(q, r)$ and vary Φ_0 and $\bar{\Phi}_0$ as two real independent quantities. In the view of the authors of Ref. [73] this is a non-systematic way of including fluctuations since they require that $\langle\mathbf{A}_4\rangle$ is Hermitian, and thus any way of obtaining $|\Phi_0| \neq |\bar{\Phi}_0|$ requires treatment of the fluctuations in the gauge field. However, since we find that $\Phi(q, ir)$ and $\bar{\Phi}(q, ir)$ are both real and different, as we see from (2.7.9) and (2.7.10), we might regard viewing Φ_0 and $\bar{\Phi}_0$ as real independent quantities as equivalent to introducing a complex background mean field where we let $r \rightarrow ir$. Thus realizing that $\langle\mathbf{A}_4\rangle \notin \mathfrak{su}(3)$ is possible justifies the use of the term mean field for the case when Φ_0 and $\bar{\Phi}_0$ are varied as real independent quantities.

There is one more problem we must face. Let us drop the 0-subscripts on Φ_0 and $\bar{\Phi}_0$. For the case of $\mu = 0$, the thermal contribution to the quark effective potential,

$$\begin{aligned} \mathcal{U}_q = & -2T \int \frac{d^3p}{(2\pi)^3} \ln \left[1 + 3\Phi e^{-\beta(\omega_{\mathbf{p}} - \mu)} + 3\bar{\Phi} e^{-2\beta(\omega_{\mathbf{p}} - \mu)} + e^{-3\beta(\omega_{\mathbf{p}} - \mu)} \right] \\ & - 2T \int \frac{d^3p}{(2\pi)^3} \ln \left[1 + 3\bar{\Phi} e^{-\beta(\omega_{\mathbf{p}} + \mu)} + 3\Phi e^{-2\beta(\omega_{\mathbf{p}} + \mu)} + e^{-3\beta(\omega_{\mathbf{p}} + \mu)} \right] \end{aligned} \quad (3.5.7)$$

⁵Remember that elements of $\mathfrak{su}(3)$ are Hermitian.

⁶It is also seen on the lattice based on a μ/T expansion [71] and in a $SU(3)$ spin model similar to QCD [70].

is real for any $q, r \in \mathbb{R}$ since the two terms are complex conjugates of each other. However, on the introduction of $\mu \neq 0$ this argument breaks down, and the potential becomes complex in general. As discussed, the solution suggested in Refs. [21, 77, 78] is to keep q real and let $r \rightarrow ir$ so that the Polyakov loops and thus the potential become real. This, however, leads to problems with unbounded potentials, which is a subject we will return to discuss when we specify the explicit form of the Polyakov loop potentials we will consider. Another option is to keep q and r real and to minimize $\text{Re} \Omega$ with respect to (Δ, q, r) , which is what is suggested in Refs. [73, 74]. We will see later that this leads to $r = 0$, which in the end gives a real effective potential. Either way, if we make the speculative assumption that a complex energy density represents an unstable state, we should choose some way of determining the parameters q and r so that they in the end yield a real potential and real Polyakov loops. However, the problem is that the standard thermodynamical principle of minimizing $\Omega(\Delta, q, r)$ with respect to (Δ, q, r) no longer applies if Ω is a complex quantity.

The Polyakov Loop Quark-Meson Model

In the previous chapter we showed how a temporal background gauge field could be used to model quark confinement in a statistical sense. However, to construct an effective model that approximates QCD, additional ingredients are needed. In particular, the model presented in Chapter 3 does not include chiral symmetry breaking, which is an essential feature of QCD. Furthermore, interactions between quarks should be incorporated without involving dynamical gauge fields.

In the following we present the quark-meson model for two quark flavors and show how it exhibits chiral symmetry breaking similar to QCD. Then we summarize the work from Refs. [1, 81–83], where the coupling constants of the QM model are calculated at the one-loop level when mesonic fluctuations are neglected. Following this we augment the QM model with the Polyakov loop and justify why the resulting model, which we refer to as a PQM model, provides an effective model of QCD.

4.1 An $O(4)$ Model with Spontaneous Symmetry Breaking

Before tackling the QM model, we will consider an $O(4)$ -symmetric Lagrangian with four neutral scalar fields with a quartic interaction:

$$\mathcal{L} = \frac{1}{2} (\partial\boldsymbol{\chi})^2 + \frac{1}{2} m^2 \boldsymbol{\chi} \cdot \boldsymbol{\chi} - \frac{\lambda}{4!} (\boldsymbol{\chi} \cdot \boldsymbol{\chi})^2. \quad (4.1.1)$$

Here $\boldsymbol{\chi}$ is a four-component field $\boldsymbol{\chi}^T = (\chi_1, \chi_2, \chi_3, \chi_4)$ and $(\partial\boldsymbol{\chi})^2 \equiv \partial_\mu \boldsymbol{\chi} \cdot \partial^\mu \boldsymbol{\chi}$. The $O(4)$ symmetry means that the Lagrangian is invariant under transformations

$$\chi_i \rightarrow R_{ij} \chi_j, \quad (4.1.2)$$

for an orthogonal 4×4 matrix R_{ij} . $O(4)$ is the group defined by these transformations. The symmetry is manifest since all terms, up to irrelevant derivatives, are of the form $(\boldsymbol{\chi} \cdot \boldsymbol{\chi})^n$, and

$$(R\boldsymbol{\chi}) \cdot (R\boldsymbol{\chi}) = (R\boldsymbol{\chi})^T (R\boldsymbol{\chi}) = \boldsymbol{\chi}^T R^T R \boldsymbol{\chi} = \boldsymbol{\chi}^T \boldsymbol{\chi} = \boldsymbol{\chi} \cdot \boldsymbol{\chi}, \quad (4.1.3)$$

where we used that for orthogonal matrices, $R^T = R^{-1}$.

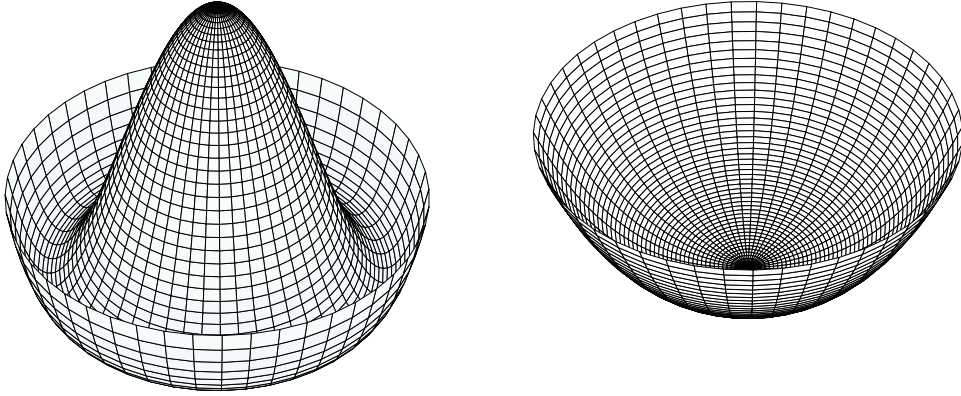


Figure 4.1: Comparison of a potential of the form $-a\boldsymbol{\chi}^2 + b\boldsymbol{\chi}^4$ (left) to a potential of the form $a\boldsymbol{\chi}^2 + b\boldsymbol{\chi}^4$ (right) for a two-component field $\boldsymbol{\chi}$ with $a, b > 0$. The two plots have different scales.

It should be noted that the quadratic term in \mathcal{L} has a positive sign, which is opposite of a standard mass term. The potential

$$U_0(\boldsymbol{\chi}) = -\frac{1}{2}m^2\boldsymbol{\chi} \cdot \boldsymbol{\chi} + \frac{\lambda}{4!}(\boldsymbol{\chi} \cdot \boldsymbol{\chi})^2 \quad (4.1.4)$$

does not have a minimum at $\boldsymbol{\chi} = 0$, but rather a maximum. Figure 4.1 shows two potentials of the same form as (4.1.4) with different signs for the quadratic term. Because the value of $U_0(\boldsymbol{\chi})$ is invariant under $O(4)$ transformations, the minimum is not unique. Thus, since at the classical level the ground state is the constant field configuration that minimizes $U_0(\boldsymbol{\chi})$, we see that we will have an arbitrary ground state chosen via spontaneous symmetry breaking. Let us assume, without loss of generality, that the non-zero value is acquired by the first $\boldsymbol{\chi}$ -component.¹ We define the field σ to be the deviation of χ_1 from the minimum value v and rename the remaining components as $\boldsymbol{\pi}$:

$$\sigma = \chi_1 - v, \quad (4.1.5)$$

$$\boldsymbol{\pi} = (\chi_2, \chi_3, \chi_4) = (\pi_1, \pi_2, \pi_3). \quad (4.1.6)$$

¹It is always possible to find an $O(4)$ -rotation which makes only one component nonzero.

The $\boldsymbol{\pi}$ fields will be interpreted as pions, with the convention that π_3 corresponds to the neutral pion π^0 , while the combinations

$$\pi^\pm = \frac{1}{\sqrt{2}}(\pi_1 \pm i\pi_2) \quad (4.1.7)$$

correspond to the charged pions π^\pm . Inserting (4.1.5) and (4.1.6) into (4.1.1) gives

$$\mathcal{L} = \frac{1}{2}(\partial\boldsymbol{\pi})^2 + \frac{1}{2}(\partial\sigma)^2 + \frac{1}{2}m^2\boldsymbol{\pi} \cdot \boldsymbol{\pi} + \frac{1}{2}m^2(v + \sigma)^2 - \frac{\lambda}{4!}[\boldsymbol{\pi} \cdot \boldsymbol{\pi} + (v + \sigma)^2]^2. \quad (4.1.8)$$

We find v at the classical level by extremizing the classical potential U_0 :

$$\frac{\partial}{\partial\chi_1} \left(-\frac{1}{2}m^2\chi_1^2 + \frac{\lambda}{4!}\chi_1^4 \right) = 0. \quad (4.1.9)$$

This gives minima at

$$\chi_{1,\min} = v = \pm\sqrt{\frac{6}{\lambda}}m, \quad (4.1.10)$$

and a maximum at $\chi_{1,\max} = 0$. We can choose the positive minimum solution without loss of generality since the negative solution always can be rotated to the positive one by applying the $O(4)$ -transformation $\chi_1 \rightarrow -\chi_1$. Inserting this value for v gives the Lagrangian

$$\mathcal{L} = \frac{1}{2}(\partial\boldsymbol{\pi})^2 + \frac{1}{2}(\partial\sigma)^2 - m^2\sigma^2 - \sqrt{\frac{\lambda}{6}}m\sigma^3 - \sqrt{\frac{\lambda}{6}}m\sigma\boldsymbol{\pi}^2 - \frac{\lambda}{4!}\sigma^4 - \frac{\lambda}{4!}\boldsymbol{\pi}^4 - \frac{\lambda}{12}\boldsymbol{\pi}^2\sigma^2, \quad (4.1.11)$$

where we introduced the notation $\mathbf{V}^{2n} \equiv (\mathbf{V} \cdot \mathbf{V})^n$ for vectors \mathbf{V} and dropped an irrelevant constant term. We see that the σ -field is massive, with a mass $m_\sigma = \sqrt{2}m$, while the three π -fields are massless. This is expected from Goldstone's theorem which says that for a Lorentz-invariant theory, if a continuous symmetry is spontaneously broken, a massless boson appears for each generator corresponding to a broken symmetry [84–86]. These particles are known as Nambu-Goldstone (NG) bosons. After spontaneous symmetry breaking, the ground state has a manifest $O(3)$ symmetry, which constitutes rotating the $\boldsymbol{\pi}$ fields. Since the orthogonal group $O(N)$ has $\frac{1}{2}N(N-1)$ generators, each corresponding to a plane in \mathbb{R}^N , we see that reducing a symmetry $O(4) \rightarrow O(3)$ corresponds to removing three generators. Thus, the appearance of three massless fields is as expected. Note however that when Lorentz invariance does not hold, which will be the case when a chemical potential is present, the one-to-one relationship between broken generators and massless bosons is not guaranteed. See Ref. [87] for details.

Consider now the addition of a term linear in χ_1 in the Lagrangian:

$$\mathcal{L} = \frac{1}{2}(\partial\boldsymbol{\chi})^2 + \frac{1}{2}m^2\boldsymbol{\chi} \cdot \boldsymbol{\chi} - \frac{\lambda}{4!}(\boldsymbol{\chi} \cdot \boldsymbol{\chi})^2 + h\chi_1. \quad (4.1.12)$$

The $O(4)$ symmetry is reduced to an $O(3)$ symmetry since any rotation involving χ_1 will change the linear term, and we can thus only rotate between the last three components.

After introducing the σ and π -fields like earlier, but without yet specifying what v is, we find the Lagrangian to be

$$\mathcal{L} = \frac{1}{2}(\partial\sigma)^2 + \frac{1}{2}(\partial\pi)^2 - \frac{1}{2}m_\pi^2\pi^2 - \frac{1}{2}m_\sigma^2\sigma^2 - (m_\pi^2v - h)\sigma - U(v) + \mathcal{L}_I, \quad (4.1.13)$$

where \mathcal{L}_I contains all interaction terms, and we defined

$$m_\sigma^2 = \frac{1}{2}\lambda v^2 - m^2, \quad (4.1.14)$$

$$m_\pi^2 = \frac{1}{6}\lambda v^2 - m^2, \quad (4.1.15)$$

and

$$U(v) = -\frac{1}{2}m^2v^2 + \frac{\lambda}{4!}v^4 - hv. \quad (4.1.16)$$

Consider what happens if we choose v be a minimum of $U(v)$, meaning that v satisfies

$$\frac{\partial U}{\partial v} = -m^2v + \frac{\lambda}{6}v^3 - h = m_\pi^2v - h = 0. \quad (4.1.17)$$

This is the prefactor of the linear term, which thus vanishes when v is evaluated at the classical minimum. We also see that this implies, at the classical level,

$$vm_\pi^2 = h, \quad (4.1.18)$$

which means that $m_\pi^2 \neq 0$ if $h \neq 0$. Thus, the explicit breaking of the $O(4)$ symmetry generates a pion mass, and the pion no longer is a true Nambu-Goldstone boson. We will refer to the limit where $h = 0$ as the chiral limit and the case where $h \neq 0$ as the physical point, since h can be adusted so that $m_\pi = 140$ MeV, which is roughly the measured pion mass [8].

Note that even though we considered what happens when v attains the value corresponding to the classical minimum, we do not want to assume that this happens, since we will treat the model quantum mechanically. In the full quantum theory v will take on the value which minimizes the effective potential and not the classical potential $U(v)$. Thus, we leave v unspecified until we have calculated loop corrections to the effective potential. We will in the following refer to $U(v)$ as the tree-level potential, since it is the lowest order approximation in QFT where no loop diagrams are involved.

4.2 The Quark-Meson Model

To obtain the two-flavor quark-meson model we couple the mesonic theory described by the Lagrangian in (4.1.12) to two N_c -plets of fermionic fields via Yukawa interactions. The fields ψ_1 and ψ_2 are taken to represent up and down quarks, respectively. Let ψ be the flavor doublet

$$\psi = \begin{pmatrix} \psi_1 \\ \psi_2 \end{pmatrix}. \quad (4.2.1)$$

The QM model is then given by

The Quark-Meson Model

$$\mathcal{L} = \bar{\psi} i \gamma^\mu \partial_\mu \psi - g \bar{\psi} (\chi_1 + i \boldsymbol{\pi} \cdot \boldsymbol{\tau} \gamma_5) \psi + \frac{1}{2} (\partial \boldsymbol{\chi})^2 + \frac{1}{2} m^2 \boldsymbol{\chi} \cdot \boldsymbol{\chi} - \frac{\lambda}{4!} (\boldsymbol{\chi} \cdot \boldsymbol{\chi})^2 + h \chi_1. \quad (4.2.2)$$

Here τ_i are the Pauli matrices which act in flavor space and $\gamma^5 \equiv i \gamma^0 \gamma^1 \gamma^2 \gamma^3$.

The reason for choosing an interaction of the form $\bar{\psi} (\chi_1 + i \boldsymbol{\pi} \cdot \boldsymbol{\tau} \gamma_5) \psi$ is as follows: Because the QCD Lagrangian is invariant under parity transformations, we also want the QM model to be parity invariant. Since it is known that the pion is a pseudoscalar [8], meaning that it transforms as $\boldsymbol{\pi} \rightarrow -\boldsymbol{\pi}$ under parity transformations, the simplest fermionic term we can couple it to that yields a parity-even interaction is $\bar{\psi} i \gamma_5 \psi$. This is because a spinor term $\bar{\psi} i \gamma_5 \psi$ transforms as [28]

$$\bar{\psi} i \gamma_5 \psi \rightarrow -\bar{\psi} i \gamma_5 \psi, \quad (4.2.3)$$

under parity and is a Lorentz scalar, and it thus combines with $\boldsymbol{\pi}$ to produce a parity even Lorentz scalar. The σ field will be identified with the $f_0(500)$ resonance, which is the lightest parity even meson that has been measured [8]. Thus we couple it to the parity even Lorentz scalar $\bar{\psi} \psi$, which is the simplest choice that yields a parity even interaction with the σ .

Let us identify the continuous symmetries of the QM model. In the chiral limit the QM Lagrangian has a global $SU(N_c) \times SU(2)_L \times SU(2)_R \times U(1)_B$ symmetry, while at the physical point the symmetry is $SU(N_c) \times SU(2)_V \times U(1)_B$. The subscripts L, R, V, B will be described in the following. Explicit derivations of all claims made about the symmetries of the QM model in the rest of this section can be found in Appendix A.3. Before proceeding we note that $SU(2) \times SU(2)$ is locally isomorphic to $O(4)$ [88], so, up to some symmetries containing discrete transformations, the $O(4)$ symmetry of the mesonic sector is preserved in the chiral limit.²

The global $SU(N_c)$ symmetry is realized by acting on ψ as

$$\psi \rightarrow \begin{pmatrix} \Omega \psi_1 \\ \Omega \psi_2 \end{pmatrix}, \quad (4.2.4)$$

for any $\Omega \in SU(N_c)$. Since Ω commutes with matrices that act in flavor space or on Dirac spinor components, we see that both fermionic terms in (4.2.2) are invariant under (4.2.4). We will not consider any non-zero color chemical potential corresponding to the conserved charges resulting from the $SU(N_c)$ symmetry, since this would imply a net color charge in the system we are considering.

The $SU(2)_L \times SU(2)_R$ -symmetry is what we refer to as chiral symmetry, and the L, R subscripts refer to the fact that independent $SU(2)$ mixing of the left- and right-handed

²Local isomorphism means that they have the same Lie algebra and thus behave the same close to the identity.

spinor components of different flavors is a symmetry. To better see this, we rewrite the QM Lagrangian as

$$\begin{aligned} \mathcal{L} = & \bar{\psi}_R i\gamma^\mu \partial_\mu \psi_R + \bar{\psi}_L i\gamma^\mu \partial_\mu \psi_L - 2g\bar{\psi}_L \Theta \psi_R - 2g\bar{\psi}_R \Theta^\dagger \psi_L \\ & + \text{Tr} \left(\partial_\mu \Theta^\dagger \partial^\mu \Theta \right) + m^2 \text{Tr} \left(\Theta^\dagger \Theta \right) - \frac{\lambda}{6} \left[\text{Tr} \left(\Theta^\dagger \Theta \right) \right]^2 + \frac{1}{2} h \text{Tr} \left(\Theta + \Theta^\dagger \right), \end{aligned} \quad (4.2.5)$$

where the left- and right-handed spinors are defined as

$$\psi_R = \frac{1}{2}(1 + \gamma_5)\psi, \quad (4.2.6)$$

$$\psi_L = \frac{1}{2}(1 - \gamma_5)\psi, \quad (4.2.7)$$

and

$$\Theta = \frac{1}{2}(\chi_1 + i\boldsymbol{\pi} \cdot \boldsymbol{\tau}) = \frac{1}{2} \begin{bmatrix} \chi_1 + i\pi_3 & i\pi_1 + \pi_2 \\ i\pi_1 - \pi_2 & \chi_1 - i\pi_3 \end{bmatrix}. \quad (4.2.8)$$

For two independent transformations $\Omega_R, \Omega_L \in SU(2)$ that are taken to act on flavor components and the components of Θ , we have that the Lagrangian is invariant under

$$\psi_R \rightarrow \Omega_R \psi_R, \quad (4.2.9)$$

$$\psi_L \rightarrow \Omega_L \psi_L, \quad (4.2.10)$$

$$\Theta \rightarrow \Omega_L \Theta \Omega_R^\dagger. \quad (4.2.11)$$

Since Ω_R and Ω_L are unitary and that a trace is cyclic, we see that every term in (4.2.5) except the $h \text{Tr}(\Theta + \Theta^\dagger)$ term is manifestly invariant under this transformation. However, one must check that the transformation (4.2.11) leaves the mesonic fields real. Otherwise, the rewriting of the Lagrangian given by (4.2.5) is invalid. In Appendix A.3 it is explicitly shown that the mesonic fields are left real under (4.2.11) and that (4.2.5) is equivalent to (4.2.2).

The conserved currents corresponding to the chiral symmetry are

$$j_{i,R}^\mu = \partial^\mu \pi_i \chi_1 - \partial^\mu \chi_1 \pi_i + \epsilon_{ijk} \pi_j \partial^\mu \pi_k + \bar{\psi}_R \gamma^\mu \tau_i \psi_R, \quad (4.2.12)$$

$$j_{i,L}^\mu = -\partial^\mu \pi_i \chi_1 + \partial^\mu \chi_1 \pi_i + \epsilon_{ijk} \pi_j \partial^\mu \pi_k + \bar{\psi}_L \gamma^\mu \tau_i \psi_L, \quad (4.2.13)$$

where $i \in \{1, 2, 3\}$. Taking linear combinations of these currents we get the so-called vector (V) and axial (A) currents, which are also conserved:

$$j_{i,V}^\mu = \frac{1}{2} \left(j_{i,R}^\mu + j_{i,L}^\mu \right) = \epsilon_{ijk} \pi_j \partial^\mu \pi_k + \frac{1}{2} \bar{\psi} \gamma^\mu \tau_i \psi, \quad (4.2.14)$$

$$j_{i,A}^\mu = \frac{1}{2} \left(j_{i,R}^\mu - j_{i,L}^\mu \right) = \partial^\mu \pi_i \chi_1 - \partial^\mu \chi_1 \pi_i + \frac{1}{2} \bar{\psi} \gamma^\mu \gamma^5 \tau_i \psi. \quad (4.2.15)$$

The names vector and axial here refers to the fact that $j_{i,V}^\mu$ is parity-even while $j_{i,A}^\mu$ is parity-odd.

At the physical point chiral symmetry is broken due to the term linear in χ_1 , since the transformation (4.2.11) generally changes χ_1 . However, a single $SU(2)$ transformation remains. It turns out that if we choose $\Omega_L = \Omega_R$, only the π components are mixed, while χ_1 is left invariant. The conserved current corresponding to this symmetry is exactly the vector current (4.2.14), and we refer to the remaining $SU(2)$ symmetry, which is also known as isospin symmetry, as $SU(2)_V$. It can also be seen that the transformation that corresponds to conservation of the axial current is given by setting $\Omega_L = \Omega_R^\dagger$, and we refer to these transformations as axial transformations.³ Thus, $h \neq 0$ explicitly breaks axial symmetry.

The chemical potential corresponding to a conserved $SU(2)_V$ charge is what we call isospin chemical potential, μ_I . Note that $j_{i,V}^0$ gives rise to three potentially conserved charges, but only one of these can be conserved at any time since the charges do not commute. This is similar to how a spin-1/2 system has three spin components, but a state can only be a spin-component eigenstate of one spatial direction.

Finally, we have the $U(1)_B$ symmetry that is realized as

$$\psi \rightarrow \Omega_B \psi, \quad (4.2.16)$$

for $\Omega_B \in U(1)$. As discussed in Sec. 3.1 this gives rise to conservation of baryon number, with the associated chemical potential $\mu_B = 3\mu$. The chemical potential μ is what we refer to as the quark chemical potential, and it corresponds to quark number conservation, where the quark number is defined as the sum of up and down quarks with antiquarks counting negatively.⁴

4.3 Chiral Symmetry Breaking in the QM Model

Like in the pure bosonic model in Sec. 4.1, we expect that the mesonic field χ_1 will develop a non-zero expectation value in the vacuum. Introducing σ and v , where we assume $\langle \sigma \rangle = 0$, the QM model Lagrangian reads

$$\begin{aligned} \mathcal{L} = & U(v) + \frac{1}{2}(\partial\boldsymbol{\pi})^2 + \frac{1}{2}(\partial\sigma)^2 - \frac{1}{2}m_\sigma^2\sigma^2 - \frac{1}{2}m_\pi^2\boldsymbol{\pi}^2 + \sigma(h - m_\pi^2 v) + \mathcal{L}_{I,\sigma\pi} \\ & + \bar{\psi}i\gamma^\mu\partial_\mu\psi - m_q\bar{\psi}\psi - g\bar{\psi}(\sigma + i\boldsymbol{\pi} \cdot \boldsymbol{\tau}\gamma_5)\psi, \end{aligned} \quad (4.3.1)$$

where

$$m_q = gv \quad (4.3.2)$$

is a dynamically generated quark mass and $\mathcal{L}_{I,\sigma\pi}$ is the meson-meson interaction sector, which works out to be:

$$\mathcal{L}_{I,\sigma\pi} = -\frac{1}{6}\lambda v\sigma^3 - \frac{1}{6}v\lambda\sigma\boldsymbol{\pi}^2 - \frac{\lambda}{12}\sigma^2\boldsymbol{\pi}^2 - \frac{\lambda}{4!}\sigma^4 - \frac{\lambda}{4!}\boldsymbol{\pi}^4. \quad (4.3.3)$$

³Note that axial transformations do not form a group. If we perform two successive axial transformations $\Omega_1, \Omega_2 \in SU(2)$ on ψ_R we get $\psi_R \rightarrow \Omega_2\Omega_1\psi_R$, while ψ_L transforms as $\psi_L \rightarrow \Omega_2^\dagger\Omega_1^\dagger\psi_L \neq (\Omega_2\Omega_1)^\dagger\psi_L$. Thus, the composition of two axial transformations is not an axial transformation.

⁴Note that μ is distinct from the separate up quark chemical potential μ_u and down quark chemical potential μ_d , which are sometimes used.

$U(v)$, m_π^2 and m_σ^2 are defined like in Sec. 4.1. In the chiral limit, if we calculate the effective potential $\mathcal{U}(v, T, \mu)$ for this Lagrangian and find that the minimum of \mathcal{U} is located at $v \neq 0$, we have that the chiral symmetry is spontaneously broken, since $\langle \chi_1 \rangle = v \neq 0$ is not invariant under chiral transformations. However, $\langle \chi_1 \rangle = v$ is invariant under the $SU(2)_V$ symmetry, since, as stated earlier, these transformations do not alter χ_1 . Thus, spontaneous breaking of chiral symmetry is a violation of the axial symmetry.

At the physical point the axial (and thus chiral) symmetry is explicitly broken from the start, but we can informally say that we have a more severe breaking of the symmetry if the value of v increases significantly in some region of temperatures and chemical potentials. If we compare with an Ising system, we can identify v with the magnetization and h with the external magnetic field. Even though the magnetization is non-zero for all temperatures when an external field is present, the magnetization is still a good approximate measure for the magnitude of the symmetry breaking.

In the following we will refer to v as the chiral condensate, since we renormalize so that $\langle \chi_1 \rangle = v$ and $\langle \sigma \rangle = 0$.

4.4 Parameters of the QM Model at One Loop

To make quantitative predictions with the QM model, we need to fix the parameters m , λ , g and h to the given order that we are working in perturbation theory. By solving (4.1.14), (4.1.15), (4.1.18) and (4.3.2) with respect to the coupling constants, we find

$$\lambda = \frac{3(m_\sigma^2 - m_\pi^2)}{v^2}, \quad (4.4.1)$$

$$m^2 = \frac{m_\sigma^2 - 3m_\pi^2}{2}, \quad (4.4.2)$$

$$h = m_\pi^2 v, \quad (4.4.3)$$

$$g = \frac{m_q}{v}. \quad (4.4.4)$$

However, these relations can be used to fix the parameters only at tree-level, since at some arbitrary order in perturbation theory the equations defining m_π^2 , m_σ^2 and m_q do not actually define the physical masses of the pions, the sigma and the quarks. At higher orders in perturbation theory the particle masses receive loop corrections. Despite this, as out pointed in Ref. [81], the parameter fixing in the literature is often done at tree-level while other quantities are calculated to higher orders, which is inconsistent. To consistently fix the parameters at any order higher than tree-level we need to renormalize m , λ , g , h , v and calculate self-energy corrections to the particle masses.

In Refs. [81, 82] the running coupling constants were determined to one loop in the large- N_c limit by using dimensional regularization. To determine the running couplings, they calculate the particle self-energy corrections at $T = 0$ and then use the physically measured masses for the pions, the sigma and the quarks in the vacuum to determine the coupling constants at the one-loop level. These results were also later reproduced

in a master thesis [83] and in an unpublished project by the author leading up to this thesis [1]. We here quote the results directly and only explain schematically how the results are obtained since the detailed calculations are quite involved and not crucial for understanding the work presented in this thesis. The full derivation is for completeness included in Appendix A.4.

The large- N_c limit implies that only diagrams scaling as $\mathcal{O}(N_c)$ are kept at the one-loop level, while diagrams $\mathcal{O}(N_c^0)$ are neglected. This amounts to neglecting mesonic fluctuations. All diagrams of order $\mathcal{O}(N_c)$ at one loop are shown in Fig. 4.2.

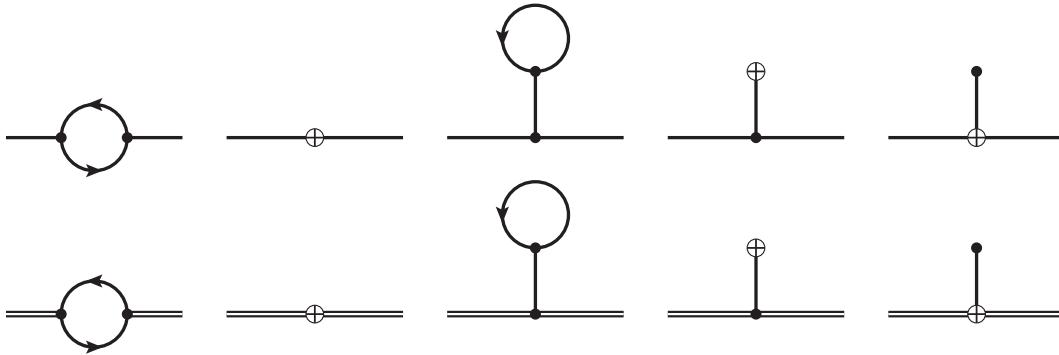


Figure 4.2: All $\mathcal{O}(N_c)$ diagrams up to one-loop order in the QM model contributing to two-point functions. The pion, sigma and quark propagators are given by double lines, full lines and arrow-lines, respectively. The crossed circles represent counterterm vertices. The renormalization condition $\langle \sigma \rangle = 0$ enforces that the sum of the last three diagrams within each row vanishes. The condition that the minimum of the effective potential is equal to the minimum of the tree-level potential causes the last diagram in each row to vanish separately since the tadpole vertex factor is proportional to $(m_\pi^2 v - h)$, which is zero exactly at the classical minimum.

The calculation of self-energies is most easily performed when we use as a renormalization condition that the sigma one-point function satisfies $\langle \sigma \rangle = 0$, so that $\langle \Phi_1 \rangle = v$. This gives a relation between the counterterm δh and the other counterterms in the problem. Furthermore, we use the $\overline{\text{MS}}$ renormalization scheme, which implies that only factors of $\frac{1}{\epsilon} + \ln(4\pi e^{-\gamma_E})$ are absorbed into counterterms. Here ϵ is defined in dimensional regulation as $d = 3 - 2\epsilon$ and γ_E is the Euler-Mascheroni constant. Finally, an additional simplifying condition we enforce is to require that the minimum of the one-loop effective potential $\mathcal{U}(v)$ at $T = \mu = 0$ is identical to the minimum of the tree-level potential $U(v)$. This fixes the renormalization scale Λ to a particular value $\Lambda = \Lambda_0$. The running couplings at some other Λ are then obtained by solving the renormalization group equations. The result is

The Large- N_c Running Couplings at One Loop

$$g_{\overline{\text{MS}}}^2(\Lambda) = \frac{g_0^2}{1 - \frac{4N_c g_0^2}{(4\pi)^2} \ln\left(\frac{\Lambda^2}{\Lambda_0^2}\right)}, \quad (4.4.5)$$

$$m_{\overline{\text{MS}}}^2(\Lambda) = \frac{m_0^2}{1 - \frac{4N_c g_0^2}{(4\pi)^2} \ln\left(\frac{\Lambda^2}{\Lambda_0^2}\right)}, \quad (4.4.6)$$

$$\lambda_{\overline{\text{MS}}}(\Lambda) = \frac{\lambda_0 - \frac{48N_c}{(4\pi)^2} g_0^4 \ln\left(\frac{\Lambda^2}{\Lambda_0^2}\right)}{\left[1 - \frac{4N_c g_0^2}{(4\pi)^2} \ln\left(\frac{\Lambda^2}{\Lambda_0^2}\right)\right]^2}, \quad (4.4.7)$$

$$h_{\overline{\text{MS}}}(\Lambda) = \frac{h_0}{1 - \frac{2N_c g_0^2}{(4\pi)^2} \ln\left(\frac{\Lambda^2}{\Lambda_0^2}\right)}, \quad (4.4.8)$$

$$v_{\overline{\text{MS}}}^2(\Lambda) = \frac{v_0^2}{1 + \frac{4N_c g_0^2}{(4\pi)^2} \ln\left(\frac{\Lambda^2}{\Lambda_0^2}\right)} \quad (4.4.9)$$

where

$$\Lambda_0^2 = m_q^2 \exp\left[-\text{Re } C(m_\pi^2) - m_\pi^2 \text{Re } C'(m_\pi^2)\right], \quad (4.4.10)$$

and

$$C(p^2) = 2 - 2\sqrt{\frac{4m_q^2}{p^2} - 1} \arctan\left(\frac{1}{\sqrt{\frac{4m_q^2}{p^2} - 1}}\right), \quad (4.4.11)$$

with $C'(p^2) = \frac{dC(p^2)}{dp^2}$. Introducing the shorthands $\text{Re } C(m_\pi^2) = C_\pi$, $\text{Re } C(m_\sigma^2) = C_\sigma$ and $\text{Re } C'(m_\pi^2) = C'_\pi$, the values g_0 , m_0 , λ_0 , v_0 and h_0 are given by

$$m_0^2 = \frac{m_\sigma^2 - 3m_\pi^2}{2} + \frac{2N_c m_q^2}{(4\pi)^2 f_\pi^2} \left[4m_q^2 + (m_\sigma^2 - 4m_q^2)C_\sigma - m_\sigma^2 C_\pi - (m_\sigma^2 - 3m_\pi^2)m_\pi^2 C'_\pi\right], \quad (4.4.12)$$

$$\lambda_0 = \frac{3(m_\sigma^2 - m_\pi^2)}{f_\pi^2} + \frac{12N_c m_q^2}{(4\pi)^2 f_\pi^4} \left[(m_\sigma^2 - 4m_q^2)(C_\sigma - C_\pi - m_\pi^2 C'_\pi) + m_\pi^4 C'_\pi\right], \quad (4.4.13)$$

$$g_0^2 = \frac{m_q^2}{f_\pi^2}, \quad (4.4.14)$$

$$h_0 = m_\pi^2 f_\pi - \frac{4N_c m_q^2 m_\pi^4}{(4\pi)^2 f_\pi} C'_\pi, \quad (4.4.15)$$

$$v_0^2 = f_\pi^2, \quad (4.4.16)$$

where f_π is the pion decay constant, which we will explain in the next section. It is important to point out that the masses m_π , m_σ and m_q occurring in (4.4.10)–(4.4.15) are the actual physical masses, so that (4.4.5)–(4.4.16) can be used to fix the coupling constants of the QM model with the measured particle masses in the vacuum. We see

that the first four equations are corrections to the tree-level relations (4.4.1)–(4.4.4) with $v = f_\pi$. The quark mass does not receive any corrections at one loop, since in the large- N_c limit all mesonic fluctuations are neglected, and only meson loops provide corrections to the quark two-point function at one loop.

Note that the mass $m_q = gv$, which we will refer to as the constituent quark mass, does not correspond to the mass parameter that occurs in the QCD Lagrangian, which is known as the current quark mass. Instead, m_q is a quark mass dynamically generated through the process of chiral symmetry breaking. In QCD this mass includes quark binding energy in the non-perturbative regime of the theory. It is this mass which is responsible for giving the proton a mass of the order of $\sim \text{GeV}$ even though the u and d current quark masses are of the order of $\sim \text{MeV}$ [8].

4.5 The Pion Decay Constant

The quantities m , g , λ and h are independent couplings in the QM Lagrangian, while v is determined once these four parameters are fixed, since it will be taken to be the minimum of the effective potential, which is a function of the couplings. Thus, in total four measurements are required to fix all parameters. However, the pion, sigma, and constituent quark masses provide only three inputs. It turns out that the value of the chiral condensate v can be identified with a measurable quantity known as the pion decay constant, thus providing the last input.

For a Nambu-Goldstone mode G corresponding to a spontaneously broken symmetry with Noether current j^μ , it can be shown that one in general can write [26]

$$\langle G(\mathbf{p}, t) | j^\mu(x) | \Omega \rangle = ip^\mu F e^{ipx}, \quad (4.5.1)$$

where $|\Omega\rangle$ is the vacuum and $|G(\mathbf{p}, t)\rangle$ a \mathbf{p} -eigenstate defined as

$$|G(\mathbf{p}, t)\rangle = \frac{-2i}{F} \int d^3x e^{i\mathbf{p}\cdot\mathbf{x}} j^0(x) | \Omega \rangle. \quad (4.5.2)$$

Here F is a normalization constant, and equation (4.5.1) is derived by enforcing the one-particle normalization condition $\langle G(\mathbf{p}, t) | G(\mathbf{k}, t) \rangle = 2\omega_{\mathbf{p}} (2\pi)^3 \delta(\mathbf{p} - \mathbf{k})$. For pions the quantity F is referred to as the pion decay constant f_π , and we can write

$$\langle \pi_j(\mathbf{p}, t) | j_{A,i}^\mu(x) | \Omega \rangle = ip^\mu f_\pi e^{ipx} \delta_{ij}, \quad (4.5.3)$$

where $j_{A,i}^\mu$ are the axial currents and $|\pi_j(\mathbf{p}, t)\rangle$ the state defined by (4.5.2) with the j -th axial current. Note that relation (4.5.3) is model independent as long as $j_{A,i}^\mu$ is chosen to be whatever currents correspond to the pions in the model studied. By using a low-energy effective theory of QCD known as chiral perturbation theory, one can relate f_π to observation by calculating the decay rate $\pi^+ \rightarrow \mu^+ \nu_\mu$, where μ^+ is the anti-muon and ν_μ a muon neutrino [26]. Since one finds that the decay rate satisfies $\Gamma \propto f_\pi^2$, one can determine f_π through a measurement of this decay.

As a consequence of the above, if we can calculate the left-hand side of (4.5.3) in the QM model, we get a relation between parameters of the QM model and f_π . After symmetry breaking we see from (4.2.15) that the axial current of the QM model is

$$j_{i,A}^\mu = v\partial^\mu\pi_i + (\text{terms containing } \sigma \text{ and } \psi). \quad (4.5.4)$$

But only the first term gives a non-zero matrix element in the left-hand side of (4.5.3) since σ or ψ cannot create or destroy a π_j state, and we find

$$\langle\pi_j(\mathbf{p}, t)|j_{A,i}^\mu(x)|\Omega\rangle = v\langle\pi_j(\mathbf{p}, t)|\partial^\mu\pi_i(x)|\Omega\rangle. \quad (4.5.5)$$

To lowest order, where we can use creation operator relations for a free theory, we can calculate this matrix element to be

$$\begin{aligned} \langle\pi_j(\mathbf{p}, t)|\partial^\mu\pi_i(x)|\Omega\rangle &= \delta_{ij}\langle\Omega|a_{\mathbf{p}}\partial^\mu\left[\int\frac{d^3k}{(2\pi)^3(2\omega_{\mathbf{k}})}\left(a_{\mathbf{k}}e^{-ikx}+a_{\mathbf{k}}^\dagger e^{ikx}\right)\right]|\Omega\rangle \\ &= \langle\Omega|i\int\frac{d^3k}{(2\pi)^3(2\omega_{\mathbf{k}})}[a_{\mathbf{p}},a_{\mathbf{k}}^\dagger]k^\mu e^{ikx}|\Omega\rangle = ip^\mu e^{ipx}, \end{aligned} \quad (4.5.6)$$

where $a_{\mathbf{p}}$ is the creation operator for the $i = j$ pion with the normalization $[a_{\mathbf{k}}, a_{\mathbf{p}}^\dagger] = (2\pi)^3 2\omega_{\mathbf{p}} \delta(\mathbf{p} - \mathbf{k})$. Hence, at tree level we have

$$\langle\pi_j(\mathbf{p}, t)|j_{A,i}^\mu(x)|\Omega\rangle = ip^\mu v e^{ipx} \delta_{ij}, \quad (4.5.7)$$

and we indentify $v = f_\pi$.

4.6 The PQM Partition Function in the One-Loop Large- N_c Limit

Consider the addition of a constant temporal background gauge field in the Polyakov-gauge to the QM Lagrangian. As we saw in Chapter 3, this amounts to adding a term $g_a\bar{\psi}i\gamma^0\mathbf{A}_4\psi$ to the Lagrangian, where we have denoted the Yang-Mills coupling constant as g_a to separate it from the Yukawa coupling. We will refer to the QM model extended with the Polyakov loop as a PQM model. Note that the addition of this term does not break any of the symmetries of the QM-model. Furthermore, it does not affect the calculation of self-energies, since this term effectively adds a constant offset $p^0 \rightarrow p^0 + g_a[\mathbf{A}_4]_{jj}$ in the quark propagator of the j -th color, which can be seen by writing the Dirac Lagrangian in momentum space:

$$\bar{\psi}(x)i\gamma^\mu\partial_\mu\psi(x) + g_a\bar{\psi}(x)i\gamma^0\mathbf{A}_4\psi(x) \rightarrow \bar{\psi}(p)i\gamma^\mu(p_\mu + \delta_{\mu 0}g_a\mathbf{A}_4)\psi(p). \quad (4.6.1)$$

Remembering that \mathbf{A}_4 is diagonal in the Polyakov-gauge, this effect is reversed by a simple shift of the p^0 variable in the loop integrals.

With the parameters of the QM model known to one loop in the large- N_c limit, we proceed to write down the partition function to one loop in the same approximation.

4.6. THE PQM PARTITION FUNCTION IN THE ONE-LOOP LARGE- N_c LIMIT 53

Since the partition function is given by the sum of connected vacuum diagrams with no external sources, calculating Z to one loop is equivalent to closing all propagators on themselves, meaning that no interaction vertices appear. Hence, the one-loop perturbative calculation of Z amounts to neglecting all interaction terms. Furthermore, neglecting both thermal and quantum mesonic fluctuations means that the only mesonic contribution to Z is the tree-level potential $U(v)$. Thus, if we work at zero isospin chemical potential, we can directly use our result from Sec. 3.1, except we now have two quark flavors, yielding an extra factor of two. The result is

$$\begin{aligned} \ln Z = & 4V \int \frac{d^3p}{(2\pi)^3} \left\{ \text{tr}_c \ln \left[1 + L e^{-\beta(\omega_{\mathbf{p}} - \mu)} \right] + \text{tr}_c \ln \left[1 + \bar{L} e^{-\beta(\omega_{\mathbf{p}} + \mu)} \right] \right\} \\ & + 4V N_c \beta \int \frac{d^3p}{(2\pi)^3} \omega_{\mathbf{p}} - \beta V U(v), \end{aligned} \quad (4.6.2)$$

with $\omega_{\mathbf{p}} = \sqrt{\mathbf{p}^2 + \Delta^2}$, where we use the notation $\Delta = gv$ instead of m_q , since gv is temperature dependent and not equal to the vacuum constituent quark mass for nonzero temperatures (we must keep in mind that v is to be chosen as the minimum of $\Omega(v, T, \mu)$). We will reserve m_q for the zero-temperature constituent quark mass.

After introducing the renormalized couplings in the $\overline{\text{MS}}$ scheme, the vacuum energy becomes finite and the effective potential to one loop reads (see Appendix A.4)

$$\Omega(\Delta, \Phi, \bar{\Phi}, T, \mu) = \mathcal{U}_{q,T}(\Delta, \Phi, \bar{\Phi}, T, \mu) + \mathcal{U}_{q,\text{vac}}(\Delta) + \mathcal{U}_{\chi}(\Delta), \quad (4.6.3)$$

where

$$\mathcal{U}_{q,T}(\Delta, T, \mu, \Phi, \bar{\Phi}) = -4T \int \frac{d^3p}{(2\pi)^3} \left\{ \text{tr}_c \ln \left[1 + L e^{-\beta(\omega_{\mathbf{p}} - \mu)} \right] + \text{tr}_c \ln \left[1 + \bar{L} e^{-\beta(\omega_{\mathbf{p}} + \mu)} \right] \right\} \quad (4.6.4)$$

is the contribution from thermal quark fluctuations,

$$\mathcal{U}_{q,\text{vac}}(\Delta) = \frac{2N_c \Delta^4}{(4\pi)^2} \left[\frac{3}{2} + \ln \left(\frac{m_q^2}{\Delta^2} \right) - C_\pi - m_\pi^2 C'_\pi \right] \quad (4.6.5)$$

is the vacuum contribution from quark quantum fluctuations and

$$\mathcal{U}_{\chi}(\Delta) = -\frac{1}{2} m_0^2 f_\pi^2 \frac{\Delta^2}{m_q^2} + \frac{1}{4!} \lambda_0 f_\pi^4 \frac{\Delta^4}{m_q^4} - h_0 f_\pi \frac{\Delta}{m_q} \quad (4.6.6)$$

the tree-level mesonic potential. The parameters m_0^2 , λ_0 and h_0 are as defined in the previous section. We have chosen to write Ω as a function of Δ instead of v since, since Δ is independent of the renormalization scheme. It turns out that in the large- N_c limit to one loop, $\delta(gv) = v\delta g + g\delta v = 0$, where δg and δv are the one-loop counterterms of g and v (again, see Appendix A.4).

After inserting m_0 , λ_0 , h_0 and adding a not yet specified Polyakov loop potential $\mathcal{U}_{\text{glue}}$, we find

Large- N_c One-Loop Effective Potential of the PQM model

$$\begin{aligned}
\Omega(\Delta, T, \mu) = & \frac{3}{4} m_\pi^2 f_\pi^2 \left\{ 1 - \frac{4N_c m_q^2}{(4\pi)^2 f_\pi^2} m_\pi^2 C'_\pi \right\} \frac{\Delta^2}{m_q^2} + \frac{2N_c m_q^4}{(4\pi)^2} \left(\frac{3}{2} - \ln \frac{\Delta^2}{m_q^2} \right) \frac{\Delta^4}{m_q^4} \\
& - \frac{m_\sigma^2 f_\pi^2}{4} \left\{ 1 + \frac{4N_c m_q^2}{(4\pi)^2 f_\pi^2} \left[\left(1 - \frac{4m_q^2}{m_\sigma^2} \right) C_\sigma - C_\pi - m_\pi^2 C'_\pi + \frac{4m_q^2}{m_\sigma^2} \right] \right\} \frac{\Delta^2}{m_q^2} \\
& + \frac{m_\sigma^2 f_\pi^2}{8} \left\{ 1 + \frac{4N_c m_q^2}{(4\pi)^2 f_\pi^2} \left[\left(1 - \frac{4m_q^2}{m_\sigma^2} \right) C_\sigma - C_\pi - m_\pi^2 C'_\pi \right] \right\} \frac{\Delta^4}{m_q^4} \\
& - \frac{m_\pi^2 f_\pi^2}{8} \left\{ 1 - \frac{4N_c m_q^2}{(4\pi)^2 f_\pi^2} m_\pi^2 C'_\pi \right\} \frac{\Delta^4}{m_q^4} - m_\pi^2 f_\pi^2 \left[1 - \frac{4N_c m_q^2}{(4\pi)^2 f_\pi^2} m_\pi^2 C'_\pi \right] \frac{\Delta}{m_q} \\
& - 4T \int \frac{d^3 p}{(2\pi)^3} \left\{ \text{tr}_c \ln \left[1 + L e^{-\beta(\sqrt{\mathbf{p}^2 + \Delta^2} - \mu)} \right] + \text{tr}_c \ln \left[1 + \bar{L} e^{-\beta(\sqrt{\mathbf{p}^2 + \Delta^2} + \mu)} \right] \right\} \\
& + \mathcal{U}_{\text{glue}}(\Phi, \bar{\Phi}, T). \tag{4.6.7}
\end{aligned}$$

In Fig. 4.3 we see the phase diagram resulting from the effective potential (4.6.7) in the case where $\mathbf{A}_4 = 0$, i.e. without the Polyakov loop, as calculated by the author in Ref. [1]. The parameters are chosen so that $m_\sigma = 550$ MeV, $m_q = 300$ MeV and $m_\pi = 0$ or $m_\pi = 140$ MeV, depending on whether one assumes $h = 0$ or $h \neq 0$. For $\mu_q = 0$ there is a second-order phase transition occurring at roughly $T_c = 160$ MeV in the chiral limit. For μ_q greater than ~ 270 MeV the transition becomes first-order. A first-order transition also happens at the physical point, for chemical potentials close to 300 MeV. When $h \neq 0$ there is no true thermodynamic phase transition, but rather a crossover between large and small Δ . We can define a pseudocritical temperature as the inflection point of the order parameter. This is how we will define the phase transition in the case of a crossover for the rest of the thesis.

4.7 The PQM Model as an Effective Model of QCD

Before proceeding to choose $\mathcal{U}_{\text{glue}}$ and investigating the thermodynamics of the PQM model, we should justify why it is sensible to consider the PQM model to be an effective model of QCD. Let us consider the QCD Lagrangian for the two light quark flavors u and d ,

$$\mathcal{L} = \mathcal{L}_A + \bar{u}(i\gamma^\mu D_\mu - m_u)u + \bar{d}(i\gamma^\mu D_\mu - m_d)d. \tag{4.7.1}$$

Here \mathcal{L}_A is the gluonic sector term and u and d two N_c -plets of spinors. We can decompose the spinors into right- and left-handed parts, and for $m_u = m_d = 0$, which we also refer to as the chiral limit, we find

$$\mathcal{L} = \mathcal{L}_A + i\bar{\psi}^L \gamma^\mu D_\mu \psi^L + i\bar{\psi}^R \gamma^\mu D_\mu \psi^R, \tag{4.7.2}$$

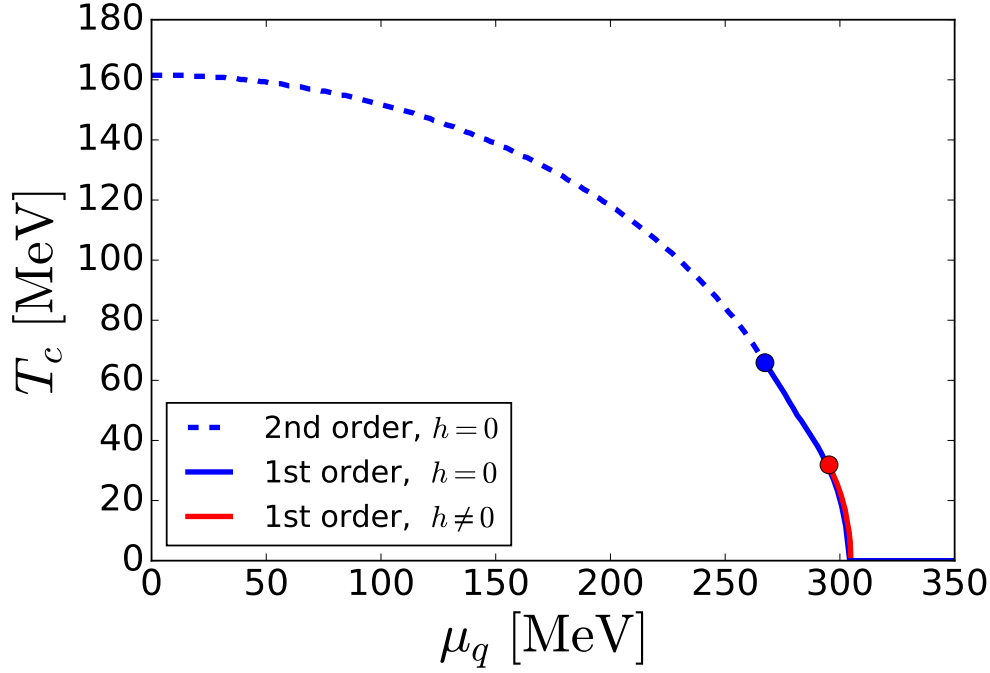


Figure 4.3: Phase diagram of Δ in the one-loop large- N_c limit without the Polyakov loop. μ_q is the quark chemical potential. The region bounded by the axes and the blue lines show where chiral symmetry is spontaneously broken in the chiral limit, i.e. where $\Delta \neq 0$.

where $\psi = (u, d)^T$. Exactly like for the (P)QM model we have a global $SU(2)_R \times SU(2)_L$ symmetry. The Lagrangian also has two $U(1)$ symmetries given by applying a phase transformation to ψ_L and ψ_R separately. However, there exist symmetries of a Lagrangian that are not symmetries of the corresponding quantum theory due to a phenomenon called an anomaly. It is caused by that fact that the integration measure in the partition function is not invariant under a symmetry of the action. It will not be shown here, but it turns out that the $U(1)_L \times U(1)_R$ symmetry of the QCD Lagrangian for massless quarks is such a symmetry. The reader is referred to Refs. [11, 26, 28] for details. The result is that only a single $U(1)$ that acts as

$$\psi \rightarrow e^{i\alpha}\psi \quad (4.7.3)$$

remains. However, this is exactly the $U(1)_B$ symmetry of the (P)QM model. Hence, both QCD and the (P)QM model have a $U(1)_B \times SU(2)_R \times SU(2)_L$ global symmetry in the chiral limit.

It is also known that the global $SU(2)_R \times SU(2)_L$ symmetry is spontaneously broken down to a $SU(2)_V$ symmetry in the QCD vacuum, generating the pions as Nambu-Goldstone bosons in the process [26]. The exact mechanism for this process remains mysterious, but the fact is well established. The order parameters for this symmetry

breaking are the quark bilinears $\langle \bar{u}u \rangle$ and $\langle \bar{d}d \rangle$, which on the lattice are determined to be [89, 90]

$$\langle \bar{u}u \rangle = \langle \bar{d}d \rangle \approx -(250 \text{ MeV})^3, \quad (4.7.4)$$

for $m_u = m_d$.

The symmetry breaking pattern described in the above is exactly the spontaneous symmetry breaking pattern observed in the (P)QM model in the chiral limit, although in the (P)QM model we describe pions with fundamental fields, while in nature the pions are bound states of quarks. $\langle \bar{\psi}\psi \rangle$ is the order parameter for chiral symmetry breaking in QCD, while in the (P)QM model it is v which plays this role. Nevertheless, we expect both QCD and the (P)QM model to have a phase transition associated with the restoration of chiral symmetry at high temperatures, which is what we refer to as the chiral phase transition. Note that the quark bilinear $\bar{\psi}\psi$ in the (P)QM model should not be expected to behave like the quark bilinear in QCD.

At the physical point, if we assume $m_u = m_d$, two-flavor QCD has no chiral symmetry but instead an $SU(2)_V$ symmetry, which is also the case in the (P)QM model. However, our intuition from the chiral limit still holds, but the chiral symmetry is now approximate. Instead of a true thermodynamic phase transition we expect, when reaching high temperatures, a crossover to where we have approximate chiral symmetry and thus a small chiral condensate. The symmetry breaking patterns of QCD and the (P)QM model are illustrated in Table 4.1.

Model	Symmetry before SSB (high T)	Symmetry after SSB (low T)
QCD, chiral limit	$SU(2)_R \times SU(2)_L$	$SU(2)_V$
QM, chiral limit	$SU(2)_R \times SU(2)_L$	$SU(2)_V$
QCD, $m_u = m_d \neq 0$	$SU(2)_V$, approx. $SU(2)_R \times SU(2)_L$	$SU(2)_V$
QM, $h \neq 0$	$SU(2)_V$, approx. $SU(2)_R \times SU(2)_L$	$SU(2)_V$

Table 4.1: Chiral symmetry breaking patterns of two-flavor QCD and the quark-meson model.

For the most realistic case of $m_u \neq m_d$, the QCD Lagrangian has no $SU(2)$ symmetry at all. However, the mass difference between m_u and m_d is so small compared to the relevant mass scale in QCD, Λ_{QCD} , that $m_u = m_d$ is a very good approximation [26].

If we choose a gluon potential similar to one of those discussed in Sec. 3.4, we also expect the PQM model to have a deconfining phase transition. However, the similarity between the deconfinement transitions in these two theories is harder to assess a priori, since center symmetry is not a symmetry of either theory, neither at the physical point nor in the chiral limit. In the PQM model there is no gauge-invariance, so speaking about twisted gauge transformations does not make sense, while in QCD the finite quark mass explicitly breaks the center symmetry.

Finally, a natural objection to the PQM model is that we combine fundamental quark and mesonic degrees of freedom, even though mesons in reality are composite

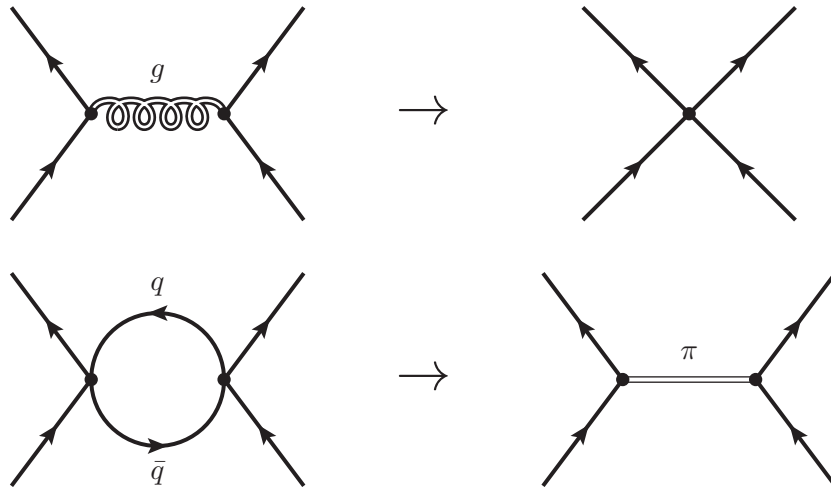


Figure 4.4: Integrating out the gauge fields gives rise to an effective theory where a 4-quark interaction vertex (upper right) replaces the quark-quark interactions that is really mediated by gluons (upper left). Connecting two or more such vertices (lower left) gives rise to an effective meson exchange (lower right). Time should be read as running vertically.

states of quarks. It is not immediately evident that combining separate meson fields with quarks makes sense. However, since we are dealing with a description of quarks without dynamical gauge fields, we cannot expect that the fermionic fields will exhibit bound states and give rise to mesons. Actually, in Sec. 3.2 we saw that a model with non-interacting quarks in a static temporal background gauge field describes baryons in the confined phase and free quarks in the deconfined phase. We did not find any mesons, which justifies the addition of separate meson fields, at least in the confined phase. However, the presence of mesons in the deconfined phase might be puzzling, since we expect bound states to “melt” in the quark-gluon plasma phase. Nevertheless, we can still think of free quarks as interacting via meson exchange. To see why, let us first imagine an effective field theory where we integrate out all the gauge fields so that we get effective 4-quark interactions (such as in the NJL-model [49, 50]). If we connect two such vertices with two quark propagators, we have an effective meson exchange, as illustrated in Fig. 4.4. Thus, it still appears reasonable to consider the exchange of mesons between the quarks in deconfined phase. Nevertheless, the only real justification is to compare the results obtained with the PQM model to lattice data to see if reasonable quantitative and qualitative agreement is achieved, which we do in the following chapter.

Thermodynamics of the PQM and χM Models

We are now ready to investigate the thermodynamics of the one-loop renormalized PQM model in the large- N_c limit. In addition to the case of $\mu > 0$, which is mostly inaccessible to lattice simulations, the intermediate temperature region 130 MeV–400 MeV for $\mu = 0$ is especially interesting. Below roughly 130 MeV a model known as the Hadron Resonance Gas (HRG) model appears to describe QCD thermodynamics well. The model assumes that all hadrons are separate non-interacting degrees of freedom, and comparison with lattice data shows good agreement [91, 92]. For temperatures above roughly 400 MeV, finite-temperature perturbation theory with a method known as hard thermal loops (HTL) can be applied [91–94]. The latter technique also works for non-zero chemical potentials, given that the temperature is high enough [95, 96]. Thus, it is in the intermediate region where HRG and HTL do not work (and the region of $\mu > 0$) that it is the most important for the PQM model to describe correctly. Incidentally, this region is exactly where the deconfinement and chiral phase transitions occur.

We will in the following investigate two different gluonic potentials. The first one is a slightly modified version of the potential proposed by Ratti, Rößner, Thaler and Weise (RRTW) [62], which was discussed in Sec. 3.4. We repeat it here for convenience:

$$\frac{\mathcal{U}_{\text{RRTW}}}{T^4} = -\frac{1}{2}a(T)\Phi\bar{\Phi} + b(T)\ln\left[1 - 6\Phi\bar{\Phi} + 4(\Phi^3 + \bar{\Phi}^3) - 3(\Phi\bar{\Phi})^2\right], \quad (5.0.1)$$

with

$$a(T) = a_1 + a_2\left(\frac{T_0}{T}\right) + a_3\left(\frac{T_0}{T}\right)^2, \quad (5.0.2)$$

$$b(T) = b_1\left(\frac{T_0}{T}\right)^3, \quad (5.0.3)$$

with all the parameters except T_0 as given in the original paper, meaning

$$a_1 = 3.51, \quad a_2 = -2.47, \quad a_3 = 15.2, \quad b_1 = -1.75. \quad (5.0.4)$$

However, we make one modification. In their original paper, Ratti et al. finds that $T_c \approx 215$ MeV when their potential is combined with the NJL model [69].¹ This is ~ 45 MeV higher than what is found in most two-flavor lattice data, as we will discuss in Sec. 5.4. To attempt to correct for this we use the prescription proposed in Ref. [66], which involves including the backreaction of the fermions onto the gluonic sector via a dependence $T_0(N_f)$ in the way that was discussed in Sec. 3.4. With the parametrisation of $T_0(N_f)$ given by (3.4.7), we find

$$T_0 = 208 \text{ MeV} \quad (5.0.5)$$

for $N_f = 2$.

When we in the following mention the PQM model, we mean the PQM model with the potential (5.0.1) with the parameters (5.0.4) and (5.0.5). The other model we investigate comes from a recent publication by Pisarski and Skokov [21], where they construct a chiral matrix model for three quark flavors. The model is similar to the PQM model, but instead of choosing a gluonic potential that is composed of polynomials and logarithms of Φ and $\bar{\Phi}$, the gluonic potential is written directly in terms of the eigenvalues of the matrix background gauge field \mathbf{A}_4 , which is what gives rise to the term ‘‘matrix model’’. Furthermore, the Pisarski-Skokov chiral matrix model, from here on just the χM model, contains a new phenomenological term in the effective potential which causes the quark mass Δ to approach the current quark mass in the high-temperature limit.

In the following we calculate several of the same quantities as Pisarski and Skokov do in Ref. [21], except for various susceptibilities. We adapt the χM model to describe the two light quark flavors only. This makes the model less similar to real QCD, but on the other hand, it allows us to use the results from Chapter 4 to determine the coupling constants of the chiral sector to one loop. This is different from Ref. [21], where they calculate the potential to one loop but match the parameters at tree-level. Furthermore, we extend on the work in Ref. [21] by studying the case $\mu > 0$.

Note that since the strange quark has a constituent mass that is roughly 500 MeV [97], we can hope that our model is not too affected by the omission of the strange quark at low temperatures, since it is reasonable to assume that the strange quark degrees of freedom are ‘‘frozen out’’ for low T .²

5.1 The Gluonic Sector of the χM Model

Let us parameterize the background gauge field \mathbf{A}_4 in the Polyakov gauge as in Sec. 2.7, so that

$$\Phi = \frac{e^{2\pi ir/3}}{3} \left[e^{-2\pi ir} + 2 \cos\left(\frac{2\pi q}{3}\right) \right] \quad (5.1.1)$$

¹They defined the critical temperature via the Polyakov loop.

²This assumes that the constituent mass of the strange quark does not rapidly decrease at the chiral phase transition. This assumption is valid, as lattice data show [98].

for two real degrees of freedom r and q . The gluonic part of the χM model was developed as an effective model for pure $SU(3)$ gauge theory in Refs. [99, 100], where the degrees of freedom of the model are r and q only. The gluonic model consists of two effective potential terms: one is calculated by integrating out all but the condensate mode of \mathbf{A}_4 to one loop in perturbation theory, and one is a phenomenological term modeling the contribution in the non-perturbative regime of pure Yang-Mills theory. We summarize the results in the rest of this section, following Pisarski and Skokov [21].

Define the functions

$$B_1(x) = |x|_{\text{mod}1} (1 - |x|_{\text{mod}1}), \quad (5.1.2)$$

$$B_2(x) = |x|_{\text{mod}1}^2 (1 - |x|_{\text{mod}1})^2, \quad (5.1.3)$$

where $|x|_{\text{mod}1}$ is the modulo 1 operation for a real number x . We define the boundary case so that $0 \leq |x|_{\text{mod}1} < 1$. We for example have $|-0.3|_{\text{mod}1} = 0.7$ and $|1.3|_{\text{mod}1} = 0.3$. Define also

$$\mathcal{V}_1(q, r) = B_1\left(\frac{2q}{3}\right) + B_1\left(\frac{q}{3} + r\right) + B_1\left(\frac{q}{3} - r\right), \quad (5.1.4)$$

$$\mathcal{V}_2(q, r) = B_2\left(\frac{2q}{3}\right) + B_2\left(\frac{q}{3} + r\right) + B_2\left(\frac{q}{3} - r\right). \quad (5.1.5)$$

The one-loop perturbative contribution to the effective potential of pure $SU(3)$ Yang-Mills theory then reads

$$\mathcal{V}_{\text{pt}}(q, r) = \pi^2 T^4 \left[-\frac{8}{45} + \frac{4}{3} \mathcal{V}_2(q, r) \right]. \quad (5.1.6)$$

The term proportional to \mathcal{V}_2 is known as the Weiss potential, and it was first calculated by Weiss [47, 101] and Gross, Pisarski and Yaffe [35]. The first term gives rise to the Stefan-Boltzmann pressure, which is the pressure in a non-interacting system of N massless bosonic degrees of freedom [36]:

$$P_{\text{SB}} = N \frac{\pi^2}{90} T^4 = 2(N_c^2 - 1) \frac{\pi^2}{90} T^4 = \frac{8\pi^4}{45} T^4, \quad (5.1.7)$$

where

$$N = 2(N_c^2 - 1), \quad (5.1.8)$$

is the number of gluonic degrees of freedom, with $N_c^2 - 1$ being the number of gluons and the factor 2 coming from the two independent spin polarizations. Since we saw in Sec. 2.7 that one of the deconfined states is characterized by $r = q = 0$, which gives $\mathcal{V}_2(0, 0) = 0$, we find that the pressure contribution of \mathcal{V}_{pt} goes to the Stefan-Boltzmann value in the high-temperature limit. However, if we only include the perturbative term, the pure glue system will always be deconfined, since confinement is never energetically favored. A fully confined state can for example be characterized by $r = 0$, $q = 1$, and $\mathcal{V}_2(q, 0)$ always increases as function of q when $0 \leq q \leq 1$.

To drive the system to confinement at low temperatures, one adds a phenomenological potential, which is chosen to be of the form

$$\mathcal{V}_{\text{nonpt}}(q, r) = -\frac{8\pi^2}{45}T^2T_d^2 \left[\frac{c_1}{5}\mathcal{V}_1(q, r) + c_2\mathcal{V}_2(q, r) - \frac{2}{15}c_3 \right], \quad (5.1.9)$$

with four fit parameters c_1 , c_2 , c_3 and T_d . At low temperatures this $\sim T^2$ term will dominate over the $\sim T^4$ perturbative term, and with an appropriate choice of the fit parameters it can drive the system to confinement. The T^2 behavior is chosen since it has been observed in lattice data that the subleading contribution to the pressure goes as $\sim T^2$ [102, 103]. The parameters c_1 and c_3 are chosen so that the pressure in the confined phase of the pure gauge theory is zero and that a phase transition happens at T_d . The former is an approximation, but it is reasonable since the pressure of the confined phase in $SU(3)$ gauge theory is very low compared to the deconfined phase, as lattice data show [57]. Furthermore, T_d is chosen to be $T_d = 270$ MeV, which is roughly the deconfinement temperature in $SU(3)$ gauge theory [57]. Then only c_2 remains as a fit parameter. It is determined by fitting the interaction measure $(\mathcal{E} - 3P)/T^4$ predicted by the full gluonic potential,

$$\mathcal{U}_{\chi M} = \mathcal{V}_{\text{pt}} + \mathcal{V}_{\text{nonpt}}, \quad (5.1.10)$$

to lattice data. The result is

$$c_1 = 0.315, \quad c_2 = 0.830, \quad c_3 = 1.13. \quad (5.1.11)$$

The potentials $\mathcal{V}_{\text{nonpt}}(q, r)/(T_d^2T^2)$ and $\mathcal{V}_{\text{pt}}(q, r)/T^4$ are shown in Fig. 5.1. Both potentials have multiple degenerate minima corresponding to different center phases. The combination $q = r = 0$, which gives $\Phi = 1$, is a minimum for \mathcal{V}_{pt} and a maximum for $\mathcal{V}_{\text{nonpt}}$. For $q = 1, r = 0$, which corresponds to $\Phi = 0$, it is opposite. For high temperatures \mathcal{V}_{pt} (left) dominates while for low temperatures $\mathcal{V}_{\text{nonpt}}$ (right) dominates. For comparison we show the thermal quark potential $\mathcal{U}_{q,T}(q, r)$ at $T = 100$ MeV and $\Delta = 300$ MeV in Fig. 5.2. We see that this potential, whose qualitative shape is mostly unchanged for other values of Δ or T , drives (q, r) towards $q = r = 0$, which corresponds to deconfinement. Thus, it is reasonable that the addition of quarks to pure gauge theory lowers the deconfinement temperature.

5.2 A Phenomenological Quark Term

In addition to the (partly) phenomenological gluonic sector, Pisarski and Skokov add to the χM model a phenomenological quark term not usually found in the PQM model, which in the two-flavor case is given by

$$\mathcal{U}_{q,\text{cur}}(\Delta, q, r, T, \mu) = -m_{\text{cur}} \frac{\partial}{\partial \Delta} \mathcal{U}_{q,T}, \quad (5.2.1)$$

were m_{cur} is the current quark mass. This purely phenomenological term is added to achieve that $\lim_{T \rightarrow \infty} \Delta(T) = m_{\text{cur}}$, since without it we have $\lim_{T \rightarrow \infty} \Delta(T) = 0$. Let us

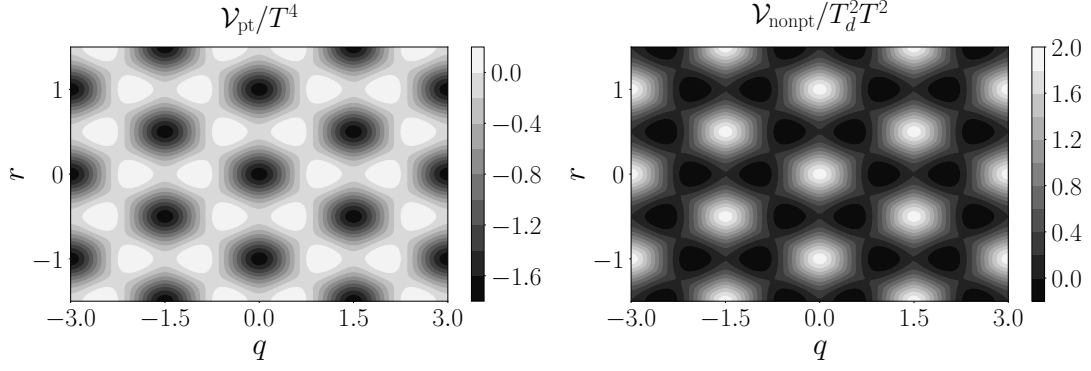


Figure 5.1: Contour plots of the perturbative (left) and non-perturbative (right) contributions to the gluonic potential in the χM model.

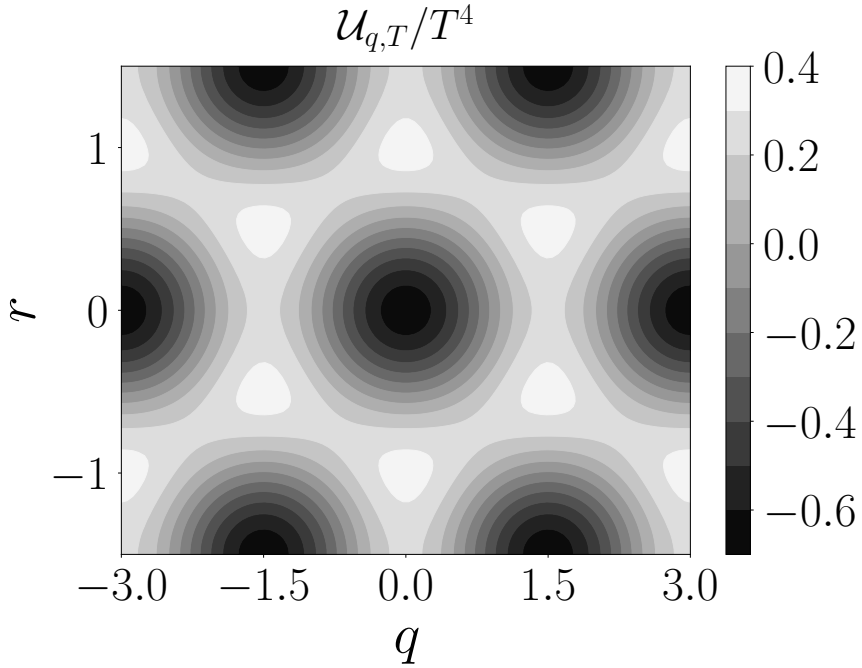


Figure 5.2: Contour plot of $\mathcal{U}_{q,T}(q, r)$ for $\mu = 0$, $\Delta = 300$ MeV, $T = 100$ MeV.

show how this term works: In the high-temperature limit we expect $\Phi = \bar{\Phi} = 1$. Let us furthermore assume that $\mu = 0$ and that $T \gg \Delta$. It is possible to expand $\mathcal{U}_{q,T}$ for $\mu = 0$, $\Phi = \bar{\Phi} = 1$ in decreasing powers of T and increasing powers of Δ , with the result being³

$$\mathcal{U}_{q,T}/N_f N_c = -4T \int \frac{d^3 p}{(2\pi)^3} \ln [1 + e^{-\beta\omega_{\mathbf{p}}}] \approx -\frac{7\pi^2}{180} T^4 + \frac{T^2 \Delta^2}{12} + \mathcal{O}\left(\Delta^4 \ln \frac{\Delta}{T}\right). \quad (5.2.2)$$

Thus, to leading order we find

$$\mathcal{U}_{q,\text{cur}}/N_f N_c = -\frac{1}{6} m_{\text{cur}} T^2 \Delta + \mathcal{O}\left(\Delta^3 \ln \frac{\Delta}{T}\right). \quad (5.2.3)$$

Since we assume high temperatures, we consider the potential only up to subleading temperature dependence $\sim T^2$. Furthermore, we assume that $\Delta \ll T$, which we expect in the high-temperature phase where chiral symmetry is approximately restored. Using this we keep only leading and subleading terms in Δ . Thus, taking Ω as given in (4.6.3) and adding \mathcal{U}_{cur} , we find that the effective potential goes as

$$\frac{\Omega}{N_f N_c} \approx -\frac{7\pi^2}{180} T^4 + \frac{T^2 \Delta^2}{12} - \frac{1}{6} m_{\text{cur}} T^2 \Delta + \mathcal{O}(\Delta) + \mathcal{O}\left(\Delta^4 \ln \frac{\Delta}{T}\right), \quad (5.2.4)$$

for high temperatures, where the neglected $\mathcal{O}(\Delta)$ term is the leading term $\sim h\Delta$ from the mesonic potential. Minimizing (5.2.4) with respect to Δ , we immediately find

$$\Delta = m_{\text{cur}}, \quad (5.2.5)$$

and we thus expect $\Delta \rightarrow m_{\text{cur}}$ in the high-temperature limit.

When we later in this chapter investigate the thermodynamics of the PQM and χM models, we will assess the effects of $\mathcal{U}_{q,\text{cur}}$ on thermodynamics. Due to its ad hoc nature, it should preferably affect the thermodynamics minimally while still achieving its purpose of ensuring the constituent quark mass to approach the current quark mass in the (approximately) chirally restored phase.

5.3 The Complete PQM and χM Models

We now have all the ingredients needed to investigate the thermodynamics of the PQM and χM models at one loop in the large- N_c limit. For a given temperature we numerically solve

$$\frac{\partial \Omega}{\partial r} = 0, \quad \frac{\partial \Omega}{\partial q} = 0, \quad \frac{\partial \Omega}{\partial \Delta} = 0, \quad (5.3.1)$$

requiring that we have a minimum, where Ω is one of the potentials

$$\Omega_{\chi M} = \mathcal{U}_{q,T}(\Delta, r, q, T, \mu) + \mathcal{U}_{q,\text{vac}}(\Delta) + \mathcal{U}_{\chi}(\Delta) + \mathcal{U}_{\chi M}(r, q, T) + \mathcal{U}_{q,\text{cur}}(\Delta, r, q, T, \mu) - P_0, \quad (5.3.2)$$

$$\Omega_{\text{PQM}} = \mathcal{U}_{q,T}(\Delta, r, q, T, \mu) + \mathcal{U}_{q,\text{vac}}(\Delta) + \mathcal{U}_{\chi}(\Delta) + \mathcal{U}_{\text{RRTW}}(r, q, T) + \mathcal{U}_{q,\text{cur}}(\Delta, r, q, T, \mu) - P_0. \quad (5.3.3)$$

³Since the Taylor series at $\Delta = 0$ does not exist, it is more complicated than expected to derive this series. We refer the reader to Refs. [39, 104] for derivations.

P_0 is a constant. The explicit forms of $\mathcal{U}_{q,T}$, $\mathcal{U}_{q,\text{vac}}$, \mathcal{U}_χ are given in (4.6.4)–(4.6.6), $\mathcal{U}_{\chi M}$ in (5.1.10), $\mathcal{U}_{\text{RRTW}}$ in (5.0.1) and $\mathcal{U}_{q,\text{cur}}$ in (5.2.1). We also add the phenomenological term $\mathcal{U}_{q,\text{cur}}$ to the PQM model, for the same reason that it is added to the χM model and for better comparison between the models. The parameters q and r are assumed real so that the Euclidean gauge field is Hermitian and $\bar{L} = L^\dagger \Rightarrow \bar{\Phi}^* = \bar{\Phi}$. We will get back to the more complicated case of $\mu \neq 0$ later in the chapter.

The parameter P_0 is a constant that we add to the effective potential so that the condition

$$P(T = \mu = 0) = 0, \quad (5.3.4)$$

is satisfied. This constant will turn out to be small and has a negligible effect on the thermodynamics. However, it makes thermodynamic quantities normalized with $1/T^4$ better behaved at temperatures close to zero.

Once we determine Δ , r and q as functions of T and μ , we can find Ω as a function of T and μ only. We can then calculate the pressure P , quark density $n_q = \langle N \rangle / V$, energy density \mathcal{E} and interaction measure $(\mathcal{E} - 3P)$ as functions of μ and T via the relations

$$P(T, \mu) = -\Omega, \quad (5.3.5)$$

$$n_q(T, \mu) = \frac{\partial P}{\partial \mu}, \quad (5.3.6)$$

$$\mathcal{E}(T, \mu) = \mu n_q - P + T \frac{\partial P}{\partial T}. \quad (5.3.7)$$

To determine the one-loop couplings we set

$$m_q = 300 \text{ MeV}, \quad (5.3.8)$$

$$m_\pi = 140 \text{ MeV}, \quad (5.3.9)$$

$$m_\sigma = 500 \text{ MeV}, \quad (5.3.10)$$

$$f_\pi = 93 \text{ MeV}, \quad (5.3.11)$$

which input in (4.4.12)–(4.4.15) yield

$$\lambda_0 = 61.5, \quad (5.3.12)$$

$$m_0 = 449 \text{ MeV}, \quad (5.3.13)$$

$$g_0 = 3.23, \quad (5.3.14)$$

$$h_0 = (121 \text{ MeV})^3. \quad (5.3.15)$$

These are the one-loop values of the running couplings in the $\overline{\text{MS}}$ scheme at the renormalization scale

$$\Lambda_0^2 = m_q^2 \exp \left[-\text{Re } C(m_\pi^2) - m_\pi^2 \text{Re } C'(m_\pi^2) \right] = (289 \text{ MeV})^2. \quad (5.3.16)$$

The value of the constituent quark mass is roughly one third of the nucleon mass, while the value of the sigma mass corresponds to the mass of the $f_0(500)$ resonance, which has a measured mass in the range from 400 MeV to 550 MeV [8]. The value $f_\pi = 93 \text{ MeV}$

corresponds roughly to the measured value of $f_\pi = 92.2$ [8].⁴ We round it up to agree with numerous other papers on the QM model. For the current quark mass we choose

$$m_{\text{cur}} = 3 \text{ MeV}. \quad (5.3.17)$$

This is roughly the average of the current quark masses for the u and d quarks, which by the Particle Data Group are reported to be $m_u = 2.2 \text{ MeV}$ and $m_d = 4.7 \text{ MeV}$ in the $\overline{\text{MS}}$ -scheme at the renormalization scale $\Lambda = 2 \text{ GeV}$.

If we determine the couplings at tree-level using (4.4.1)–(4.4.4), we find $\lambda_{\text{tree}} = 79.9$, $m_{\text{tree}} = 309 \text{ MeV}$, $g_{\text{tree}} = 3.23$ and $h_{\text{tree}} = (122 \text{ MeV})^3$. Thus, we see that λ and m are altered quite significantly by bosonic self-energy corrections.

5.4 QCD Lattice Results

To compare model predictions with lattice data, we should understand what lattice simulations predict. Some works indicate that the chiral and deconfinement phase transitions coincide [105, 106], while others find the deconfinement transition to happen at 25–30 MeV higher temperatures [107–109]. However, it is hard to unambiguously define whether the transitions coincide or not, since the transition temperatures are not well defined.⁵ This is because at the physical point neither the deconfinement nor the chiral phase transitions are real thermodynamic phase transitions, but rather crossovers. The deconfinement transition is also a crossover in the chiral limit.

For the location of the chiral transition, there seems to be better agreement. For 2+1 flavors, meaning two light flavors and one heavier strange flavor, the chiral transition is found to occur at approximately $T_c^{(2+1)} = (155 \pm 9) \text{ MeV}$ by the HotQCD collaboration [98, 110]. Within the uncertainty this agrees with the findings of Aoki et al. [107, 108] and the Wuppertal-Budapest collaboration [17]. For two flavors the chiral phase transition is found to be $T_c = (171 \pm 4) \text{ MeV}$ by the CP-PACS collaboration [111], $T_c = (174 \pm 3 \pm 6) \text{ MeV}$ by the QCDSF-DIK collaboration [106] and $T_c = (172 \pm 3 \pm 6) \text{ MeV}$ by Bornyakov et al. [112]. Note that for two flavors, Ref. [106] finds that the chiral and deconfinement transitions coincide.

For comparison of thermodynamics at zero chemical potential, our primary sources for (2+1)-flavor lattice simulations are the results from the Wuppertal-Budapest [91] and HotQCD [92] collaborations that were published in 2014. Several older papers on (2+1)-flavor simulations exist, but since inconsistencies and disagreements between various data sets were resolved more recently [17], we use only these two papers for (2+1)-flavor thermodynamics. For two flavors, data are more scarce, and we use results from the CP-PACS collaboration from 2001 [113].

For data on the Polyakov loop as a function of temperature for (2+1) flavors we use data from the 2013 publication by Bazavov and Petreczky [114] and the 2010 publication

⁴The Particle Data Group's definition of f_π differs by a factor $\sqrt{2}$ from our convention, and they find $f_\pi = 130.41 \text{ MeV}$ [8].

⁵Not well defined in the sense that calculating the inflection point for different observables give different critical temperatures.

by Cheng et al. [115]. For data on the Polyakov loop with two flavors we use data from Kaczmarek and Zantow from 2005 [116].

Data on thermodynamics from lattice simulations at finite chemical potential also exist. This relies on a Taylor series expansion of the fermion determinant in powers of μ/T around $\mu/T = 0$. In the following we compare model calculations at nonzero quark chemical potentials with lattice simulations performed to order $\mathcal{O}((\mu/T)^6)$ in the effective potential by Allton et al. in 2005 [117].

Since we expect a ~ 20 MeV difference in the critical temperature between the (2+1)-flavor lattice data and the two-flavor lattice and model data, we plot thermodynamic quantities against T/T_c , where T_c in the lattice data is taken to be $T_c^{(2+1)} = 155$ MeV whenever the data are not already given as a function of T/T_c .⁶ This allows us to more easily assess the similarities and differences between the two- and (2 + 1)-flavor data which is not related to the obvious difference in critical temperature. Furthermore, we plot quantities normalized to the Stefan-Boltzmann (SB) pressure

$$P_{\text{SB}} = \left(8 \frac{\pi^2}{45} + 2N_c N_f \frac{7\pi^2}{180} \right) T^4, \quad (5.4.1)$$

$2N_c N_f$ is the number of fermionic degrees of freedom, with the factor 2 coming from the spin.⁷ The Stefan-Boltzmann pressure is simply the pressure of a non-interacting gas of bosons and fermions in the high-temperature limit where the particles can be assumed massless [36]. By dividing out the Stefan-Boltzmann pressure, we can factor out the difference in the pressure in the two- and (2 + 1)-flavor data that stems from the fact that they have different asymptotic values for the pressure at high T . It is also useful since the two-flavor data from Ref. [113] is not extrapolated to the continuum limit, but the Stefan-Boltzmann pressure, whose value is different from (5.4.1) in a finite discretization of space-time, is still estimated. Thus P/P_{SB} from a finite lattice discretization that is not continuum extrapolated can still be compared to model and continuum extrapolated lattice data.

Finally, a comment on the acquisition of the lattice data is warranted. In the data by HotQCD and Wuppertal, Refs. [91, 92], all thermodynamical quantities are provided in tables. However, in the older papers the data are extracted from plots with a data mining tool known as WebPlotDigitizer [118].⁸ It is found that the uncertainty in the y -value of each data point caused by extracting the data with this tool is well below 1% of L_y , where L_y is the total length of the y -axis in the plot, i.e. the difference between the maximal and minimal values displayed on the y -axis. For the purpose of comparing with an effective model without any finely tuned parameters, this uncertainty is entirely inconsequential.

⁶The two-flavor data we consider is already given as T/T_c .

⁷This means that the (2 + 1) and two-flavor data are normalized with different factors.

⁸<https://automeris.io/WebPlotDigitizer/>

5.5 Numerical Results: PQM and χM Model Thermodynamics at $\mu = 0$

We solve for the minimum of the effective potential with a global optimization method known as Basin-Hopping [119] using a routine implemented in the SciPy Optimize library for Python [120].⁹ Using this method we obtain the pressure, energy density, interaction measure and order parameters as functions of temperature for $\mu = 0$. When optimizing we always have that a global minimum is located at $r = 0$, which we choose so that Φ and Ω is real.

We restrict $\Delta \in [0, \Delta_c]$, where Δ_c is an upper bound on Δ specifying the validity range of our model. This is needed, possibly because we have neglected mesonic fluctuations, since the effective potential is unbounded from below for $\Delta \in [0, \infty]$. In the large- Δ limit we have that the dominating term comes from the renormalized quark vacuum energy, which goes as $\sim -\Delta^4 \ln \Delta$, as seen from (4.6.5). However, mesonic fluctuations would contribute with terms $\mathcal{O}(+\Delta^4 \ln \Delta)$, which might have kept the potential bounded from below. Thus, in neglecting mesonic fluctuations, we always expect an upper validity range on Δ in the effective models. With mesonic fluctuations it might or might not be needed.

Figure 5.3 shows the effective potential as function of Δ for the χM model at $\mu = T = 0$ and $q = r = 0$, and with the parameters as discussed previously. We see that the effective potential is non-increasing above roughly $\Delta = 500$ MeV, which we use as our value for Δ_c . We also see that if we inconsistently match the coupling constants of the theory at tree-level, the potential would be qualitatively different, and no local minimum would be present in the effective potential for the m_σ we have chosen.

Figures 5.4 and 5.5 show the order parameters $\Delta(T)/\Delta_0$, $\Phi(T)$ and their derivatives with respect to T , where $\Delta_0 = \Delta(T = 0)$. We see in Fig. 5.4 that chiral symmetry is approximately restored at temperatures higher than ~ 200 MeV in both models. We point out that Δ does not go to zero at high temperatures, but rather towards $\Delta \approx m_{\text{cur}}$ (see Fig. 5.13), as expected from the discussion in Sec. 5.2. We find that the χM model reaches full deconfinement at $T \sim 250$ MeV, while the PQM model reaches $\Phi = 1$ more slowly and is in a “semi-deconfined” state between roughly 200 MeV to 400 MeV.

From Fig. 5.5 we see that the pseudocritical temperatures for the chiral and deconfinement transitions coincide for both models, with the inflection points of Δ being located at

$$T_c^{\chi M} = 181_{-9}^{+6} \text{ MeV}, \quad (5.5.1)$$

$$T_c^{\text{PQM}} = 169_{-3}^{+3} \text{ MeV}. \quad (5.5.2)$$

The uncertainties are obtained by varying the sigma mass within the uncertainty range, which is 400 MeV to 550 MeV. The lowest m_σ corresponds to the lowest temperature and vice versa. We see that T_c of the two models differ by 11 MeV, but the uncertainty ranges of both models overlap with the uncertainty range from the lattice,

⁹<https://docs.scipy.org/doc/scipy/reference/optimize.html>

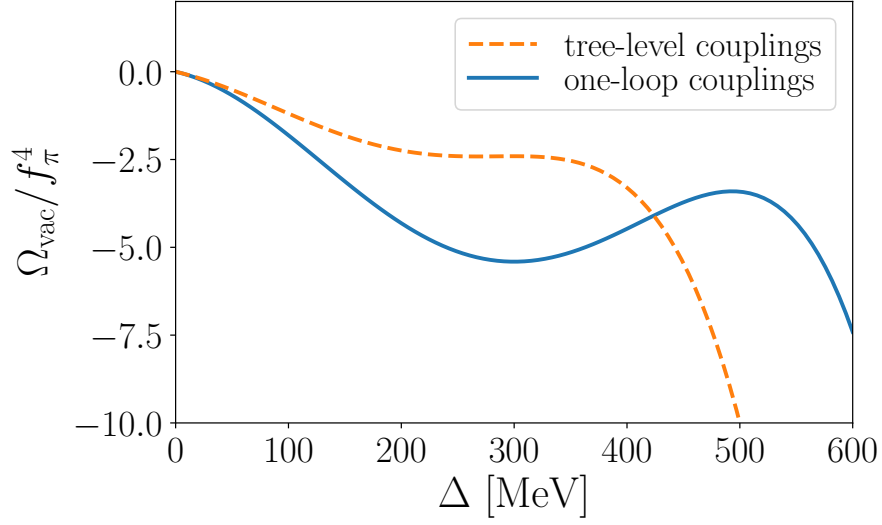


Figure 5.3: The χM model one-loop effective potential in the large- N_c limit for $q = r = 0$ and $T = \mu = 0$ with one-loop and tree-level determination of the couplings.

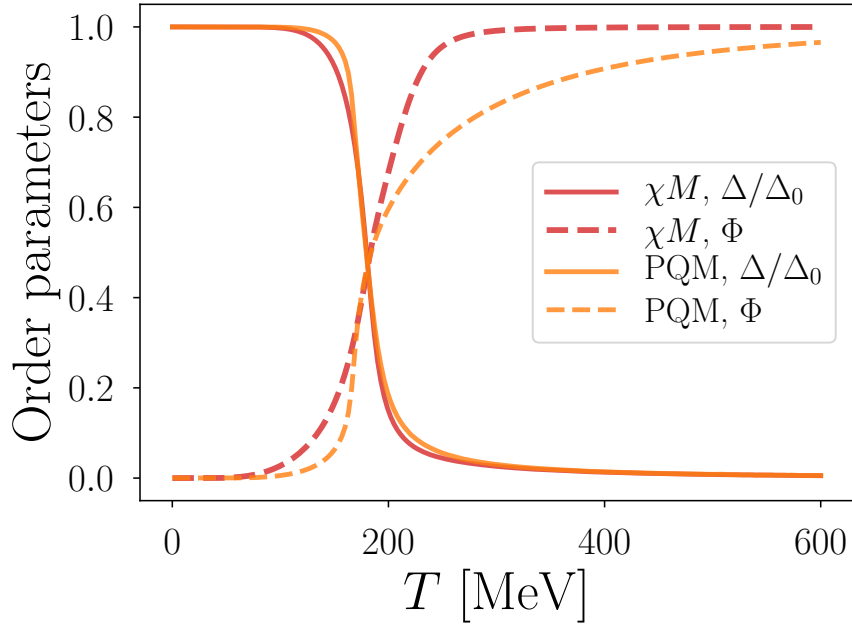


Figure 5.4: Order parameters in the χM and PQM models as function of temperature.

$T_c^{\text{lat}} = (172 \pm 3 \pm 6) \text{ MeV}$ [112]. However, the PQM model is in best agreement with lattice data for the upper sigma mass, while for the χM model it is opposite.

The coinciding of the phase transitions is natural in the PQM and χM models for

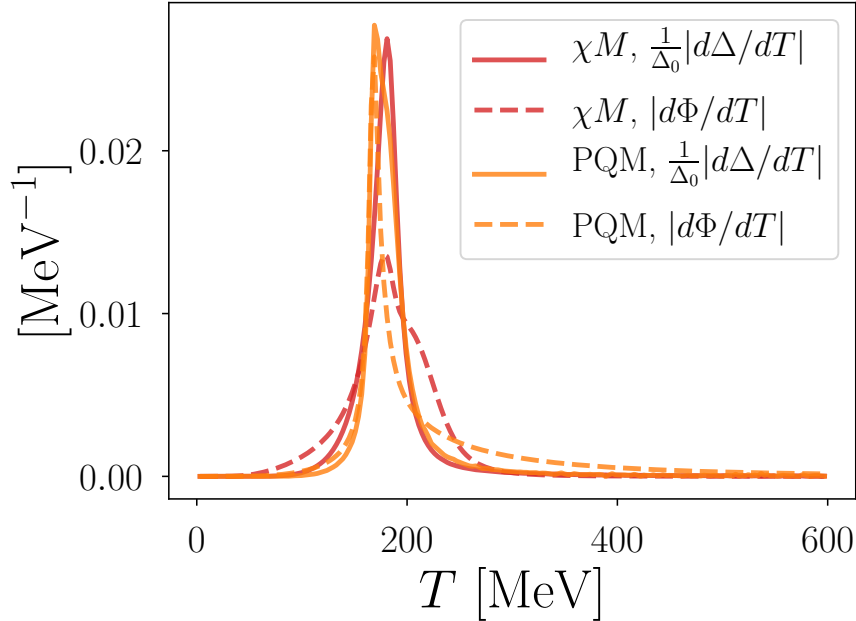


Figure 5.5: Absolute value of the differentiated order parameters as function of T . The peak locations correspond to the pseudocritical transition temperatures.

the following reason: Φ and Δ at some T are obtained by maximizing the pressure $P(\Phi, \Delta, T) = -\Omega(\Phi, \Delta, T)$ with respect to Δ and Φ .¹⁰ Below T_0 (or T_d) the gluonic contribution is pushing Φ towards zero, while the quark thermal contribution is pushing Φ towards 1, and there is competition between the two. However, when $\Delta \gg T$ the thermal contribution of the quarks to the pressure is Boltzmann-suppressed, and the pressure gained from the thermal quark term by increasing Φ is small, since we then are deconfining quark degrees of freedom that are anyway frozen out. Thus, the energy cost from the gluonic potential dominates. However, once Δ is driven to be equal to or smaller than T , the quark degrees of freedom become active (no longer Boltzmann-suppressed), and there is a sizeable potential pressure gain in deconfining them. Thus, once $\Delta < T$ it becomes much more energetically favorable to increase Φ . Hence, we expect that Φ undergoes a transition once Δ does, given that the gluonic potential is not too stiff. The argument does not work as well in reverse since the mesonic potential turns out to be too dominating at low T . We can see this as follows: we obtain the standard QM model without the Polyakov loop by setting $\mathbf{A}_4 = 0$, which gives $\Phi = \bar{\Phi} = 1$. We can view this as the PQM model that is deconfined already from $T = 0$. But the QM model displays a chiral phase transition at temperatures around $T = 150$ MeV to 200 MeV [81, 121, 122] and not already at $T = 0$. Thus, the backreaction of Φ onto Δ is not as strong. However, since the natural chiral transition temperature, meaning the transition temperature in

¹⁰Remember that we have $\Phi = \bar{\Phi}$.

the QM model, is below the natural deconfinement transition temperature, meaning the transition temperature T_0 or T_d in the pure gluonic model, we will have that the chiral condensate brings with it the Polyakov loop. If T_0 or T_d were lower than the natural chiral transition temperature, we would not expect the reverse to happen. We indeed verify this in Sec. 6.14

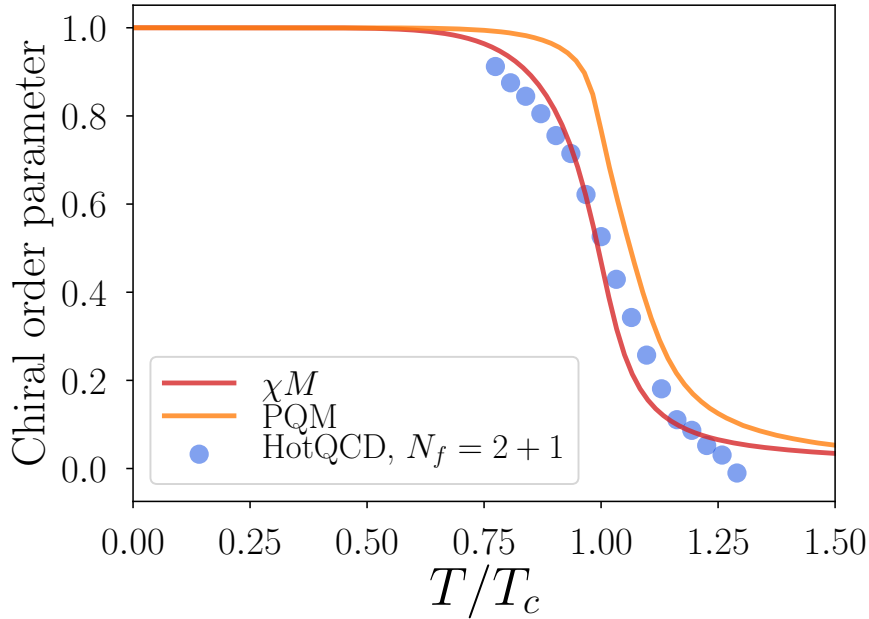


Figure 5.6: The chiral order parameter in the effective models compared with lattice data from Ref. [92].

In Figs. 5.6 and 5.7 we compare the (normalized) order parameters with the lattice results. We see that the χM model agrees fairly well with the $(2+1)$ -lattice data, while in the PQM model the chiral condensate appears to drop slightly later. However, the apparent difference between the two models is largely due to the sensitive nature of the definition of T_c as the inflection point of Δ . If we look at Fig. 5.6 we see that the chiral condensates of the PQM and χM models are nearly identical as functions of T (as opposed to T/T_c). One qualitative difference between model and lattice results is that the chiral order parameter on the lattice goes down to approximately zero shortly after the transition temperature. However, we have no particular reason to assume that the high-temperature asymptotic behavior of Δ , which is the constituent quark mass at a given temperature, should be the same as for the QCD chiral condensate $\langle \bar{\psi}\psi \rangle$.

For the Polyakov loop we find that $\Phi(T)$ in $(2+1)$ -flavor lattice data rises significantly slower than in model calculations. The two-flavor data agree well with the PQM model, while Φ in χM model rises significantly faster than in two-flavor lattice data also. Both models exhibit a fast rise of Φ around the transition temperature, and this behavior is not seen $(2+1)$ -flavor lattice data. Before proceeding to discuss the potential reason for this,

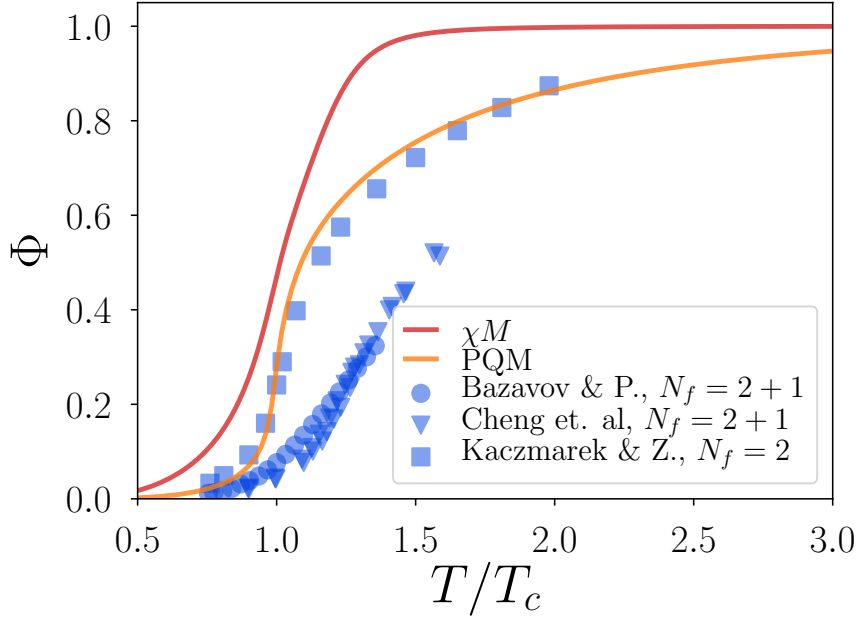


Figure 5.7: The Polyakov loop in the effective models compared with lattice data from Refs. [114–116].

a comment on the two-flavor data from Kaczmarek and Zantow [116] is warranted. In their paper they give the Polyakov loop as function of T/T_c and estimate the unusually high value $T_c = (202 \pm 4)$ MeV. If we plot their data and the model data against T , the two-flavor and $(2 + 1)$ -flavor lattice data agree to a much greater extent, while the agreement with the models become significantly worse. This is shown in Fig. 5.8. Unless there is some reason why Φ should rise faster in two-flavor data, the strong disagreement between the two- and $(2 + 1)$ -flavor lattice data in Fig. 5.7 indicates that Fig. 5.8 shows the more accurate picture and thus that both the PQM and χM models show a too fast rise in the Polyakov loop.

The fast rise of Φ is also present in the original $(2 + 1)$ -flavor χM model by Pisarski and Skokov. It is natural to assume that the nonperturbative contribution to $\mathcal{U}_{\text{glue}}$ is the problem. However, when they in Ref. [21] modify the nonperturbative gluonic potential to obtain better agreement with Φ from the lattice, the agreement for various susceptibilities and thermodynamic quantities is ruined. They let the parameters c_1 and c_2 in the non-perturbative potential (5.1.9) have a more general T -dependence by making the replacement

$$T^2 c_1 \rightarrow \alpha_1 T + \beta_1 T^2 + \gamma_1 T^3, \quad (5.5.3)$$

$$T^2 c_2 \rightarrow \alpha_2 T + \beta_2 T^3 + \gamma_2 T^3. \quad (5.5.4)$$

Then, after imposing the same conditions as for the original potential, namely that in the pure gauge theory $T_c = T_d$ and that the pressure vanishes at T_d , they fit the

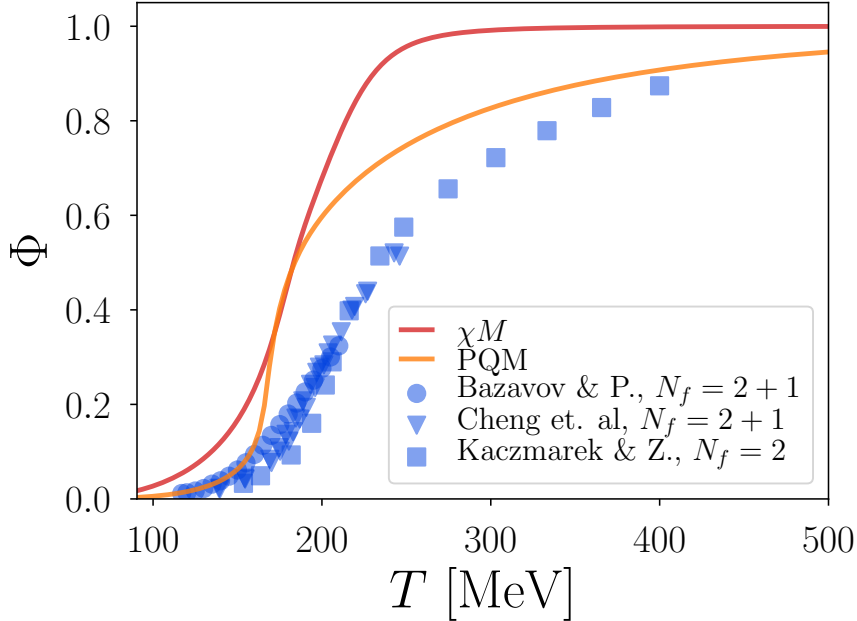


Figure 5.8: The Polyakov loop in the effective models compared with lattice data from Refs. [114–116]. The data from Ref. [116] is converted to be given as a function of T instead of T/T_c by setting $T_c = 202$ MeV, which is the value estimated in the paper.

new free parameters so that the Polyakov loop agrees with the lattice. However, as pointed out, this ruins the thermodynamics of the model. The comparison of the χM model with the PQM model in Fig. 5.7 hints to the fact that it is the choice of the Polyakov loop potential in the χM model that is the problem however, since in the PQM model we obtain better agreement with Φ on the lattice while still also obtaining equally good or better agreement with lattice data for all thermodynamic quantities (see the following). We can imagine that we should choose a qualitatively different form of the non-perturbative potential contribution. Two potentials which both can fit pure gauge theory well might still behave differently when combined with quarks.

Let us now turn to thermodynamics. Figure 5.9 shows the comparison between the SB-normalized pressure in lattice and model data, where the nearly invisible error bands are obtained by varying the sigma mass in its uncertainty range. Both the PQM and χM models show reasonable agreement with lattice data above $T = T_c$, although with a pressure lower than in data. Below and around $T = T_c$ the PQM model appears to have a pressure that is significantly lower than what lattice data show. However, below and around T_c we expect mesons to exist and contribute to the pressure, and by neglecting mesonic fluctuations in the model calculations, we have underestimated the pressure. Since the pions have masses of ~ 140 MeV below T_c while the quarks have masses of ~ 300 MeV, we expect that the mesons would provide a significant contribution to the pressure in this range. For temperatures below T_c the agreement with the χM model

is worse, since there is a small but nonzero pressure causing P/P_{SB} to blow up for low temperatures due to the $P_{\text{SB}} \propto T^4$ dependence. However, this does not mean that the pressure diverges or that it is large. It only means that a small non-zero pressure exists for $T > 0$. This pressure is insignificant, as we see if we compare the pressure of the χM and the PQM models without SB-normalizing, which is done in Fig. 5.10.

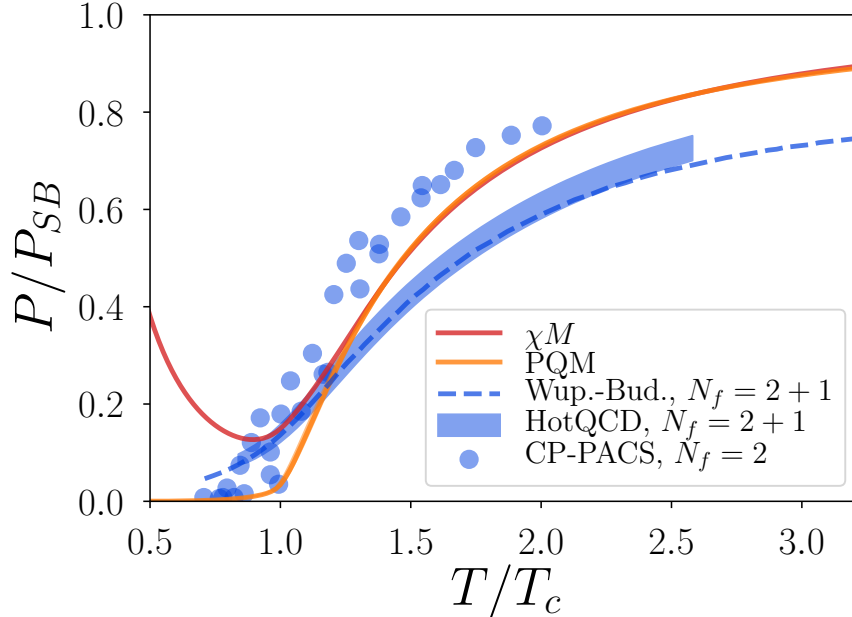


Figure 5.9: Boltzmann-normalized pressure in the χM and PQM model compared to lattice data from Refs. [91, 92, 113].

When comparing the pressure of the $(2 + 1)$ -flavor data to the two-flavor data, we see that the two-flavor model and lattice data are closer to the SB limit at temperatures above the critical temperature. This is expected since the strange quarks constitute degrees of freedom which are partly “frozen out” out at temperatures just above T_c due to their large mass. While the light quarks become nearly massless above T_c and their contribution to the pressure become close to the SB-value, the strange quark always has a mass that is at least equal to its current quark mass, which is of the order ~ 100 MeV [8]. Furthermore, the strange quark chiral condensate goes to zero much slower than the light quark chiral condensate [98], so that the strange quarks still have a large constituent quark mass just above T_c . Thus, it is expected that the SB limit is reached at higher temperatures in $(2 + 1)$ -flavor QCD than two-flavor QCD since significantly higher temperatures must be reached before the strange quark has a negligible mass. If we plot P/T^4 instead of P/P_{SB} , the pressure in the two-flavor model and $(2 + 1)$ -flavor lattice data agree well.¹¹

¹¹Remember that two-flavor and $(2+1)$ -flavor data are normalized with different Boltzmann pressures.

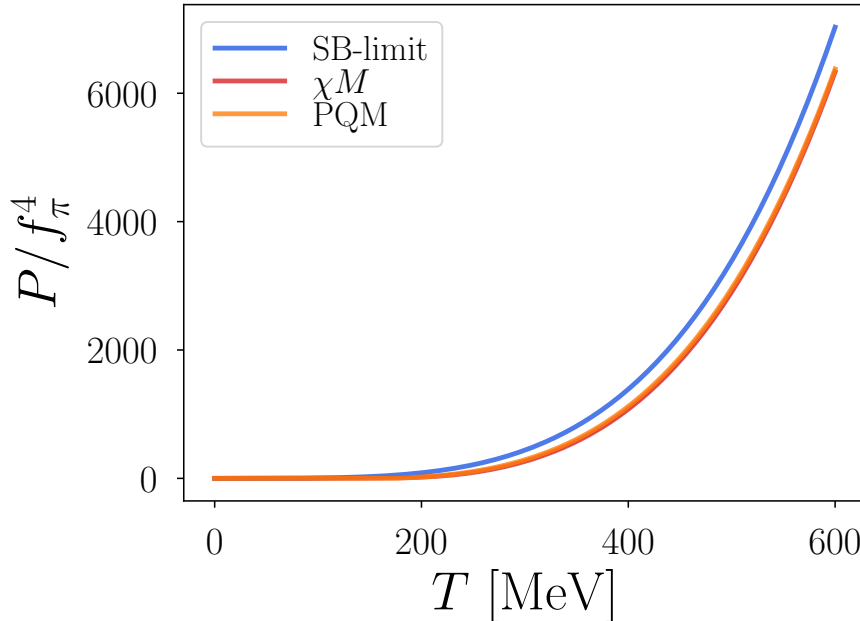


Figure 5.10: Pressure divided by f_{π}^4 in the χM and PQM models compared to the SB-limit.

For the interaction measure I and energy density \mathcal{E} , both normalized by $\mathcal{E}_{\text{SB}} = 3P_{\text{SB}}$ and shown in Figs 5.11 and 5.12 (with error bands obtained in the same way as for the pressure), we find fairly good agreement between the PQM model and two-flavor lattice data up to $T \sim 1.5T_c$. The peak of the interaction measure in the χM model is shifted to higher values than what is seen in the PQM model and two-flavor lattice data. The χM model also has an interaction measure that is negative for low temperatures and a peak that is too low.

For temperatures above $1.5T_c$ there are a few data points in the two-flavor lattice data which show a peculiar drop in the energy density. One possible explanation is that statistical errors cause the drop. The $(2+1)$ -flavor simulations and a more recent two-flavor simulation in Ref. [123] do not show this drop in energy density.¹² The drop in energy density is naturally also associated with a drop in the interaction measure above $T = 1.5T_c$, which is not seen in either model.

Given Figs. 5.4–5.11, we see that both models exhibit the essential qualitative features of QCD: chiral and deconfinement phase transitions. Furthermore, except for the Polyakov loop, there also appears to be reasonable quantitative agreement with lattice data, especially for the PQM model. We remind that except for the Polyakov loop potentials that are fitted to $SU(3)$ gauge theory without quarks, there is no fitting in the models.

¹²The two-flavor simulation in Ref. [123] uses an unphysical pion mass of $m_{\pi} \geq 360$, which is the reason it is not used for comparison with the models.

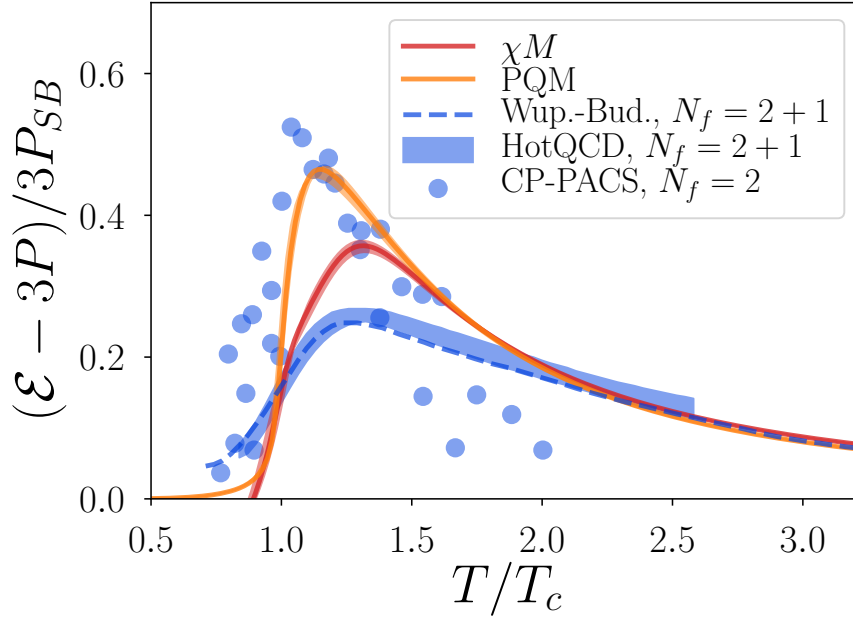


Figure 5.11: SB-normalized interaction measure in the effective models compared to lattice data from Refs. [91, 92, 113].

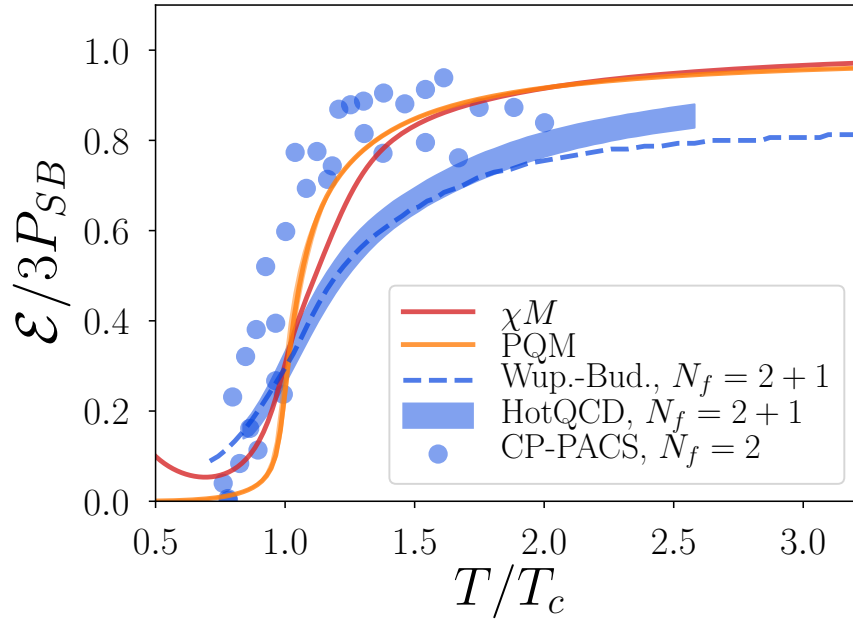


Figure 5.12: SB-normalized energy density in the effective models compared to lattice data from Refs. [91, 92, 113].

Before proceeding to study the models at a nonzero chemical potential, we should comment on the significance of two aspects which are untypical about our study: the phenomenological quark term and the one-loop determination of the couplings.

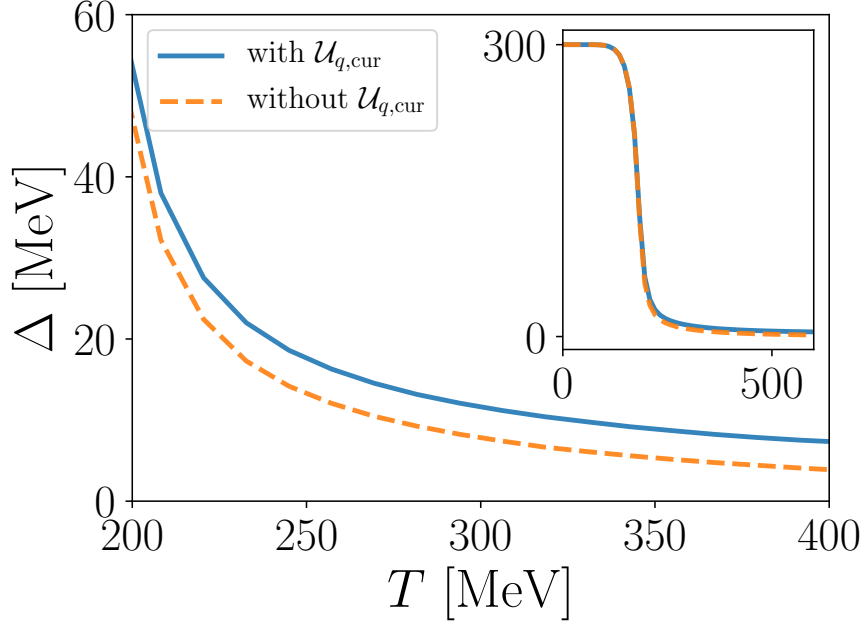


Figure 5.13: Comparison of $\Delta(T)$ in the PQM model with and without the phenomenological quark term.

We find that $\mathcal{U}_{q,\text{cur}}$ has only the effect of changing the high-temperature behavior of $\Delta(T)$, while the thermodynamics for all purposes is unaffected. $\Delta(T)$ is shown in Fig. 5.13 for the PQM model both with and without the term included. Below $T \approx 200$ MeV, Δ is practically unaffected. The inclusion of $\mathcal{U}_{q,\text{cur}}$ has no measurable effect on T_c , and when we plot the pressure, energy density and interaction measure with and without $\mathcal{U}_{q,\text{cur}}$ we find no visible difference. For this reason we omit $\mathcal{U}_{q,\text{cur}}$ in the section where we study the effective models at $\mu > 0$. This is because the numerical evaluation of $\mathcal{U}_{q,\text{cur}}$ is fairly intensive, and the minimization of the effective potential requires a large number of function evaluations. We will instead live with the fact that the quark mass goes towards zero for high temperatures which, as we have pointed out, is irrelevant for thermodynamics.¹³

When it comes to the couplings, we find that for low sigma masses it does not even make sense to consider the model with tree-level couplings combined with one-loop corrections to the potential. This is because with tree-level couplings we find that the point $\Delta = m_q = 300$ MeV at $T = 0$ corresponds to an inflection point rather than a

¹³Due to the μ -dependence of $\mathcal{U}_{q,\text{cur}}$ it contributes to the quark density as $-\frac{\partial \mathcal{U}_{q,\text{cur}}}{\partial \mu} = m_{\text{cur}} \frac{\partial \mathcal{U}_{q,T}}{\partial \Delta \partial \mu}$. It has been verified that this contribution is entirely negligible, just like for the other thermodynamic quantities.

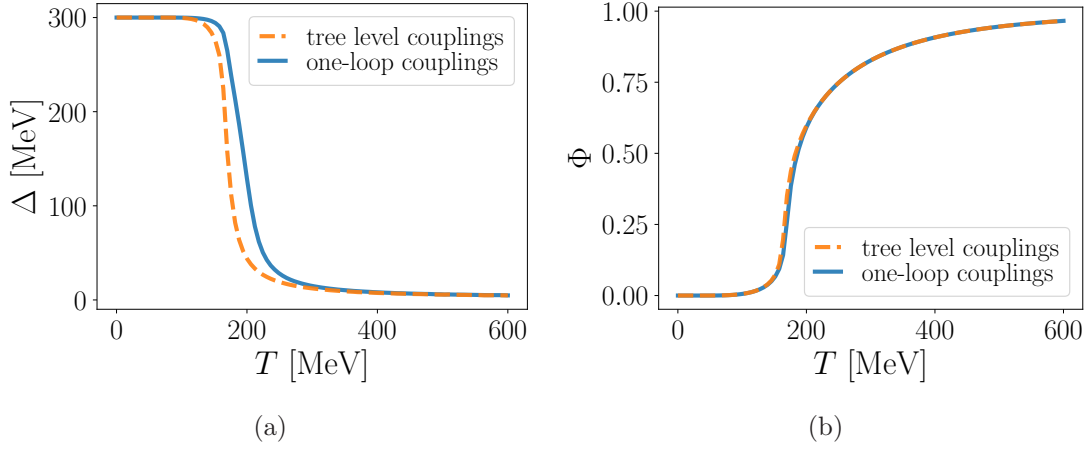


Figure 5.14: Comparison of the order parameters resulting from using tree-level and one-loop couplings in the PQM model with the one-loop potential in the large- N_c limit with $m_\sigma = 600$ MeV.

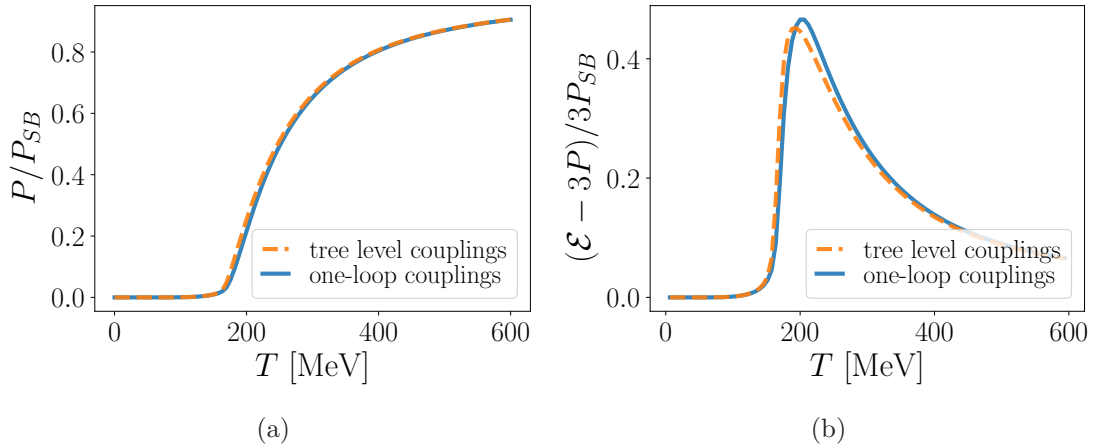


Figure 5.15: Comparison of the thermodynamics resulting from using tree-level and one-loop couplings in the PQM model with the one-loop potential in the large- N_c limit with the value of $m_\sigma = 600$ MeV.

local minimum, and the effective potential becomes non-increasing for all Δ . This can be seen from Fig. 5.3. However, for higher sigma masses a minimum is still present. In Fig. 5.14 we show the effect of using tree-level couplings at the higher sigma mass of $m_\sigma = 600$ MeV. For this m_σ the model has a minimum for Δ at $T = 0$ also when tree-level parameters are used. We see that in this case, the tree-level parameters cause the chiral phase transition to happen earlier – roughly at a temperature which is 25 MeV lower. On the other hand, the Polyakov loop and thus the location of the deconfinement phase transition is nearly unchanged. Consequently, using tree-level parameter matching

causes a discrepancy between the pseudocritical temperature of the deconfinement and chiral phase transitions. Additionally, as shown in Fig. 5.15, we see a slight difference in the interaction measure for intermediate temperatures, although it is not very significant. For the pressure and energy density (not shown) the difference is minuscule. Thus, if one is lucky enough to use a set of input parameters where the use of tree-level matching does not entirely break the model by removing the minimum in $\Omega(\Delta)$, it appears that the thermodynamics is not too strongly affected.

We finally note that the tree-level determination of the parameters corresponds to using (4.4.1)–(4.4.4) and a renormalization scale that satisfies

$$\ln \frac{\Lambda^2}{m_q^2} + 1 = 0, \quad (5.5.5)$$

as shown in Ref. [124]. The latter condition ensures that $h - m_\pi^2 v = 0$ at $T = 0$ with tree-level parameter matching and one-loop potential contributions.

5.6 Minimizing Ω at $\mu \neq 0$

We now return to the issue of minimizing Ω at $\mu \neq 0$, which we first discussed in Sec. 3.5. It is suggested in Refs. [21, 77, 78] to let the background gauge field become non-Hermitian by setting $q \in \mathbb{R}$ and $r = iR$, with $R \in \mathbb{R}$. Inserting $r = iR$ into the expressions for the Polyakov loops, (2.7.9) and (2.7.10), we get

$$\Phi = \frac{e^{-2\pi R/3}}{3} \left[e^{2\pi R} + 2 \cos \left(\frac{2\pi q}{3} \right) \right], \quad (5.6.1)$$

$$\bar{\Phi} = \frac{e^{2\pi R/3}}{3} \left[e^{-2\pi R} + 2 \cos \left(\frac{2\pi q}{3} \right) \right], \quad (5.6.2)$$

which give that both are real, but with different values in general. For the RRTW potential, which is a function of Φ and $\bar{\Phi}$ directly, it is clear that the Polyakov loop potential becomes real, and thus the full potential is real for all $(q, R) \in \mathbb{R}^2$, since $\mathcal{U}_{q,T}$ can also be written in terms of Φ and $\bar{\Phi}$. For the χM model this is also the case, since the only potentially complex terms in (5.1.4) and (5.1.5) are

$$B_1 \left(\frac{q}{3} + iR \right) + B_1 \left(\frac{q}{3} - iR \right) = 2 \operatorname{Re} B_1 \left(\frac{q}{3} - iR \right), \quad (5.6.3)$$

and

$$B_2 \left(\frac{q}{3} + iR \right) + B_2 \left(\frac{q}{3} - iR \right) = 2 \operatorname{Re} B_2 \left(\frac{q}{3} - iR \right). \quad (5.6.4)$$

However, the problem is that $\Omega_{\chi M}$ is unbounded in R for low temperatures, and Ω_{PQM} is unbounded in R for all temperatures. The part of the potential that depends on R in the χM model, $\tilde{\mathcal{V}} = \mathcal{U}_{q,T} + \mathcal{U}_{\chi M}$, is shown in Fig. 5.16 as function of (q, R) . We see that there is no minimum below $R < 1$. This behavior persists for any R .

In Refs. [77, 78] they suggest choosing the physically realized state to be the lowest saddle point of $\Omega(q, R)$. The method has the benefit of yielding $\Phi \neq \bar{\Phi}$ with $\Phi, \bar{\Phi} \in \mathbb{R}$,

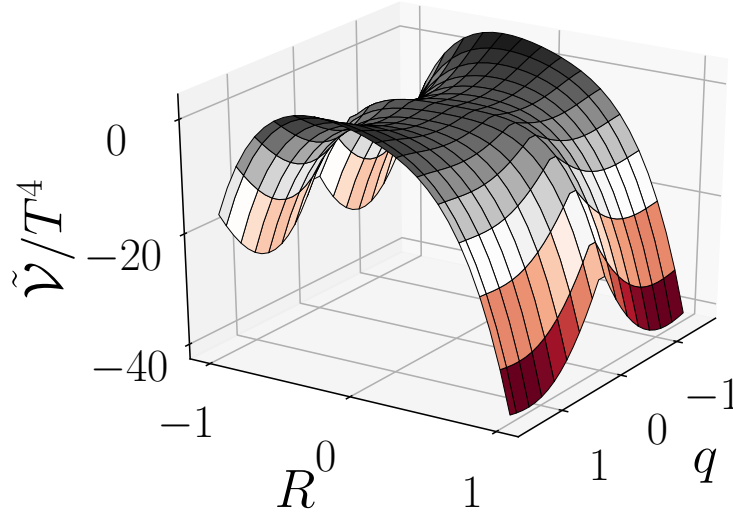


Figure 5.16: Normalized R -dependent part of the effective potential in the χM model at $T = \mu = 200$ MeV, $\Delta = 150$ MeV.

and we avoid a complex potential. However, choosing a saddle point is highly arbitrary and does not follow from any known principle of thermodynamics. Furthermore, it is not clear why r should be purely imaginary and q purely real. In Ref. [74] it is argued that the saddle point approach is problematic since it is impossible to calculate interface tensions with this scheme. Instead they suggest, together with Ref. [73], that r and q should stay real, and that we instead should minimize $\text{Re } \Omega$. This scheme has the unfortunate consequence of giving $\Phi = \bar{\Phi}$ also at $\mu \neq 0$. However, it allows for the calculation of interface tensions and is partly based on the potential minimization principle. Furthermore, a minimum of $\text{Re } \Omega$ still lies at $r = 0$ even though $\mu \neq 0$, such that at the minimum of $\text{Re } \Omega$ we have $\text{Im } \Omega = 0$ (see Fig. 5.17). If we are of the opinion that $\Phi \neq \bar{\Phi}$ mainly is a result of fluctuations in \mathbf{A}_4 , then $\Phi = \bar{\Phi}$ is not a pathology but a natural consequence of the mean field treatment of \mathbf{A}_4 combined with keeping \mathbf{A}_4 Hermitian.

Unlike for the saddle point method, we can also provide an (admittedly speculative) interpretation of the minimization of $\text{Re } \Omega$: When a complex energy appears in quantum mechanics, it usually signals a decaying quantity, and $\text{Im } E$ plays the role of a decay rate Γ . To see this, consider a generic physical state $\Psi(t) = \psi e^{-iEt}$, with the factor e^{-iEt} determining its time evolution. Then

$$\Psi(t) = \psi e^{-iEt} = \psi e^{-i \text{Re } Et} e^{\text{Im } Et} = \psi e^{i \text{Re } Et} e^{-\Gamma t}, \quad (5.6.5)$$

which is a state decaying with rate $\Gamma = -\text{Im } E$. An even closer analogy is provided when

we try to calculate the one-loop effective potential for a Lagrangian with spontaneous symmetry breaking without expanding about the minimum of the tree-level potential. Consider the complex scalar theory

$$\mathcal{L} = \partial_\mu \chi^\dagger \partial^\mu \chi + m^2 \chi^\dagger \chi - \lambda (\chi^\dagger \chi)^2. \quad (5.6.6)$$

Normally we would expand about the potential minimum $\chi = v + \sigma$. However, if we directly calculate the one-loop effective potential, we find that the thermal contribution is [36]

$$\mathcal{U}_T = -2V \int \frac{d^3 p}{(2\pi)^3} \ln \left(1 - e^{-\beta \omega_{\mathbf{p}}} \right), \quad (5.6.7)$$

where $\omega_{\mathbf{p}} = \sqrt{\mathbf{p}^2 - m^2}$. However, $\omega_{\mathbf{p}}$ is complex for low momenta, and thus \mathcal{U}_T becomes complex. The reason for this is that we have expanded around the potential maximum, which is unstable, instead of the stable potential minimum. Thus, if we interpret states with $\text{Im } \Omega \neq 0$ as unstable states that are not realized in an equilibrium system, then we imagine that the equilibrium state is the state that satisfies the constrained minimization problem¹⁴

$$\frac{\partial \text{Re } \Omega(q, r)}{\partial q} = 0, \quad \frac{\partial \text{Re } \Omega(q, r)}{\partial r} = 0, \quad \text{Im } \Omega(q, r) = 0, \quad r, q \in \mathbb{R}, \quad (5.6.8)$$

with the additional requirement that we choose the global minimum. However, in the case studied in this thesis, the condition $\text{Im } \Omega(q, r) = 0$ can be automatically satisfied when

$$\frac{\partial \text{Re } \Omega(q, r)}{\partial q} = 0, \quad \frac{\partial \text{Re } \Omega(q, r)}{\partial r} = 0, \quad r, q \in \mathbb{R}, \quad (5.6.9)$$

is satisfied, given that we chose the global minimum with $r = 0$. We see that this will be the case from Fig. 5.17, which shows the real and imaginary part of the quark thermal potential. The minimum of $\text{Re } \mathcal{U}_{q,T}$ is at $r = 0$ also for $\mu \neq 0$. However, we speculate that (5.6.8) is the correct criterion in general.

Due to the lack of physical interpretation, the seeming arbitrariness of setting $q \in \mathbb{R}$, $ir \in \mathbb{R}$, and the impossibility of calculating surface tensions, we avoid the saddle point scheme and instead use (5.6.8). As for the consequences of this choice, it is pointed out in Ref. [74] that the two methods always agree for $(T = 0, \mu = \mu_{\text{max}})$ and $(T = T_{\text{max}}, \mu = 0)$, where μ_{max} is the largest chemical potential for which there is a (pseudo) phase transition and $T_{\text{max}} = T_c(\mu = 0)$. Thus, the phase diagrams obtained from the two methods converge on the endpoints of the critical curves.

5.7 Numerical Results: PQM and χM Model Thermodynamics at $\mu > 0$

Now that we have verified that the models provide reasonable approximations to the QCD thermodynamics up to $T \approx 2T_c$, we proceed to investigate the predictions of these

¹⁴We ignore Δ at the moment.

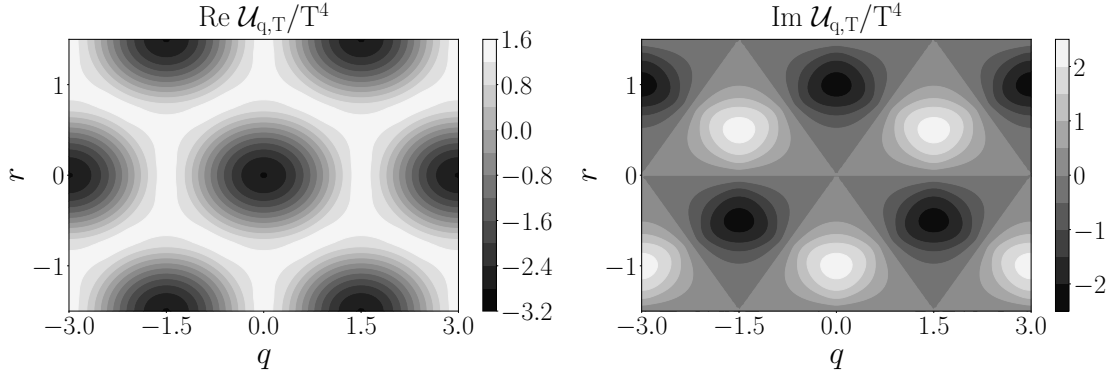


Figure 5.17: The real and imaginary parts of the quark thermal potential at $T = \mu = \Delta = 150$ MeV. $\text{Im}\mathcal{U}_{q,T}$ has a discontinuity at $q = r = 0$, with $\text{Im}\mathcal{U}_{q,T} = 0$ exactly at this point.

models at nonzero quark chemical potential. Due to the existence of lattice simulations at finite chemical potentials based on Taylor expansions in powers of μ/T , as discussed in Sec. 5.4, we also carry out checks on our results at $\mu > 0$. Lattice data are however only available for $\mu/T \leq 1$, since for large μ/T the Taylor series is not expected to converge.

In the following we calculate the pressure increase and quark number caused by a nonzero quark chemical potential and compare with lattice data. Furthermore, we calculate the chiral and deconfinement phase diagrams of the two models.

To study the pressure, we define the quantity $\Delta P(T, \mu)$ as

$$\Delta P(T, \mu) = P(T, \mu) - P(T, 0). \quad (5.7.1)$$

This corresponds to the pressure increase at a given temperature that is caused by a nonzero quark chemical potential. Figure 5.18 shows the comparison of ΔP from lattice and models as function of T/T_c for different fixed ratios of μ/T . The lattice data are taken from Ref. [117]. We see that the PQM model agrees well with lattice simulations, especially up to temperatures of $T \sim 1.5T_c$. Between $T = 1.5T_c$ and $T = 2T_c$ the deviation is slightly larger at the high μ/T ratios, but still not much more than 10%. For the χM model ΔP is larger than what is found in lattice data. However, the qualitative shape of the $\Delta P/T^4$ curves for the χM model appears to be in good agreement with lattice data, with a fast saturation in $\Delta P/T^4$ after the initial rise around $T = T_c$.

In Fig. 5.19 we see $n_q(T, \mu)/T^3$ for constant μ/T compared to lattice data. Here n_q is the quark number density which is given by (3.2.9), except that we now have two quark flavors. We see reasonable quantitative agreement between PQM model and lattice data. However, like for $\Delta P/T^4$, we find that the curves given by the χM model have a shape more similar to lattice data.

Figures 5.20 and 5.21 display the phase diagrams for both models, where the pseudo-critical temperatures corresponding to the inflection points of Δ and Φ are indicated, in

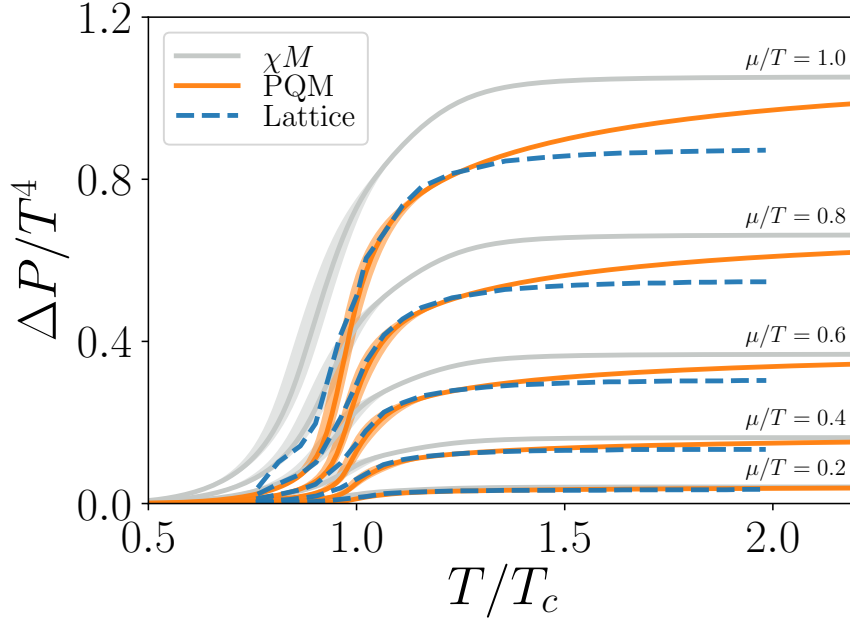


Figure 5.18: Pressure increase as function of T for fixed μ/T ratios in the PQM and χM models compared to lattice data from Allton et al. [117].

addition to the temperature where $\Phi = \frac{1}{2}$.¹⁵ We see that the chiral and deconfinement phase transitions also coincide for nonzero chemical potentials. However, referring to the inflection point of the Polyakov loop as deconfinement at high chemical potentials is misleading. It is correct that the chiral symmetry in the models is approximately restored above the lines of the chiral phase transition in Figs. 5.20 and 5.21, as we see in Fig. 5.22, but it is not correct to assume that quarks are deconfined everywhere outside the phase boundaries given by the inflection point of Φ . This is clear since the temperatures where $\Phi = \frac{1}{2}$ extends well beyond the temperature where the inflection point occurs – especially for the PQM model. We have a phase where chiral symmetry is restored and where the quarks are confined or semi-confined. In Fig 5.23 we see the value of the Polyakov loop in the $\mu - T$ plane. Interestingly, we see that the χM model approaches deconfinement in the high-density limit, which is not the case in the PQM model. This is a radical difference between the two models, and it is hard to assess which behavior best reflects QCD due to the lack of lattice data for $\mu > T$. The chirally restored and confined phase predicted for $\mu \gg T$ in the PQM model is sometimes referred to as a quarkyonic phase [125].

We also note that at sufficiently high temperatures some of the crossovers become

¹⁵The inflection point for each μ -value is extracted by fitting the $\partial\Delta/\partial T$ and $\partial\Phi/\partial T$ curves with Gaussians in a small range around the peak value. A more direct method would be to directly extract the temperature value on the discretized T -axis where the peak occurs, but the former method works better as it is more stable against varying step sizes in the discretization of the T -axis.

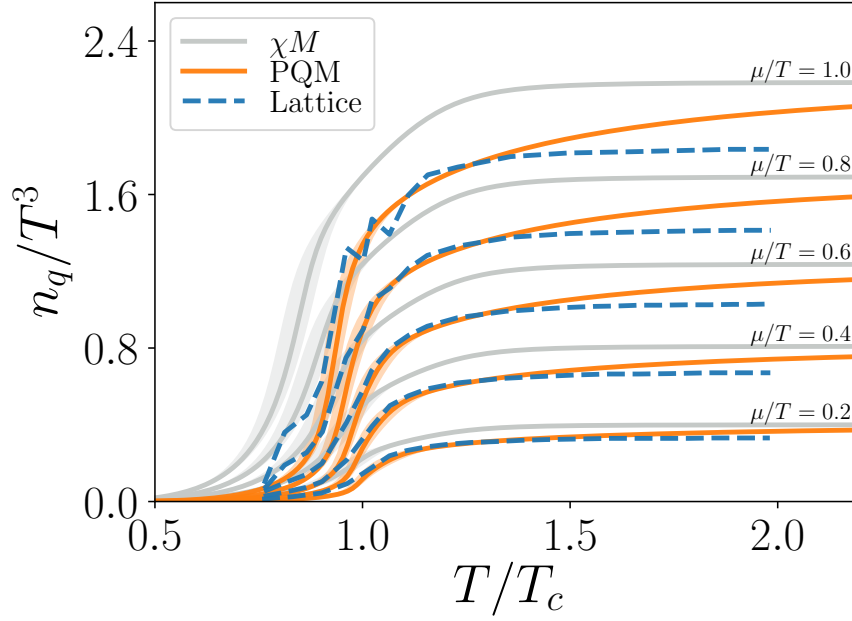


Figure 5.19: Normalized quark density as function of T for fixed μ/T ratios in the PQM and χM model compared to lattice data from Allton et al. [117].

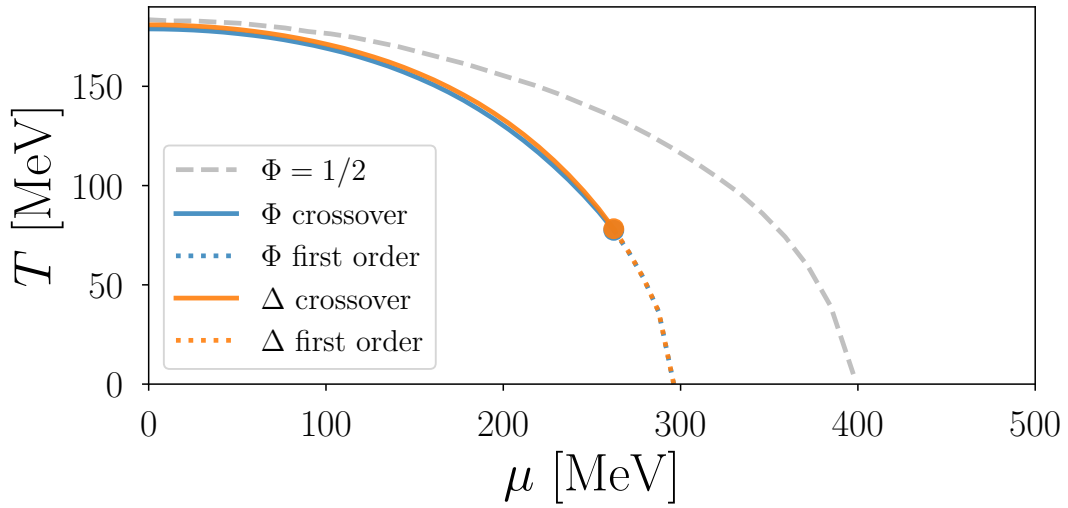


Figure 5.20: Phase diagram of the χM model.

first order phase transitions, with the transition from crossover to first order marked by a critical point. In the χM model the critical points of the chiral condensate and the

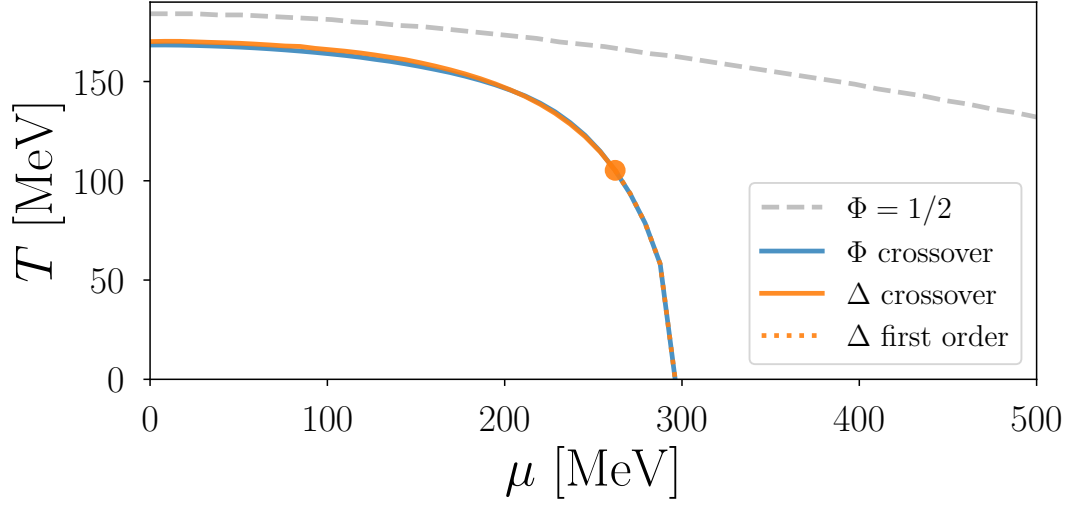


Figure 5.21: Phase diagram of the PQM model.

Polyakov loop coincide, and they are located at

$$(\mu^*, T^*) = (262 \text{ MeV}, 78 \text{ MeV}). \quad (5.7.2)$$

For PQM model only the chiral transition has a critical point, which is another qualitative difference between the two models. The chiral critical point of the PQM model is located at

$$(\mu^*, T^*) = (262 \text{ MeV}, 105 \text{ MeV}). \quad (5.7.3)$$

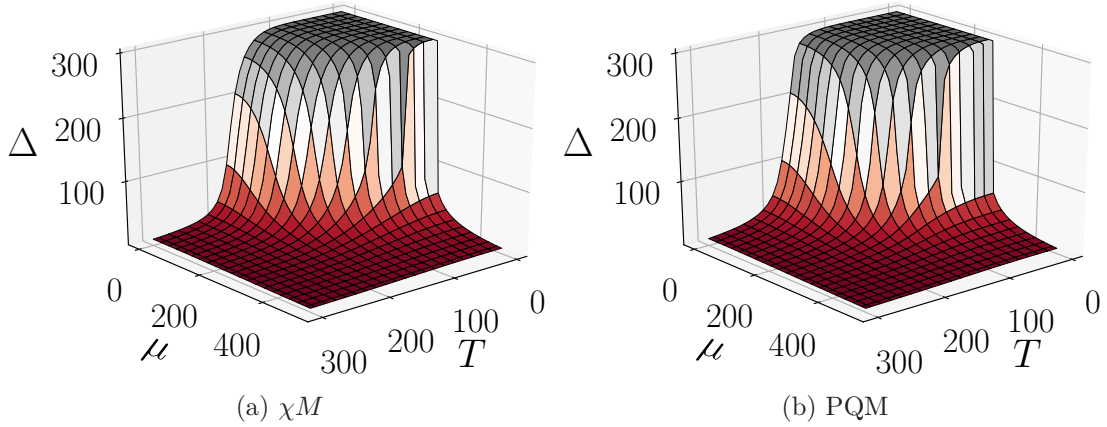


Figure 5.22: The chiral condensate as function of (μ, T) in the two models. Units of Δ , μ and T are in MeV.

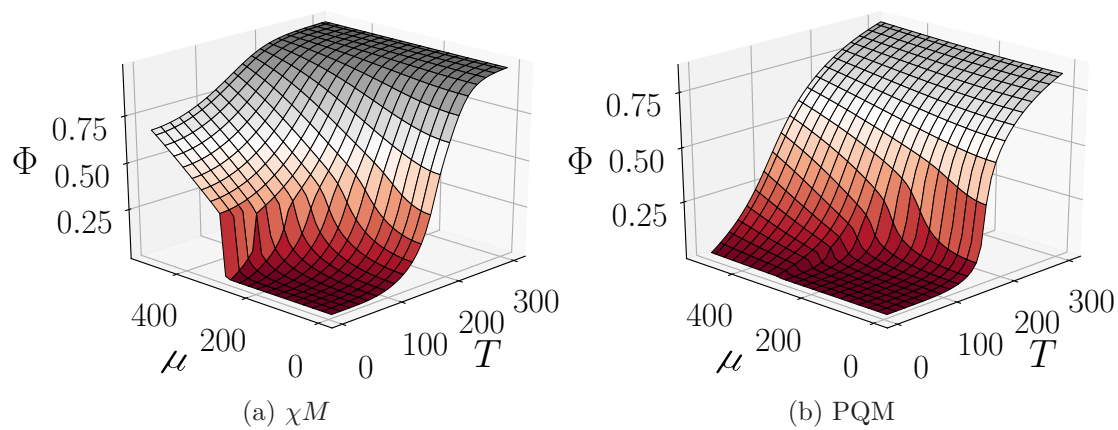


Figure 5.23: The Polyakov loop as function of (μ, T) in the two models. Units of μ and T are in MeV.

The PQM Model in a Magnetic Field

Strongly interacting matter in magnetic fields is relevant for the study of various physical phenomena, such as heavy-ion collisions, compact stars, and the early universe [126]. In heavy-ion collisions it is known that strong time-dependent magnetic fields are created when collisions are non-central [127–129], with the magnetic field strength in the LHC estimated to reach up to values of $|eB| \approx 15m_\pi^2$ [128], where e is the electron charge and B the magnetic field. In the case of compact stars there is a class of neutron stars known as magnetars that have magnetic fields reaching 10^{10} T to 10^{11} T on the surface [130] and possibly $\sim 10^{14}$ T in the core [131], with the latter field corresponding to $|eB| \approx 0.3m_\pi^2$.¹ Furthermore, if large magnetic fields existed in the early universe, it has potential consequences for early universe phase transitions [126]. Thus, the study of strongly interacting matter in a magnetic field is well motivated, and it is the goal of this chapter.

In both model [132–137] and lattice calculations [138–141] an effect known as magnetic catalysis is found in the vacuum. In the context of QCD, magnetic catalysis is the effect where an external B -field strengthens chiral symmetry breaking by increasing the value of the chiral condensate. In the chiral limit, it can also refer to the effect where a nonzero B -field breaks the chiral symmetry that was present at $B = 0$. This could happen at $T > T_c$ where chiral symmetry is not spontaneously broken for $B = 0$.

In lattice simulations one also finds what is known as inverse magnetic catalysis [141–143], which is the decrease of the chiral transition temperature with increasing magnetic field. It is also found that the chiral and deconfinement phase transitions coincide at $B > 0$ [139]. These two findings are not reproduced in model calculations [132–137, 144,

¹ $1 \text{ T} = 1 \text{ kgs}^{-1}\text{C}^{-1} \approx (5.61 \times 10^{35} \text{ eV}) (6.58 \times 10^{-16} \text{ eV}) (1.6 \times 10^{-19} \text{ e}^{-1}) \approx 195 \text{ eV}^2$, where we use the relations $1 = \hbar \approx 6.58 \times 10^{-16} \text{ eVs}$, $0.303 \approx 1 e \approx 1.60 \times 10^{-19} \text{ C}$ and $1 \text{ kg} = (1.66 \times 10^{-27})^{-1} m_p$, where $m_p = 931 \text{ MeV}$ is the proton mass.

145] and represent cases where the naive application of effective models is qualitatively wrong.

In the following we study magnetic catalysis in the PQM and χM models at the one-loop large- N_c level with consistent parameter fixing. Furthermore, we investigate the findings of Ozaki et al. in Ref. [146], where they find inverse magnetic catalysis in a Polyakov loop model without a chiral sector, which is opposite to what is found in models with a chiral sector. Finally, we briefly explore the effect a B -dependent gluonic potential in the χM model.

We note in passing that we do not look at the case of $\mu \neq 0$ in a magnetic field, since the authors of Ref. [147] have shown that high magnetic fields and nonzero baryon chemical potentials lead to a fundamentally altered vacuum structure of QCD, with neutral pion domain walls favored over nuclear matter.

6.1 The PQM Lagrangian Coupled to the EM field

Let \mathcal{A}_μ be the electromagnetic gauge field. We want to minimally couple it to the quarks and the pions so that we take the effect of an external magnetic field into account. To couple to the pions, we must identify the fields corresponding to charged pions, π^\pm . Knowing that the electromagnetic field should be $U(1)$ gauge invariant, we should identify mesonic fields which are also $U(1)$ gauge invariant. Define the complex field

$$\pi = \frac{1}{\sqrt{2}}(\pi_1 + i\pi_2). \quad (6.1.1)$$

Rewriting the non-interacting π_1, π_2 sector of (4.2.2), we find

$$\mathcal{L}_{\pi_1\pi_2} = \partial_\mu \pi^\dagger \partial^\mu \pi - m_\pi^2 \pi^\dagger \pi, \quad (6.1.2)$$

which is clearly invariant under global $U(1)$ transformations. To obtain gauge invariance we follow the canonical prescription of replacing the partial derivative with the gauge-covariant derivative. Doing this we find that the mesonic sector reads

$$\mathcal{L}_\pi = (D_\mu \pi)^\dagger (D^\mu \pi) - m_\pi^2 \pi^\dagger \pi + \frac{1}{2}(\partial\pi_3)^2 - \frac{1}{2}m_\pi \pi_3^2 + \frac{1}{2}(\partial\sigma)^2 - \frac{1}{2}m_\sigma \sigma^2 + \mathcal{L}_{I,\sigma\pi}, \quad (6.1.3)$$

where $\mathcal{L}_{I,\sigma\pi}$ is given by (4.3.3) and $D_\mu \pi$ is

$$D_\mu \pi = (\partial_\mu - ie\mathcal{A}_\mu - ig_a \mathbf{A}_\mu)\pi, \quad (6.1.4)$$

where we set $\mathbf{A}_\mu = \delta_\mu^0 \mathbf{A}_0$ as usual. We have written the gluon gauge coupling as g_a to avoid confusion with the Yukawa-coupling. The coupling e is the electric elementary charge. The choice of coupling the EM field to π_1 and π_2 is entirely arbitrary and has no physical content – it is just a matter of labeling. What is important is that only a complex field couple to the EM field, meaning that one of the pion fields cannot couple

minimally to the EM gauge field without breaking gauge invariance.² This field, here chosen to be π_3 , will represent the neutral pion, π^0 .

In the quark sector we also couple to the EM fields by replacing the partial derivative with gauge covariant derivatives. However, since ψ_1 and ψ_2 represent up and down quarks that have charges $q_1 = \frac{2}{3}e$ and $q_2 = -\frac{1}{3}e$ respectively, we must couple to gauge-covariant derivatives with different charges. The quark sector, not including the Yukawa interactions, then reads

$$\mathcal{L}_\psi = \sum_{j=1}^{N_f} \bar{\psi}_j i\gamma^\mu (\partial_\mu - iq_j \mathcal{A}_\mu - ig_a \mathbf{A}_\mu) \psi_j - gv\bar{\psi}\psi. \quad (6.1.5)$$

The Yukawa interaction is unchanged. Note that the introduction of different EM charges for the two flavors breaks both chiral symmetry and isospin symmetry, and only $SU(N_c) \times U(1)_B$ remains.

6.2 Quarks in a Constant Magnetic Field

Let us now consider the partition function to one loop in the large- N_c limit, so that we can neglect mesonic fluctuations. We consider a constant magnetic field in the z -direction, given in the Landau gauge by

$$\mathcal{A}_\mu = (0, 0, -Bx, 0). \quad (6.2.1)$$

We treat the EM field as a classical background field. The quark contribution to the one-loop partition function reads

$$Z_q = \int_{\text{ABPC}} \prod_{j=1}^{N_f} \prod_{k=1}^{N_c} i\mathcal{D}\psi_{jk}^\dagger \mathcal{D}\psi_{jk} \exp \left\{ \int_0^\beta d\tau \int d^3x \psi_{jk}^\dagger D_{jk} \psi_{jk} \right\}, \quad (6.2.2)$$

with ψ_{jk} being Dirac spinors of flavor j and color k with no implicit sum over either index, and

$$\begin{aligned} D_{jk} &= -\partial_\tau - i\gamma^0 \gamma^i \partial_i + ig[\mathbf{A}_4]_{kk} + \mu - \gamma^0 \Delta + q_j \gamma^0 \gamma^\mu \mathcal{A}_\mu \\ &= -\partial_\tau - i\gamma^0 \gamma^i \partial_i + \tilde{\mu}_k - \gamma^0 \Delta + q_j Bx \gamma^0 \gamma^2. \end{aligned} \quad (6.2.3)$$

The above result is obtained by generalizing (3.1.8) by adding a second flavor and coupling the two flavors to the EM gauge field with different charges. Furthermore, we have assumed that \mathbf{A}_4 is constant and in the Polyakov gauge, and we have defined

$$\tilde{\mu}_k = \mu + ig[\mathbf{A}_4]_{kk}. \quad (6.2.4)$$

²We emphasize that the coupling is minimal, since the so-called chiral anomaly allows for a coupling between π^0 and photons [148, 149]. It is this coupling which causes the modified vacuum structure of QCD at nonzero baryon chemical potential [147].

Using the Gaussian Grassman integral, (3.1.15), we find that

$$Z_q = \prod_{j=1}^{N_f} \prod_{k=1}^{N_c} \det D_{jk}. \quad (6.2.5)$$

In using the Gaussian integral in the case where D_{jk} is a differential operator, we must clarify what the determinant here means. For matrices the determinant can be defined as the product of the eigenvalues of the matrix. This is a definition we can carry over to differential operators, with the difference being that the number of eigenvalues usually is infinite. To see that the formula is correct also for differential operators one could discretize space, carry out the Gaussian integrals and then again take the continuum limit.

6.3 Landau Levels

We now want to find the spectrum of the operator D_{jk} . Thus, we consider the eigenvalue problem

$$D\psi = \lambda\psi, \quad (6.3.1)$$

where we for the moment consider a single flavor and color and thus suppress the flavor index j and color index k . We can rewrite this equation as

$$(-\partial_\tau + \tilde{\mu} - \lambda)\psi = (i\gamma^0\gamma^i\partial_i + \gamma^0\Delta - qBx\gamma^0\gamma^2)\psi. \quad (6.3.2)$$

Writing $\psi(\tau, \mathbf{x})$ in terms of its Matsubara frequencies ω_l ,³

$$\psi(\tau, \mathbf{x}) = \sum_{l=-\infty}^{l=\infty} \tilde{\psi}_l(\mathbf{x})e^{-i\omega_l\tau}, \quad (6.3.3)$$

we obtain

$$(i\omega_l + \tilde{\mu} - \lambda)\tilde{\psi}_l = (i\gamma^0\gamma^i\partial_i + \gamma^0\Delta - qBx\gamma^0\gamma^2)\tilde{\psi}_l. \quad (6.3.4)$$

Choosing the Dirac representation of the gamma matrices, setting

$$\tilde{\psi}_l = \begin{pmatrix} \chi_- \\ \chi_+ \end{pmatrix}, \quad (6.3.5)$$

and defining

$$\eta = i\omega_l + \tilde{\mu} - \lambda, \quad (6.3.6)$$

we find

$$(\eta \pm \Delta)\chi_\pm = (i\sigma^i\partial_i - qBx\sigma^y)\chi_\mp. \quad (6.3.7)$$

Inserting one into the other yields

$$(\eta^2 - \Delta^2)\chi_+ = (i\sigma^i\partial_i - qBx\sigma^y)^2\chi_+. \quad (6.3.8)$$

³There is no factor $V^{-\frac{1}{2}}$, since we do not Fourier expand the spatial part.

Simplifying the operator on the left hand side, we obtain

$$(i\sigma^i \partial_i - qBx\sigma^y)^2 = \left[-\partial_x^2 - \partial_z^2 - (\partial_y + iqBx)^2 + qB\sigma^z \right], \quad (6.3.9)$$

where we used $\sigma^i \sigma^j = \delta^{ij} + i\epsilon^{ijk} \sigma^k$. Thus, we find the equation

$$\left[\eta^2 - \Delta^2 + \partial_x^2 + \partial_z^2 + (\partial_y + iqBx)^2 - qB\sigma^z \right] \chi_+ = 0. \quad (6.3.10)$$

The equation for χ_- is identical, so to find the spectrum of D we only need to consider (6.3.10). The z and y parts of the equation are solved by plane waves. Thus, we see that we have two independent solutions of the form

$$\chi_+ = \begin{pmatrix} 0 \\ f_-(x) \end{pmatrix} e^{ip_z z + ip_y y}, \quad \chi_- = \begin{pmatrix} f_+(x) \\ 0 \end{pmatrix} e^{ip_z z + ip_y y}. \quad (6.3.11)$$

Note that to satisfy the specific boundary conditions of the problem, one might have to take linear combinations of these solutions. Furthermore, the boundary conditions might put quantization conditions on p_y and p_z , which we will get back to later.

Inserting (6.3.11) into (6.3.10), we get

$$\left[\eta^2 - \Delta^2 - p_z^2 + \partial_x^2 - (p_y + qBx)^2 - qBs \right] f_{\mp} = 0, \quad (6.3.12)$$

where $s = \pm 1$. Defining $w = x + p_y/qB$, changing variables and dividing by $2|qB|$, we find

$$\left[-\frac{1}{2|qB|} \partial_w^2 + \frac{1}{2}|qB|w^2 \right] f_{\mp}(w) = \frac{\eta^2 - \Delta^2 - p_z^2 - qBs}{2|qB|} f_{\mp}(w). \quad (6.3.13)$$

But this is just the well-known harmonic oscillator equation where the parameters m , ω , and E now correspond to $|qB|$, 1 and $(\eta^2 - \Delta^2 - p_z^2 - qBs)/2|qB|$. Thus, we find that solutions exist when

$$(\eta^2 - \Delta^2 - p_z^2 - qBs)/2|qB| = n + \frac{1}{2} \quad (6.3.14)$$

for some integer $n \geq 0$. Since we later will sum over $s = \pm 1$, we can replace $qBs \rightarrow |qB|s$. Insertion of η into (6.3.14) gives

$$(\lambda - \tilde{\mu} - i\omega_l)^2 = \Delta^2 + p_z^2 + |qB|(2n + 1 + s). \quad (6.3.15)$$

The energies $E(p_z, n, s)^2 = \Delta^2 + p_z^2 + |qB|(2n + 1 + s)$ are known as Landau levels and correspond to the energy eigenstates of fermions in a constant magnetic field at $T = 0$ with no chemical potential or background gluon field. Now, (6.3.15) is a quadratic equation in λ with two solutions. We write the equation as

$$(\lambda + \alpha)^2 = \gamma^2, \quad (6.3.16)$$

with $\alpha = -\tilde{\mu} - i\omega_l$ and γ equal to the right hand side of (6.3.15). We have two solutions

$$\lambda_{\pm} = \pm\gamma - \alpha. \quad (6.3.17)$$

6.4 The Quark Partition Function at One Loop: Part I

We now return to evaluate the partition function. With the index j summing over the whole eigenvalue spectrum, which includes summing over p_z , p_y , l , n and s , we have that the contribution of one quark flavor is

$$\begin{aligned}
\ln Z_q &= \ln \det D = \ln \prod_j \lambda_j = \sum_j \ln \lambda_j = \sum_j \ln \lambda_{+,j} + \sum_j \ln \lambda_{-,j} \\
&= \sum_j \frac{1}{2} \ln (\lambda_{+,j}^2 \lambda_{-,j}^2) = \sum_j \frac{1}{2} \ln [(\gamma^2 - \alpha^2)^2] = \sum_j \ln (\gamma^2 - \alpha^2) \\
&= \sum_j \ln [(\omega_l - i\tilde{\mu})^2 + \Delta^2 + p_z^2 + |qB|(2n + 1 + s)]. \tag{6.4.1}
\end{aligned}$$

We observe that (6.4.1) is dimensionally inconsistent since we have something of mass dimension two in the logarithm. This is because we really should have inserted the Matsubara frequency expansion in the path integral (6.2.2), which would give us a factor β in the action, and the Euclidean action would be of the form

$$-S_E = \sum_l \int d^3x \psi_l(\mathbf{x})^\dagger \beta D(\omega_l, \mathbf{x}) \psi_l(\mathbf{x}). \tag{6.4.2}$$

Thus, we should really replace $D \rightarrow \beta D$ in the previous section, which leads to the replacements $\lambda_i \rightarrow \beta \lambda_i$, which finally gives

$$\ln Z_q = \sum_i \ln \left\{ \beta^2 [(\omega_l - i\tilde{\mu})^2 + \Delta^2 + p_z^2 + |qB|(2n + 1 + s)] \right\}. \tag{6.4.3}$$

The sum over the eigenvalues is given by

$$\sum_j = \sum_{n=0}^{\infty} \sum_{l=-\infty}^{\infty} \sum_{s=\pm 1} \sum_{p_z, p_y} \tag{6.4.4}$$

Even though the eigenvalues are degenerate in the p_y quantum number, the p_y sum is non-trivial since it is not obvious what the degeneracy factor is. A heuristic non-rigorous argument commonly found in the literature goes as follows: From the fact that (6.3.13) is a harmonic oscillator equation with the quadratic potential centered at $x_c = -p_y/qB$, we know that the solutions are $f_n(x + \frac{p_y}{qB})$, with f_n being the eigenfunctions of the harmonic oscillator. If we put the system in a finite cubic volume of size $V = L^3$ and assume periodic boundary conditions,⁴ we have that the momentum p_y must be quantized, satisfying

$$p_y = \frac{2\pi}{L} m, \tag{6.4.5}$$

⁴The background gauge field $A_\mu = (0, 0, -Bx, 0)$ is not compatible with periodic boundary conditions in the x -direction, but periodicity in the y -direction is sufficient for this argument.

for some integer m . Assume for a moment that $qB < 0$. Wanting the center of our eigenstate to be localized within the box, and letting $x \in [0, L]$ define the x -coordinates of the box, we have the requirement

$$0 < x_c = \frac{-2\pi m}{qBL} = \frac{2\pi m}{|qB|L} < L, \quad (6.4.6)$$

which implies

$$0 < m < \frac{|qB|L^2}{2\pi}. \quad (6.4.7)$$

This gives a degeneracy of

$$\left\lfloor \frac{|qB|L^2}{2\pi} \right\rfloor \approx \frac{|qB|L^2}{2\pi}, \quad (6.4.8)$$

where we assume that $|qB|L^2/2\pi \gg 1$, so that the effect of the floor function $\lfloor \cdot \rfloor$ is negligible. Clearly the argument also applies for $qB > 0$ with trivial modifications. Whether or not one buys this argument, it can anyhow be verified by checking that the $B \rightarrow 0$ limit reproduces the correct $B = 0$ result. This uniquely and rigorously fixes the degeneracy factor. For a rigorous direct derivation of the degeneracy factor of the Landau levels the reader is referred to Ref. [150].

Taking the thermodynamic limit where $\sum_{p_z} \rightarrow L \int \frac{dp_z}{2\pi}$, we find

$$\sum_i = \frac{|qB|L^2}{2\pi} \sum_{n=0}^{\infty} \sum_{l=-\infty}^{\infty} \sum_{s=\pm 1} L \int \frac{dp_z}{2\pi}. \quad (6.4.9)$$

We thus finally obtain, for a single color and flavor,

$$\ln Z = \frac{|qB|V}{2\pi} \sum_{n=0}^{\infty} \sum_{l=-\infty}^{\infty} \sum_{s=\pm 1} \int \frac{dp_z}{2\pi} \ln \left\{ \beta^2 \left[(\omega_l - i\tilde{\mu})^2 + \Delta^2 + p_z^2 + |qB|(2n+1+s) \right] \right\}. \quad (6.4.10)$$

The Matsubara frequency sum is the same as the one encountered for non-interacting fermions with no external EM field if we identify an effective mass

$$M_B^2 = \Delta^2 + |qB|(2n+1+s), \quad (6.4.11)$$

replace $\int \frac{d^3p}{(2\pi)^3} \rightarrow \int \frac{dp_z}{2\pi}$ and notice that we have an explicit factor of two less that is replaced by the sum $\sum_{s=\pm}$. Using the derivations in Appendix A.1 and A.2 with these replacements, we obtain

$$\ln Z = \frac{|qB|V}{2\pi} \sum_{n=0}^{\infty} \sum_{s=\pm 1} \int \frac{dp_z}{2\pi} \left\{ \beta \sqrt{p_z^2 + M_B^2} + \sum_{k=\pm 1} \ln \left[1 + e^{-\beta(\sqrt{p_z^2 + M_B^2} - k\tilde{\mu})} \right] \right\}. \quad (6.4.12)$$

6.5 Interlude: Regularization of the Vacuum Energy

As is the case for a system without a magnetic field, we find a divergent vacuum energy, except in this case the divergent integral corresponds to quantum fluctuations in one dimension only. We regularize the integral with dimensional regularization by letting

$$\int_{-\infty}^{\infty} \frac{dp_z}{2\pi} \sqrt{p_z^2 + M_B^2} \rightarrow \Lambda^{2\epsilon} \int \frac{d^{d-2\epsilon} p_z}{(2\pi)^{d-2\epsilon}} \sqrt{p_z^2 + M_B^2} \equiv I, \quad (6.5.1)$$

for some small ϵ . Here Λ is the renormalization scale, $d = 1$ and $d^{d-2\epsilon} p_z$ the volume element in $d - 2\epsilon$ dimensions. The analytic continuation of the volume element to non-integer dimensions is obtained by using that $d^d p = p^{d-1} dp d\Omega_d$ and the fact that the solid angle integration $\int d\Omega_d$ can be analytically continued to non-integer d , since

$$\int d\Omega_d = \frac{2\pi^{\frac{d}{2}}}{\Gamma\left(\frac{d}{2}\right)} \quad (6.5.2)$$

is defined for non-integer d . Since the integrand of (6.5.1) is spherically symmetric, we can use the above relation to get

$$I = \frac{(4\pi\Lambda^2)^\epsilon}{\sqrt{\pi}\Gamma\left(\frac{1}{2} - \epsilon\right)} \int_0^\infty dp \frac{p^{-2\epsilon}}{(p^2 + M_B^2)^{-1/2}}. \quad (6.5.3)$$

This integral is essentially the Euler beta function, and we use the well-known integral formula [26]⁵

$$\int_0^\infty dx \frac{x^a}{(x^2 + M^2)^b} = (M^2)^{\frac{a+1}{2}-b} \frac{\Gamma\left(\frac{a+1}{2}\right)\Gamma\left(b - \frac{a+1}{2}\right)}{2\Gamma(b)} \quad (6.5.4)$$

with $a = -2\epsilon$ and $b = -\frac{1}{2}$ to obtain

$$I = -\frac{M_B^2}{4\pi} \left(\frac{4\pi\Lambda^2}{M_B^2}\right)^\epsilon \Gamma(-1 + \epsilon), \quad (6.5.5)$$

where we used that $\Gamma\left(-\frac{1}{2}\right) = -2\sqrt{\pi}$. Like in Chapter 4 we adopt the $\overline{\text{MS}}$ renormalization scheme, which means we absorb all factors $(\epsilon^{-1} + \ln 4\pi e^{-\gamma_E})$ into counterterms. The effect of this is equivalent to redefining $\Lambda^2 \rightarrow \Lambda^2/4\pi e^{-\gamma_E}$ everywhere and absorbing factors of ϵ^{-1} into counterterms. Doing this we finally get that

$$I = -\frac{M_B^2}{4\pi} \left(\frac{e^{\gamma_E}\Lambda^2}{M_B^2}\right)^\epsilon \Gamma(-1 + \epsilon). \quad (6.5.6)$$

Usually at this point we expand in the $\epsilon \rightarrow 0$ limit. However, keeping I on the form given will help us regulate the sum over the Landau levels, as we see in the next section.

⁵The Euler beta function satisfies $B(x, y) = \frac{\Gamma(x)\Gamma(y)}{\Gamma(x+y)}$ and is defined by $B(x, y) = \int \frac{u^{x-1} du}{(1+u)^{x+y}}$ [151].

6.6 The Quark Partition Function to One Loop: Part II

Now that we have regulated the diverging integral, we want to sum over the Landau levels. Unfortunately, we cannot do this explicitly, but we can rewrite our expressions more succinctly.

Combining (6.4.12) and (6.5.5) gives an effective potential

$$\Omega = \frac{|qB|}{2\pi} \sum_{n=0}^{\infty} \sum_{s=\pm 1} \left\{ \frac{M_B^{2-2\epsilon} (e^{\gamma_E} \Lambda^2)^\epsilon}{4\pi} \Gamma(-1+\epsilon) - \sum_{k=\pm 1} T \int \frac{dp_z}{2\pi} \ln \left[1 + e^{-\beta(\sqrt{p_z^2 + M_B^2} - k\tilde{\mu})} \right] \right\}. \quad (6.6.1)$$

Let us first deal with the vacuum energy. We must consider the sum

$$S \equiv \sum_{n=0}^{\infty} \sum_{s=\pm 1} M_B^{2-2\epsilon} = \sum_{s=\pm 1} \sum_{n=0}^{\infty} \left[\Delta^2 + |qB|(2n+1+s) \right]^{1-\epsilon}, \quad (6.6.2)$$

which for large n goes as $\sim \sum_n n^{1-\epsilon}$. Conveniently, ϵ acts as a regulator on the sum. Carrying out the $s = \pm 1$ sum:

$$\begin{aligned} S &= (2|qB|)^{1-\epsilon} \sum_{s=\pm 1} \sum_{n=0}^{\infty} \left(n + \frac{\Delta^2}{2|qB|} + \frac{1+s}{2} \right)^{1-\epsilon} \\ &= (2|qB|)^{1-\epsilon} \left[\sum_{n=1}^{\infty} \left(n + \frac{\Delta^2}{2|qB|} \right)^{1-\epsilon} + \sum_{n=0}^{\infty} \left(n + \frac{\Delta^2}{2|qB|} \right)^{1-\epsilon} \right] \\ &= 2(2|qB|)^{1-\epsilon} \sum_{n=0}^{\infty} \left(n + \frac{\Delta^2}{2|qB|} \right)^{1-\epsilon} - \Delta^{2-2\epsilon}. \end{aligned} \quad (6.6.3)$$

The above sum is of the same form as the definition of the Hurwitz zeta function, which is given by [152]

$$\zeta(s, a) = \sum_{n=0}^{\infty} (n+a)^{-s}. \quad (6.6.4)$$

The Hurwitz zeta function is defined by (6.6.4) only for $\text{Re } s > 1$, but it can be analytically continued with the formula

$$\zeta(s, a) = \frac{1}{s-1} \sum_{n=0}^{\infty} \sum_{k=0}^n \frac{(-1)^k}{n+1} \binom{n}{k} (a+k)^{1-s}, \quad (6.6.5)$$

which is valid for all real numbers $a > -1$ and complex numbers $s \neq 1$ [152].⁶ Defining

$$\delta = \frac{\Delta^2}{2|qB|}, \quad (6.6.6)$$

we find that

$$S = 2(2|qB|)^{1-\epsilon} \left[\zeta(-1+\epsilon, \delta) - \frac{1}{2} \delta^{1-\epsilon} \right]. \quad (6.6.7)$$

⁶The Hurwitz zeta function can be analytically continued to any real a and complex s as long as $s \neq -1$ [152].

Hence, the vacuum energy contribution to the effective potential is

$$\begin{aligned}\Omega_{T=0} &= \frac{2|qB|}{(4\pi)^2} \left(e^{\gamma_E} \Lambda^2 \right)^\epsilon \Gamma(-1 + \epsilon) 2(2|qB|)^{1-\epsilon} \left[\zeta(-1 + \epsilon, \delta) - \frac{1}{2} \delta^{1-\epsilon} \right] \\ &= \frac{8(qB)^2}{(4\pi)^2} \left(\frac{e^{\gamma_E} \Lambda^2}{2|qB|} \right)^\epsilon \Gamma(-1 + \epsilon) \left[\zeta(-1 + \epsilon, \delta) - \frac{1}{2} \delta^{1-\epsilon} \right].\end{aligned}\quad (6.6.8)$$

To take the $\epsilon \rightarrow 0$ limit we use that

$$\zeta(-1 + \epsilon, \delta) = \zeta(-1, \delta) + \epsilon \zeta^{(1,0)}(-1, \delta) + \mathcal{O}(\epsilon^2), \quad (6.6.9)$$

$$\Gamma(-1 + \epsilon) = -\frac{1}{\epsilon} - 1 + \gamma_E + \mathcal{O}(\epsilon), \quad (6.6.10)$$

$$\delta^\epsilon = 1 + \epsilon \ln \delta + \mathcal{O}(\epsilon^2), \quad (6.6.11)$$

where $\zeta^{(1,0)}(s, \delta) = \partial_x \zeta(x, \delta)|_{x=s}$. We can further simplify (6.6.9) by using the known relation [153]

$$\zeta(-n, \delta) = -\frac{B_{n+1}(\delta)}{n+1}, \quad n \in \mathbb{N}, \quad (6.6.12)$$

where $B_n(x)$ is the n -th Bernoulli polynomial. Thus we find

$$\zeta(-1, q) = -\frac{1}{2} B_2(\delta) = -\frac{1}{12} + \frac{\delta}{2} - \frac{\delta^2}{2}. \quad (6.6.13)$$

Inserting (6.6.9)–(6.6.13) into (6.6.8) and neglecting terms going as $\mathcal{O}(\epsilon)$ we find

$$\begin{aligned}\Omega_{T=0} &= \frac{8(qB)^2}{(4\pi)^2} \left\{ \left[\frac{1}{\epsilon} + 1 + \ln \left(\frac{\Lambda^2}{2|qB|} \right) \right] \left[\frac{1}{12} + \frac{\delta^2}{2} \right] - \frac{1}{2} \delta \ln \delta - \zeta^{(1,0)}(-1, \delta) \right\} \\ &= \frac{8(qB)^2}{(4\pi)^2} \left[\frac{1}{12} + \frac{\delta^2}{2} - \frac{1}{2} \delta \ln \delta - \zeta^{(1,0)}(-1, \delta) + \ln \left(\frac{\Lambda^2}{2|qB|} \right) \left(\frac{1}{12} + \frac{\delta^2}{2} \right) \right] \\ &\quad + \delta \Omega^{\text{div}},\end{aligned}\quad (6.6.14)$$

with the divergent part

$$\delta \Omega^{\text{div}} = \frac{8(qB)^2}{(4\pi)^2} \left(\frac{1}{12} + \frac{\delta^2}{2} \right) \frac{1}{\epsilon}, \quad (6.6.15)$$

which will be absorbed by counterterms later.

For the thermal contribution to the effective potential we consider

$$\Omega_T = -\frac{|qB|}{2\pi} \sum_{k=\pm 1} \sum_{n=0}^{\infty} \sum_{s=\pm 1} T \int_{-\infty}^{\infty} \frac{dp_z}{2\pi} \ln \left[1 + e^{-\beta(\sqrt{p_z^2 + M_B^2} - k\tilde{\mu})} \right]. \quad (6.6.16)$$

This integral converges, and it is thus not necessary to regularize it. We use that $\int_{-\infty}^{\infty} = 2 \int_0^{\infty}$ since the integrand is symmetric in p_z and perform a partial integration to obtain

$$\begin{aligned}\Omega_T &= -\frac{|qB|}{2\pi} \sum_{k=\pm 1} \sum_{n=0}^{\infty} \sum_{s=\pm 1} 2 \int_0^{\infty} \frac{dp_z}{2\pi} \frac{p_z^2}{\sqrt{p_z^2 + M_B^2}} \frac{1}{1 + e^{\beta(\sqrt{p_z^2 + M_B^2} - k\tilde{\mu})}} \\ &= -\frac{8|qB|T^2}{(4\pi)^2} \sum_{n=0}^{\infty} \sum_{s=\pm 1} K(M_B, \tilde{\mu}),\end{aligned}\quad (6.6.17)$$

where we defined the dimensionless function $K_\beta(m^2, \mu)$:

$$K_\beta(m^2, \mu) = \beta^2 \int_0^\infty dp_z \frac{p_z^2}{\sqrt{p_z^2 + m^2}} \left[\frac{1}{1 + e^{\beta(\sqrt{p_z^2 + m^2} - \mu)}} + \frac{1}{1 + e^{\beta(\sqrt{p_z^2 + m^2} + \mu)}} \right], \quad (6.6.18)$$

Again we can sum over s by using that, for any function f and parameters a, b ,

$$\begin{aligned} \sum_{n=0}^\infty \sum_{s=\pm 1} f(a + b(2n + 1 + s)) &= \sum_{n=0}^\infty [f(a + 2b(n + 1)) + f(a + 2bn)] \\ &= \sum_{n=1}^\infty f(a + 2bn) + \sum_{n=0}^\infty f(a + 2bn) \\ &= f(a) + 2 \sum_{n=1}^\infty f(a + 2bn). \end{aligned} \quad (6.6.19)$$

This gives us

$$\Omega_T = -\frac{8|qB|T^2}{(4\pi)^2} \sum_{n=0}^\infty (2 - \delta_{n0}) K_\beta(\Delta^2 + 2|qB|n, \tilde{\mu}). \quad (6.6.20)$$

Since we have summed out the s quantum number, from here and onward we redefine

$$M_B^2 = \Delta^2 + 2|qB|n. \quad (6.6.21)$$

6.7 The PQM Partition Function

We now proceed to write down the full one-loop partition function of the PQM model in the large- N_c limit. To absorb the diverging vacuum energy that is proportional to $|qB|$ we include the tree-level energy term from the EM gauge field itself, which is

$$\mathcal{U}_{EM}^{\text{tree}} = -\frac{1}{4} \mathcal{F}_{\mu\nu} \mathcal{F}^{\mu\nu} = \frac{1}{2} (\mathbf{E}^2 + \mathbf{B}^2) = \frac{1}{2} \mathbf{B}^2, \quad (6.7.1)$$

where $\mathcal{F}_{\mu\nu} = \partial_\mu \mathcal{A}_\nu - \partial_\nu \mathcal{A}_\mu$ is the EM field strength tensor. We could of course also have included one-loop contributions to Ω from the pure gauge sector, which would be given by

$$\begin{aligned} \mathcal{U}_{EM}^{1\text{-loop}} &= \int \frac{d^3p}{(2\pi)^3} [|\mathbf{p}| + 2T \ln(1 - e^{-\beta|\mathbf{p}|})] \\ &= -\frac{\pi^2}{45} T^4 + \int \frac{d^3p}{(2\pi)^3} |\mathbf{p}|. \end{aligned} \quad (6.7.2)$$

In dimensional regularization the last integral vanishes. We see this immediately since it has no momentum scale to go in the logarithm $\ln\left(\frac{\Lambda}{\cdot}\right)$ that usually arises in these integrals. Furthermore, the nonzero thermal contribution is not proportional to N_c , and should not be included in the large- N_c limit. Even if the nonzero T^4 contribution does affect the pressure of the model, it does not affect the minimization of the potential with

respect to Δ , q and r . Hence, while the neglect of mesonic fluctuations does affect the phase diagram, the phase diagram is not affected by neglecting thermal fluctuations in the photon field.

Adding the chiral sector and summing over all the quark flavors and colors, we have the effective potential

$$\begin{aligned} \Omega = & \frac{1}{2}B^2 - \frac{1}{2}mv^2 + \frac{1}{4!}\lambda v^4 - hv + \delta\Omega^{\text{div}} + \mathcal{U}_{\text{glue}} \\ & + N_c \sum_f \frac{8(q_f B)^2}{(4\pi)^2} \left[\frac{1}{12} + \frac{\delta_f^2}{2} - \frac{1}{2}\delta_f \ln \delta_f - \zeta^{(1,0)}(-1, \delta_f) + \ln \left(\frac{\Lambda^2}{2|q_f B|} \right) \left(\frac{1}{12} + \frac{\delta_f^2}{2} \right) \right] \\ & - \sum_c \sum_f \frac{8|q_f B|T^2}{(4\pi)^2} \sum_{n=0}^{\infty} (2 - \delta_{n0}) K_\beta(\Delta^2 + 2|q_f B|n, \tilde{\mu}_c). \end{aligned} \quad (6.7.3)$$

The index f runs over $1, \dots, N_f = 2$, while c runs over $1, \dots, N_c = 3$, and

$$\delta_f = \frac{\Delta^2}{2|q_f B|}, \quad (6.7.4)$$

$$\tilde{\mu}_c = \mu + ig[\mathbf{A}_4]_{cc}. \quad (6.7.5)$$

The diverging part is given by

$$\delta\Omega^{\text{div}} = N_c \sum_f \frac{8(q_f B)^2}{(4\pi)^2} \left(\frac{1}{12} + \frac{\delta_f^2}{2} \right) \frac{1}{\epsilon} = N_c \sum_f \frac{2(q_f B)^2}{3} \frac{1}{(4\pi)^2} \frac{1}{\epsilon} + \frac{2N_c \Delta^4}{(4\pi)^2} \frac{1}{\epsilon}. \quad (6.7.6)$$

We now need to take care of renormalization. Conveniently, everything from chapter 4 carries over, as the particle masses still are identified with the masses measured in the vacuum where $B = 0$, and we have no photon loops shifting particle masses in the one-loop large- N_c limit. Letting all couplings $s \in \{g, \lambda, v, m, h\}$ be given by $s = s_{\overline{\text{MS}}} + \delta s_{\overline{\text{MS}}}$ and inserting the running couplings given in (4.4.5)–(4.4.9) and the counterterms given in (A.4.84), we find that the chiral sector is

$$\mathcal{U}_\chi = -\frac{1}{2}m_0^2 f_\pi^2 \frac{\Delta^2}{m_q^2} + \frac{1}{4!}\lambda_0 f_\pi^4 \frac{\Delta^4}{m_q^4} - h_0 f_\pi \frac{\Delta}{m_q} + \delta\Omega_{\text{chiral}}^{\overline{\text{MS}}}, \quad (6.7.7)$$

with

$$\delta\Omega_{\text{chiral}}^{\overline{\text{MS}}} = -\frac{2N_c \Delta^4}{(4\pi)^2} \frac{1}{\epsilon}. \quad (6.7.8)$$

Here λ_0 , m_0 , h_0 are given by (4.4.13)–(4.4.15). We see that the counterterm from the renormalization of the couplings in the tree-level mesonic potential exactly cancels the divergence that is independent of B .

We remind that $\Delta = gv = g_{\overline{\text{MS}}} v_{\overline{\text{MS}}}$, as was pointed out Sec. 4.6. This means that all occurrences of Δ in the last two lines of (6.7.3) can be kept as they are upon introducing the $\overline{\text{MS}}$ couplings.

Everything that remains is the renormalization of the B -field. We could just let $B^2 \rightarrow (1 + \delta Z)B^2$, and demand that $\delta Z B^2$ absorbs the B -dependent divergences. However, since the underlying dynamics of the B -field is known, we can do better. The renormalization of B is a consequence of the renormalization of the gauge field \mathcal{A}_μ . If we calculate the self-energy corrections to the photon propagator to one loop and demand that it is zero, we find an expression for δZ in the on-shell scheme. Since this is a standard result of QED, we quote the final expression and refer to textbooks for a derivation [11, 26, 28]. Letting $\mathcal{A}_\mu = \sqrt{Z^{\text{OS}}}\mathcal{A}_\mu^{\text{OS}}$ with $Z^{\text{OS}} = 1 + \delta Z^{\text{OS}}$, we find that⁷

$$\delta Z_{\text{OS}} = -\frac{4N_c}{3(4\pi)^2} \sum_f q_f^2 \left[\frac{1}{\epsilon} + \ln\left(\frac{\Lambda^2}{m_q^2}\right) \right]. \quad (6.7.9)$$

Note that we should use m_q and not Δ , since the renormalization is carried out at $T = 0$. Furthermore, compared to the alternative approach outlined in the beginning of this paragraph we have gained an extra $\ln\left(\frac{\Lambda^2}{m_q^2}\right)$ term. This term only affects the pressure of the model and has no effect on the phase diagram, since it is independent of the order parameters.

Since the bare magnetic field should be independent of the renormalization scheme, we have

$$Z_{\text{OS}} B_{\text{OS}}^2 = Z_{\overline{\text{MS}}} B_{\overline{\text{MS}}}^2, \quad (6.7.10)$$

which gives, to one-loop order,

$$B_{\overline{\text{MS}}}^2 = \frac{1 + \delta Z_{\text{OS}}}{1 + \delta Z_{\overline{\text{MS}}}} B_{\text{OS}}^2 \approx (1 + \delta Z_{\text{OS}} - \delta Z_{\overline{\text{MS}}}) B_{\text{OS}}^2, \quad (6.7.11)$$

which evaluates to

$$B_{\overline{\text{MS}}}^2 = \left[1 - \frac{4N_c}{3(4\pi)^2} \ln\left(\frac{\Lambda^2}{m_q^2}\right) \sum_f q_f^2 \right] B_{\text{OS}}^2. \quad (6.7.12)$$

Inserting $B = B_{\overline{\text{MS}}} + \delta B_{\overline{\text{MS}}}$ we see that the B -dependent divergence cancels, and we find, after some rewriting, that the vacuum part of the potential reads

$$\begin{aligned} \Omega_{\text{vac}} = & -\frac{1}{2} m_0^2 f_\pi^2 \frac{\Delta^2}{m_q^2} + \frac{1}{4!} \lambda_0 f_\pi^4 \frac{\Delta^4}{m_q^4} - h_0 f_\pi \frac{\Delta}{m_q} + \frac{2N_c \Delta^4}{(4\pi)^2} \left[\frac{3}{2} + \ln\left(\frac{\Lambda^2}{\Delta^2}\right) \right] \\ & + \frac{8N_c}{(4\pi)^2} \sum_f (q_f B)^2 \left[\frac{1}{12} - \zeta^{(1,0)}(-1, \delta_f) - \frac{1}{2} \delta_f \ln \delta_f - \frac{\delta_f^2}{4} + \frac{1}{2} \delta_f^2 \ln \delta_f \right] \\ & + \frac{1}{2} B^2 \left[1 + \frac{4N_c}{3(4\pi)^2} \sum_f q_f^2 \ln\left(\frac{m_q^2}{2|q_f B|}\right) \right], \end{aligned} \quad (6.7.13)$$

⁷Again we have redefined $\Lambda^2 \rightarrow \Lambda^2/4\pi e^{-\gamma_E}$. Furthermore, our result differs by a factor two in the ϵ^{-1} -term from Refs. [26, 28], since we define $d = 4 - 2\epsilon$ in dimensional regularization, while in Refs. [26, 28] they let $d = 4 - \epsilon$.

where we wrote $B_{\text{OS}} = B$. Note that for all terms except the tree-level term $\frac{1}{2}B^2$, we can set $B_{\overline{\text{MS}}} = B_{\text{OS}}$, since working to one-loop order means we are working up to $\mathcal{O}(q_f^2)$, and $|q_f B_{\overline{\text{MS}}}|$ and $|q_f B_{\text{OS}}|$ differs only at higher orders in q_f . Furthermore, we have rewritten the potential so that the first line is the $B = 0$ contribution, while the second and third lines are the additional terms arising due to the magnetic field. Again we point out that if we are only studying the order parameters, the term on the last line is irrelevant.

The term on the second line of (6.7.13) superficially appears to be nonzero even if $B = 0$ due to terms $\sim B^2 \delta_f^2 \sim \mathcal{O}(B^0)$ and $\sim B^2 \delta_f^2 \ln \delta_f \sim \mathcal{O}(-\ln B)$. However, it turns out that these contributions are cancelled by similar contributions from the $\sim B^2 \zeta^{(1,0)}(-1, \delta_f)$ term. Noting that small B corresponds to large δ_f , and using the large- δ_f expansion [126]

$$\zeta^{(1,0)}(-1, \delta_f) = -\frac{1}{4}\delta_f^2 + \delta_f^2 \ln \delta_f - \frac{1}{2}\delta_f \ln \delta_f + \frac{1}{12} \ln \delta_f + \frac{1}{12} + \mathcal{O}\left(\frac{1}{\delta_f^2}\right), \quad (6.7.14)$$

we see that

$$\lim_{B \rightarrow 0} (q_f B)^2 \left[\frac{1}{12} - \zeta^{(1,0)}(-1, \delta_f) - \frac{1}{2}\delta_f \ln \delta_f - \frac{\delta_f^2}{4} + \frac{1}{2}\delta_f^2 \ln \delta_f \right] = 0. \quad (6.7.15)$$

Inserting the couplings λ_0 , m_0 and h_0 and setting $\Lambda = \Lambda_0$, with Λ_0 as defined in (4.4.10), we finally find

Large- N_c One-Loop Effective Potential of the PQM model in a B -field

$$\begin{aligned} \Omega = & \frac{3}{4} m_\pi^2 f_\pi^2 \left\{ 1 - \frac{4N_c m_q^2}{(4\pi)^2 f_\pi^2} m_\pi^2 C'_\pi \right\} \frac{\Delta^2}{m_q^2} + \frac{2N_c m_q^4}{(4\pi)^2} \left\{ \frac{3}{2} + \ln \left(\frac{m_q^2}{\Delta^2} \right) \right\} \frac{\Delta^4}{m_q^4} \\ & - \frac{m_\sigma^2 f_\pi^2}{4} \left\{ 1 + \frac{4N_c m_q^2}{(4\pi)^2 f_\pi^2} \left[\left(1 - \frac{4m_q^2}{m_\sigma^2} \right) C_\sigma - C_\pi - m_\pi^2 C'_\pi + \frac{4m_q^2}{m_\sigma^2} \right] \right\} \frac{\Delta^2}{m_q^2} \\ & + \frac{m_\sigma^2 f_\pi^2}{8} \left\{ 1 + \frac{4N_c m_q^2}{(4\pi)^2 f_\pi^2} \left[\left(1 - \frac{4m_q^2}{m_\sigma^2} \right) C_\sigma - C_\pi - m_\pi^2 C'_\pi \right] \right\} \frac{\Delta^4}{m_q^4} \\ & - \frac{m_\pi^2 f_\pi^2}{8} \left\{ 1 - \frac{4N_c m_q^2}{(4\pi)^2 f_\pi^2} m_\pi^2 C'_\pi \right\} \frac{\Delta^4}{m_q^4} - m_\pi^2 f_\pi^2 \left\{ 1 - \frac{4N_c m_q^2}{(4\pi)^2 f_\pi^2} m_\pi^2 C'_\pi \right\} \frac{\Delta}{m_q} \\ & - \frac{8N_c}{(4\pi)^2} \sum_f (q_f B)^2 \left[\zeta^{(1,0)}(-1, \delta_f) + \frac{1}{2}\delta_f \ln \delta_f + \frac{\delta_f^2}{4} - \frac{1}{2}\delta_f^2 \ln \delta_f - \frac{1}{12} \right] \\ & - \frac{8|q_f B| T^2}{(4\pi)^2} \sum_{n,c,f} (2 - \delta_{n0}) K_\beta \left(\Delta^2 + 2|q_f B| n, \tilde{\mu}_c(q, r) \right) \\ & + \frac{1}{2} B^2 \left[1 + \frac{4N_c}{3(4\pi)^2} \sum_f q_f^2 \ln \left(\frac{m_q^2}{2|q_f B|} \right) \right] + \mathcal{U}_{\text{glue}}(\Phi(q, r), \bar{\Phi}(q, r), T). \end{aligned} \quad (6.7.16)$$

We have

$$\beta\tilde{\mu}_1 = \beta\mu + i\frac{2\pi}{3}(q+r), \quad \beta\tilde{\mu}_2 = \beta\mu + i\frac{2\pi}{3}(-q+r), \quad \beta\tilde{\mu}_3 = \beta\mu - i\frac{4\pi}{3}r, \quad (6.7.17)$$

as can be seen from the definition of $\tilde{\mu}_c$ in (6.2.4) and the parametrization of \mathbf{A}_4 in Sec. 2.7. Note that here q is the Polyakov loop eigenvalue and not an electric charge.

6.8 A Fugacity Expansion of Ω_T

The expression for Ω_T given in (6.6.20) appears to be the one usually quoted in the literature. However, the integral $K_\beta(m^2, \mu)$ is computationally intensive to evaluate numerically. For this reason we will derive an alternative expression for Ω_T in terms of Bessel functions. With this expression we can take advantage of preexisting code libraries for highly efficient computation of Bessel functions.

We find that (6.6.16) generalized to N_c colors reads

$$\Omega_T = -\frac{|q_f B|}{2\pi} T \sum_c \sum_{k=\pm 1} \sum_{n=0}^{\infty} (2 - \delta_{n0}) \int_{-\infty}^{\infty} \frac{dp_z}{2\pi} \ln \left[1 + e^{-\beta(\sqrt{p_z^2 + M_B^2} - k\tilde{\mu}_c)} \right], \quad (6.8.1)$$

for a single flavor f . Introducing $x = \beta p_z$, $y = \beta M_B$ and $z_c = \beta\tilde{\mu}_c$, we find

$$\Omega_T = -\frac{|q_f B|}{2\pi^2} T^2 \sum_{n=0}^{\infty} (2 - \delta_{n0}) \sum_c \sum_{k=\pm 1} \int_0^{\infty} dx \ln \left(1 + e^{-\sqrt{x^2 + y^2} + kz_c} \right). \quad (6.8.2)$$

We now Taylor expand the logarithm, sum over k , and find

$$\Omega_T = -\frac{|q_f B|}{2\pi^2} T^2 \sum_{n=0}^{\infty} (2 - \delta_{n0}) \sum_c \sum_{l=1}^{\infty} \frac{(-1)^{l+1}}{l} (e^{lz_c} + e^{-lz_c}) \int_0^{\infty} dx e^{-l\sqrt{x^2 + y^2}} \quad (6.8.3)$$

Performing a change of variables we have

$$I \equiv \int_0^{\infty} dx e^{-l\sqrt{x^2 + y^2}} = y \int_1^{\infty} du \frac{u}{\sqrt{u^2 - 1}} e^{-(ly)u}, \quad (6.8.4)$$

where $u = \sqrt{(x/y)^2 + 1}$. Setting $u = \cosh t$ we find

$$I = y \int_0^{\infty} dt \cosh t e^{-(ly) \cosh t}. \quad (6.8.5)$$

Up to a factor, I can be identified with a modified Bessel function of the second kind K_ν with $\nu = 1$ through the integral representation [153]

$$K_\nu(z) = \int_0^{\infty} dt \cosh(\nu t) e^{-z \cosh t}, \quad (6.8.6)$$

and we thus find

$$I = y K_1(ly) = \beta M_B K_1(l\beta M_B). \quad (6.8.7)$$

We also have that

$$\sum_c (e^{lz_c} + e^{-lz_c}) = N_c \left(e^{l\beta\mu} \Phi_l + e^{-l\beta\mu} \bar{\Phi}_l \right), \quad (6.8.8)$$

where

$$\Phi_l = \frac{1}{N_c} \text{tr}_c L^l, \quad \bar{\Phi}_l = \frac{1}{N_c} \text{tr}_c \bar{L}^l, \quad (6.8.9)$$

are ‘‘Polyakov loops’’ winding imaginary time l times. For more flavors we thus find the expression

Ω_T Fugacity Expansion

$$\Omega_T = - \sum_f \frac{8N_c |q_f B| T}{(4\pi)^2} \sum_{n=0}^{\infty} (2 - \delta_{n0}) M_B \sum_{l=1}^{\infty} \frac{(-1)^{l+1}}{l} K_1(l\beta M_B) \left(e^{l\beta\mu} \Phi_l + e^{-l\beta\mu} \bar{\Phi}_l \right). \quad (6.8.10)$$

We refer to this as a fugacity expansion, since the quantity $e^{\beta\mu}$ is known as the fugacity of the system. In the case where $\mu = 0$, where we can always set $r = 0$ and which is the case we will be studying, we find

$$N_c(\Phi_l + \bar{\Phi}_l) = 2 + 4 \cos \left(\frac{2\pi ql}{3} \right), \quad (6.8.11)$$

and finally obtain

$$\Omega_T = - \sum_f \frac{8|q_f B| T}{(4\pi)^2} \sum_{n=0}^{\infty} (2 - \delta_{n0}) M_B \sum_{l=1}^{\infty} \frac{(-1)^{l+1}}{l} K_1(l\beta M_B) \left[2 + 4 \cos \left(\frac{2\pi ql}{3} \right) \right], \quad (6.8.12)$$

with $M_B = \sqrt{\Delta^2 + 2|q_f B|n}$.

6.9 Numerical Methods

We now proceed to study numerically how the effective potential changes in the presence of a magnetic field and its consequences for the transitions. To calculate the thermal contribution to the effective potential, we must sum over Landau levels. This causes the computational burden to increase significantly compared to the $B = 0$ case. In practice we must truncate the sum over Landau levels and, if we use (6.8.12), the sum over Bessel functions. However, for either large Δ or large magnetic fields, the sum over Landau levels should rapidly converge since we effectively sum up thermal fluctuations from one-dimensional particles with mass $M_B = \sqrt{\Delta^2 + 2|q_f B|n}$. Increasing n leads to increasing effective masses and a high degree of Boltzmann suppression. Since $K_1(z)$ decays very rapidly for $z > 1$, we see that Landau levels are strongly suppressed once $lM_B > T$, as expected. For either small B or Δ both the number of Landau levels and ‘‘ l -levels’’ required in the sum increase significantly.

We truncate the sum over Landau levels when the difference between two consecutive terms is less than $10^{-4}f_\pi^4$. This is significantly smaller than the expected value of the potential at the minimum at any temperature. From Fig. 5.3 we see that the potential at the minimum is of the order $\Omega \sim f_\pi^4$ at $T = 0$, while from Fig. 5.10 we see that the minimum is of the order $\Omega \sim 10^3 f_\pi^4$ for $T = 400$ MeV. The value of the potential at the minimum will of course change in the presence of a magnetic field, but it will not change so much that $10^{-4}f_\pi^4$ no longer can be considered small. This would require the pressure to decrease by many orders of magnitude upon the introduction of a magnetic field, which is not the case.

For the sum over Bessel functions, we truncate the sum when the difference between two terms is less than $10^{-6}f_\pi^4$. Thus the main error comes from the truncation of Landau levels.

With these convergence requirements, we find that we get roughly a factor ten speed-up by summing over Bessel functions instead of evaluating K_β for each Landau level, even though both methods produce identical plots. This comparison is clearly dependent on the particular libraries, programming language and implementation used. Here we have used the `scipy.integrate.quad` routine in SciPy [120] for the numerical integration needed to evaluate K_β , with is an adaptive integration scheme from the Fortran library QUADPACK [154].⁸ For faster integration we have implemented the integrand in C and accessed it through the `scipy.LowLevelCallable` class. For the modified Bessel functions we use the `scipy.special.kn` routine, which is a wrapper to the Fortran library AMOS [155].⁹ The Hurwitz zeta function derivative is calculated with the `mpmath` library for Python [156], which has an implementation of the Hurwitz zeta function.¹⁰

For the global minimization, we again used the Basin-Hopping method for finding the global minimum of $\Omega(\Delta, q)$ in the domain $\Delta \in [0, \Delta_c]$, where Δ_c is an upper validity range of the effective potential. Δ_c is set to a value just below where Ω becomes non-increasing with increasing Δ . As mentioned, we only study the case where $\mu = 0$ where we can minimize Ω with respect to q and Δ only, and with r set to zero.

6.10 Numerical Results: The Effective Potential

In Fig. 6.1 we see the normalized effective potential $\tilde{\Omega}(\Delta) = \Omega(\Delta) - \Omega(\Delta = 0)$ as function of Δ at $\Phi = 0$, $T = 0$ for various magnetic fields. The parameters are the same as the ones used in Chapter 5, meaning $m_\pi = 140$ MeV, $m_\sigma = 500$ MeV and $m_q = 300$ MeV.

It is clear that the minimum of the potential moves to higher Δ for increasing B , indicating that we have magnetic catalysis at $T = 0$. We also see from Fig. 6.1 that the model is only valid up to roughly $\Delta_c = 500$ MeV. For larger values of Δ it becomes non-increasing. Furthermore, the potential becomes non-increasing for magnetic fields of around $|eB| = 10m_\pi^2$ and larger, and thus the model is only valid for magnetic fields below this value. With a larger sigma mass, as is frequently used in the literature, both

⁸<http://www.netlib.org/quadpack/>

⁹<http://www.netlib.org/amos/>

¹⁰<http://mpmath.org/>

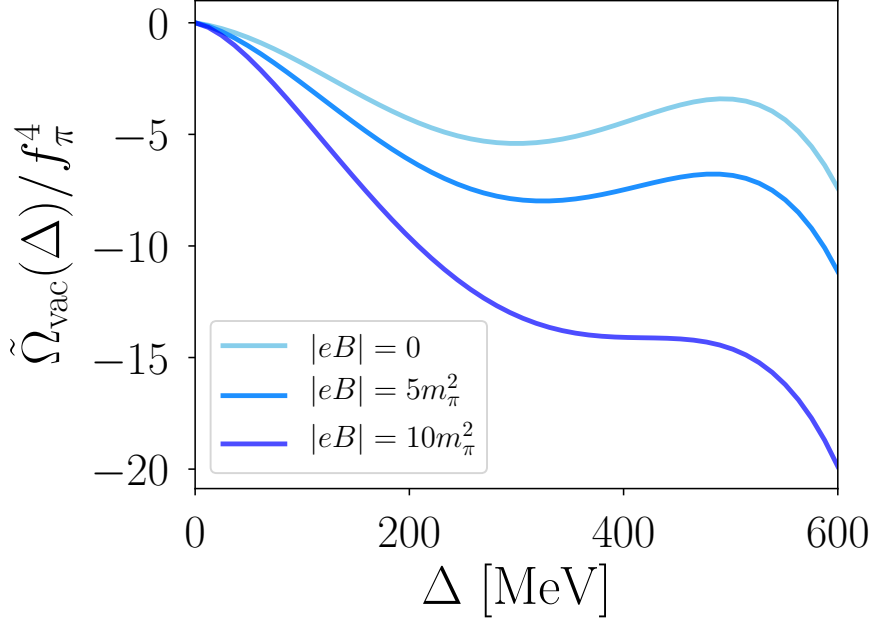


Figure 6.1: Normalized effective potential for increasing magnetic fields at $\Phi = 0$ and $T = 0$.

the validity range in Δ and B increases. For $m_\sigma = 700$ MeV the model is valid up to roughly $\Delta_c = 1100$ MeV and $|eB| = 100m_\pi^2$ at $T = 0$. For a sigma mass of 400 MeV, which is the lower estimate for the mass of the $f_0(500)$ resonance, the model breaks down already at $|eB| = 4m_\pi^2$. Thus, for lower sigma masses it seems more important to include mesonic fluctuations, which potentially, if the relative coupling strengths allow, can stabilize the potential with their $\mathcal{O}(\Delta \ln \Delta)$ contribution.

In Fig. 6.2 we see $\tilde{\Omega}(\Delta)$ for increasing values of T at $\Phi = 0$ and $|eB| = 5m_\pi^2$. As in the $B = 0$ case we see that as temperature increases the minimum moves towards $\Delta = 0$.

Figures 6.3 and 6.4 show the normalized effective potential $\bar{\Omega}(\Phi) = \Omega(\Phi) - \Omega(\Phi = 1)$ at $T = \Delta = 150$ MeV for the two different Polyakov loop potentials. Choosing $r = 0$ implies that $\Phi \in \mathbb{R}$ and $-\frac{1}{3} \leq \Phi \leq 1$, which explains the plotted range on the x -axis. We see that for both the PQM and χM models the minimum moves to larger Φ for increasing B . Interestingly, remembering that $\Phi(T)$ behaves oppositely to $\Delta(T)$, this indicates the possibility of inverse magnetic catalysis for the Polyakov loop. However, this does not show that inverse magnetic catalysis actually occurs. To investigate this, we must solve for $\Phi(T)$ and $\Delta(T)$ by minimizing $\Omega(\Delta, \Phi, T)$ with respect to Δ and Φ , as usual. Before moving on to doing this in the next section, we also note that the PQM and χM models are significantly different in their sensitivity to Φ and B . We see that the minimum of the PQM model moves much less than the minimum of the χM model upon the introduction of a magnetic field.

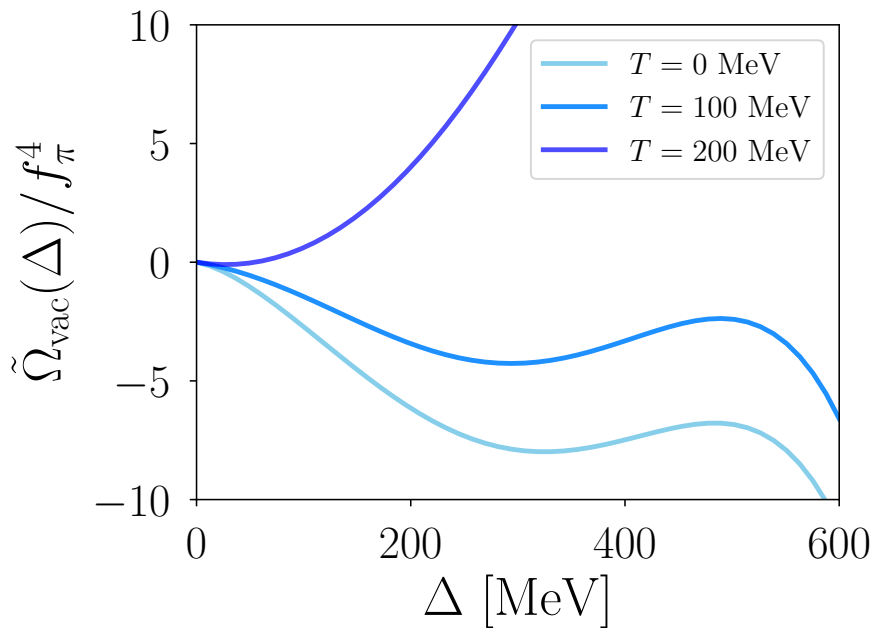


Figure 6.2: Normalized effective potential for increasing temperatures at $|eB| = 5m_\pi^2$ and $\Phi = 1$.

6.11 Numerical Results: Magnetic Catalysis

The chiral condensate and the Polyakov loop as a function of temperature for different magnetic fields are shown in Figs. 6.5 and 6.6. For both models we see the same behavior. The chiral condensate increases as a function of magnetic field everywhere, meaning the system displays magnetic catalysis at any temperature. At low temperatures this is the right behavior, but lattice data show that inverse magnetic catalysis occurs around the transition temperature, causing T_c to be lowered. This is not reproduced in the models, as is also reported in other model studies. Instead, we have a slight increase in T_c , which is plotted in Fig. 6.7.

We also see that the Polyakov loop is practically unchanged, meaning that we have a slight splitting between the chiral and deconfinement transition temperatures. Again, this is not in line with the lattice data [141–143], which shows a decreasing $T_c(B)$ (see Fig. 6.10).

6.12 Numerical Results: The Effect of the Chiral Sector on Magnetic Catalysis

Interestingly, by varying m_σ and m_q we find that it is possible to obtain inverse magnetic catalysis for the Polyakov loop while we still have magnetic catalysis for the chiral

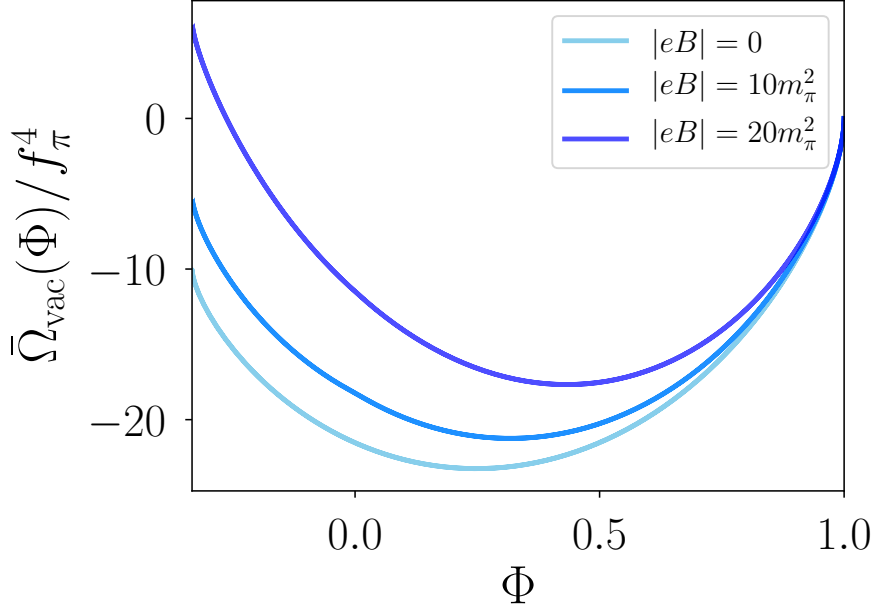


Figure 6.3: Normalized effective potential with $\Delta = T = 150$ MeV as function of the Polyakov loop $\Phi = \bar{\Phi}$ at different magnetic fields for the χM model.

condensate. In Fig. 6.8 we see $\Delta(T)$ and $\Phi(T)$ for $m_\sigma = 600$ MeV and $m_q = 200$ MeV. This is a useful observation since Ozaki et al. in Ref. [146] find inverse magnetic catalysis in a simple effective model with one quark flavor and the RRTW potential, but with no chiral sector. The finding that inverse magnetic catalysis for Φ does not imply inverse magnetic catalysis for $\Delta(T)$ is useful have in mind when looking at the results of Ref. [146], since it means that it cannot be considered a solution to the problem of lacking inverse magnetic catalysis in effective models.

We can go further and investigate what happens if we add a chiral sector to the model investigated in Ref. [146]. We obtained the model as the one studied in Ref. [146] if we remove the chiral sector of the PQM model, use the RRTW potential, and study only one quark flavor with charge $q_f = e$.^{11,12} Since we are only looking at the behaviour $\Phi(q(T))$, which is determined by the solutions of $\partial_q \Omega = 0$, we can drop all terms that do not depend on the Polyakov loop eigenvalue q . Thus, we can optimize the potential

$$\mathcal{V} = \mathcal{U}_{\text{RRTW}}(\Phi(q), \bar{\Phi}(q), T) - \frac{8|eB|T}{(4\pi)^2} \sum_{n=0}^{\infty} (2 - \delta_{n0}) M_B \sum_{l=1}^{\infty} \frac{(-1)^{l+1}}{l} K_1(l\beta M_B) \left[2 + 4 \cos\left(\frac{2\pi ql}{3}\right) \right] \quad (6.12.1)$$

¹¹The quark thermal contribution is written in a different form in Ref. [146], since they instead use the Schwinger proper time method to calculate the thermal quark term.

¹²To remove the vacuum energy divergence in the case where we have no chiral sector we would simply add a vacuum energy counterterm $\delta\mathcal{L} \propto m_q^4 \epsilon^{-1}$ to the Lagrangian at one loop.

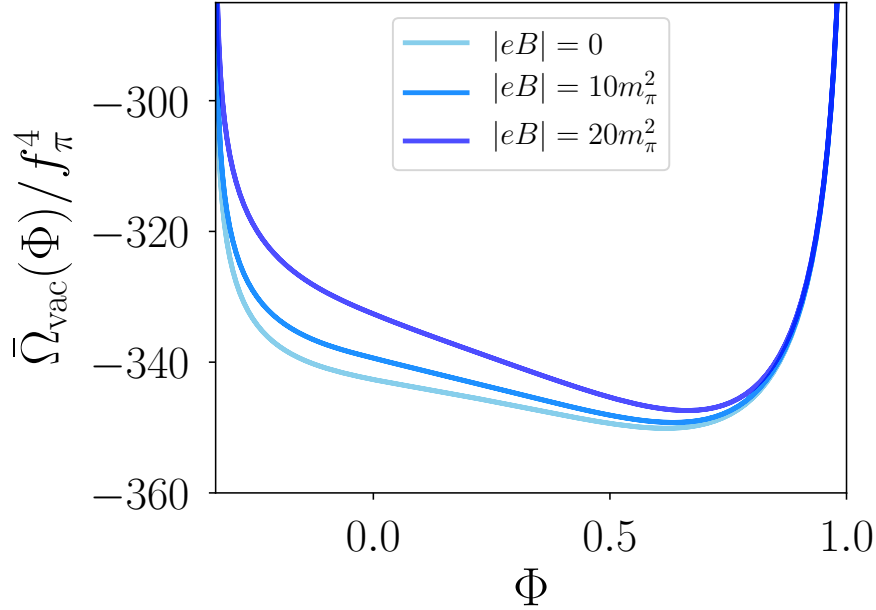


Figure 6.4: Normalized effective potential with $\Delta = T = 150$ MeV as function of the Polyakov loop $\Phi = \bar{\Phi}$ at different magnetic fields for the PQM model.

with respect to q to find $\Phi(T)$. For a direct comparison we use the same parameters as Ref. [146], which means that we set $T_0 = 270$ MeV in the RRTW potential and $m_q = 350$ MeV.

In the left plot of Fig. 6.9 we see $\Phi(T)$ as predicted by the model given by (6.12.1). The left plot is in full agreement with Fig. 10 in Ref. [146], and we see that inverse magnetic catalysis occurs. However, in the right plot we see the resulting $\Phi(T)$ when we reintroduce chiral sector. When reintroducing the chiral sector, we add only one quark flavor with a charge $q_f = e$.¹³ Furthermore, we use a sigma with $m_\sigma = 800$ MeV to be able to reach the very high magnetic field of $|eB| = 0.75 \text{ GeV}^2 \sim 38m_\pi^2$, which is the highest magnetic field considered in Ref. [146]. We see that the addition of the chiral sector removes the inverse magnetic catalysis.

6.13 Inverse Magnetic Catalysis

To gain a better understanding of the reason for inverse magnetic catalysis, we repeat the main points presented Ref. [143].

Consider QCD with a single quark flavor. One can show that the chiral condensate

¹³Note that with one quark flavor, the one-loop corrections to the couplings, equations (4.4.13)-(4.4.15), are halved.

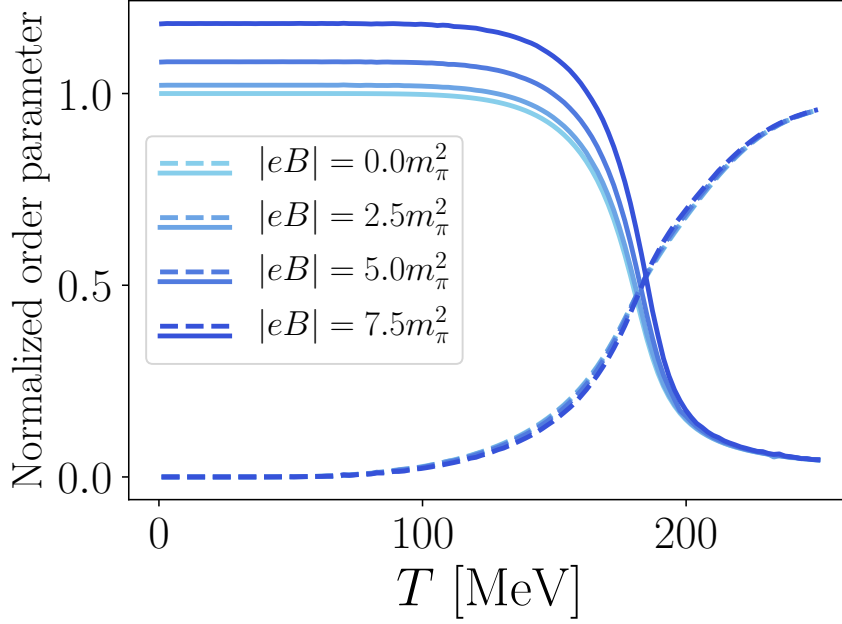


Figure 6.5: The normalized chiral condensate $\Delta/\Delta(T=0, B=0)$ and the Polyakov loop in the χM model as function of temperature for different magnetic fields. A full line represents the chiral condensate and a dashed line the Polyakov loop.

is given by

$$\langle \bar{\psi}\psi \rangle = \frac{1}{Z} \int \mathcal{D}A_\mu e^{-S_{YM}} \det(\not{D}(B) + m) \text{tr}(\not{D}(B) + m)^{-1}, \quad (6.13.1)$$

with the partition function being

$$Z = \int \mathcal{D}A_\mu e^{-S_{YM}} \det(\not{D}(B) + m), \quad (6.13.2)$$

and $\not{D} = \gamma_\mu D_\mu$.¹⁴ Let B be small compared to all other scales in the problem of the same dimension, so that it is reasonable to assume that

$$\det(\not{D}(B) + m) = \det(\not{D}(0) + m) + \delta_{\det}(B) \quad (6.13.3)$$

$$\text{tr}(\not{D}(B) + m)^{-1} = \text{tr}(\not{D}(0) + m)^{-1} + \delta_{\text{tr}}(B). \quad (6.13.4)$$

with the δ -terms being small compared to the trace and determinant terms. We can now write

$$\langle \bar{\psi}\psi \rangle \approx \langle \bar{\psi}\psi \rangle^{\text{val}} + \langle \bar{\psi}\psi \rangle^{\text{sea}}, \quad (6.13.5)$$

¹⁴Here γ_μ are Euclidean gamma matrices, whose exact form are entirely irrelevant to our argument.

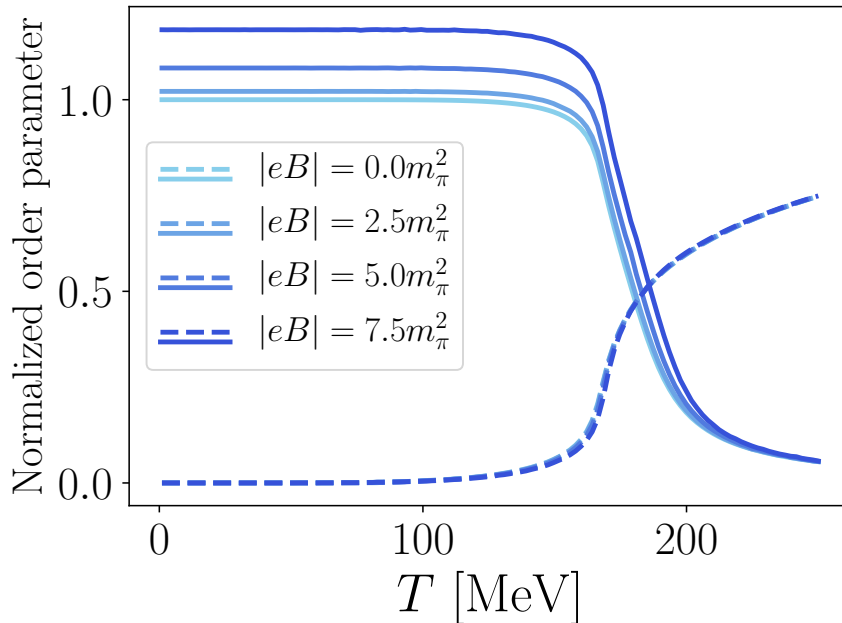


Figure 6.6: The normalized chiral condensate $\Delta/\Delta(T=0, B=0)$ and the Polyakov loop in the PQM model as function of temperature for different magnetic fields. A full line represents the chiral condensate and a dashed line the polyakov loop.

where we have defined the valence and sea quark contributions

$$\langle \bar{\psi}\psi \rangle^{\text{val}} = \frac{1}{Z} \int \mathcal{D}A_\mu e^{-S_{YM}} \det(\not{D}(0) + m) \text{tr}(\not{D}(B) + m)^{-1}, \quad (6.13.6)$$

$$\langle \bar{\psi}\psi \rangle^{\text{sea}} = \frac{1}{Z} \int \mathcal{D}A_\mu e^{-S_{YM}} \det(\not{D}(B) + m) \text{tr}(\not{D}(0) + m)^{-1}, \quad (6.13.7)$$

and neglected $\delta_{\text{tr}}\delta_{\text{det}}$. In the low- B regime we see that the change in the chiral condensate from the introduction of a magnetic field arises from two effects: The term $e^{-S_{YM}} \det(\not{D}(B) + m)$ represents the probability distribution for a given gauge field configuration, and the introduction of a magnetic field in the determinant thus changes the relative weighting of different gauge field configurations in the path integral. This is the sea effect. The valence contribution comes from the change in the eigenvalue spectrum of the quark propagator $(\not{D}(B) + m)^{-1}$.¹⁵

It is shown on the lattice [138] that (6.13.5) is a very good approximation at low magnetic fields. Furthermore, it is shown in Ref. [143] that $\langle \bar{\psi}\psi \rangle^{\text{val}}$ is positive for all T and B , while around the critical temperature $\langle \bar{\psi}\psi \rangle^{\text{sea}}$ becomes negative. Thus, it is the sea effect which drives inverse magnetic catalysis. The sea effect can be seen as a backreaction from the quark sector onto the gluonic sector. However, since the PQM or

¹⁵Taking the trace corresponds to summing over all the eigenvalues.

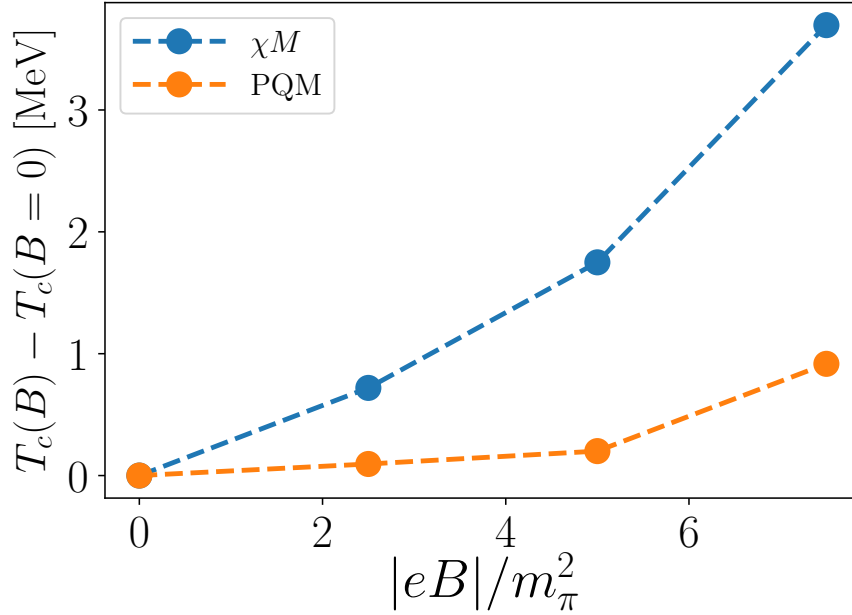


Figure 6.7: The critical temperature for the chiral phase transition for (a) the χM model and (b) the PQM model.

χM models do not contain dynamical gluons, this effect is not taken into account in our models.

A natural way to attempt to take the quark backreaction onto the gluonic sector into account in the PQM or χM models is to add a dependence on the magnetic field in the gluonic potential. This was systematically investigated for the PQM model with the RRTW potential at the mean field level in Ref. [144] and later also with fluctuations with the functional renormalization group (FRG) in Ref. [145].¹⁶ Both papers find that even for an arbitrary dependence $T_0 = T_0(B)$ in the RRTW potential, inverse magnetic catalysis can only be obtained for a range small range of magnetic fields.¹⁷ In Ref. [144] they find that inverse magnetic catalysis cannot be obtained for $|eB| > 15m_\pi^2$ for any functional dependence $T_0(B)$, while in Ref. [145] they find that it cannot be obtained for magnetic fields $|eB| > m_\pi^2$. Note that the latter paper uses a sigma mass of $m_\sigma = 530$ MeV, while for the first paper it is not clear what m_σ is. The two papers mentioned above also investigate a dependence on the magnetic field in the Yukawa coupling, $g = g(B)$, and similarly find that this cannot reproduce inverse magnetic catalysis.

¹⁶The functional renormalization group is a non-perturbative method to take fluctuations into account.

¹⁷Note that both papers require that the chiral transition should not become first order, in order to agree with lattice data [143].

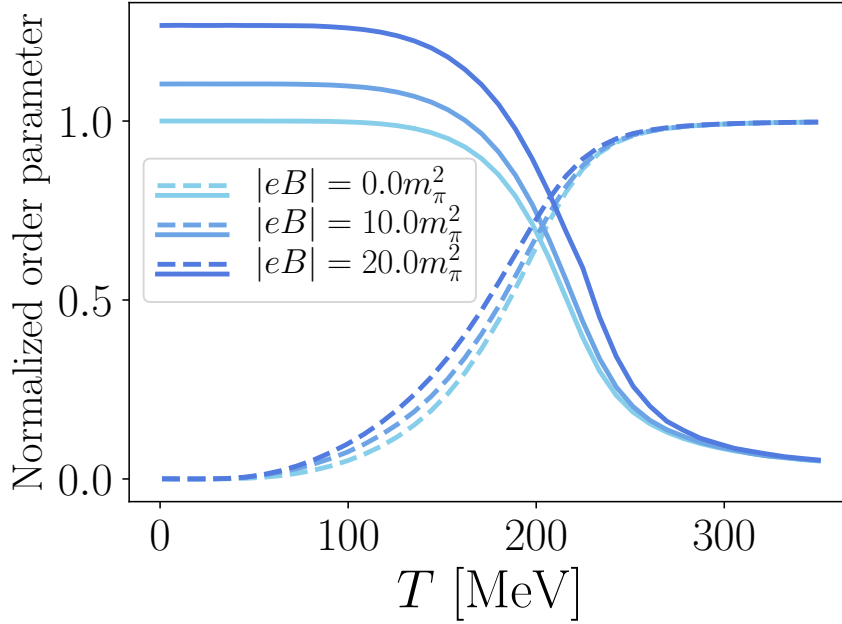


Figure 6.8: The normalized chiral condensate and the Polyakov loop for the unphysical particle masses $m_q = 200$ MeV and $m_\sigma = 600$ MeV. A full line represents the chiral condensate and a dashed line the Polyakov loop.

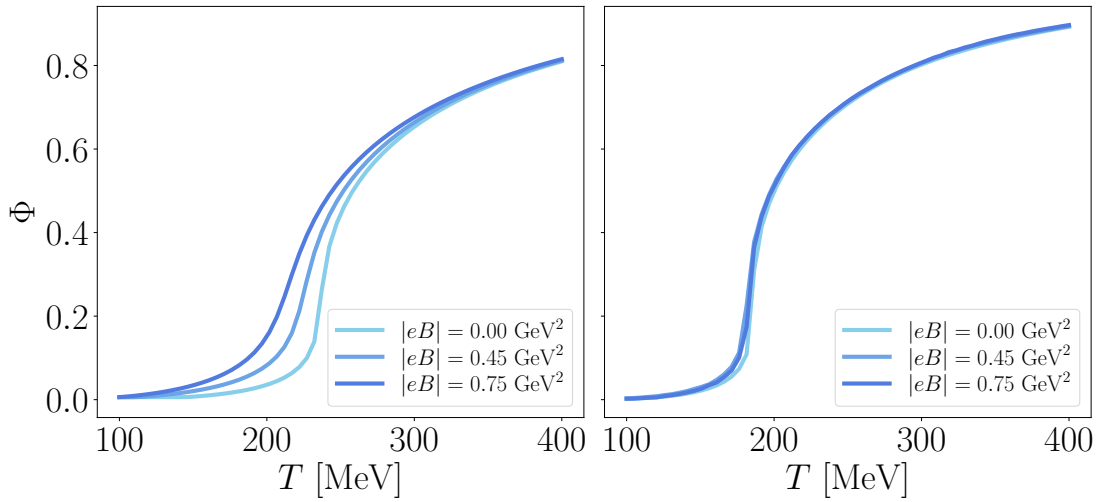


Figure 6.9: The Polyakov loop in a quark model without (left) and with (right) a chiral sector.

6.14 Numerical Results: A B -Dependent Gluonic Sector

We end this chapter with a brief investigation of the effect letting T_d decrease with B in the χM model. We choose

$$T_d(B) = T_d(B=0)e^{-\left(\frac{eB}{bm_\pi^2}\right)^2}, \quad (6.14.1)$$

with the dimensionless constant b setting the decay scale of $T_d(B)$, and $T_d(B = 0) = 270$ MeV.

The resulting phase diagram with $b = 70$ is shown in Fig. 6.10. We have chosen a sigma mass of $m_\sigma = 800$ MeV to be able to reach magnetic fields comparable to the largest magnetic fields in Ref. [142]. It is clear that the critical temperature of the Polyakov loop is driven down by a decreasing T_d , while the chiral sector still displays magnetic catalysis. The result is a splitting between the chiral and deconfinement temperatures which is not found on the lattice [141, 142, 157]. We are not able to choose any value for b the remedies this problem. Hence, with a magnetic field included it appears that the χM model is suffering from the same problems as the PQM model.

It appears that some mechanism that tends to keep $T_{\text{chiral}} \leq T_{\text{deconf}}$ is lacking in the PQM model. We argued in Chapter 5 that there is a strong drive for deconfinement to happen once the chiral transition has taken place, which tends to keep $T_{\text{deconf}} \leq T_{\text{chiral}}$. However, the opposite does not appear to be the case, and it seems that some essential physics is lacking from the PQM and χM models at $B \neq 0$.

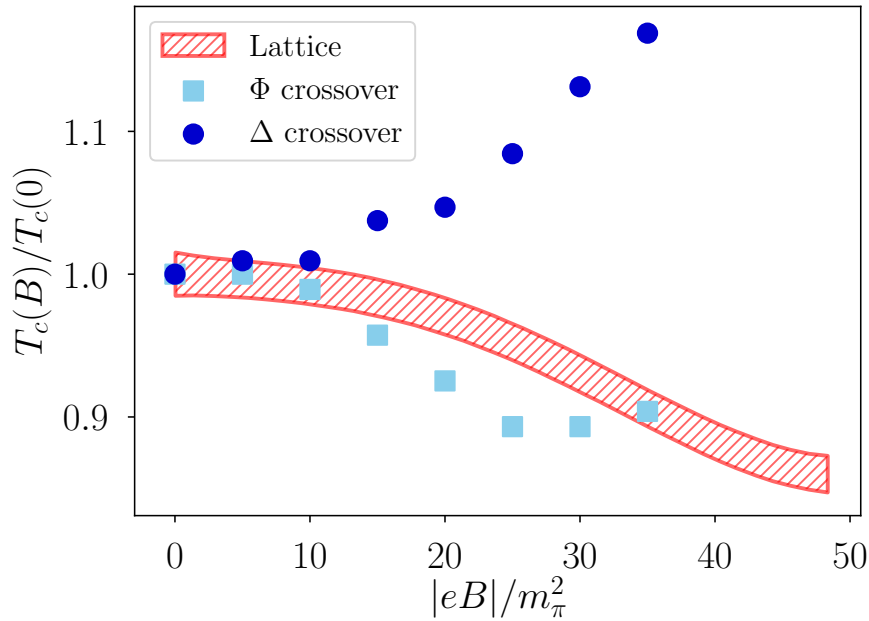


Figure 6.10: Phase diagram of the χM model with $T_d(B)$ as given by (6.14.1) with $b = 70$ compared to the phase diagram from the lattice. The sigma mass is $m_\sigma = 800$ MeV. $(2 + 1)$ -flavor lattice data is taken from Bali et al. [142].

Conclusion and Outlook

7.1 Summary

In this work we have studied spontaneous symmetry breaking and thermodynamics in the two-flavor Polyakov-loop extended quark-meson model and Pisarski-Skokov chiral matrix model. We worked at the one-loop order and investigated the cases of nonzero temperature and baryon chemical potentials, and nonzero temperature and magnetic fields. As a simplifying approximation, we have neglected mesonic fluctuations, which is equivalent to working in the large- N_c limit. Furthermore, we have fixed the coupling constants consistently at the one-loop level, in contrast to what is most often done in the literature on the QM model.

The Effect of One-Loop Couplings

We find that the one-loop determination of couplings could affect the validity range of the models in terms of what particle masses yield an effective potential that has a local minimum. Furthermore, we found that one-loop couplings could have a significant effect on the location of the chiral transition, with the chiral transition being lowered by approximately 25 MeV when using a tree-level determination of the couplings. When it comes to thermodynamics, the introduction of loop corrections to the particle masses have only a small effect.

The Phase Transition and Thermodynamics at $\mu = 0$

We find that both models exhibit coinciding chiral and deconfinement phase transitions, with the inflection points of the chiral condensates located at

$$T_c^{\chi M} = 181_{-9}^{+6} \text{ MeV}, \quad (7.1.1)$$

$$T_c^{\text{PQM}} = 169_{-3}^{+3} \text{ MeV}, \quad (7.1.2)$$

which both lie in the uncertainty range of the transition temperature found on the lattice for two flavors, which is $T_c = (172 \pm 3 \pm 6)$ MeV [112]. We find that both models undergo crossovers at the physical point, rather than true phase transitions.

Furthermore, at zero baryon chemical potential we find that the PQM and χM models have similar predictions for thermodynamic quantities, and they mostly agree reasonably well with QCD lattice data up to $T \approx 2T_c$ – both qualitatively and quantitatively. However, the PQM model appears to be in better agreement with data when it comes to the interaction measure.

For the chiral order parameter both models agree with lattice simulations. However, when it comes to the Polyakov loop, neither model reproduce the lattice result, since Φ in the models show a faster rise with T . However, the PQM model has a functional form $\Phi(T)$ which resembles lattice data, with a slower approach to the asymptotic value $\Phi = 1$ that is associated with a semi-deconfined region.

The Phase Diagram and Thermodynamics at $\mu \neq 0$

At $\mu \neq 0$ we face the problem of how to deal with a complex effective potential or a complex gauge field. We chose to minimize the real part of the potential with a gluonic mean field in $\langle \mathbf{A}_4 \rangle \in \mathfrak{su}(3)$. This has the benefit of giving a bounded effective potential and yields a real effective potential at the minimum of the real part. However, it comes at the cost of having the unphysical effect $\Phi = \bar{\Phi}$.

We find that the PQM model agrees well with both the pressure and quark density from two-flavor lattice data at nonzero chemical potentials in the region $\mu/T \leq 1$ and $T \leq 1.5T_c$. For $T > 1.5T_c$ the PQM model starts to overshoot the pressure and quark number from the lattice. For the χM model we find that the pressure and quark density is too large in the regime $\mu/T \geq 0.4$, but the curves have the correct qualitative shape.

In the μ – T phase diagram, the chiral condensate in the two models behaves similarly. The chiral transition starts out as a crossover and then becomes a first order transition at sufficiently high chemical potentials. The change of transition order is marked by a critical point, which is located at

$$(\mu^*, T^*) = (262 \text{ MeV}, 78 \text{ MeV}), \quad \text{for the } \chi M \text{ model}, \quad (7.1.3)$$

$$(\mu^*, T^*) = (262 \text{ MeV}, 105 \text{ MeV}), \quad \text{for the PQM model}. \quad (7.1.4)$$

A significant difference between the models was found in the deconfinement phase diagram. In the χM model the deconfinement transition also goes from a crossover to a first order transition, with the critical point located at the same place as the critical point for the chiral transition. This is not the case in the PQM model, where the deconfinement transition is a crossover for all μ . Thus, the latter model predicts that the chiral and deconfinement phase transitions are of different order at high chemical potentials.¹ Furthermore, the χM model predicts deconfinement in the low T , high

¹Note that when we say deconfinement phase transition, we are only talking about an inflection point in Φ . We are not claiming that $\Phi \approx 0.5$ or even that it is much larger than zero at the critical temperature.

μ regime, while the PQM model predicts a quarkyonic phase. Thus, the two models predict entirely different phases of matter in the low-temperature, high-density regime, which is the most significant difference between the two models.

The Phase Diagram at $B \neq 0$

With a nonzero magnetic field, we find that both the PQM and the χM models in their standard form exhibit magnetic catalysis at all temperatures. This is in line with lattice data at low temperatures but contradicts them for temperatures around $T = T_c$. We also find that for certain unphysical particle masses, it is possible to obtain inverse magnetic catalysis for the Polyakov loop while still having magnetic catalysis for the chiral condensate. Additionally, we see that a model without a chiral sector predicts inverse magnetic catalysis for Φ .

Finally, we briefly discussed the topic of making the gluon potential dependent on the magnetic field. We find that a B -dependent T_d in the gluonic sector cannot make the χM model display inverse magnetic catalysis, and it thus suffers from the same problems as the PQM model at $B \neq 0$.

7.2 Conclusion

We find that the two-flavor χM and PQM models are in reasonable agreement with two-flavor QCD thermodynamics at zero baryon chemical potential for temperatures up to $T \sim 2T_c$. The main problem with the models is the temperature dependence of the Polyakov loop. At nonzero μ the PQM model appears to agree with the lattice for $T \leq 1.5T_c$ in the regime of μ/T -values where data exist. The χM model overshoots the quark number and pressure in this regime. Furthermore, the χM and PQM models strongly disagree in the high- μ and low- T phase, predicting different states of matter. At nonzero magnetic fields, both models do not show inverse magnetic catalysis in their standard form and disagree qualitatively with lattice results.

7.3 Outlook

There are several natural ways to continue and extend on the work presented in this thesis. In the following we summarize some possibilities.

Including Mesonic Fluctuations

In this work we have used the large- N_c approximation. The most obvious generalization of our approach is to drop this assumption and include fluctuations from mesons. Several studies taking mesonic fluctuations into account have been carried out, both with [121, 122, 158, 159] and without [160] the functional renormalization group (FRG). They seem to indicate possible qualitative effects on the phase diagram. For example, in Ref. [122] they find that the phase diagram splits into two branches after the critical point.

If we would include mesonic fluctuations and still carry out consistent parameter fixing at one loop, it would require the calculation of significantly many more diagrams in the one-loop parameter matching procedure. Thus, the process of renormalizing the theory becomes much more involved. Furthermore, if we do not use FRG we face the problem of m_π^2 becoming negative once the temperature becomes high enough.² Solving this problem would require more advanced methods of perturbative thermal field theory such as hard thermal loops, which is a reorganization of the perturbative expansion [36, 37, 39].

Investigating Minimization Scheme at $\mu \neq 0$

We have chosen a scheme where we minimize the real part of the effective potential. It would be illuminating to see how different the results are between this method and saddle point method. Both methods have been compared in the PQM model, and while they always agree at the endpoints of the phase diagram, they show potentially large differences for the location of the critical point [74]. Since at the time of writing there are no publications on the χM model at $\mu \neq 0$, the saddle point method has not been used with the χM model.

Calculation of Susceptibilities

In Ref. [21] they calculate various susceptibilities for the χM model, including baryon number susceptibilities. Susceptibilities provide more opportunities to compare model data to lattice simulations. Thus, more stringent tests can be put on the χM and PQM models if we extend the study performed in this work also to include susceptibilities.

Isospin Chemical Potential

Since QCD does not suffer from a sign problem at nonzero isospin chemical potentials μ_I , the scenario is open to lattice studies, and the phase diagram in the $\mu_I - T$ plane was recently calculated in Ref. [161]. The PQM model can readily be extended to include nonzero isospin, where a pion condensate appears as a new order parameter. Studies of the PQM model at nonzero isospin has been carried out previously in Ref. [162] and recently also with one-loop couplings in Refs. [163, 164]. Since the PQM and χM models differ the most in their behavior at nonzero baryon chemical potential, it would be interesting to see how the χM model behaves at nonzero μ_I .

²In the chiral limit m_π^2 becomes negative for any $T > 0$, since $m_\pi^2 = 0$ in the vacuum, and m_π^2 decreases with decreasing Δ .

Bibliography

- [1] Å. Folkestad. “The Chiral Phase Transition in the Quark-Meson Model at One Loop”. Unpublished project. 2017.
- [2] A. S. Eve and J. Chadwick. “Lord Rutherford, 1871 - 1937”. In: *Obituary Notices of Fellows of the Royal Society* 2.6 (1936), pp. 394–423.
- [3] N. Kemmer. “Hideki Yukawa, 23 January 1907 - 8 September 1981”. In: *Biographical Memoirs of Fellows of the Royal Society* 29 (1983), pp. 660–676.
- [4] M. Gell-Mann. “A schematic model of baryons and mesons”. In: *Physics Letters* 8.3 (1964), pp. 214–215.
- [5] G. Zweig. “An SU(3) model for strong interaction symmetry and its breaking. Version 2”. In: *Developments in the Quark Theory of Hadrons. Vol. 1. 1964 - 1978*. Ed. by D. Lichtenberg and S. P. Rosen. 1964, pp. 22–101.
- [6] H. Fritzsch, M. Gell-Mann, and H. Leutwyler. “Advantages of the color octet gluon picture”. In: *Physics Letters B* 47.4 (1973), pp. 365–368.
- [7] B. Capdevila et al. “Patterns of New Physics in $b \rightarrow s\ell^+\ell^-$ transitions in the light of recent data”. In: *ArXiv e-prints* (Apr. 2017).
- [8] Particle Data Group, C. Patrignani et al. “Review of Particle Physics”. In: *Chin. Phys.* C40.10 (2016), p. 100001.
- [9] D. J. Gross and F. Wilczek. “Ultraviolet Behavior of Non-Abelian Gauge Theories”. In: *Phys. Rev. Lett.* 30 (26 June 1973), pp. 1343–1346.
- [10] H. D. Politzer. “Reliable Perturbative Results for Strong Interactions?” In: *Phys. Rev. Lett.* 30 (26 June 1973), pp. 1346–1349.
- [11] M. Peskin and D. Schroeder. *An Introduction to Quantum Field Theory*. Westview Press, 1995.
- [12] The STAR Collaboration, J. Adams et al. “Experimental and theoretical challenges in the search for the quark–gluon plasma: The STAR Collaboration’s critical assessment of the evidence from RHIC collisions”. In: *Nuclear Physics A* 757.1 (2005). First Three Years of Operation of RHIC, pp. 102–183.
- [13] The PHOBOS collaboration, B. Back et al. “The PHOBOS perspective on discoveries at RHIC”. In: *Nuclear Physics A* 757.1 (2005). First Three Years of Operation of RHIC, pp. 28–101.

- [14] The BRAHMS collaboration, I. Arsene et al. “Quark–gluon plasma and color glass condensate at RHIC? The perspective from the BRAHMS experiment”. In: *Nuclear Physics A* 757.1 (2005). First Three Years of Operation of RHIC, pp. 1–27.
- [15] The PHENIX Collaboration, K. Adcox et al. “Formation of dense partonic matter in relativistic nucleus–nucleus collisions at RHIC: Experimental evaluation by the PHENIX Collaboration”. In: *Nuclear Physics A* 757.1 (2005). First Three Years of Operation of RHIC, pp. 184–283.
- [16] ALICE Collaboration, K. Aamodt et al. “Elliptic Flow of Charged Particles in Pb-Pb Collisions at $\sqrt{s_{NN}} = 2.76$ TeV”. In: *Phys. Rev. Lett.* 105 (25 Dec. 2010), p. 252302.
- [17] S. Borsányi et al. “Is there still any T_c mystery in lattice QCD? Results with physical masses in the continuum limit III”. In: *Journal of High Energy Physics* 2010.9 (Sept. 2010), p. 73.
- [18] K. Fukushima and T. Hatsuda. “The phase diagram of dense QCD”. In: *Reports on Progress in Physics* 74.1 (2011), p. 014001.
- [19] A. Andronic et al. “Hadron production in ultra-relativistic nuclear collisions: Quarkyonic matter and a triple point in the phase diagram of QCD”. In: *Nuclear Physics A* 837.1 (2010), pp. 65–86.
- [20] G. Aarts. “Introductory lectures on lattice QCD at nonzero baryon number”. In: *Journal of Physics: Conference Series* 706.2 (2016), p. 022004.
- [21] R. D. Pisarski and V. V. Skokov. “Chiral matrix model of the semi-QGP in QCD”. In: *Phys. Rev. D* 94 (3 Aug. 2016), p. 034015.
- [22] L. D. McLerran and B. Svetitsky. “Quark liberation at high temperature: A Monte Carlo study of SU(2) gauge theory”. In: *Phys. Rev. D* 24 (2 July 1981), pp. 450–460.
- [23] L. S. Brown and W. I. Weisberger. “Remarks on the static potential in quantum chromodynamics”. In: *Phys. Rev. D* 20 (12 Dec. 1979), pp. 3239–3245.
- [24] K. Fukushima. “Chiral effective model with the Polyakov loop”. In: *Physics Letters B* 591.3 (2004), pp. 277–284.
- [25] E. Wigner. “On Unitary Representations of the Inhomogeneous Lorentz Group”. In: *Annals of Mathematics* 40.1 (1939), pp. 149–204.
- [26] M. D. Schwartz. *Quantum Field Theory and the Standard Model*. Cambridge University Press, 2014.
- [27] C. N. Yang and R. L. Mills. “Conservation of Isotopic Spin and Isotopic Gauge Invariance”. In: *Phys. Rev.* 96 (1 Oct. 1954), pp. 191–195.
- [28] M. Srednicki. *Quantum field theory*. Cambridge University Press, 2007.
- [29] M. Creutz. “Monte Carlo study of quantized SU(2) gauge theory”. In: *Phys. Rev. D* 21 (8 Apr. 1980), pp. 2308–2315.

- [30] G. S. Bali. “QCD forces and heavy quark bound states”. In: *Physics Reports* 343.1 (2001), pp. 1–136.
- [31] L. L. Foldy and S. A. Wouthuysen. “On the Dirac Theory of Spin 1/2 Particles and Its Non-Relativistic Limit”. In: *Phys. Rev.* 78 (1 Apr. 1950), pp. 29–36.
- [32] F. Schwabl. *Advanced Quantum Mechanics*. Springer-Verlag Berlin Heidelberg, 2008.
- [33] A. Polyakov. “Thermal properties of gauge fields and quark liberation”. In: *Physics Letters B* 72.4 (1978), pp. 477–480.
- [34] L. Susskind. “Lattice models of quark confinement at high temperature”. In: *Phys. Rev. D* 20 (10 Nov. 1979), pp. 2610–2618.
- [35] D. J. Gross, R. D. Pisarski, and L. G. Yaffe. “QCD and instantons at finite temperature”. In: *Rev. Mod. Phys.* 53 (1 Jan. 1981), pp. 43–80.
- [36] J. Kapusta and C. Gale. *Finite-Temperature Field Theory: Principles and Applications*. Cambridge Monographs on Mathematical Physics. Cambridge University Press, 2006.
- [37] M. Le Bellac. *Thermal Field Theory*. Cambridge Monographs on Mathematical Physics. Cambridge University Press, 1996.
- [38] A. Dumitru, R. D. Pisarski, and D. Zschiesche. “Dense quarks, and the fermion sign problem, in a $SU(N)$ matrix model”. In: *Phys. Rev. D* 72 (6 Sept. 2005), p. 065008.
- [39] M. Laine and A. Vuorinen. *Basics of Thermal Field Theory*. Springer International Publishing, 2007.
- [40] H. A. Kramers and G. H. Wannier. “Statistics of the Two-Dimensional Ferromagnet. Part I”. In: *Phys. Rev.* 60 (3 Aug. 1941), pp. 252–262.
- [41] H. A. Kramers and G. H. Wannier. “Statistics of the Two-Dimensional Ferromagnet. Part II”. In: *Phys. Rev.* 60 (3 Aug. 1941), pp. 263–276.
- [42] M. Kardar. *Statistical Physics of Fields*. Cambridge University Press, 2007.
- [43] B. Svetitsky and L. G. Yaffe. “Critical behavior at finite-temperature confinement transitions”. In: *Nuclear Physics B* 210.4 (1982), pp. 423–447.
- [44] K. Fukushima and V. Skokov. “Polyakov loop modeling for hot QCD”. In: *Progress in Particle and Nuclear Physics* 96 (2017), pp. 154–199.
- [45] G. ’t Hooft and M. Veltman. “Regularization and renormalization of gauge fields”. In: *Nuclear Physics B* 44.1 (1972), pp. 189–213.
- [46] K. James and P. Landshoff. “Finite-temperature field theory in the temporal gauge: the imaginary-time formalism”. In: *Phys. Letters B* 251.1 (1990), pp. 167–174.
- [47] N. Weiss. “Effective potential for the order parameter of gauge theories at finite temperature”. In: *Phys. Rev. D* 24 (2 July 1981), pp. 475–480.

- [48] S. Nadkarni. “Dimensional reduction in finite-temperature quantum chromodynamics”. In: *Phys. Rev. D* 27 (4 Feb. 1983), pp. 917–931.
- [49] Y. Nambu and G. Jona-Lasinio. “Dynamical Model of Elementary Particles Based on an Analogy with Superconductivity. I”. In: *Phys. Rev.* 122 (1 Apr. 1961), pp. 345–358.
- [50] Y. Nambu and G. Jona-Lasinio. “Dynamical Model of Elementary Particles Based on an Analogy with Superconductivity. II”. In: *Phys. Rev.* 124 (1 Oct. 1961), pp. 246–254.
- [51] M. Gell-Mann and M. Lévy. “The axial vector current in beta decay”. In: *Il Nuovo Cimento (1955-1965)* 16.4 (May 1960), pp. 705–726.
- [52] F. Schwabl. *Statistical Mechanics*. Springer-Verlag Berlin Heidelberg, 2006.
- [53] H. Callen. *Thermodynamics and an Introduction to Thermostatistics*. Wiley, 1985.
- [54] R. Fukuda and E. Kyriakopoulos. “Derivation of the effective potential”. In: *Nuclear Physics B* 85.2 (1975), pp. 354–364.
- [55] B. Lucini, M. Teper, and U. Wenger. “The high temperature phase transition in SU(N) gauge theories”. In: *Journal of High Energy Physics* 2004.01 (2004), p. 061.
- [56] L. G. Yaffe and B. Svetitsky. “First-order phase transition in the SU(3) gauge theory at finite temperature”. In: *Phys. Rev. D* 26 (4 Aug. 1982), pp. 963–965.
- [57] G. Boyd et al. “Thermodynamics of SU(3) lattice gauge theory”. In: *Nuclear Physics B* 469.3 (1996), pp. 419–444.
- [58] S. Borsányi et al. “Precision SU(3) lattice thermodynamics for a large temperature range”. In: *Journal of High Energy Physics* 2012.7 (July 2012), p. 56.
- [59] L. Giusti and M. Pepe. “Equation of state of the SU(3) Yang–Mills theory: A precise determination from a moving frame”. In: *Physics Letters B* 769 (2017), pp. 385–390.
- [60] O. Kaczmarek et al. “Heavy quark–antiquark free energy and the renormalized Polyakov loop”. In: *Physics Letters B* 543.1 (2002), pp. 41–47.
- [61] C. Ratti, M. A. Thaler, and W. Weise. “Phases of QCD: Lattice thermodynamics and a field theoretical model”. In: *Phys. Rev. D* 73 (1 Jan. 2006), p. 014019.
- [62] C. Ratti et al. “Thermodynamics of the PNJL model”. In: *The European Physical Journal C* 49.1 (Jan. 2007), pp. 213–217.
- [63] K. Fukushima. “Phase diagrams in the three-flavor Nambu–Jona-Lasinio model with the Polyakov loop”. In: *Phys. Rev. D* 77 (11 June 2008), p. 114028.
- [64] V. A. Dexheimer and S. Schramm. “Novel approach to modeling hybrid stars”. In: *Phys. Rev. C* 81 (4 Apr. 2010), p. 045201.
- [65] B.-J. Schaefer, M. Wagner, and J. Wambach. “Thermodynamics of (2 + 1)-flavor QCD: Confronting models with lattice studies”. In: *Phys. Rev. D* 81 (7 Apr. 2010), p. 074013.

- [66] B.-J. Schaefer, J. M. Pawłowski, and J. Wambach. “Phase structure of the Polyakov-quark-meson model”. In: *Phys. Rev. D* 76 (7 Oct. 2007), p. 074023.
- [67] T. K. Herbst, J. M. Pawłowski, and B.-J. Schaefer. “The phase structure of the Polyakov–quark–meson model beyond mean field”. In: *Physics Letters B* 696.1 (2011), pp. 58–67.
- [68] J. O. Andersen, W. R. Naylor, and A. Tranberg. “Chiral and deconfinement transitions in a magnetic background using the functional renormalization group with the Polyakov loop”. In: *Journal of High Energy Physics* 2014.4 (Apr. 2014), p. 187.
- [69] S. Rößner, C. Ratti, and W. Weise. “Polyakov loop, diquarks, and the two-flavor phase diagram”. In: *Phys. Rev. D* 75 (3 Feb. 2007), p. 034007.
- [70] F. Karsch and H. W. Wyld. “Complex Langevin Simulation of the SU(3) Spin Model with Nonzero Chemical Potential”. In: *Phys. Rev. Lett.* 55 (21 Nov. 1985), pp. 2242–2245.
- [71] C. R. Allton et al. “QCD thermal phase transition in the presence of a small chemical potential”. In: *Phys. Rev. D* 66 (7 Oct. 2002), p. 074507.
- [72] H. Abuki and K. Fukushima. “Gauge dynamics in the PNJL model: Color neutrality and Casimir scaling”. In: *Physics Letters B* 676.1 (2009), pp. 57–62.
- [73] S. Rößner et al. “The chiral and deconfinement crossover transitions: PNJL model beyond mean field”. In: *Nuclear Physics A* 814.1 (2008), pp. 118–143.
- [74] B. W. Mintz et al. “Phase diagram and surface tension in the three-flavor Polyakov-quark-meson model”. In: *Phys. Rev. D* 87 (3 Feb. 2013), p. 036004.
- [75] C. Altes. “Constrained effective potential in hot QCD”. In: *Nuclear Physics B* 420.3 (1994), pp. 637–668.
- [76] T. Bhattacharya et al. “Z(N) interface tension in a hot SU(N) gauge theory”. In: *Nuclear Physics B* 383.3 (1992), pp. 497–524.
- [77] J. Maelger, U. Reinosa, and J. Serreau. “Perturbative study of the QCD phase diagram for heavy quarks at nonzero chemical potential: Two-loop corrections”. In: *Phys. Rev. D* 97 (7 Apr. 2018), p. 074027.
- [78] U. Reinosa, J. Serreau, and M. Tissier. “Perturbative study of the QCD phase diagram for heavy quarks at nonzero chemical potential”. In: *Phys. Rev. D* 92 (2 July 2015), p. 025021.
- [79] C. Ratti, M. A. Thaler, and W. Weise. “Phases of QCD: Lattice thermodynamics and a field theoretical model”. In: *Phys. Rev. D* 73 (1 Jan. 2006), p. 014019.
- [80] S. Mukherjee, M. G. Mustafa, and R. Ray. “Thermodynamics of the Polyakov-Nambu-Jona-Lasinio model with nonzero baryon and isospin chemical potentials”. In: *Phys. Rev. D* 75 (9 May 2007), p. 094015.
- [81] P. Adhikari, J. O. Andersen, and P. Kneschke. “On-shell parameter fixing in the quark-meson model”. In: *Phys. Rev. D* 95 (3 Feb. 2017), p. 036017.

- [82] P. Adhikari, J. O. Andersen, and P. Kneschke. “Inhomogeneous chiral condensate in the quark-meson model”. In: *Phys. Rev. D* 96 (1 July 2017), p. 016013.
- [83] S. L. Grøver. “The quark-meson model in a magnetic field”. MA thesis. Norwegian University of Science and Technology, 2017.
- [84] J. Goldstone. “Field theories with « Superconductor » solutions”. In: *Il Nuovo Cimento (1955-1965)* 19.1 (Jan. 1961), pp. 154–164.
- [85] J. Goldstone, A. Salam, and S. Weinberg. “Broken Symmetries”. In: *Phys. Rev.* 127 (3 Aug. 1962), pp. 965–970.
- [86] Y. Nambu. “Quasi-Particles and Gauge Invariance in the Theory of Superconductivity”. In: *Phys. Rev.* 117 (3 Feb. 1960), pp. 648–663.
- [87] H. Nielsen and S. Chadha. “On how to count Goldstone bosons”. In: *Nuclear Physics B* 105.3 (1976), pp. 445–453.
- [88] M. Grahl and D. H. Rischke. “Functional renormalization group study of the two-flavor linear sigma model in the presence of the axial anomaly”. In: *Phys. Rev. D* 88 (5 Sept. 2013), p. 056014.
- [89] H. Fukaya et al. “Determination of the Chiral Condensate from (2 + 1)-Flavor Lattice QCD”. In: *Phys. Rev. Lett.* 104 (12 Mar. 2010), p. 122002.
- [90] L. Giusti et al. “The QCD chiral condensate from the lattice”. In: *Nuclear Physics B* 538.1 (1999), pp. 249–277.
- [91] S. Borsányi et al. “Full result for the QCD equation of state with 2+1 flavors”. In: *Physics Letters B* 730 (2014), pp. 99–104.
- [92] HotQCD Collaboration, A. Bazavov et al. “Equation of state in (2 + 1)-flavor QCD”. In: *Phys. Rev. D* 90 (9 Nov. 2014), p. 094503.
- [93] J. O. Andersen et al. “NNLO hard-thermal-loop thermodynamics for QCD”. In: *Physics Letters B* 696.5 (2011), pp. 468–472.
- [94] J. O. Andersen et al. “Three-loop HTL QCD thermodynamics”. In: *Journal of High Energy Physics* 2011.8 (Aug. 2011), p. 53.
- [95] N. Haque, M. G. Mustafa, and M. Strickland. “Two-loop hard thermal loop pressure at finite temperature and chemical potential”. In: *Phys. Rev. D* 87 (10 May 2013), p. 105007.
- [96] S. Mogliacci et al. “Equation of state of hot and dense QCD: resummed perturbation theory confronts lattice data”. In: *Journal of High Energy Physics* 2013.12 (Dec. 2013), p. 55.
- [97] D. J. Griffiths. *Introduction to elementary particles; 2nd rev. version*. Physics textbook. New York, NY: Wiley, 2008.
- [98] HotQCD Collaboration, A. Bazavov et al. “Chiral and deconfinement aspects of the QCD transition”. In: *Phys. Rev. D* 85 (5 Mar. 2012), p. 054503.
- [99] A. Dumitru et al. “How wide is the transition to deconfinement?” In: *Phys. Rev. D* 83 (3 Feb. 2011), p. 034022.

- [100] A. Dumitru et al. “Effective matrix model for deconfinement in pure gauge theories”. In: *Phys. Rev. D* 86 (10 Nov. 2012), p. 105017.
- [101] N. Weiss. “Wilson line in finite-temperature gauge theories”. In: *Phys. Rev. D* 25 (10 May 1982), pp. 2667–2672.
- [102] P. N. Meisinger, T. R. Miller, and M. C. Ogilvie. “Phenomenological equations of state for the quark-gluon plasma”. In: *Phys. Rev. D* 65 (3 Jan. 2002), p. 034009.
- [103] R. D. Pisarski. “Effective theory of Wilson lines and deconfinement”. In: *Phys. Rev. D* 74 (12 Dec. 2006), p. 121703.
- [104] L. Dolan and R. Jackiw. “Symmetry behavior at finite temperature”. In: *Phys. Rev. D* 9 (12 June 1974), pp. 3320–3341.
- [105] A. Bazavov et al. “Equation of state and QCD transition at finite temperature”. In: *Phys. Rev. D* 80 (1 July 2009), p. 014504.
- [106] QCDSF-DIK Collaboration, V. G. Bornyakov et al. “Probing the finite temperature phase transition with $N_f = 2$ nonperturbatively improved Wilson fermions”. In: *Phys. Rev. D* 82 (1 July 2010), p. 014504.
- [107] Y. Aoki et al. “The QCD transition temperature: Results with physical masses in the continuum limit”. In: *Physics Letters B* 643.1 (2006), pp. 46–54.
- [108] Y. Aoki et al. “The QCD transition temperature: results with physical masses in the continuum limit II”. In: *Journal of High Energy Physics* 2009.06 (2009), p. 088.
- [109] TUMQCD Collaboration, A. Bazavov et al. “Polyakov loop in 2 + 1 flavor QCD from low to high temperatures”. In: *Phys. Rev. D* 93 (11 June 2016), p. 114502.
- [110] HotQCD Collaboration, T. Bhattacharya et al. “QCD Phase Transition with Chiral Quarks and Physical Quark Masses”. In: *Phys. Rev. Lett.* 113 (8 Aug. 2014), p. 082001.
- [111] CP-PACS Collaboration, A. Ali Khan et al. “Phase structure and critical temperature of two-flavor QCD with a renormalization group improved gauge action and clover improved Wilson quark action”. In: *Phys. Rev. D* 63 (3 Dec. 2000), p. 034502.
- [112] V. G. Bornyakov et al. “Finite temperature phase transition with two flavors of improved Wilson fermions”. In: *PoS Lattice2010* (2014), p. 170.
- [113] CP-PACS Collaboration, A. Ali Khan et al. “Equation of state in finite-temperature QCD with two flavors of improved Wilson quarks”. In: *Phys. Rev. D* 64 (7 Sept. 2001), p. 074510.
- [114] A. Bazavov and P. Petreczky. “Polyakov loop in 2+1 flavor QCD”. In: *Phys. Rev. D* 87 (9 May 2013), p. 094505.
- [115] M. Cheng et al. “Equation of state for physical quark masses”. In: *Phys. Rev. D* 81 (5 Mar. 2010), p. 054504.

- [116] O. Kaczmarek and F. Zantow. “Static quark-antiquark interactions in zero and finite temperature QCD: I. Heavy quark free energies, running coupling, and quarkonium binding”. In: *Phys. Rev. D* 71 (11 June 2005), p. 114510.
- [117] C. R. Allton et al. “Thermodynamics of two flavor QCD to sixth order in quark chemical potential”. In: *Phys. Rev. D* 71 (5 Mar. 2005), p. 054508.
- [118] A. Rohatgi. *WebPlotDigitizer Version 4.0*. Oct. 2017.
- [119] D. J. Wales and J. P. K. Doye. “Global Optimization by Basin-Hopping and the Lowest Energy Structures of Lennard-Jones Clusters Containing up to 110 Atoms”. In: *The Journal of Physical Chemistry A* 101.28 (1997), pp. 5111–5116.
- [120] E. Jones, T. Oliphant, P. Peterson, et al. *SciPy: Open source scientific tools for Python*. 2001–. URL: <http://www.scipy.org/>.
- [121] K. Kamikado et al. “Fluctuations in the quark-meson model for QCD with isospin chemical potential”. In: *Physics Letters B* 718.3 (2013), pp. 1044–1053.
- [122] B.-J. Schaefer and J. Wambach. “The phase diagram of the quark–meson model”. In: *Nuclear Physics A* 757.3 (2005), pp. 479–492.
- [123] tmfT Collaboration, F. Burger et al. “Equation of state of quark-gluon matter from lattice QCD with two flavors of twisted mass Wilson fermions”. In: *Phys. Rev. D* 91 (7 Apr. 2015), p. 074504.
- [124] J. O. Andersen and R. Khan. “Chiral transition in a magnetic field and at finite baryon density”. In: *Phys. Rev. D* 85 (6 Mar. 2012), p. 065026.
- [125] L. McLerran and R. D. Pisarski. “Phases of dense quarks at large N_c ”. In: *Nuclear Physics A* 796.1 (2007), pp. 83–100.
- [126] J. O. Andersen, W. R. Naylor, and A. Tranberg. “Phase diagram of QCD in a magnetic field”. In: *Rev. Mod. Phys.* 88 (2 Apr. 2016), p. 025001.
- [127] D. E. Kharzeev, L. D. McLerran, and H. J. Warringa. “The effects of topological charge change in heavy ion collisions: “Event by event P and CP violation””. In: *Nuclear Physics A* 803.3 (2008), pp. 227–253.
- [128] V. V. Skokov, A. Y. Illarionov, and V. D. Toneev. “Estimate of the magnetic field strength in heavy-ion collisions”. In: *International Journal of Modern Physics A* 24.31 (2009), pp. 5925–5932.
- [129] A. Bzdak and V. Skokov. “Event-by-event fluctuations of magnetic and electric fields in heavy ion collisions”. In: *Physics Letters B* 710.1 (2012), pp. 171–174.
- [130] R. C. Duncan and C. Thompson. “Formation of very strongly magnetized neutron stars - Implications for gamma-ray bursts”. In: *Astrophysical Journal* 392 (June 1992), pp. L9–L13.
- [131] D. Lai and S. L. Shapiro. “Cold equation of state in a strong magnetic field - Effects of inverse beta-decay”. In: *Astrophysical Journal* 383 (Dec. 1991), pp. 745–751.

- [132] A. J. Mizher, M. N. Chernodub, and E. S. Fraga. “Phase diagram of hot QCD in an external magnetic field: Possible splitting of deconfinement and chiral transitions”. In: *Phys. Rev. D* 82 (10 Nov. 2010), p. 105016.
- [133] R. Gatto and M. Ruggieri. “Deconfinement and chiral symmetry restoration in a strong magnetic background”. In: *Phys. Rev. D* 83 (3 Feb. 2011), p. 034016.
- [134] R. Gatto and M. Ruggieri. “Dressed Polyakov loop and phase diagram of hot quark matter in a magnetic field”. In: *Phys. Rev. D* 82 (5 Sept. 2010), p. 054027.
- [135] K. Kashiwa. “Entanglement between chiral and deconfinement transitions under strong uniform magnetic background field”. In: *Phys. Rev. D* 83 (11 June 2011), p. 117901.
- [136] J. O. Andersen, W. R. Naylor, and A. Tranberg. “Chiral and deconfinement transitions in a magnetic background using the functional renormalization group with the Polyakov loop”. In: *Journal of High Energy Physics* 2014.4 (Apr. 2014), p. 187.
- [137] J. O. Andersen and A. Tranberg. “The chiral transition in a magnetic background: finite density effects and the functional renormalization group”. In: *Journal of High Energy Physics* 2012.8 (Aug. 2012), p. 2.
- [138] M. D’Elia and F. Negro. “Chiral properties of strong interactions in a magnetic background”. In: *Phys. Rev. D* 83 (11 June 2011), p. 114028.
- [139] M. D’Elia, S. Mukherjee, and F. Sanfilippo. “QCD phase transition in a strong magnetic background”. In: *Phys. Rev. D* 82 (5 Sept. 2010), p. 051501.
- [140] M. D’Elia and F. Negro. “Chiral properties of strong interactions in a magnetic background”. In: *Phys. Rev. D* 83 (11 June 2011), p. 114028.
- [141] G. S. Bali et al. “QCD quark condensate in external magnetic fields”. In: *Phys. Rev. D* 86 (7 Oct. 2012), p. 071502.
- [142] G. S. Bali et al. “The QCD phase diagram for external magnetic fields”. In: *Journal of High Energy Physics* 2012.2 (Feb. 2012), p. 44.
- [143] F. Bruckmann, G. Endr3odi, and T. G. Kov3acs. “Inverse magnetic catalysis and the Polyakov loop”. In: *Journal of High Energy Physics* 2013.4 (Apr. 2013), p. 112.
- [144] E. Fraga, B. Mintz, and J. Schaffner-Bielich. “A search for inverse magnetic catalysis in thermal quark–meson models”. In: *Physics Letters B* 731 (2014), pp. 154–158.
- [145] J. O. Andersen, W. R. Naylor, and A. Tranberg. “Inverse magnetic catalysis and regularization in the quark-meson model”. In: *Journal of High Energy Physics* 2015.2 (Feb. 2015), p. 42.
- [146] S. Ozaki et al. “Euler-Heisenberg-Weiss action for QCD + QED”. In: *Phys. Rev. D* 92 (1 July 2015), p. 016002.
- [147] D. T. Son and M. A. Stephanov. “Axial anomaly and magnetism of nuclear and quark matter”. In: *Phys. Rev. D* 77 (1 Jan. 2008), p. 014021.

- [148] J. Wess and B. Zumino. “Consequences of anomalous ward identities”. In: *Physics Letters B* 37.1 (1971), pp. 95–97.
- [149] E. Witten. “Global aspects of current algebra”. In: *Nuclear Physics B* 223.2 (1983), pp. 422–432.
- [150] A. Altland and B. Simons. *Condensed Matter Field Theory*. Cambridge University Press, 2006.
- [151] E. Weisstein. *Beta Function*. From *MathWorld—A Wolfram Web Resource*. Visited on 16/05/2018. URL: <http://mathworld.wolfram.com/HurwitzZetaFunction.html>.
- [152] J. Sondow and E. Weisstein. *Hurwitz Zeta Function*. From *MathWorld—A Wolfram Web Resource*. Visited on 19/04/2018. URL: <http://mathworld.wolfram.com/HurwitzZetaFunction.html>.
- [153] *NIST Digital Library of Mathematical Functions*. <http://dlmf.nist.gov/>, Release 1.0.18 of 2018-03-27. F. W. J. Olver, A. B. Olde Daalhuis, D. W. Lozier, B. I. Schneider, R. F. Boisvert, C. W. Clark, B. R. Miller and B. V. Saunders, eds.
- [154] R. Piessens et al. *Quadpack: A Subroutine Package for Automatic Integration*. Springer Berlin Heidelberg, 1983.
- [155] D. E. Amos. “Algorithm 644: A Portable Package for Bessel Functions of a Complex Argument and Nonnegative Order”. In: *ACM Trans. Math. Softw.* 12.3 (Sept. 1986), pp. 265–273.
- [156] F. Johansson et al. *mpmath: a Python library for arbitrary-precision floating-point arithmetic (version 0.18)*. Dec. 2013. URL: <http://mpmath.org/>.
- [157] G. Endrődi. “Critical point in the QCD phase diagram for extremely strong background magnetic fields”. In: *Journal of High Energy Physics* 2015.7 (July 2015), p. 173.
- [158] T. K. Herbst, J. M. Pawłowski, and B.-J. Schaefer. “The phase structure of the Polyakov–quark–meson model beyond mean field”. In: *Physics Letters B* 696.1 (2011), pp. 58–67.
- [159] V. Skokov et al. “Meson fluctuations and thermodynamics of the Polyakov-loop-extended quark-meson model”. In: *Phys. Rev. C* 82 (1 July 2010), p. 015206.
- [160] R. Khan and L. T. Kyllingstad. “The chiral phase transition and the role of vacuum fluctuations”. In: *AIP Conference Proceedings* 1343.1 (2011), pp. 504–506.
- [161] B. B. Brandt, G. Endrődi, and S. Schmalzbauer. “QCD phase diagram for nonzero isospin-asymmetry”. In: *Phys. Rev. D* 97 (5 Mar. 2018), p. 054514.
- [162] H. Ueda et al. “QCD phase diagram at finite baryon and isospin chemical potentials in the Polyakov loop extended quark meson model with vector interaction”. In: *Phys. Rev. D* 88 (7 Oct. 2013), p. 074006.

- [163] J. O. Andersen and P. Kneschke. “Chiral density wave versus pion condensation at finite density and zero temperature”. In: *Phys. Rev. D* 97 (7 Apr. 2018), p. 076005.
- [164] P. Adhikari, J. O. Andersen, and P. Kneschke. “Pion condensation and phase diagram in the Polyakov-loop quark-meson model”. In: (2018).
- [165] M. Chanowitz, M. Furman, and I. Hinchliffe. “The axial current in dimensional regularization”. In: *Nuclear Physics B* 159.1 (1979), pp. 225–243.

Additional Derivations

A.1 Calculation of the Fermion Partition Function

We here finish the calculation of the Fermion partition function from Sec. 3.1. Using the Dirac representation,

$$\gamma^0 = \begin{pmatrix} I_2 & 0 \\ 0 & -I_2 \end{pmatrix} \quad \gamma^i = \begin{pmatrix} 0 & \sigma^i \\ -\sigma^i & 0 \end{pmatrix}, \quad (\text{A.1.1})$$

where σ^i are the Pauli matrices, we have that

$$K + gA_{cc} \equiv \frac{D_c}{i\beta} = \begin{pmatrix} [-i\omega_n + \mu + gA_{cc} - m] I_2 & \sigma^i p_i \\ \sigma^i p_i & [-i\omega_n + \mu + gA_{jj} + m] I_2 \end{pmatrix}, \quad (\text{A.1.2})$$

where K is defined as

$$K = -i\omega_n + \mu + \gamma^0 \gamma^i p_i - \gamma^0 m. \quad (\text{A.1.3})$$

Let

$$K_{\pm} = -i\omega_n + \mu + gA_{cc} \pm m. \quad (\text{A.1.4})$$

Then D_{cc} reads

$$\frac{D_{cc}}{i\beta} = \begin{pmatrix} K_- I_2 & \sigma^i p_i \\ \sigma^i p_i & K_+ I_2 \end{pmatrix} = \begin{pmatrix} K_- & 0 & p_z & p_x - ip_y \\ 0 & K_- & p_x + ip_y & -p_z \\ p_z & p_x - ip_y & K_+ & 0 \\ p_x + ip_y & -p_z & 0 & K_+ \end{pmatrix}, \quad (\text{A.1.5})$$

which gives a determinant

$$\begin{aligned} \det D_{cc} &= \beta^4 [-K_+ K_- + \mathbf{p}^2]^2 = \beta^4 [-(-i\omega_n + \mu + gA_{cc})^2 + m^2 + \mathbf{p}^2]^2 \\ &= \beta^4 [(\omega_n + i\mu + igA_{cc})^2 + \omega_{\mathbf{p}}^2]^2 \\ &= \beta^4 [(\omega_n + i\tilde{\mu}_c)^2 + \omega_{\mathbf{p}}^2]^2, \end{aligned} \quad (\text{A.1.6})$$

where

$$\tilde{\mu}_c \equiv \mu + gA_{cc}. \quad (\text{A.1.7})$$

Using (3.1.16), which reads

$$\ln Z = \sum_{n, \mathbf{p}} \sum_{c=1}^{N_c} \ln \det D_c(\mathbf{p}, n), \quad (\text{A.1.8})$$

we get

$$\begin{aligned} \ln Z &= 2 \sum_{c=1}^{N_c} \sum_{n, \mathbf{p}} \ln (\beta^2 [(\omega_n + i\tilde{\mu}_c)^2 + \omega_{\mathbf{p}}^2]) \\ &= \sum_{c=1}^{N_c} \sum_{n, \mathbf{p}} \ln (\beta^4 [(\omega_n + i\tilde{\mu}_c)^2 + \omega_{\mathbf{p}}^2] [(-\omega_n + i\tilde{\mu}_c)^2 + \omega_{\mathbf{p}}^2]) \\ &= \sum_{c=1}^{N_c} \sum_{n, \mathbf{p}} \ln (\beta^4 [\omega_n^2 + (\omega_{\mathbf{p}} - \tilde{\mu}_c)^2] [\omega_n^2 + (\omega_{\mathbf{p}} + \tilde{\mu}_c)^2]) \\ &= \sum_{c=1}^{N_c} \sum_{n, \mathbf{p}} \ln (\beta^2 [\omega_n^2 + (\omega_{\mathbf{p}} - \tilde{\mu}_c)^2]) + \ln (\beta^2 [\omega_n^2 + (\omega_{\mathbf{p}} + \tilde{\mu}_c)^2]), \end{aligned} \quad (\text{A.1.9})$$

where we have used that we sum over all $n \in \mathbb{Z}$, so that the sum is unchanged under $\omega_n \rightarrow -\omega_n$. Remembering that $\omega_n = (2n + 1)\pi T$ and using the integral

$$\int_1^{\beta^2 \omega_{\mathbf{p}}^2} \frac{dx^2}{x^2 + \omega_n^2} = \ln [\omega_n^2 + \beta^2 \omega_{\mathbf{p}}^2] - \ln [(2n + 1)^2 \pi^2 + 1], \quad (\text{A.1.10})$$

we find

$$\ln Z = \sum_{c=1}^{N_c} \sum_{\mathbf{p}} \sum_n \left(\int_1^{\beta^2 (\omega_{\mathbf{p}} + \tilde{\mu}_c)^2} \frac{dx^2}{x^2 + (2n + 1)^2 \pi^2} + \int_1^{\beta^2 (\omega_{\mathbf{p}} - \tilde{\mu}_c)^2} \frac{dx^2}{x^2 + (2n + 1)^2 \pi^2} \right),$$

where we dropped an irrelevant additive factor that does not affect thermodynamics. Carrying out the Matsubara frequency sums, which are shown in Appendix A.2, and taking the large volume limit, where

$$\sum_{\mathbf{p}} \rightarrow V \int \frac{d^3 p}{(2\pi)^3}, \quad (\text{A.1.11})$$

we finally get

$$\ln Z = 2V \sum_{c=1}^{N_c} \int \frac{d^3 p}{(2\pi)^3} \left\{ \beta \omega_{\mathbf{p}} + \ln [1 + e^{-\beta(\omega_{\mathbf{p}} - \tilde{\mu}_c)}] + \ln [1 + e^{-\beta(\omega_{\mathbf{p}} + \tilde{\mu}_c)}] \right\}. \quad (\text{A.1.12})$$

A.2 Matsubara Frequency Sums

Bosonic Sum

Consider the sum

$$\frac{1}{4\pi i} \sum_{i=-\infty}^{\infty} \oint_{C_i} dp_0 f(p_0) \coth\left(\frac{1}{2}\beta p_0\right) \quad (\text{A.2.1})$$

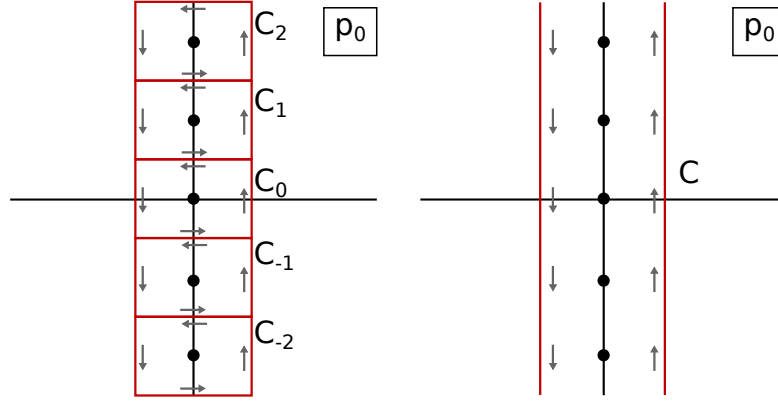


Figure A.1: Left: each square C_n is an integration path in the complex plane. Right: Equivalent integration path C .

where the paths C_i are shown in Fig. A.1. We have that

$$\coth\left(\frac{1}{2}\beta p_0\right) = \frac{1 + e^{-\beta p_0}}{1 - e^{-\beta p_0}} \quad (\text{A.2.2})$$

has poles at

$$p_0 = 2\pi i n T \equiv i\omega_n \quad n \in \mathbb{Z}, \quad (\text{A.2.3})$$

and it is analytic everywhere else. We have here introduced the bosonic Matsubara frequencies ω_n . If $f(p_0)$ is analytic we can use the residue theorem for each path C_n . Furthermore, we use that the integral over all paths C_n is equivalent to integrating over the path C shown in Fig. A.1. As a result we get

$$\frac{1}{2} \sum_{n=-\infty}^{\infty} f(i\omega_n) \operatorname{Res}_{p_0=i\omega_n} \coth\left(\frac{1}{2}\beta p_0\right) = \frac{1}{4\pi i} \oint_C dp_0 f(p_0) \coth\left(\frac{1}{2}\beta p_0\right) \quad (\text{A.2.4})$$

The pole is of first order, and the residue thus is given by

$$\operatorname{Res}_{p_0=i\omega_n} \coth\left(\frac{1}{2}\beta p_0\right) = \lim_{p_0 \rightarrow i\omega_n} (p_0 - i\omega_n) \frac{\cosh\left(\frac{1}{2}\beta p_0\right)}{\sinh\left(\frac{1}{2}\beta p_0\right)} \quad (\text{A.2.5})$$

$$= 2i\pi T \lim_{k \rightarrow n} (k - n) \frac{\cosh(i\pi k)}{\sinh(i\pi k)} \quad (\text{A.2.6})$$

$$= 2\pi T \lim_{k \rightarrow n} (k - n) \frac{\cos(\pi k)}{\sin(\pi k)} \quad (\text{A.2.7})$$

$$= 2\pi T \lim_{q \rightarrow 0} q \frac{\cos(\pi q + \pi n)}{\sin(\pi q + \pi n)} \quad (\text{A.2.8})$$

$$= 2\pi T \lim_{q \rightarrow 0} q \frac{\cos(\pi q)}{\sin(\pi q)} \quad (\text{A.2.9})$$

$$= 2\pi T \lim_{q \rightarrow 0} q \frac{1}{\pi q} \quad (\text{A.2.10})$$

$$= 2T \quad (\text{A.2.11})$$

Thus we get

$$T \sum_{n=-\infty}^{\infty} f(i\omega_n) = \frac{1}{4\pi i} \oint_C dp_0 f(p_0) \coth\left(\frac{1}{2}\beta p_0\right). \quad (\text{A.2.12})$$

Let us now calculate the sum for

$$f(p_0) = \frac{1}{x^2 - \beta^2 p_0^2}. \quad (\text{A.2.13})$$

Using that we can rewrite

$$\oint_C = \int_{-\epsilon+i\infty}^{-\epsilon-i\infty} + \int_{\epsilon-i\infty}^{\epsilon+i\infty}, \quad (\text{A.2.14})$$

we find

$$\sum_n \frac{1}{x^2 + (2\pi n)^2} = \frac{\beta}{4\pi i} \left(\int_{-\epsilon+i\infty}^{-\epsilon-i\infty} + \int_{\epsilon-i\infty}^{\epsilon+i\infty} \right) dp_0 \frac{\coth\left(\frac{1}{2}\beta p_0\right)}{x^2 - (\beta p_0)^2} \quad (\text{A.2.15})$$

We can now close each of the line integrals with a half-circle to negative and positive real infinity, so that we again can use the residue theorem. We have poles at $p_0 = \pm \frac{x}{\beta}$, giving

$$\sum_n \frac{1}{x^2 + (2\pi n)^2} = \frac{\beta}{4\pi i} 2\pi i \left[\text{Res}_{p_0=x/\beta} g(p_0) + \text{Res}_{p_0=-x/\beta} g(p_0) \right], \quad (\text{A.2.16})$$

for

$$g(p_0) = \frac{\coth\left(\frac{1}{2}\beta p_0\right)}{x^2 - (\beta p_0)^2}. \quad (\text{A.2.17})$$

The poles are of first order, and the sum of the residues are

$$\frac{\coth\left(\frac{x}{2}\right)}{2x\beta} - \frac{-\coth\left(\frac{x}{2}\right)}{2x\beta} = \frac{\coth\left(\frac{x}{2}\right)}{x\beta} = \frac{1}{\beta x} \left(1 + \frac{2}{e^x - 1} \right). \quad (\text{A.2.18})$$

Thus

$$\sum_n \frac{1}{x^2 + (2\pi n)^2} = \frac{1}{2x} \left(1 + \frac{2}{e^x - 1} \right). \quad (\text{A.2.19})$$

Using this gives

$$\int_1^{\beta^2 \omega_{\mathbf{p}}^2} \sum_n \frac{dx^2}{x^2 + (2\pi n)^2} = \int_1^{\beta^2 \omega_{\mathbf{p}}^2} \frac{dx}{2\sqrt{x}} \left(1 + \frac{2}{e^{\sqrt{x}} - 1} \right) \quad (\text{A.2.20})$$

$$= \beta \omega_{\mathbf{p}} + 2 \ln(1 - e^{-\beta \omega_{\mathbf{p}}}) + \text{const.} \quad (\text{A.2.21})$$

Fermionic Sum

With the same argument as for the bosonic sum, except with Matsubara frequencies $\omega_n = (2n + 1)\pi T$ and the replacement

$$\coth\left(\frac{1}{2}\beta p_0\right) \rightarrow \tanh\left(\frac{1}{2}\beta p_0\right), \quad (\text{A.2.22})$$

which has poles at $p_0 = i\omega_n$, we find

$$T \sum_{n=-\infty}^{\infty} f(i\omega_n) = \frac{1}{4\pi i} \oint_C dp_0 f(p_0) \tanh\left(\frac{1}{2}\beta p_0\right). \quad (\text{A.2.23})$$

Let us calculate the same sum as for the bosons, except with the Fermionic Matsubara frequencies. We find

$$\sum_n \frac{1}{x^2 + (2n+1)^2\pi^2} = \frac{\beta}{4\pi i} 2\pi i \left[\text{Res}_{p_0=x/\beta} g(p_0) + \text{Res}_{p_0=-x/\beta} g(p_0) \right], \quad (\text{A.2.24})$$

where $g(p_0)$ now is

$$g(p_0) = \frac{\tanh\left(\frac{1}{2}\beta p_0\right)}{x^2 - (\beta p_0)^2}. \quad (\text{A.2.25})$$

The sum of the residues is

$$\frac{\tanh\left(\frac{x}{2}\right)}{2\beta x} - \frac{\tanh\left(\frac{x}{2}\right)}{-2\beta x} = \frac{\tanh\left(\frac{x}{2}\right)}{\beta x} = \frac{1}{\beta x} \left(1 - \frac{2}{e^x + 1}\right) \quad (\text{A.2.26})$$

Using this gives

$$\int_1^{\beta^2(\omega_{\mathbf{p}} \pm \mu)^2} \sum_n \frac{dx^2}{x^2 + (2n+1)^2\pi^2} = \int_1^{\beta^2(\omega_{\mathbf{p}} \pm \mu)^2} \frac{dx}{2\sqrt{x}} \left(1 - \frac{2}{e^{\sqrt{x}} + 1}\right) \quad (\text{A.2.27})$$

$$= (\beta\omega_{\mathbf{p}} \pm \mu) + 2 \ln\left(1 + e^{-\beta(\omega_{\mathbf{p}} \pm \mu)}\right) + \text{const.} \quad (\text{A.2.28})$$

A.3 Symmetries of the QM Model

One can show that γ^5 satisfies $(\gamma^5)^2 = 1$, $(\gamma^5)^\dagger = \gamma^5$ and $\{\gamma^5, \gamma^\mu\} = 0$. Define the operators P_R and P_L as

$$P_R = \frac{1}{2}(1 + \gamma^5), \quad P_L = \frac{1}{2}(1 - \gamma^5). \quad (\text{A.3.1})$$

Using that $(\gamma^5)^2 = 1$, we find that $P_R^2 = P_R$ and $P_L^2 = P_L$, which means that they are projection operators. Since $P_R + P_L = 1$, we can write

$$\psi = P_R\psi + P_L\psi = \psi_R + \psi_L, \quad (\text{A.3.2})$$

where we in the last equality defined the right- and left-handed spinors, $\psi_R = P_R\psi$ and $\psi_L = P_L\psi$. We see that

$$\gamma^5\psi_R = \psi_R, \quad (\text{A.3.3})$$

$$\gamma^5\psi_L = -\psi_L. \quad (\text{A.3.4})$$

Inserting these relations into the Yukawa term gives

$$-\mathcal{L}_Y = g\bar{\psi}_L(\chi_1 + i\boldsymbol{\pi} \cdot \boldsymbol{\tau})\psi_R + g\bar{\psi}_R(\chi_1 - i\boldsymbol{\pi} \cdot \boldsymbol{\tau})\psi_L + g\bar{\psi}_L(\chi_1 - i\boldsymbol{\pi} \cdot \boldsymbol{\tau})\psi_L + g\bar{\psi}_R(\chi_1 + i\boldsymbol{\pi} \cdot \boldsymbol{\tau})\psi_R. \quad (\text{A.3.5})$$

The last two terms vanish for the following reason. Let ξ and χ be two spinors and let P be one of the two defined projection operators. Then

$$\begin{aligned} \overline{(P\chi)}(P\xi) &= [(1 \pm \gamma^5) \chi]^\dagger \gamma^0 (1 \pm \gamma^5) \xi = \chi^\dagger (1 \pm \gamma^5) \gamma^0 (1 \pm \gamma^5) \xi = \chi^\dagger \gamma^0 (1 \mp \gamma^5) (1 \pm \gamma^5) \xi \\ &= \chi^\dagger \gamma^0 [1 - (\gamma^5)^2] \xi = 0. \end{aligned}$$

For the kinetic terms we have that $\bar{\psi}_R i\gamma^\mu \partial_\mu \psi_L$ and $\bar{\psi}_L i\gamma^\mu \partial_\mu \psi_R$ vanish, as can be shown by a similar calculation. Thus, the quark sector of the Lagrangian becomes

$$\bar{\psi}_R i\gamma^\mu \partial_\mu \psi_R + \bar{\psi}_L i\gamma^\mu \partial_\mu \psi_L - g\bar{\psi}_L(\chi_1 + i\boldsymbol{\pi} \cdot \boldsymbol{\tau})\psi_R - g\bar{\psi}_R(\chi_1 - i\boldsymbol{\pi} \cdot \boldsymbol{\tau})\psi_L. \quad (\text{A.3.6})$$

To make the symmetries of the Lagrangian manifest, introduce

$$\Theta = \frac{1}{2} (\chi_1 + i\boldsymbol{\pi} \cdot \boldsymbol{\tau}) = \frac{1}{2} \begin{bmatrix} \chi_1 + i\pi_3 & i\pi_1 + \pi_2 \\ i\pi_1 - \pi_2 & \chi_1 - i\pi_3 \end{bmatrix} \quad (\text{A.3.7})$$

We see that

$$\text{Tr}(\Theta^\dagger \Theta) = \frac{1}{4} \text{Tr} \begin{bmatrix} \chi_1^2 + \pi_3^2 + 2\pi^- \pi^+ & 0 \\ 0 & \chi_1^2 + \pi_3^2 + 2\pi^- \pi^+ \end{bmatrix} = \frac{1}{2} \chi_1^2 + \frac{1}{2} \boldsymbol{\pi}^2, \quad (\text{A.3.8})$$

when the fields are real. We furthermore have that

$$\text{Tr}(\Theta^\dagger + \Theta) = 2\chi_1. \quad (\text{A.3.9})$$

Consequently we can rewrite the full quark-meson Lagrangian as

$$\begin{aligned} \mathcal{L} &= \bar{\psi}_R i\gamma^\mu \partial_\mu \psi_R + \bar{\psi}_L i\gamma^\mu \partial_\mu \psi_L - 2g\bar{\psi}_L \Theta \psi_R - 2g\bar{\psi}_R \Theta^\dagger \psi_L \\ &\quad + \text{Tr}(\partial_\mu \Theta^\dagger \partial^\mu \Theta) + m^2 \text{Tr}(\Theta^\dagger \Theta) - \frac{\lambda}{6} [\text{Tr}(\Theta^\dagger \Theta)]^2 + \frac{1}{2} h \text{Tr}(\Theta + \Theta^\dagger). \end{aligned} \quad (\text{A.3.10})$$

Assume now first that $h = 0$. Let U_1 and U_2 be two independent transformations in $SU(2)$ acting on flavor space. Consider the transformations

$$\psi_R \rightarrow U_1 \psi_R, \quad \psi_L \rightarrow U_2 \psi_L. \quad (\text{A.3.11})$$

Since U_i acts on flavor components while γ^μ acts on the spinors, we find that U_i commutes with γ^μ . Thus the kinetic quark terms are invariant:

$$\overline{U_1 \psi_R} i\gamma^\mu \partial_\mu U_1 \psi_R = \psi_R^\dagger U_1^\dagger \gamma^0 i\gamma^\mu \partial_\mu U_1 \psi_R = \psi_R^\dagger U_1^{-1} U_1 \gamma^0 i\gamma^\mu \partial_\mu \psi_R = \bar{\psi}_R i\gamma^\mu \partial_\mu \psi_R,$$

and similar for ψ_L . The Yukawa-part becomes

$$-\mathcal{L}_Y = 2g\bar{\psi}_L U_2^{-1} \Theta' U_1 \psi_R + g\bar{\psi}_R U_1^{-1} \Theta'^\dagger U_2 \psi_L, \quad (\text{A.3.12})$$

where we assume Θ has transformed into some Θ' . We see that if we transform Θ as

$$\Theta' = U_2 \Theta U_1^{-1}, \quad (\text{A.3.13})$$

both these terms are invariant, since $U_i^\dagger = U_i^{-1}$. However, we must check that the transformed σ and $\boldsymbol{\pi}$ fields are still real; otherwise the way we have written the Lagrangian in (A.3.10) is not valid. If this is the case, as we will show that it is in the following, we see that also the meson sector of the Lagrangian invariant, since

$$\text{Tr}[(U_2 \Theta U_1^{-1})^\dagger (U_2 \Theta U_1^{-1})] = \text{Tr}[U_1 \Theta^\dagger U_2^{-1} U_2 \Theta U_1^{-1}] = \text{Tr}(\Theta^\dagger \Theta), \quad (\text{A.3.14})$$

where we use the cyclic property of the trace. Thus, the Lagrangian is invariant under $SU(2)_R \times SU(2)_L$, where we have included subscripts to indicate that the Lagrangian is invariant under separate $SU(2)$ transformations on left- and right-handed components of the doublet.

Let us now verify that χ_1 and $\boldsymbol{\pi}$ are still real after an $SU(2)_R \times SU(2)_L$ transformation. We can write

$$U_1 = e^{-\frac{i}{2}\boldsymbol{\alpha}\cdot\boldsymbol{\tau}} = 1 - \frac{i}{2}\boldsymbol{\alpha}\cdot\boldsymbol{\tau}, \quad U_2 = e^{-\frac{i}{2}\boldsymbol{\beta}\cdot\boldsymbol{\tau}} = 1 - \frac{i}{2}\boldsymbol{\beta}\cdot\boldsymbol{\tau}, \quad (\text{A.3.15})$$

for two general infinitesimal transformations, since the Pauli matrices generates a two-dimensional representation of $SU(2)$. Here $\boldsymbol{\alpha}$ and $\boldsymbol{\beta}$ are real infinitesimal parameters. We have that the Θ transformation on infinitesimal form reads:

$$\begin{aligned} (\chi_1 + i\boldsymbol{\pi}\cdot\boldsymbol{\tau}) &\rightarrow \left(1 - \frac{i}{2}\boldsymbol{\beta}\cdot\boldsymbol{\tau}\right) (\chi_1 + i\boldsymbol{\pi}\cdot\boldsymbol{\tau}) \left(1 + \frac{i}{2}\boldsymbol{\alpha}\cdot\boldsymbol{\tau}\right) \\ &= (\chi_1 + i\boldsymbol{\pi}\cdot\boldsymbol{\tau}) + \frac{i}{2}(\boldsymbol{\alpha} - \boldsymbol{\beta})\cdot\boldsymbol{\tau}\chi_1 + \frac{1}{2}[(\boldsymbol{\beta}\cdot\boldsymbol{\tau})(\boldsymbol{\pi}\cdot\boldsymbol{\tau}) - (\boldsymbol{\pi}\cdot\boldsymbol{\tau})(\boldsymbol{\alpha}\cdot\boldsymbol{\tau})] \\ &= (\chi_1 + i\boldsymbol{\pi}\cdot\boldsymbol{\tau}) + i\left(\frac{\boldsymbol{\alpha} - \boldsymbol{\beta}}{2}\right)\cdot\boldsymbol{\tau}\chi_1 + \left(\frac{\boldsymbol{\beta} - \boldsymbol{\alpha}}{2}\right)\cdot\boldsymbol{\pi} + i\left[\left(\frac{\boldsymbol{\beta} + \boldsymbol{\alpha}}{2}\right) \times \boldsymbol{\pi}\right]\cdot\boldsymbol{\tau} \\ &= \left[\chi_1 - \left(\frac{\boldsymbol{\alpha} - \boldsymbol{\beta}}{2}\right)\cdot\boldsymbol{\pi}\right] + i\left[\boldsymbol{\pi} + \left(\frac{\boldsymbol{\alpha} - \boldsymbol{\beta}}{2}\right)\chi_1 + \left(\frac{\boldsymbol{\alpha} + \boldsymbol{\beta}}{2}\right) \times \boldsymbol{\pi}\right]\cdot\boldsymbol{\tau}, \end{aligned}$$

where we between the second and third line used the identity

$$(\mathbf{a}\cdot\boldsymbol{\tau})(\mathbf{b}\cdot\boldsymbol{\tau}) = (\mathbf{a}\cdot\mathbf{b}) + i(\mathbf{a}\times\mathbf{b})\cdot\boldsymbol{\tau}. \quad (\text{A.3.16})$$

Hence, an infinitesimal $SU(2)_R \times SU(2)_L$ transformation corresponds to changing the scalar fields as

$$\delta\chi_1 = -\left(\frac{\boldsymbol{\alpha} - \boldsymbol{\beta}}{2}\right)\cdot\boldsymbol{\pi}, \quad \delta\boldsymbol{\pi} = \left(\frac{\boldsymbol{\alpha} - \boldsymbol{\beta}}{2}\right)\chi_1 + \left(\frac{\boldsymbol{\alpha} + \boldsymbol{\beta}}{2}\right) \times \boldsymbol{\pi}. \quad (\text{A.3.17})$$

We see that the fields remain real, and the claim that \mathcal{L} is invariant under $SU(2)_R \times SU(2)_L$ is thus valid.

For the case $h \neq 0$, we see that $SU(2)_R \times SU(2)_L$ is broken since the term (A.3.9) is changed when $\delta\chi_1 \neq 0$. However, a single $SU(2)$ symmetry remains, which corresponds to choosing the two $SU(2)$ transformations to be equal, $U_1 = U_2$. This implies $\boldsymbol{\alpha} = \boldsymbol{\beta}$ in the infinitesimal case, which leads to $\delta\chi_1 = 0$. We refer to this symmetry as $SU(2)_V$.

Conserved Currents

Let us find the currents corresponding to the $SU(2)$ symmetries. Consider first $h = 0$. Choosing $\boldsymbol{\beta} = 0$ and $\alpha_j = 2\delta_j^i$ for $i \in \{1, 2, 3\}$ gives us the conserved right-handed currents

$$\begin{aligned} j_{i,R}^\mu &= \frac{\partial\mathcal{L}}{\partial(\partial_\mu\chi_1)}(-\delta_j^i\pi_j) + \frac{\partial\mathcal{L}}{\partial(\partial_\mu\pi_j)}(\chi_1\delta_j^i + \epsilon_{jkl}\delta_k^i\pi_l) + \frac{\partial\mathcal{L}}{\partial(\partial_\mu\psi)}(-i\tau_i\psi_R) \\ &= \partial^\mu\pi_i\chi_1 - \partial^\mu\chi_1\pi_i + \epsilon_{ijk}\pi_j\partial^\mu\pi_k + i(\bar{\psi}_L + \bar{\psi}_R)\gamma^\mu(-i\tau_i\psi_R). \end{aligned} \quad (\text{A.3.18})$$

Using that $\bar{\psi}_L\gamma^\mu\psi_R = 0$, we get

$$j_{i,R}^\mu = \partial^\mu\pi_i\chi_1 - \partial^\mu\chi_1\pi_i + \epsilon_{ijk}\pi_j\partial^\mu\pi_k + \bar{\psi}_R\gamma^\mu\tau_i\psi_R. \quad (\text{A.3.19})$$

Similarly we get for the conserved left-handed currents

$$j_{i,L}^\mu = -\partial^\mu\pi_i\chi_1 + \partial^\mu\chi_1\pi_i + \epsilon_{ijk}\pi_j\partial^\mu\pi_k + \bar{\psi}_L\gamma^\mu\tau_i\psi_L. \quad (\text{A.3.20})$$

We can also form the vector and axial currents, which are the linear combinations

$$j_{i,V}^\mu = \frac{1}{2} (j_{i,R}^\mu + j_{i,L}^\mu) = \epsilon_{ijk} \pi_j \partial^\mu \pi_k + \frac{1}{2} \bar{\psi} \gamma^\mu \tau_i \psi, \quad (\text{A.3.21})$$

$$j_{i,A}^\mu = \frac{1}{2} (j_{i,R}^\mu - j_{i,L}^\mu) = \partial^\mu \pi_i \chi_1 - \partial^\mu \chi_1 \pi_i + \frac{1}{2} \bar{\psi} \gamma^\mu \gamma^5 \tau_i \psi. \quad (\text{A.3.22})$$

In rewriting the quark contribution to these currents we have again used that the ψ_R - ψ_L cross-terms vanish. Furthermore, we have used equations (A.3.3) and (A.3.4) to rewrite

$$\bar{\psi}_R \gamma^\mu \tau_i \psi_R - \bar{\psi}_L \gamma^\mu \tau_i \psi_L = (\bar{\psi}_R + \bar{\psi}_L) \gamma^\mu \tau_i (\psi_R - \psi_L) = (\bar{\psi}_R + \bar{\psi}_L) \gamma^\mu \gamma^5 \tau_i (\psi_R + \psi_L).$$

To find the conserved currents in the $h \neq 0$ case we must set $\alpha - \beta = 0$. We choose $\alpha_j + \beta_j = 2\delta_j^i$ and find that

$$\delta\psi = -\frac{i}{2} \alpha \cdot \tau \psi_R - \frac{i}{2} \beta \cdot \tau \psi_L = -\frac{i}{2} \left(\frac{\alpha + \beta}{2} \right) \cdot \tau \psi - \frac{i}{2} \gamma^5 \left(\frac{\alpha - \beta}{2} \right) \cdot \tau \psi = -\frac{i}{2} \tau_i \psi. \quad (\text{A.3.23})$$

Using this, we find exactly (A.3.21) as the conserved currents. Thus for $h \neq 0$, only the vector currents are conserved. The vector currents are, as the name suggests, the currents corresponding to the $SU(2)_V$ symmetry.

A.4 One-Loop Renormalization of the QM Model

We will here derive the one-loop self-energies in the large- N_c limit of the quark-meson model. This section is a partial summary of the work done in Ref. [1].

Renormalized Perturbation Theory

Consider the quark-meson Lagrangian. Let the coupling constants and fields before renormalization be denoted with a subscript B , standing for bare. After we have expanded about $\chi_{1,B} = v_B + \sigma_B$ we have:

$$\begin{aligned} \mathcal{L} = & U(v_B) + \frac{1}{2} (\partial \boldsymbol{\pi}_B)^2 + \frac{1}{2} (\partial \sigma_B)^2 - \frac{1}{2} m_{\sigma,B}^2 \sigma_B^2 - \frac{1}{2} m_{\pi,B}^2 \boldsymbol{\pi}_B^2 + \sigma_B (h_B - m_{\pi,B}^2 v_B) \\ & + \bar{\psi}_B i \not{\partial} \psi_B - m_{q,B} \bar{\psi}_B \psi_B - g_B \bar{\psi}_B (\sigma_B + i \boldsymbol{\pi}_B \cdot \boldsymbol{\tau} \gamma_5) \psi_B + \mathcal{L}_{i,B}, \end{aligned} \quad (\text{A.4.1})$$

where

$$\mathcal{L}_{i,B} = -\frac{1}{6} v_B \lambda_B \sigma_B \boldsymbol{\pi}_B^2 - \frac{\lambda_B}{12} \sigma_B^2 \boldsymbol{\pi}_B^2 - \frac{1}{6} \lambda_B v_B \sigma_B^3 - \frac{\lambda_B}{4!} \sigma_B^4 - \frac{\lambda_B}{4!} \boldsymbol{\pi}_B^4 \quad (\text{A.4.2})$$

contains all interactions except the Yukawa-term. We introduce the renormalized fields and couplings via

$$\begin{aligned} \boldsymbol{\pi}_B &= \sqrt{Z_\pi} \boldsymbol{\pi}, & \sigma_B &= \sqrt{Z_\sigma} \sigma, & \psi_B &= \sqrt{Z_\psi} \psi, \\ m_B^2 &= Z_m m^2, & \lambda_B &= Z_\lambda \lambda, & g_B &= \sqrt{Z_g} g, \\ h_B &= Z_h h, & v_B &= \sqrt{Z_v} v, \end{aligned} \quad (\text{A.4.3})$$

where the Z -factors are the field, mass and coupling renormalizations. Inserting (A.4.3) into (A.4.1) gives the Lagrangian

$$\begin{aligned} \mathcal{L} = & U(v) + \delta U + \frac{1}{2}Z_\pi(\partial\boldsymbol{\pi})^2 + \frac{1}{2}Z_\sigma(\partial\sigma)^2 - \frac{1}{2}Z_\sigma \left(\frac{Z_\lambda\lambda}{2}Z_v v^2 - Z_m m^2 \right) \sigma^2 \\ & - \frac{1}{2}Z_\pi \left(\frac{Z_\lambda\lambda}{6}Z_v v^2 - Z_m m^2 \right) \boldsymbol{\pi}^2 + \sigma\sqrt{Z_\sigma} \left(Z_h h - \frac{Z_\lambda\lambda}{6}(Z_v v^2)^{\frac{3}{2}} + Z_m m^2 \sqrt{Z_v v^2} \right) \\ & + Z_\psi \bar{\psi} i \not{\partial} \psi - Z_\psi \sqrt{Z_g Z_v} m_q \bar{\psi} \psi - Z_\psi \sqrt{Z_g} g \bar{\psi} (\sqrt{Z_\sigma} \sigma + i\sqrt{Z_\pi} \boldsymbol{\pi} \cdot \boldsymbol{\tau} \gamma_5) \psi + \mathcal{L}_i + \delta\mathcal{L}_i. \end{aligned} \quad (\text{A.4.4})$$

Here δU is the change in the tree-level potential, which we will look at later, while the counterterms coming from the non-Yukawa interactions, $\delta\mathcal{L}_i$, will not be needed at one-loop level in the large- N_c limit for the renormalization scheme we will adopt. Introducing

$$Z = 1 + \delta Z \quad (\text{A.4.5})$$

for all the quantities in (A.4.3), we find that the quadratic part of the meson sector becomes

$$\begin{aligned} & \frac{1}{2}(\partial\boldsymbol{\pi})^2 + \frac{1}{2}(\partial\sigma)^2 - \frac{1}{2}(1 + \delta Z_\sigma)(m_\sigma^2 + \delta m_\sigma^2)\sigma^2 - \frac{1}{2}(1 + \delta Z_\pi)(m_\pi^2 + \delta m_\pi^2)\boldsymbol{\pi}^2 \\ & + \frac{1}{2}\delta Z_\pi(\partial\boldsymbol{\pi})^2 + \frac{1}{2}\delta Z_\sigma(\partial\sigma)^2, \end{aligned} \quad (\text{A.4.6})$$

where we have introduced

$$\delta m_\sigma^2 = \frac{1}{2}\delta\lambda v^2 - \delta m^2 + \frac{1}{2}\lambda\delta v^2, \quad (\text{A.4.7})$$

$$\delta m_\pi^2 = \frac{1}{6}\delta\lambda v^2 - \delta m^2 + \frac{1}{6}\lambda\delta v^2, \quad (\text{A.4.8})$$

$$\delta m^2 = \delta Z_m m^2, \quad \delta\lambda = \delta Z_\lambda \lambda, \quad \delta v^2 = \delta Z_v v^2. \quad (\text{A.4.9})$$

To one-loop order, where we can drop products of counterterms, we see that the quadratic meson part gives the counterterms

$$i\frac{1}{2}[\delta Z_\sigma(p^2 - m_\sigma^2) - \delta m_\sigma^2] \equiv \sigma \text{---}\otimes\text{---}\sigma, \quad (\text{A.4.10})$$

$$i\frac{1}{2}[\delta Z_\pi(p^2 - m_\pi^2) - \delta m_\pi^2] \equiv \boldsymbol{\pi} \text{---}\otimes\text{---}\boldsymbol{\pi}. \quad (\text{A.4.11})$$

Note that in the definition of the vertex factor, we do not include a factor of 2! coming from the fact that a σ or π -field can attach to the counterterm in two ways. We will instead multiply with these factors explicitly when summing diagrams.

We notice that to one-loop order, to find the counterterms corresponding to a product of renormalized quantities, we can effectively take the variation of the product. For example, if A and B are being renormalized at one loop, then the counterterms corresponding to the product AB is given by

$$\delta(AB) \equiv (A + \delta A)(B + \delta B) - AB = (\delta A)B + A(\delta B) + \underbrace{\delta A \delta B}_{\text{two-loop term}}. \quad (\text{A.4.12})$$

Using this we see that to one-loop order the linear counterterm becomes

$$\frac{1}{2}\delta Z_\sigma \sigma (h - m_\pi^2 v) + \sigma \left(\delta h - \delta m_\pi^2 v - \frac{1}{2}m_\pi^2 v \frac{\delta v^2}{v^2} \right), \quad (\text{A.4.13})$$

$$\begin{aligned}
\sigma \text{ --- } \sigma &= \frac{i}{p^2 - m_\sigma^2}, & \pi \text{ - - - } \pi &= \frac{i}{p^2 - m_\pi^2}, \\
\psi \text{ --- } \psi &= \frac{i(\not{p} + m_q)}{p^2 - m_q^2}, & \bullet \text{ --- } \sigma &= i(h - m_\pi^2 v), \\
\begin{array}{c} \sigma \\ \diagdown \quad \diagup \\ \bullet \\ \diagup \quad \diagdown \\ \sigma \end{array} &= -i \frac{\lambda}{4!}, & \begin{array}{c} \sigma \\ | \\ \bullet \\ \diagdown \quad \diagup \\ \sigma \quad \sigma \end{array} &= -i \frac{1}{6} \lambda v, & \begin{array}{c} \pi_i \quad \sigma \\ \diagdown \quad \diagup \\ \bullet \\ \diagup \quad \diagdown \\ \pi_i \quad \sigma \end{array} &= -i \frac{\lambda}{12} \\
\begin{array}{c} \pi_i \\ \diagdown \quad \diagup \\ \bullet \\ \diagup \quad \diagdown \\ \pi_i \quad \sigma \end{array} &= -i \frac{1}{6} \lambda v, & \begin{array}{c} \pi_i \quad \pi_j \\ \diagdown \quad \diagup \\ \bullet \\ \diagup \quad \diagdown \\ \pi_i \quad \pi_j \end{array} &= \begin{cases} -i \frac{2\lambda}{4!}, & i \neq j \\ -i \frac{\lambda}{4!}, & i = j \end{cases} \\
\begin{array}{c} \psi_\alpha \\ \diagdown \quad \diagup \\ \bullet \\ \diagup \quad \diagdown \\ \pi_i \quad \psi_\beta \end{array} &= g[\tau_i]_{\alpha\beta} \gamma^5, & \begin{array}{c} \psi_\alpha \\ \diagdown \quad \diagup \\ \bullet \\ \diagup \quad \diagdown \\ \sigma \quad \psi_\alpha \end{array} &= -ig.
\end{aligned}$$

Figure A.2: Vertex factors and propagators in the quark-meson model. Note that in this definition of the vertex factors, we do not include in the vertex itself a factor $n!$ for n equal external legs.

with

$$\sqrt{Z_\sigma} \approx 1 + \frac{1}{2} \delta Z_\sigma, \quad \delta v = \frac{1}{2v} \delta v^2. \quad (\text{A.4.14})$$

Thus, we have the counterterm

$$i \left[\frac{1}{2} \delta Z_\sigma (h - m_\pi^2 v) - \frac{1}{2} m_\pi^2 v \frac{\delta v^2}{v^2} + \delta h - \delta m_\pi^2 v \right] \equiv \otimes \text{---} \sigma \equiv i \delta t, \quad (\text{A.4.15})$$

where we have defined the δt as the expression in the braces.

From the Lagrangian we read off the rest of the Feynman rules. They are displayed in Fig. A.2. As we will see in the following, in the large- N_c limit at one loop we will not need any more counterterms than the ones we have derived when we use the appropriate renormalization conditions.

Simplifications in the One-Loop Large- N_c Limit

From now on we assume that N_c is large so that we can neglect all $\mathcal{O}(N_c^0)$ -terms. This allows us to derive several useful relations between the various counterterms at the one-loop level. In

this limit the quark mass receives no corrections at one loop, since the pion and sigma loops that would renormalize the quark propagator goes as $\mathcal{O}(N_c^0)$. Thus, for our approximation scheme to be consistent, we must have that the counterterms which would cancel these contributions must vanish. This means that

$$\psi \longrightarrow \otimes \longrightarrow \psi = 0. \quad (\text{A.4.16})$$

In other words, the counterterm corresponding to $\bar{\psi}i\cancel{\partial}\psi - m_q\bar{\psi}\psi$ must be zero:

$$\delta Z_\psi i\not{p} - \delta Z_\psi m_q - \delta m_q = 0 \quad \forall p. \quad (\text{A.4.17})$$

For this to hold for all p we must have that

$$\delta Z_\psi = 0, \quad \delta m_q = 0. \quad (\text{A.4.18})$$

This gives

$$\delta m_q = g\delta v + \delta gv = g\frac{\delta v^2}{2v} + v\frac{\delta g^2}{2g} = \frac{1}{2}\left(\frac{\delta g^2}{g^2} + \frac{\delta v^2}{v^2}\right) = 0, \quad (\text{A.4.19})$$

giving that

$$\frac{\delta g^2}{g^2} = -\frac{\delta v^2}{v^2}. \quad (\text{A.4.20})$$

We also have that the one-loop contribution to the $\pi\bar{\psi}\psi$ vertex goes as $\mathcal{O}(N_c^0)$ and thus is neglected in the large- N_c approximation. Hence, we must have that the corresponding counterterm also vanishes:

$$\begin{array}{c} \bar{\psi}_\alpha \\ \nearrow \\ \pi_j \text{ --- } \otimes \\ \searrow \\ \psi_\beta \end{array} = 0 \Rightarrow Z_\psi \sqrt{Z_g g^2} \sqrt{Z_\pi} \approx g \left(1 + \frac{1}{2}\frac{\delta g^2}{g^2} + \frac{1}{2}\delta Z_\pi\right) = g, \quad (\text{A.4.21})$$

where we used $Z_\psi = 1$ and discarded two-loop corrections. This implies that we need

$$\delta g^2 = -g^2 \delta Z_\pi. \quad (\text{A.4.22})$$

Combining this relation with equation (A.4.20), we find

$$\frac{\delta v^2}{v^2} = \delta Z_\pi. \quad (\text{A.4.23})$$

From the definitions (A.4.7) and (A.4.8) we can find additional relations between the counterterms. We see that

$$\delta\lambda = \frac{3(\delta m_\sigma^2 - \delta m_\pi^2)}{v^2} - \lambda \frac{\delta v^2}{v^2}, \quad (\text{A.4.24})$$

$$\delta m^2 = \frac{(\delta m_\sigma^2 - 3\delta m_\pi^2)}{2}. \quad (\text{A.4.25})$$

Combining (A.4.23) with (A.4.24) we find

$$\delta\lambda = \frac{3(\delta m_\sigma^2 - \delta m_\pi^2)}{v^2} - \lambda \delta Z_\pi. \quad (\text{A.4.26})$$

Subtleties in Dimensional Regularization

In four space-time dimensions one has a multitude of gamma-matrix identities, but in $d = 4 - 2\epsilon$ dimensions several of these relations either must be modified or becomes undefined. In the original paper by t'Hooft and Veltmann where dimensional regularization is introduced, Ref. [45], it is illustrated how ambiguities arise in integrals involving γ^5 . In four space-time dimensions γ^5 is defined by

$$\gamma^5 = i\gamma^0\gamma^1\gamma^2\gamma^3. \quad (\text{A.4.27})$$

However, in $d = 4 - 2\epsilon$ it is not clear how to define γ^5 . We will assume that it is somehow possible to define γ^5 in $4 - 2\epsilon$ dimensions such that it satisfies

$$\{\gamma^5, \gamma^\mu\} = 0, \quad (\gamma^5)^2 = 1. \quad (\text{A.4.28})$$

We will not need to take the trace of γ^5 , since we will only evaluate diagrams where two γ^5 matrices occur and thus can be combined to square to one. The justification for using these properties of γ^5 in arbitrary dimensions is discussed in Ref. [165].

The only other identities we need in the following are

$$\text{Tr } \gamma^\mu = 0, \quad \text{Tr } I = 4, \quad \text{Tr } \gamma^\mu \gamma^\nu = g^{\mu\nu}, \quad (\text{A.4.29})$$

which are not modified [11].

Pion and Sigma Self-Energies

We are now ready to calculate the self-energies of the sigma and the pions. All the relevant one-loop terms proportional to N_c and counterterms at the same order are shown in Fig. 4.2. Let us label the σ diagrams $i\Sigma_\sigma^1$, $i\Sigma_\sigma^{1,ct}$, $i\Sigma_\sigma^2$, $i\Sigma_\sigma^{2,ct}$ from left to right, respectively, and similarly for π . We note that in a general renormalization scheme, we would also need to account for the rightmost diagrams in Fig. 4.2. However, we will renormalize so that $m_\pi^2 v - h = 0$ holds also after renormalization, so that these diagrams vanish.

Sigma Self-Energy Diagrams

The first loop diagram is

$$\begin{aligned}
i\Sigma_\sigma^1(p^2) &= \text{---} \bullet \text{---} \text{---} \text{---} \bullet \text{---} \text{---} \\
&= 2N_c(-1)(-ig)^2\Lambda^{4-d} \int \frac{d^d k}{(2\pi)^d} \text{Tr} \left[\frac{i(\not{k} + \not{p} + m_q)}{(k+p)^2 - m_q^2} \frac{i(\not{k} + m_q)}{k^2 - m_q^2} \right] \\
&= -8N_c g^2 \Lambda^{4-d} \int \frac{d^d k}{(2\pi)^d} \frac{k^2 + p \cdot k + m_q^2}{[(k+p)^2 - m_q^2][k^2 - m_q^2]} \\
&= -8N_c g^2 \Lambda^{4-d} \int \frac{d^d k}{(2\pi)^d} \frac{(k+p)^2 - m_q^2 - p \cdot k - p^2 + 2m_q^2}{[(k+p)^2 - m_q^2][k^2 - m_q^2]} \\
&= -8N_c g^2 \left\{ A(m_q^2) + \Lambda^{4-d} \int \frac{d^d k}{(2\pi)^d} \frac{-p \cdot k - p^2 + 2m_q^2}{[(k+p)^2 - m_q^2][k^2 - m_q^2]} \right\}. \quad (\text{A.4.30})
\end{aligned}$$

where we have defined

$$A(m_q^2) = \Lambda^{4-d} \int \frac{d^d k}{(2\pi)^d} \frac{1}{k^2 - m_q^2}. \quad (\text{A.4.31})$$

In the second line we calculated the trace to be

$$\text{Tr} [(\not{k} + \not{p} + m_q)(\not{k} + m_q)] = 4(k^2 + p \cdot k + m_q^2) \quad (\text{A.4.32})$$

by using that $\text{Tr}(\gamma^\mu \gamma^\nu) = 4g^{\mu\nu}$. We can rewrite the last integral in the parenthesis of equation (A.4.30) as

$$I \equiv \Lambda^{4-d} \int \frac{d^d k}{(2\pi)^d} \frac{-p \cdot k - p^2 + 2m_q^2}{[(k+p)^2 - m_q^2][k^2 - m_q^2]} = \Lambda^{4-d} \int \frac{d^d q}{(2\pi)^d} \frac{p \cdot q + 2m_q^2}{[q^2 - m_q^2][(q+p)^2 - m_q^2]}, \quad (\text{A.4.33})$$

where we changed variable $q = -k - p$ in the last step. Adding both ways of writing the integral, we find that

$$I = \frac{I}{2} + \frac{I}{2} = \Lambda^{4-d} \int \frac{d^d k}{(2\pi)^d} \frac{-\frac{1}{2}p^2 + 2m_q^2}{[(k+p)^2 - m_q^2][k^2 - m_q^2]} \equiv -\frac{1}{2}(p^2 - 4m_q^2)B(p^2),$$


where we defined

$$B(p^2) = \Lambda^{4-d} \int \frac{d^d k}{(2\pi)^d} \frac{1}{[(k+p)^2 - m_q^2][k^2 - m_q^2]}. \quad (\text{A.4.34})$$

Thus we have

$$i\Sigma_\sigma^1(p^2) = -8N_c g^2 \left[A(m_q^2) - \frac{1}{2}(p^2 - 4m_q^2)B(p^2) \right]. \quad (\text{A.4.35})$$

The other diagram we consider is



$$i\Sigma_\sigma^2(p^2) = \text{---} \bullet \text{---} = 3!(-1)(2N_c) \left(\frac{-i\lambda v}{6} \right) \frac{i}{-m_\sigma^2} (-ig) \Lambda^{4-d} \int \frac{d^d k}{(2\pi)^d} \text{Tr} \frac{i(\not{k} + m_q)}{k^2 - m_q^2}$$

$$= \frac{8N_c \lambda g v m_q}{m_\sigma^2} \Lambda^{4-d} \int \frac{d^d k}{(2\pi)^d} \frac{1}{k^2 - m_q^2} = \frac{8N_c \lambda m_q^2}{m_\sigma^2} A(m_q^2). \quad (\text{A.4.36})$$

The factor $3!$ comes from the fact that external propagators can attach to the σ^3 vertex in $3!$ ways, the (-1) comes from the fermion loop and $2N_c$ from the fact that we have 2 different flavors and N_c different colors. Λ is a dimensionful scale keeping the dimensions of the integrals the same as in $d = 4$. We have also used that $\text{Tr} \gamma^\mu = 0 \Rightarrow \text{Tr}(\not{k} + m_q) = 4m_q$.

Adding up the two diagrams, we find

$$i\Sigma_\sigma^2(p^2) + i\Sigma_\sigma^1(p^2) = -8N_c g^2 \left[A(m_q^2) - \frac{1}{2}(p^2 - 4m_q^2)B(p^2) \right] + \frac{8N_c \lambda m_q^2}{m_\sigma^2} A(m_q^2). \quad (\text{A.4.37})$$

Pion Self-Energy Diagrams

The Σ_π^1 diagram is new since we here have the pseudoscalar Yukawa vertex associated with the term

$$g\bar{\psi}i\gamma^5\tau_i\pi_i\psi = gi[\pi_1(\bar{\psi}_1\gamma^5\psi_2 + \bar{\psi}_2\gamma^5\psi_1) + \pi_2i(-\bar{\psi}_1\gamma^5\psi_2 + \bar{\psi}_2\gamma^5\psi_1) + \pi_3(\bar{\psi}_1\gamma^5\psi_1 - \bar{\psi}_2\gamma^5\psi_2)]. \quad (\text{A.4.38})$$

Due to the $SU(2)_V$ symmetry which mixes components of $\boldsymbol{\pi}$, the contribution of these interactions to the self-energy is necessarily the same for all the components of $\boldsymbol{\pi}$. For π_3 we find N_c diagrams for each flavor:

$$i\Sigma_\pi^2(p^2) = N_c \left(\begin{array}{c} \psi_1 \\ \text{---} \pi_3 \text{---} \bullet \text{---} \pi_3 \text{---} \\ \psi_1 \end{array} \right) + N_c \left(\begin{array}{c} \psi_2 \\ \text{---} \pi_3 \text{---} \bullet \text{---} \pi_3 \text{---} \\ \psi_2 \end{array} \right) \quad (\text{A.4.39})$$

$$\begin{aligned} &= (-1)(\pm g)^2 2N_c \Lambda^{4-d} \int \frac{d^d k}{(2\pi)^d} \text{Tr} \left[\frac{\gamma^5 i(\not{k} + \not{p} + m_q)}{(k+p)^2 - m_q^2} \frac{\gamma^5 i(\not{k} + m_q)}{k^2 - m_q^2} \right] \\ &= -2N_c g^2 \Lambda^{4-d} \int \frac{d^d k}{(2\pi)^d} \text{Tr} \left[\frac{(\not{k} + \not{p} - m_q)(\not{k} + m_q)}{(k+p)^2 - m_q^2 [k^2 - m_q^2]} \right] \\ &= -8N_c g^2 \Lambda^{4-d} \int \frac{d^d k}{(2\pi)^d} \frac{k^2 + p \cdot k - m_q^2}{[(k+p)^2 - m_q^2][k^2 - m_q^2]} = -8N_c g^2 \left[A(m_q^2) - \frac{1}{2} p^2 B(p^2) \right]. \end{aligned} \quad (\text{A.4.40})$$

We here used that $\{\gamma^5, \gamma^\mu\} = 0$ and performed the same kind of manipulation on the integral as with σ . If we look at π_1 or π_2 instead, we would have loops with two different quark flavors at each vertex, but the final result is the same.

The Σ_π^2 diagram is

$$i\Sigma_\pi^2(p^2) = \begin{array}{c} \text{---} \bullet \text{---} \\ \uparrow \\ \text{---} \bullet \text{---} \end{array} = \frac{1}{3} \cdot \begin{array}{c} \text{---} \bullet \text{---} \\ \uparrow \\ \text{---} \bullet \text{---} \end{array} \quad (\text{A.4.41})$$

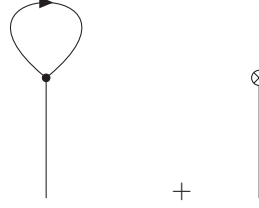
The factor $\frac{1}{3}$ difference is simply a result of the fact that the external pion propagators only can connect to the $\sigma\pi\pi$ vertex in $2!$ ways instead of $3!$.

The two diagrams add up to

$$i\Sigma_\pi^1(p^2) + i\Sigma_\pi^2(p^2) = -8N_c g^2 \left[A(m_q^2) - \frac{1}{2} p^2 B(p^2) \right] + \frac{8N_c \lambda m_q^2}{3m_\sigma^2} A(m_q^2). \quad (\text{A.4.42})$$

The On-Shell Renormalization Scheme

In the on-shell renormalization scheme we demand, at $T = 0$, that $v = \frac{\hbar}{m_\pi^2}$ and $\langle \sigma \rangle = 0$ also after loop corrections. The latter means that we have the condition



$$+ \quad = -8N_c g m_q A(m_q^2) + i\delta t = 0, \quad (\text{A.4.43})$$

since these are the diagrams that contribute to the one-point function in the large N_c limit. This gives

$$\delta t = -8iN_c g m_q A(m_q^2) = -8iN_c g^2 v A(m_q^2). \quad (\text{A.4.44})$$

This fixes δt , and thus gives an expression for δh in terms of δZ_σ , δv^2 and δm_π^2 through equation (A.4.15). Condition (A.4.43) also gives us that

$$\Sigma_\sigma^2(p^2) + \Sigma_\sigma^{2,ct}(p^2) = 0, \quad \Sigma_\pi^2(p^2) + \Sigma_\pi^{2,ct}(p^2) = 0, \quad (\text{A.4.45})$$

since these sums are proportional to (A.4.43). Using this we then have the inverse propagators

$$G_\sigma(p^2)^{-1} = p^2 - m_\sigma^2 + \Sigma_\sigma^1(p^2) + \Sigma_\sigma^{1,ct}(p^2), \quad (\text{A.4.46})$$

$$G_\pi(p^2)^{-1} = p^2 - m_\pi^2 + \Sigma_\pi^1(p^2) + \Sigma_\pi^{1,ct}(p^2). \quad (\text{A.4.47})$$

The on-shell scheme is defined by the fact that the masses receive no radiative corrections [11, 26]. Hence, we demand that the full propagators have poles at the location of the renormalized masses, meaning¹

$$\Sigma_\sigma^1(m_\sigma^2) + \Sigma_\sigma^{1,ct}(m_\sigma^2) = 0, \quad (\text{A.4.48})$$

$$\Sigma_\pi^1(m_\pi^2) + \Sigma_\pi^{1,ct}(m_\pi^2) = 0. \quad (\text{A.4.49})$$

The terms $i\Sigma_\sigma^{1,ct}$ and $i\Sigma_\pi^{1,ct}$ are, up to a factor of two, given by equations (A.4.10) and (A.4.11). Using that $\Sigma_\sigma^{1,ct}(m_\sigma^2) = -\delta m_\sigma^2$ and $\Sigma_\pi^{1,ct}(m_\pi^2) = -\delta m_\pi^2$, we find

$$\delta m_\sigma^2 = \Sigma_\sigma^1(m_\sigma^2) = 8iN_c g^2 \left[A(m_q^2) - \frac{1}{2}(m_\sigma^2 - 4m_q^2)B(m_\sigma^2) \right], \quad (\text{A.4.50})$$

$$\delta m_\pi^2 = \Sigma_\pi^1(m_\pi^2) = 8iN_c g^2 \left[A(m_q^2) - \frac{1}{2}m_\pi^2 B(m_\pi^2) \right]. \quad (\text{A.4.51})$$

In the on-shell scheme one also takes as a renormalization condition that the residue of the propagators at the mass poles are equal to i . Using the formula for a simple pole gives the criterion

$$i = \text{Res}_{p^2=m^2} G(p^2) = \lim_{p^2 \rightarrow m^2} (p^2 - m^2) \frac{i}{p^2 - m^2 + \Sigma(p^2)} = \frac{i}{1 + \frac{d\Sigma(p^2)}{dp^2} \Big|_{p^2=m^2}}, \quad (\text{A.4.52})$$

¹We actually here mean the real part of the inverse propagators. In order to not clutter the notation we will suppress this and discard imaginary parts. We will comment on this more in the following.

where we used L'Hôpital's rule. We thus find the on-shell condition

$$\left. \frac{d\Sigma(p^2)}{dp^2} \right|_{p^2=m^2} = 0. \quad (\text{A.4.53})$$

This condition gives

$$\left. \frac{d}{dp^2} [\Sigma_\sigma^1(p^2) + \Sigma_\sigma^{1,ct}(p^2)] \right|_{p^2=m_\sigma^2} = \left. \frac{d\Sigma_\sigma^1(p^2)}{dp^2} \right|_{p^2=m_\sigma^2} + \delta Z_\sigma = 0, \quad (\text{A.4.54})$$

and similarly for π . We find the expressions

$$\delta Z_\sigma = - \left. \frac{d\Sigma_\sigma^1(p^2)}{dp^2} \right|_{p^2=m_\sigma^2}, \quad \delta Z_\pi = - \left. \frac{d\Sigma_\pi^1(p^2)}{dp^2} \right|_{p^2=m_\pi^2}. \quad (\text{A.4.55})$$

Differentiating (A.4.35) and (A.4.40), we find

$$\delta Z_\sigma = 4iN_c g^2 [B(m_\sigma^2) + (m_\sigma^2 - 4m_q^2)B'(m_\sigma^2)], \quad (\text{A.4.56})$$

$$\delta Z_\pi = 4iN_c g^2 [B(m_\pi^2) + m_\pi^2 B'(m_\pi^2)], \quad (\text{A.4.57})$$

where $B'(m^2) = \left. \frac{dB(p^2)}{dp^2} \right|_{p^2=m^2}$.

To find an expression for δh , we combine (A.4.15), (A.4.23) and (A.4.44), and find

$$-8iN_c g^2 v A(m_q^2) = \frac{1}{2} \delta Z_\sigma (h - m_\pi^2 v) - \frac{1}{2} m_\pi^2 v \delta Z_\pi + \delta h - \delta m_\pi^2 v, \quad (\text{A.4.58})$$

which gives

$$\delta h = -8iN_c g^2 v A(m_q^2) + v \delta m_\pi^2 + \frac{1}{2} m_\pi^2 v \delta Z_\pi - \frac{1}{2} \delta Z_\sigma (h - m_\pi^2 v). \quad (\text{A.4.59})$$

Note that the last term vanishes since we renormalize so the minimum of the potential does not change.

Having determined δm_σ^2 , δm_π^2 , δZ_σ and δZ_π , we are in position to use relations (A.4.22), (A.4.25), (A.4.26) and (A.4.59) to find δg^2 , δv^2 , $\delta \lambda$, δm^2 and δh . We find the on-shell expressions

$$\delta m_{\text{OS}}^2 = -8iN_c g^2 \left[A(m_q^2) + \frac{1}{4}(m_\sigma^2 - 4m_q^2)B(m_\sigma^2) - \frac{3}{4}m_\pi^2 B(m_\pi^2) \right], \quad (\text{A.4.60})$$

$$\delta \lambda_{\text{OS}} = - \frac{12iN_c g^2}{v^2} [(m_\sigma^2 - 4m_q^2)B(m_\sigma^2) - m_\pi^2 B(m_\pi^2)] - 4i\lambda N_c g^2 [B(m_\pi^2) + m_\pi B'(m_\pi^2)], \quad (\text{A.4.61})$$

$$\delta g_{\text{OS}}^2 = -4iN_c g^4 [B(m_\pi^2) + m_\pi^2 B'(m_\pi^2)], \quad (\text{A.4.62})$$

$$\delta h_{\text{OS}} = -2iN_c g^2 m_\pi^2 v [B(m_\pi^2) - m_\pi^2 B'(m_\pi^2)], \quad (\text{A.4.63})$$

$$\delta v_{\text{OS}}^2 = 4iN_c g^2 v^2 [B(m_\pi^2) + m_\pi^2 B'(m_\pi^2)], \quad (\text{A.4.64})$$

$$\delta Z_\sigma^{\text{OS}} = 4iN_c g^2 [B(m_\sigma^2) + (m_\sigma^2 - 4m_q^2)B'(m_\sigma^2)], \quad (\text{A.4.65})$$

$$\delta Z_\pi^{\text{OS}} = 4iN_c g^2 [B(m_\pi^2) + m_\pi^2 B'(m_\pi^2)], \quad (\text{A.4.66})$$

where we have listed δZ_σ and δZ_π again for completeness.

Calculating the Loop Integrals

We want to calculate the integrals $A(m_q^2)$ and $B(p^2)$ and separate out the divergent parts so that we can relate the counterterms and couplings in the on-shell and $\overline{\text{MS}}$ schemes.

In the following we will use the integral formula

$$\int \frac{d^d k}{(2\pi)^d} \frac{k^{2a}}{(k^2 - \eta)^b} = i(-1)^{a-b} \frac{1}{(4\pi)^{\frac{d}{2}}} \eta^{\frac{d}{2}+a-b} \frac{\Gamma(a + \frac{d}{2}) \Gamma(b - a - \frac{d}{2})}{\Gamma(b) \Gamma(\frac{d}{2})}, \quad (\text{A.4.67})$$

with $d = 4 - 2\epsilon$. We find

$$\begin{aligned} A(m_q^2) &= \Lambda^{4-d} \int \frac{d^d k}{(2\pi)^4} \frac{1}{k^2 - m_q^2} = \frac{-im_q^2}{(4\pi)^{\frac{d}{2}}} \left(\frac{\Lambda}{m_q}\right)^{4-d} \Gamma\left(1 - \frac{d}{2}\right) = \frac{-im_q^2}{(4\pi^2)^2} \left(\frac{4\pi\Lambda^2}{m_q^2}\right)^\epsilon \Gamma(-1 + \epsilon) \\ &= \frac{im_q^2}{(4\pi)^2} \left[\frac{1}{\epsilon} + 1 + \ln(4\pi e^{-\gamma_E}) + \ln\left(\frac{\Lambda}{m_q^2}\right) \right], \end{aligned} \quad (\text{A.4.68})$$

where we only keep terms up to order $\mathcal{O}(\epsilon^0)$. For the integral $B(p^2)$ we use that

$$\frac{1}{XY} = \int_0^1 \frac{dx}{[X + (Y - X)x]^2}, \quad (\text{A.4.69})$$

where we have introduced a so-called Feynman parameter x . Defining

$$\eta(x) = p^2 x(x - 1) + m_q^2, \quad (\text{A.4.70})$$

we then find

$$\begin{aligned} B(p^2) &= \Lambda^{4-d} \int \frac{d^d k}{(2\pi)^4} \frac{1}{[(k+p)^2 - m_q^2][k^2 - m_q^2]} = \Lambda^{4-d} \int_0^1 dx \frac{i\eta(x)^{\frac{d}{2}-2}}{(4\pi)^{\frac{d}{2}}} \Gamma\left(2 - \frac{d}{2}\right) \\ &= \frac{i}{(4\pi)^2} \int_0^1 dx \left(\frac{4\pi\Lambda^2}{\eta(x)}\right)^\epsilon (\epsilon - 1) \Gamma(-1 + \epsilon) \\ &\equiv \frac{i}{(4\pi)^2} \left[\frac{1}{\epsilon} + \ln(4\pi e^{-\gamma_E}) + \ln\left(\frac{\Lambda}{m_q^2}\right) + C(p^2) \right], \end{aligned} \quad (\text{A.4.71})$$

where we have defined the function

$$C(p^2) = - \int_0^1 dx \ln\left(\frac{\eta(x)}{m_q^2}\right) = - \int_0^1 dx \ln\left[\frac{p^2}{m_q^2} x(x - 1) + 1\right]. \quad (\text{A.4.72})$$

This integral can be calculated exactly and is found in standard integral tables. The result is

$$C(p^2) = 2 - 2\sqrt{\frac{4m_q^2}{p^2} - 1} \arctan\left(\frac{1}{\sqrt{\frac{4m_q^2}{p^2} - 1}}\right). \quad (\text{A.4.73})$$

Differentiating gives

$$C'(p^2) = \frac{4m_q^2}{p^4 \sqrt{\frac{4m_q^2}{p^2} - 1}} \arctan\left(\frac{1}{\sqrt{\frac{4m_q^2}{p^2} - 1}}\right) - \frac{1}{p^2}. \quad (\text{A.4.74})$$

Note that for $p^2 > 4m_q^2$, $C(p^2)$ and $C'(p^2)$ get an imaginary part. Thus, the self-energy also gets an imaginary part. This is the case for $C(m_\sigma^2)$ and $C'(m_\sigma^2)$ if $m_\sigma > 2m_q$, because the sigma then will have a finite lifetime, since the decay $\sigma \rightarrow \bar{\psi}\psi$ through the Yukawa-vertex becomes kinematically allowed. For the pions this decay will be kinematically forbidden, since we will use a quark mass satisfying $m_\pi < m_q$. In the following we will only keep the real parts of $C(m_\sigma^2)$ and $C'(m_\sigma^2)$. We can do this since the requirement that the inverse propagators vanish when evaluated at the physical masses, equations (A.4.48) and (A.4.49), should really have been

$$\text{Re } G_\sigma(m_\sigma^2)^{-1} = 0, \quad (\text{A.4.75})$$

$$\text{Re } G_\pi(m_\pi)^{-1} = 0. \quad (\text{A.4.76})$$

To avoid writing $\ln(4\pi e^{-\gamma_E})$ everywhere we redefine $\Lambda \rightarrow \Lambda e^{\gamma_E}/4\pi$. Inserting our analytical expressions for the integrals, equations (A.4.68) and (A.4.71), into equations (A.4.60)–(A.4.66), we get

$$\begin{aligned} \delta m_{\text{os}}^2 &= \delta m_{\overline{\text{MS}}}^2 + \frac{2N_c m_q^2}{(4\pi)^2 v^2} (m_\sigma^2 - 3m_\pi^2) \ln\left(\frac{\Lambda}{m_q^2}\right) \\ &\quad + \frac{4N_c m_q^2}{(4\pi)^2 v^2} \left[2m_q^2 + \frac{1}{2}(m_\sigma^2 - 4m_q^2)C(m_\sigma^2) - \frac{3}{2}m_\pi^2 C(m_\pi^2) \right], \end{aligned} \quad (\text{A.4.77})$$

$$\begin{aligned} \delta \lambda_{\text{os}} &= \delta \lambda_{\overline{\text{MS}}} + \frac{12N_c m_q^2}{(4\pi)^2 v^4} \left[2(m_\sigma^2 - m_\pi^2 - 2m_q^2) \ln\left(\frac{\Lambda}{m_q^2}\right) + (m_\sigma^2 - 4m_q^2)C(m_\sigma^2) \right], \\ &\quad + \frac{12N_c m_q^4}{(4\pi)^2 v^4} \left[(m_\sigma^2 - 2m_\pi^2)C(m_\pi^2) + (m_\sigma^2 - m_\pi^2)m_\pi^2 C'(m_\pi^2) \right], \end{aligned} \quad (\text{A.4.78})$$

$$\delta g_{\text{os}}^2 = \delta g_{\overline{\text{MS}}}^2 + \frac{4N_c m_q^4}{(4\pi)^2 v^4} \left[\ln\left(\frac{\Lambda}{m_q^2}\right) + C(m_\pi^2) + m_\pi^2 C'(m_\pi^2) \right], \quad (\text{A.4.79})$$

$$\delta h_{\text{os}} = \delta h_{\overline{\text{MS}}} + \frac{2N_c g^2 m_\pi^2 v}{(4\pi)^2} \left[\ln\left(\frac{\Lambda}{m_q^2}\right) + C(m_\pi^2) - m_\pi^2 C'(m_\pi^2) \right], \quad (\text{A.4.80})$$

$$\delta v_{\text{os}}^2 = \delta v_{\overline{\text{MS}}}^2 - \frac{4N_c m_q^2}{(4\pi)^2} \left[\ln\left(\frac{\Lambda}{m_q^2}\right) + C(m_\pi^2) + m_\pi^2 C'(m_\pi^2) \right], \quad (\text{A.4.81})$$

$$\delta Z_\sigma^{\text{OS}} = \delta Z_\sigma^{\overline{\text{MS}}} - \frac{4N_c m_q^2}{(4\pi)^2 v^2} \left[\ln\left(\frac{\Lambda}{m_q^2}\right) + C(m_\sigma^2) + (m_\sigma^2 - 4m_q^2)C'(m_\sigma^2) \right], \quad (\text{A.4.82})$$

$$\delta Z_\pi^{\text{OS}} = \delta Z_\pi^{\overline{\text{MS}}} - \frac{4N_c m_q^2}{(4\pi)^2 v^2} \left[\ln\left(\frac{\Lambda}{m_q^2}\right) + C(m_\pi^2) + m_\pi^2 C'(m_\pi^2) \right], \quad (\text{A.4.83})$$

where the $\frac{1}{\epsilon}$ -parts, which will be common to both subtraction schemes, are

$$\begin{aligned} \delta m_{\overline{\text{MS}}}^2 &= \frac{4N_c g^2 m^2}{(4\pi)^2} \frac{1}{\epsilon}, & \delta \lambda_{\overline{\text{MS}}} &= \frac{8N_c g^2}{(4\pi)^2} (\lambda - 6g^2) \frac{1}{\epsilon}, & \delta g_{\overline{\text{MS}}}^2 &= \frac{4N_c g^4}{(4\pi)^2} \frac{1}{\epsilon}, & \delta h_{\overline{\text{MS}}} &= \frac{2N_c g^2 h}{(4\pi)^2} \frac{1}{\epsilon}, \\ \delta v_{\overline{\text{MS}}}^2 &= -\frac{4N_c g^2 v^2}{(4\pi)^2} \frac{1}{\epsilon}, & \delta Z_\sigma^{\overline{\text{MS}}} &= -\frac{4N_c g^2}{(4\pi)^2} \frac{1}{\epsilon}, & \delta Z_\pi^{\overline{\text{MS}}} &= -\frac{4N_c g^2}{(4\pi)^2} \frac{1}{\epsilon}. \end{aligned} \quad (\text{A.4.84})$$

These are the counterterms in the $\overline{\text{MS}}$ scheme. Note, very importantly, that the masses present in equations (A.4.77)–(A.4.83) are the physical masses, since the renormalized and the physical pole masses coincide in the on-shell scheme.

We should now determine the value for Λ that is consistent with our assumption that $m_\pi^2 v - h = 0$. This assumption is valid if

$$\left. \frac{\partial \Omega_{\text{vac}}}{\partial v} \right|_{v=\frac{h}{m_\pi^2}} = 0, \quad (\text{A.4.85})$$

i.e. if the minimum of the effective potential is the same as the minimum of the tree-level potential. Dropping terms not proportional to N_c gives that the vacuum effective potential is,

$$\Omega_{\text{vac}}(v) = U(v) + \delta U(v) + \frac{2N_c g^4 v^4}{(4\pi)^2} \left[\frac{1}{\epsilon} + \frac{3}{2} + \ln \left(\frac{\Lambda^2}{g^2 v^2} \right) \right], \quad (\text{A.4.86})$$

We will show later that the infinite part of δU cancels the divergent part in the last term. Assuming this, requirement (A.4.85) reads

$$\left. \frac{\partial}{\partial v} \left\{ \delta U(v)_{\text{finite}} + \frac{2N_c g^4 v^4}{(4\pi)^2} \left[\frac{3}{2} + \ln \left(\frac{\Lambda^2}{g^2 v^2} \right) \right] \right\} \right|_{v=\frac{h}{m_\pi^2}} = 0, \quad (\text{A.4.87})$$

where we have that

$$\delta U = -\frac{1}{2} \delta m^2 v^2 - \frac{1}{2} m^2 \delta v^2 + \frac{\delta \lambda}{4!} v^4 + \frac{\lambda}{4!} 2v^2 \delta v^2 - \delta h v - h \frac{\delta v^2}{2v}. \quad (\text{A.4.88})$$

Inserting the finite parts of the on-shell counterterms into equation (A.4.87) and calculating the derivative in Wolfram Mathematica, we find

$$C(m_\pi^2) + m_\pi^2 C'(m_\pi^2) + \ln \left(\frac{\Lambda_0^2}{m_q^2} \right) = 0. \quad (\text{A.4.89})$$

Thus, equations (A.4.77)–(A.4.83) are valid when the renormalization scale is

$$\Lambda_0^2 \equiv m_q^2 \exp\{-C(m_\pi^2) - m_\pi^2 C'(m_\pi^2)\}. \quad (\text{A.4.90})$$

The $\overline{\text{MS}}$ Renormalization Scheme

We must have that the bare quantities are independent of renormalization scheme. Hence, we have

$$m_B^2 = Z_m^{\overline{\text{MS}}} m_{\overline{\text{MS}}}^2 = Z_m^{\text{OS}} m^2, \quad (\text{A.4.91})$$

which implies

$$m_{\overline{\text{MS}}}^2 + \delta m_{\overline{\text{MS}}}^2 = m^2 + \delta m_{\text{OS}}^2. \quad (\text{A.4.92})$$

Hence, $m_{\overline{\text{MS}}}^2$, and all the other couplings by the same argument, can be found by

$$\begin{aligned} m_{\overline{\text{MS}}}^2(\Lambda) &= m^2 + \delta m_{\text{OS}}^2 - \delta m_{\overline{\text{MS}}}^2, & \lambda_{\overline{\text{MS}}}(\Lambda) &= \lambda + \delta \lambda_{\text{OS}} - \delta \lambda_{\overline{\text{MS}}}, & g_{\overline{\text{MS}}}^2(\Lambda) &= g^2 + \delta g_{\text{OS}}^2 - \delta g_{\overline{\text{MS}}}^2, \\ h_{\overline{\text{MS}}}(\Lambda) &= h + \delta h_{\text{OS}} - \delta h_{\overline{\text{MS}}}, & v_{\overline{\text{MS}}}^2(\Lambda) &= v^2 + \delta v_{\text{OS}}^2 - \delta v_{\overline{\text{MS}}}^2. \end{aligned} \quad (\text{A.4.93})$$

The difference between the OS and $\overline{\text{MS}}$ counterterms can be read off directly from the expressions (A.4.77)–(A.4.83). Since the masses are measured in vacuum, where the minimum of the potential

is $v = f_\pi$ by assumption, we find that the running couplings are

$$m_{\overline{\text{MS}}}^2(\Lambda) = \frac{m_\sigma^2 - 3m_\pi^2}{2} + \frac{2N_c m_q^2}{(4\pi)^2 f_\pi^2} (m_\sigma^2 - 3m_\pi^2) \ln\left(\frac{\Lambda}{m_q^2}\right) + \frac{4N_c m_q^2}{(4\pi)^2 f_\pi^2} \left[2m_q^2 + \frac{1}{2}(m_\sigma^2 - 4m_q^2)C(m_\sigma^2) - \frac{3}{2}m_\pi^2 C(m_\pi^2) \right], \quad (\text{A.4.94})$$

$$\lambda_{\overline{\text{MS}}}(\Lambda) = \frac{3(m_\sigma^2 - m_\pi^2)}{f_\pi^2} + \frac{12N_c m_q^2}{(4\pi)^2 f_\pi^4} \left[2(m_\sigma^2 - m_\pi^2 - 2m_q^2) \ln\left(\frac{\Lambda}{m_q^2}\right) + (m_\sigma^2 - 4m_q^2)C(m_\sigma^2) \right] + \frac{12N_c m_q^2}{(4\pi)^2 f_\pi^4} [(m_\sigma^2 - 2m_\pi^2)C(m_\pi^2) + (m_\sigma^2 - m_\pi^2)m_\pi^2 C'(m_\pi^2)], \quad (\text{A.4.95})$$

$$g_{\overline{\text{MS}}}^2(\Lambda) = \frac{m_q^2}{f_\pi^2} + \frac{4N_c m_q^4}{(4\pi)^2 f_\pi^4} \left[\ln\left(\frac{\Lambda}{m_q^2}\right) + C(m_\pi^2) + m_\pi^2 C'(m_\pi^2) \right], \quad (\text{A.4.96})$$

$$h_{\overline{\text{MS}}}(\Lambda) = m_\pi^2 f_\pi + \frac{2N_c g^2 m_\pi^2 f_\pi}{(4\pi)^2} \left[\ln\left(\frac{\Lambda}{m_q^2}\right) + C(m_\pi^2) - m_\pi^2 C'(m_\pi^2) \right], \quad (\text{A.4.97})$$

$$v_{\overline{\text{MS}}}^2(\Lambda) = f_\pi^2 - \frac{4N_c m_q^2}{(4\pi)^2} \left[\ln\left(\frac{\Lambda}{m_q^2}\right) + C(m_\pi^2) + m_\pi^2 C'(m_\pi^2) \right], \quad (\text{A.4.98})$$

We again emphasize that the masses on the right hand side of those equations are the physical masses, and thus we can use these relations to calculate the running couplings at the scale Λ_0 . Later we find the expressions for the couplings valid at any scale Λ via the renormalization group equations.

Let us now find the effective potential in the large- N_c limit. In the $\overline{\text{MS}}$ scheme the vacuum potential reads

$$\Omega_{\text{vac}}(v) = U(v_{\overline{\text{MS}}}) + \delta U_{\overline{\text{MS}}} + \frac{2N_c g_{\overline{\text{MS}}}^4 v_{\overline{\text{MS}}}^4}{(4\pi)^2} \left[\frac{1}{\epsilon} + \frac{3}{2} + \ln\left(\frac{\Lambda^2}{g_{\overline{\text{MS}}}^2 v_{\overline{\text{MS}}}^2}\right) \right]. \quad (\text{A.4.99})$$

Since we have not explicitly demanded that the vacuum energy is finite, we should check that this is the case. If we plug in all the counterterms in the $\overline{\text{MS}}$ -scheme into equation (A.4.88), we find

$$\delta U_{\overline{\text{MS}}} = -\frac{2N_c g_{\overline{\text{MS}}}^4 v_{\overline{\text{MS}}}^4}{(4\pi)^2} \frac{1}{\epsilon}. \quad (\text{A.4.100})$$

But this exactly cancels the divergence in (A.4.99). Including the temperature dependent term and defining $\Delta = v_{\overline{\text{MS}}} g_{\overline{\text{MS}}}$, we find

$$\Omega(\Delta, T, \mu_q) = -\frac{1}{2} \frac{m_{\overline{\text{MS}}}^2(\Lambda)}{g_{\overline{\text{MS}}}^2(\Lambda)} \Delta^2 + \frac{1}{4!} \frac{\lambda_{\overline{\text{MS}}}(\Lambda)}{g_{\overline{\text{MS}}}^4(\Lambda)} \Delta^4 - \frac{h_{\overline{\text{MS}}}(\Lambda)}{g_{\overline{\text{MS}}}(\Lambda)} \Delta + \frac{2N_c \Delta^4}{(4\pi)^2} \left[\frac{3}{2} + \ln\left(\frac{\Lambda^2}{\Delta^2}\right) \right] - 4N_c T \int \frac{d^3 p}{(2\pi)^3} \left\{ \ln \left[1 + e^{-\beta(\sqrt{\mathbf{p}^2 + \Delta^2} - \mu_q)} \right] + \ln \left[1 + e^{-\beta(\sqrt{\mathbf{p}^2 + \Delta^2} + \mu_q)} \right] \right\}. \quad (\text{A.4.101})$$

Note that since $\delta(gv) = 0$, we have, to order $\mathcal{O}(N_c^1)$, that $\Delta = v_{\overline{\text{MS}}} g_{\overline{\text{MS}}} = v_{\text{os}} g_{\text{os}}$, which is independent of Λ .

Renormalization Group Equations

In the previous we found the grand potential in the $\overline{\text{MS}}$ scheme. However, since we have required that the minimum of $\Omega_{\text{vac}}(v)$ equals the minimum of the tree-level potential, we have a requirement on Λ , which is given in equation (A.4.90). A fundamental idea of quantum field theory is that physical quantities should be independent of the choice of the renormalization scale Λ . This leads us to the renormalization group (RG) equations, which is a class of equations implementing this requirement.

We obtain the RG equations for the running couplings by simply differentiating relations (A.4.94)–(A.4.97) and inserting the expressions for h , m^2 , λ and g^2 in terms of $h_{\overline{\text{MS}}}$, $m_{\overline{\text{MS}}}^2$, $\lambda_{\overline{\text{MS}}}$ and $g_{\overline{\text{MS}}}^2$ to lowest order in the $\overline{\text{MS}}$ quantities. We find

$$\begin{aligned} \frac{dm_{\overline{\text{MS}}}^2(\Lambda)}{d \ln \Lambda} &= \frac{8N_c}{(4\pi)^2} m_{\overline{\text{MS}}}^2(\Lambda) g_{\overline{\text{MS}}}^2(\Lambda), & \frac{dg_{\overline{\text{MS}}}^2(\Lambda)}{d \ln \Lambda} &= \frac{8N_c}{(4\pi)^2} g_{\overline{\text{MS}}}^4(\Lambda), \\ \frac{dh_{\overline{\text{MS}}}(\Lambda)}{d \ln \Lambda} &= \frac{4N_c}{(4\pi)^2} g_{\overline{\text{MS}}}^2(\Lambda) h_{\overline{\text{MS}}}(\Lambda), & \frac{d\lambda_{\overline{\text{MS}}}(\Lambda)}{d \ln \Lambda} &= \frac{16N_c}{(4\pi)^2} [g_{\overline{\text{MS}}}^2(\Lambda) \lambda_{\overline{\text{MS}}}(\Lambda) - 6g_{\overline{\text{MS}}}^4(\Lambda)], \end{aligned} \quad (\text{A.4.102})$$

where we used $\frac{d}{d \ln \Lambda} = \Lambda \frac{d}{d\Lambda}$. These are standard ordinary differential equations, and we find that the solutions are

$$\begin{aligned} m_{\overline{\text{MS}}}^2(\Lambda) &= \frac{m_0^2}{1 - \frac{4N_c g_0^2}{(4\pi)^2} \ln \left(\frac{\Lambda^2}{\Lambda_0^2} \right)}, & g_{\overline{\text{MS}}}^2(\Lambda) &= \frac{g_0^2}{1 - \frac{4N_c g_0^2}{(4\pi)^2} \ln \left(\frac{\Lambda^2}{\Lambda_0^2} \right)}, \\ h_{\overline{\text{MS}}}(\Lambda) &= \frac{h_0}{1 - \frac{2N_c g_0^2}{(4\pi)^2} \ln \left(\frac{\Lambda^2}{\Lambda_0^2} \right)}, & \lambda_{\overline{\text{MS}}}(\Lambda) &= \frac{\lambda_0 - \frac{48N_c}{(4\pi)^2} g_0^4 \ln \left(\frac{\Lambda^2}{\Lambda_0^2} \right)}{\left[1 - \frac{4N_c g_0^2}{(4\pi)^2} \ln \left(\frac{\Lambda^2}{\Lambda_0^2} \right) \right]^2}, \end{aligned} \quad (\text{A.4.103})$$

where the values with the 0-subscript are the values of the couplings at the given scale Λ_0 . These relations together with the values g_0 , m_0 , λ_0 and h_0 calculated at the specific scale Λ_0 thus gives us these couplings at any other scale.

The Effective Potential

Inserting the running couplings into the potential gives

$$\Omega_{\text{vac}}(\Delta) = -\frac{1}{2} m_0^2 f_\pi^2 \frac{\Delta^2}{m_q^2} + \frac{1}{4!} \lambda_0 f_\pi^4 \frac{\Delta^4}{m_q^4} - h_0 f_\pi \frac{\Delta}{m_q} \quad (\text{A.4.104})$$

$$+ \frac{2N_c \Delta^4}{(4\pi)^2} \left[\frac{3}{2} + \ln \left(\frac{m_q^2}{\Delta^2} \right) - C(m_\pi^2) - m_\pi^2 C'(m_\pi^2) \right], \quad (\text{A.4.105})$$

where we used

$$\frac{h_{\overline{\text{MS}}}(\Lambda)}{g_{\overline{\text{MS}}}(\Lambda)} = \frac{h_0}{g_0} \frac{\sqrt{1 - \frac{4N_c g_0^2}{(4\pi)^2} \log \left(\frac{\Lambda^2}{\Lambda_0^2} \right)}}{1 - \frac{2N_c g_0^2}{(4\pi)^2} \log \left(\frac{\Lambda^2}{\Lambda_0^2} \right)} = \frac{h_0}{g_0} + \mathcal{O} \left(N_c^2 \log^2 \left(\frac{\Lambda^2}{\Lambda_0^2} \right) \right). \quad (\text{A.4.106})$$

We drop the $\mathcal{O}(N_c^2)$ term as this is a two loop term. We now see that the grand potential is independent of Λ .

Code

In the following we provide the Python and C routines used to minimize the effective potential. The code used for plotting is voluminous and not included.

B.1 Implementation of the Effective Potential in Python

```
import numpy as np
import scipy
from scipy import integrate, LowLevelCallable
import mpmath
import math
import cmath
import os, ctypes
import time

#Import C functions for integrands for faster integration
lib = ctypes.CDLL(os.path.abspath('quarkIntegrand.so'))
lib.quark_integrand.restype = ctypes.c_double
lib.quark_integrand.argtypes = (ctypes.c_int, ctypes.
    POINTER(ctypes.c_double))
quark_integrand = LowLevelCallable(lib.quark_integrand)

lib = ctypes.CDLL(os.path.abspath('quarkIntegrand.so'))
lib.quark_integrand_noB.restype = ctypes.c_double
lib.quark_integrand_noB.argtypes = (ctypes.c_int, ctypes.
    POINTER(ctypes.c_double))
quark_integrand_noB = LowLevelCallable(lib.
    quark_integrand_noB)

#Global variable specifying when the B=0 expressions
    should be utilized
```

```

mpi = 140
B_cutoff = 1.e-2 *mpi**2

class CouplingSet:
    def __init__(self, m_pi, m_sigma, m_quark, f_pi,
                 n_colors = 3):

        self.m_quark = m_quark
        self.m_pi = m_pi
        self.m_sigma = m_sigma
        self.f_pi = f_pi
        self.n_colors = n_colors

        self.renorm_MS0 = np.sqrt( m_quark**2 * np.exp(
            - self.C(m_pi) - m_pi**2 * self.C_prime(m_pi) )
        )
        self.m0 = self.calc_m_MS()
        self.lambda0 = self.calc_lambda_MS()
        self.g0 = self.calc_g_MS()
        self.h0 = self.calc_h_MS()
        self.renorm_MS = self.renorm_MS0
        self.m_MS = self.m0
        self.lambda_MS = self.lambda0
        self.g_MS = self.g0
        self.h_MS = self.h0

    def convertToTreeLevel(self):
        self.m0 = np.sqrt((self.m_sigma**2 - 3.0*self.m_pi
            **2)/2.0)
        self.lambda0 = 3.0*(self.m_sigma**2 - self.m_pi
            **2)/self.f_pi**2
        self.g0 = self.m_quark/self.f_pi
        self.h0 = self.m_pi**2*self.f_pi
        self.renorm_MS0 = np.exp(-0.5)*self.g0*self.f_pi
        self.m_MS = self.m0
        self.lambda_MS = self.lambda0
        self.g_MS = self.g0
        self.h_MS = self.h0
        self.renorm_MS = self.renorm_MS0

    def C(self, p):
        """ C(p) is a mathematical function appearing in
            the calculation of the pion and sigma self-
            energies. """
        if (p==0):
            return 0
        else:
            q = 4.*(self.m_quark**2)/p**2 - 1. + 0j
            r = np.sqrt(q)

```

```

        return np.real(2.-2.*r*np.arctan(1.0/r))

def C_prime(self, p):
    """ The derivative of C(p). """
    if (p==0):
        return 0
    else:
        q = 4.*(self.m_quark**2)/p**2 - 1. + 0j
        r = np.sqrt(q)
        return np.real(4.*self.m_quark**2/(p**4*r)*np.
            arctan(1/r) - 1./p**2)

def calc_m_MS(self):
    n_colors = self.n_colors
    mu2 = (self.m_sigma**2 - 3.0*self.m_pi**2)/2.0
    bigBrace = 2*self.m_quark**2 + mu2*np.log(self.
        renorm_MS0**2/self.m_quark**2) + 0.5*(self.
        m_sigma**2 - 4.*self.m_quark**2)*self.C(self.
        m_sigma) - 1.5*self.m_pi**2 * self.C(self.m_pi)
    mu2 += 4.*n_colors*(self.m_quark**2)/(4.*np.pi*
        self.f_pi)**2 * bigBrace
    return np.sqrt(mu2)

def calc_lambda_MS(self):
    n_colors = self.n_colors
    Lambda = 3.0*(self.m_sigma**2 - self.m_pi**2)/self.
        .f_pi**2
    bigBrace1 = 2.0*(self.m_sigma**2 - self.m_pi**2 -
        2.0*self.m_quark**2)*np.log(self.renorm_MS0**2/
        self.m_quark**2) + (self.m_sigma**2 - 4.0*self.
        m_quark**2)*self.C(self.m_sigma)
    bigBrace2 = (self.m_sigma**2 - 2.0*self.m_pi**2)*
        self.C(self.m_pi) + (self.m_sigma**2 - self.
        m_pi**2)*self.m_pi**2 * self.C_prime(self.m_pi)
    Lambda += 12.0*n_colors*(self.m_quark**2)/((4.0*np
        .pi)**2*self.f_pi**4) * (bigBrace1 + bigBrace2)
    return Lambda

def calc_g_MS(self):
    n_colors = self.n_colors
    g2 = self.m_quark**2/self.f_pi**2 + (4.*n_colors*
        self.m_quark**4)/((4.*np.pi)**2*self.f_pi**4) *
        ( np.log(self.renorm_MS0**2/self.m_quark**2) +
        self.C(self.m_pi) + self.m_pi**2*self.C_prime(
        self.m_pi) )
    return np.sqrt(g2)

def calc_h_MS(self):
    n_colors = self.n_colors

```

```

    h = self.m_pi**2*self.f_pi + (2.*n_colors*self.
        m_quark**2*self.m_pi**2)/((4.*np.pi)**2*self.
        f_pi) * ( np.log(self.renorm_MS0**2/self.
        m_quark**2) + self.C(self.m_pi)-self.m_pi**2*
        self.C_prime(self.m_pi) )
    return h

def v_effective(parameters, T, chem_pot, B, couplings,
    scale, potential, withPhoton=False):
    """ Assume parameters of the form parameters = [delta,
        q] """
    delta = parameters[0]
    q = parameters[1]
    r_imag = 0
    r = 0

    v = 0
    v += v_qk_vac_noB(delta, couplings)
    v += v_qk_vac_B(delta, B)
    v += v_qk_thermal(delta, B, T, chem_pot, q)
    v += v_meson(delta, couplings)
    if(potential=='chiM'):
        v += v_gluon(q, r, r_imag, T)
    elif(potential=='RRTW'):
        v += v_gluon_RRTW(q, r, r_imag, T)
    else:
        print "Invalid potential. Terminating."
        return np.nan
    if(withPhoton):
        v += v_photon(couplings, B)
    return v*scale

def v_meson(delta, couplings):
    v_mes = -0.5 * couplings.m_MS**2 * delta**2 /
        couplings.g_MS**2 + couplings.lambda_MS/(4.*3.*2.*
        couplings.g_MS**4)*delta**4 \
        - couplings.h_MS*delta/couplings.g_MS
    return v_mes

def v_qk_thermal(delta, B, T, chem_pot, q):
    if(T == 0):
        print("WARNING: T identical 0 not implemented
            in thermal quark term. Choose T close to 0.
            ")
        return np.nan
    mPi = 140.
    if(B < B_cutoff):
        print "Warning: below magnetic field cutoff.
            Evaluation will use B=0 expression.\n"

```

```

        upper_lim=np.inf
        integral, err = scipy.integrate.quad(
            quark_integrand_noB, 0, upper_lim, args=(
                delta, T, chem_pot, q, 0))
        return -4*T*integral/(2*np.pi**2)
    elif( B < 0.1*mPi**2):
        print "Warning: small magnetic field.
              Evaluation will be slow.\n"

    e_charge = 0.303
    q_up = (2./3.)*e_charge
    q_down = (-1./3.)*e_charge
    v = double_sum(delta, B, T, q, q_up)
    v += double_sum(delta, B, T, q, q_down)
    return v

def v_qk_vac_B(delta, B):
    """ B-dependent part of the quark vacuum energy """
    if(B < B_cutoff):
        return 0
    n_colors = 3.
    e_charge = 0.303
    q_up = 2./3.*e_charge
    q_down = -1./3.*e_charge
    delta_up = delta**2 / (2. * np.abs(q_up * B) )
    delta_down = delta**2 / (2. * np.abs(q_down * B) )
    v = (q_up * B)**2 * (1./12. - mpmath.fp.zeta(-1,
        delta_up, 1) - 1./2. * delta_up *math.log(
        delta_up) - 1./4. * delta_up**2 + 1./2. *
        delta_up**2 * math.log(delta_up) )
    v += (q_down * B)**2 * (1./12. - mpmath.fp.zeta(-1,
        delta_down, 1) - 1./2. * delta_down*math.log(
        delta_down) - 1./4. * delta_down**2 + 1./2. *
        delta_down**2 * math.log(delta_down) )
    v *= 8*n_colors/(4*np.pi)**2
    return v

def v_photon(couplings, B):
    """ B-dependent part of the photon vacuum energy. It
        has no effect on phase diagram. """
    if(B<B_cutoff):
        return 0
    n_color = 3.
    e_charge = 0.303
    q_up = 2./3.*e_charge
    q_down = -1./3.*e_charge
    prefactor = 4.*n_color/( 3. * (4.*np.pi)**2 )
    v = 0
    v += 0.5*B**2

```

```

v += 0.5*B**2 * prefactor * (q_up**2 * math.log(
    couplings.m_quark**2 / ( 2.*np.abs(q_up *B))))
v += 0.5*B**2 * prefactor * (q_down**2 * math.log(
    couplings.m_quark**2 / ( 2.*np.abs(q_down*B))))
return v

def v_qk_vac_noB(delta, couplings):
    """ B-independent part of the quark vacuum energy """
    v = 0
    delta_cutoff = 1e-9
    if(abs(delta) > delta_cutoff):
        v += (2.0 * couplings.n_colors * delta**4)/((4.*
            np.pi)**2) * (1.5 + np.log(couplings.renorm_MS
                **2/(delta**2)))
    return v

def zetaPrime(x):
    """ Derivative of Hurwitz zeta function with respect
        to first argument evaluated at -1 """
    return mpmath.zeta(-1, x, 1)

def double_sum(delta, B, T, q, charge):
    """ Sum over Landau levels """
    fpi = 93.
    nTolerance = 1.e-4 * fpi**4
    lTolerance = nTolerance/100.

    current_sum = 0.
    prev_sum = 0.
    sumN = True
    n = 0

    prefactor = np.abs(charge*B)*T/(2*np.pi**2)
    while(sumN):
        if(n==0):
            current_sum += l_sum(delta, B, T, q, charge, n
                , lTolerance)
        else:
            current_sum += 2.*l_sum(delta, B, T, q, charge
                , n, lTolerance) #Degeneracy factor of 2
                for n>1.
        if(prefactor * np.abs(current_sum - prev_sum) <
            nTolerance):
            sumN = False
        elif(current_sum == 0):
            sumN = False
        n=n+1
        prev_sum = current_sum

```



```

    return - np.abs(charge*B)/(2*np.pi**2) * T *
           current_sum

def l_sum(delta, B, T, q, charge, n, tolerance):
    """ Sum over fugacities """
    current_sum = 0.
    prev_sum    = 0.
    l = 1
    continueSum = True

    prefactor = np.abs(charge*B)*T/(2*np.pi)
    M = math.sqrt(delta**2 + 2*np.abs(charge*B)*n)
    while(continueSum):
        l_term = (-1)**(l+1) * M * ( 2+4*math.cos( 2.*np.
            pi*q*l/(3.) ) ) / (l) * scipy.special.kn(1, l*M
            /T)
        current_sum += l_term
        if(prefactor * np.abs(current_sum - prev_sum) <
            tolerance):
            continueSum = False
        elif(l_term == 0):
            continueSum = False
        prev_sum = current_sum
        l = l+1
    return current_sum

# Gluonic potential
# B2, B4 assumes complex input.
def B2(x):
    while(x.real >= 1.):
        x = x - (1.+0j)
    while(x.real < 0.):
        x = x + (1.+0j)
    return x * ( 1 - x )

def B4(x):
    while(x.real >= 1.):
        x = x - (1.+0j)
    while(x.real < 0.):
        x = x + (1.+0j)
    return x**2 * ( 1 - x )**2

# v2, v4 assumes real input.
def v4(q, r, r_imag):
    r_imag = r_imag*(0+1j)
    return B4(2.*q/3.) + B4(q/3. + r + r_imag) + B4(q/3. -
        r - r_imag)

def v2(q, r, r_imag):

```

```

r_imag = r_imag*(0+1j)
return B2(2.*q/3.) + B2(q/3. + r + r_imag) + B2(q/3. -
      r - r_imag)

def v_gluon_perturbative(q, r, r_imag, T):
return math.pi**2 * T**4 * ( -8./45. + 4./3. * v4(q,r,
      r_imag) )

def v_gluon_nonperturbative(q, r, r_imag, T, Td):
c2 = 0.830
c1 = 50.*(1-c2)/27.
c3 = (47. - 20. * c2)/27.
return 4.* math.pi**2 /3. * T**2 * Td**2 * ( - 1./5. *
      c1 * v2(q, r, r_imag) - c2 * v4(q,r, r_imag) +
      2./15.*c3 )

def v_gluon(q, r, r_imag, T, Td = 270):
complexPot = v_gluon_perturbative(q, r, r_imag, T) +
      v_gluon_nonperturbative(q, r, r_imag, T, Td)
return complexPot.real

def v_gluon_RRTW(q, r, r_imag, T, Td = 208.):
loop = polyakov_loop(q, r, r_imag)
alooop = polyakov_antiloop(q, r, r_imag)

T0 = Td
a0 = 3.51
a1 = -2.47
a2 = 15.2
b3 = -1.75
A = a0 + (T0/T) * a1 + (T0/T)**2 * a2
B = b3 * (T0/T)**3
logArg = 1 - 6*loop*alooop - 3 * (loop*alooop)**2 + 4*(
      loop**3 + alooop**3)
U = T**4 * ( - 0.5*A*loop*alooop + B*cmath.log( logArg )
      )
return U.real

def polyakov_loop(q, r, r_imag):
r_imag = r_imag*(0+1j)
return 1/3. * cmath.exp(2*math.pi*( r+r_imag )*(0+1j)
      /3.0) * ( cmath.exp( 2*math.pi*(r+r_imag)*(0+1j) )
      + 2*math.cos(2*math.pi*q/3.0) )

def polyakov_antiloop(q, r, r_imag):
r_imag = r_imag*(0+1j)
return 1/3. * cmath.exp(-2*math.pi*( r+r_imag )*(0+1j)
      /3.0) * ( cmath.exp( -2*math.pi*(r+r_imag)*(0+1j) )
      + 2*math.cos(2*math.pi*q/3.0) )

```

B.2 Implementation of the Thermal Quark Integrand in C

```

#include <math.h>
#include <complex.h>
#include <stdio.h>

complex double quark_integrand(int n, double *x) {
    // x[0] = p, x[1] = M_B, x[2] = T, x[3] = chem_pot, x
    // [4] = q, x[5] = r_imag
    double p_squared = x[0]*x[0];
    double eff_energy = sqrt(p_squared + x[1]*x[1]);
    double beta_eff_energy = eff_energy/x[2];
    double mu_prefactor = (2.0*M_PI/3.0);
    double complex img_unit = 0.0 + 1.0 * I;
    double complex betamu1 = x[3]/x[2] + img_unit *
        mu_prefactor * ( x[4] + x[5]*img_unit);
    double complex betamu2 = x[3]/x[2] + img_unit *
        mu_prefactor * ( - x[4] + x[5]*img_unit);
    double complex betamu3 = x[3]/x[2] + img_unit *
        mu_prefactor * ( -2*x[5]*img_unit);

    double complex integrand = 0;
    integrand += 1.0/(1 + cexp(beta_eff_energy - betamu1))
        + 1.0/(1 + cexp(beta_eff_energy + betamu1));
    integrand += 1.0/(1 + cexp(beta_eff_energy - betamu2))
        + 1.0/(1 + cexp(beta_eff_energy + betamu2));
    integrand += 1.0/(1 + cexp(beta_eff_energy - betamu3))
        + 1.0/(1 + cexp(beta_eff_energy + betamu3));
    integrand *= p_squared / (eff_energy * x[2]*x[2]);
    return creal(integrand);
}

complex double quark_integrand_noB(int n, double *x) {
    // x[0] = p, x[1] = delta, x[2] = T, x[3] = chem_pot,
    // x[4] = q, x[5] = r_imag
    double complex img = 0.0 + 1.0 * I;
    double pSquared = x[0]*x[0];
    double energy = sqrt( pSquared + x[1]*x[1] );
    double complex exponent1 = - ( energy - x[3] ) / x[2]
        + 2*M_PI * img * ( x[4] + x[5]*img ) / 3.0;
    double complex exponent2 = - ( energy - x[3] ) / x[2]
        + 2*M_PI * img * ( -x[4] + x[5]*img ) / 3.0;
    double complex exponent3 = - ( energy - x[3] ) / x[2]
        + 2*M_PI * img * ( -2. * x[5]*img ) / 3.0;
    double complex exponent4 = - ( energy + x[3] ) / x[2]
        - 2*M_PI * img * ( x[4] + x[5]*img ) / 3.0;

```

```

double complex exponent5 = - ( energy + x[3] ) / x[2]
    - 2*M_PI * img * ( -x[4] + x[5]*img ) / 3.0;
double complex exponent6 = - ( energy + x[3] ) / x[2]
    - 2*M_PI * img * ( -2. * x[5]*img ) / 3.0;
double complex totIntegrand = 0;
double exponentCutoff = 10;
if(creal( exponent1 ) > exponentCutoff && creal(
    exponent2 ) > exponentCutoff && creal( exponent3 )
    > exponentCutoff &&
        creal( exponent4 ) > exponentCutoff &&
        creal( exponent5 ) >
            exponentCutoff && creal( exponent6
        ) > exponentCutoff){
    totIntegrand = pSquared*(exponent1+exponent2+
        exponent3+exponent4+exponent5+exponent6);
}
else {
    double complex arg = ( 1 + cexp(exponent1) )*(
        1 + cexp(exponent2) )*( 1 + cexp(exponent3
        ) )*( 1 + cexp(exponent4) )*( 1 + cexp(
        exponent5) )*( 1 + cexp(exponent6) );
    totIntegrand = pSquared * clog(arg);
}
return creal(totIntegrand);
}

```

B.3 Implementation of the Global Minimization in Python

```

from potentials import CouplingSet, v_effective
import numpy as np
import cmath, math
import scipy
import matplotlib.pyplot as plt
from matplotlib.backends.backend_pdf import PdfPages
from joblib import Parallel, delayed
import os
import time

# Set CPU affinity to allow multithreading with numpy/
#   scipy
# This is necessary due to a bug in the BLAS library
n_cores = 12
os.system('taskset -cp 0-%d %s' % (n_cores, os.getpid()))

def opt_function(temp, chem_pot, B, couplings, bnds, model
    ):

```

```

# Finds (Delta, q) at given T, B
scale = (8./45. + 2.*7./60.)*np.pi**2*temp**4
# Normalize potential with P_SB so it is of the
# order of 1.
optimizer = 'TNC'
kwargs = {'args':(temp, chem_pot, B, couplings, 1./
scale, model), 'method':optimizer, 'bounds':bnds}
delta_guess = 300.0
q_guess = 0.9
res = scipy.optimize.basinhopping(
    v_effective,
    np.array([delta_guess, q_guess]),
    minimizer_kwargs = kwargs,
    niter=30,
)
return res

def polyakov_loop(q, r, r_imag):
    r_imag = r_imag*(0+1j)
    return 1/3. * cmath.exp(2*math.pi*( r+r_imag )*(0+1j)
/3.0) * ( cmath.exp( 2*math.pi*(r+r_imag)*(0+1j) )
+ 2*math.cos(2*math.pi*q/3.0) )

def calc_condensates(couplings, potential, chem_pot,
B_vals, N_steps, T_lower, T_upper, delta_upper, comment
=''):
    # Calculate condensates as function of temperatures
    # for a list of B values
    # Assumes B_vals i units of mpi**2/e

    header_string = '|eB|-field values in units of m_pi^2:
    %s' % np.array2string(B_vals, precision=2)
    mpi = 140
    e_charge = 0.303
    B_vals = B_vals * mpi**2/e_charge

    # Initialize arrays
    temps = np.linspace(T_lower, T_upper, N_steps)
    delta_mins = np.zeros((len(temps), len(B_vals)))
    q_mins = np.zeros((len(temps), len(B_vals)))
    loop_mins = np.zeros((len(temps), len(B_vals)))
    results = np.empty((len(temps), len(B_vals)),
dtype = scipy.optimize.OptimizeResult)

    # Carry out minimization procedure at each temperature
    # . Minimum is always located at q<1$.
    bnds = ((0.01, delta_upper), (0.005, 0.999))
    start = time.time()
    for k in range(len(B_vals)):

```

```

        results[:, k] = Parallel(n_jobs=n_cores)(delayed(
            opt_function)(temps[i], chem_pot, B_vals[k],
                couplings, bnds, potential) for i in range(len(
                    temps)))
    print("Time spent on optimization: %.1f s" % (time.
        time() - start) )

    for k in range(0, len(B_vals)):
        for i in range(0, len(temps)):
            delta_mins[i, k], q_mins[i, k] = results[i, k
                ].x
            loop_mins[i, k] = np.abs(polyakov_loop(q_mins[
                i, k], 0, 0)) #Has imaginary part 0, but
                abs needed to convert complex float to real
                float.

#Save for postprocessing and plotting.
timestr = time.strftime("%Y%m%d-%H%M%S")
filename1 = 'temps_N%.0f_msigma%.0f_mquark%.0
    f_potential%s_Tmin%.0f_Tmax%.0f_%s_%s.csv' % (
        N_steps, couplings.m_sigma, couplings.m_quark,
        potential, T_lower, T_upper, timestr, comment)
filename2 = 'deltas_N%.0f_msigma%.0f_mquark%.0
    f_potential%s_Tmin%.0f_Tmax%.0f_%s_%s.csv' % (
        N_steps, couplings.m_sigma, couplings.m_quark,
        potential, T_lower, T_upper, timestr, comment)
filename3 = 'loop_N%.0f_msigma%.0f_mquark%.0
    f_potential%s_Tmin%.0f_Tmax%.0f_%s_%s.csv' % (
        N_steps, couplings.m_sigma, couplings.m_quark,
        potential, T_lower, T_upper, timestr, comment)
np.savetxt(filename1, temps, header =
    header_string)
np.savetxt(filename2, delta_mins, header =
    header_string)
np.savetxt(filename3, loop_mins, header =
    header_string)

#Example use
mpi = 140
msigma = 500
mquark = 300
fpi = 93
chem_pot = 0
N_steps = 20
delta_max = 450
T_min = 1
T_max = 250
B_fields = np.array([0, 4, 8])
default_couplings = CouplingSet(mpi, sigma, mquark, fpi)

```

```
calc_condensates(default_couplings, 'chiM', chem_pot,  
                 B_fields, N_steps, T_min, T_max, delta_max)
```
